ATTACHMENT 6

Holtec International Report No. HI-2033124
"Spent Fuel Storage Expansion at Clinton Power Station"
(Non-Proprietary Version)

HOLTEC INTERNATIONAL

Holtec Center, 555 Lincoln Drive West, Marlton, NJ 08053
Telephone (856) 797-0900
Fax (856) 797-0909

SPENT FUEL STORAGE EXPANSION

at

CLINTON POWER STATION

for

AMERGEN

HOLTEC PROJECT NO. 1342

HOLTEC REPORT HI-2033124

REPORT CATEGORY: A

REPORT CLASS: SAFETY RELATED

HOLTEC INTERNATIONAL

DOCUMENT ISSUANCE AND REVISION STATUS[1]

DOCUMENT NAME: Spent Fuel Storage Expansion at Clinton Power Station

DOCUMENT NO.:	HI-2033124	CATEGORY: ☐	GENERIC
PROJECT NO.:	1342	☒	PROJECT SPECIFIC

Rev. No.[2]	Date Approved	Author's Initials	VIR #	Rev. No.	Date Approved	Author's Initials	VIR #
0	1/30/04	SP	550600				
1	6/18/04	SP	666423				
2	7/16/04	SP	583678				

DOCUMENT CATEGORIZATION

In accordance with the Holtec Quality Assurance Manual and associated Holtec Quality Procedures (HQPs), this document is categorized as a:

☐ Calculation Package[3] (Per HQP 3.2)

☒ Technical Report (Per HQP 3.2) (Such as a Licensing Report)

☐ Design Criterion Document (Per HQP 3.4)

☐ Design Specification (Per HQP 3.4)

☐ Other (Specify):

DOCUMENT FORMATTING

The formatting of the contents of this document is in accordance with the instructions of HQP 3.2 or 3.4 except as noted below:

DECLARATION OF PROPRIETARY STATUS

This document is labeled:

☐ Nonproprietary ☒ Holtec Proprietary ☐ TOP SECRET

Documents labeled TOP SECRET contain extremely valuable intellectual/commercial property of Holtec International. They cannot be released to external organizations or entities without explicit approval of a company corporate officer. The recipient of Holtec's proprietary or Top Secret document bears full and undivided responsibility to safeguard it against loss or duplication.

Notes

1. This document has been subjected to review, verification and approval process set forth in the Holtec Quality Assurance Procedures Manual. Password controlled signatures of Holtec personnel who participated in the preparation, review, and QA validation of this document are saved in the N-drive of the company's network. The Validation Identifier Record (VIR) number is a unique six-digit random number that is generated by the computer after the specific revision of this document has undergone the required review and approval process, and the appropriate Holtec personnel have recorded their password-controlled electronic concurrence to the document.
2. A revision to this document will be ordered by the Project Manager and carried out if any of its contents is materially affected during evolution of this project. The determination as to the need for revision will be made by the Project Manager with input from others, as deemed necessary by him.
3. Revisions to Calculation Packages may be made by adding supplements to the document and replacing the "Table of Contents", the "Review and Certification" page and the "Revision Log".

SUMMARY OF REVISIONS

Revision 2 contains the following pages:	
COVER PAGE	1 page
DOCUMENT ISSUANCE AND REVISION STATUS	1 page
SUMMARY OF REVISIONS	1 page
TABLE OF CONTENTS	9 pages
1.0 INTRODUCTION	7 pages
2.0 CASK PIT STORAGE RACKS	20 pages
3.0 MATERIAL AND HEAVY LOADS CONSIDERATIONS	12 pages
4.0 CRITICALITY SAFETY ANALYSES	31 pages
-- APPENDIX 4A	26 pages
5.0 THERMAL-HYDRAULIC CONSIDERATIONS	33 pages
6.0 STRUCTURAL/SEISMIC CONSIDERATIONS	66 pages
7.0 FUEL HANDLING AND CONSTRUCTION ACCIDENTS	16 pages
8.0 FUEL POOL STRUCTURE INTEGRITY CONSIDERATIONS	13 pages
9.0 RADIOLOGICAL EVALUATION	5 pages
10.0 INSTALLATION	8 pages
11.0 ENVIRONMENTAL COST/BENEFIT ASSESSMENT	7 pages
TOTAL	256 pages

Revision 1 incorporates client comments. Added reference in Section 2.6 (5) and Reference Section 2.7. Revised the word "skip" to the word "intermittent" in Section 2.6.1. Corrected footers and pagination on pages 6-13 thru 6-18. Corrected wording "Cask Loading" to "Fuel Cask Storage" throughout Section 11. Corrected typographical error on page 11-4. Revised Code versions in Section 6.13 to be consistent with plant design basis. Revised Section 5 to reflect results of updated thermal-hydraulic evaluations. Revised Section 3 and other references to clarify neutron absorber material selection.

Revision 2 incorporates client comments. The word "borated" on page 1-2 is corrected to "unborated". Dimensions on Figures 1.1.1 to 1.1.3 were adjusted to reflect nominal values. The software ORIGEN2 has been added as a reference on pages 5-5 and 5-15.

TABLE OF CONTENTS

TABLE OF CONTENTS

TABLE OF CONTENTS

Tables

Figures

1.0 INTRODUCTION

The Clinton Power Station is operated by Amergen Energy Company, LLC (Amergen). The single unit nuclear power facility is located in Harp Township, DeWitt County, approximately 6 miles east of the city of Clinton, Illinois. Unit 1 of the Clinton Power Station has a boiling water reactor nuclear steam supply system with 624 fuel assemblies in the core. The plant was designed by General Electric and is designated as a BWR/6 unit and has a licensed rated power level of 3473 MWt. The unit currently uses a Spent Fuel Pool (SFP) for storage of irradiated nuclear fuel between refueling outages in order to maintain a subcritical array, remove decay heat and provide radiation shielding.

The SFP is currently licensed for 2,512 fuel assembly storage locations and 10 failed fuel container storage locations, arranged in twenty-two distinct rack modules. An additional storage capacity of 160 assemblies exists in the Upper Containment Storage Pool. However, the upper pool capacity is commonly relied upon only during refueling and is not considered for long-term fuel storage. Therefore, full core offload will be lost once the SFP contains 2,512 less 624 fuel assemblies, or 1,888 assemblies. Based on the current inventory of 1,312 fuel assemblies stored in the spent fuel pool and the anticipated future discharges of spent fuel, loss of full core reserve capacity will occur during the scheduled February 2006 refueling outage when an anticipated 312 fuel assemblies are permanently discharged and new fuel is loaded into the SFP during Operating Cycle 11.

To maintain prudent storage reserve, Amergen intends to expand spent fuel storage capacity in two phases. Phase 1 consists of adding two new 15 by 12 cell racks within the Fuel Cask Storage Pool by January 2005. The completed Fuel Cask Storage Pool configuration is shown in Figure 1.1.1. This modification would increase the licensed storage capacity from the current 2,512 storage cells to 2,872 storage cells. During Phase 2 the two racks in the Fuel Cask Storage Pool will be relocated into the SFP along with 14 more new racks. During this second phase, 12 of the existing racks will be removed from the SFP and three of these existing racks to be removed will be placed within the Fuel Cask Storage Pool. The final, Phase 2, configurations of the SFP and the Fuel Cask Storage Pool are shown in Figures 1.1.2 and 1.1.3, respectively.

This report provides the design basis, analysis methodology, and evaluation results for the proposed storage racks at Clinton Power Station to support the licensing process. The rack design and analysis methodologies employed are a direct evolution of previous license applications. This report documents the design and analyses performed to demonstrate that the racks meet all governing requirements of the applicable codes and standards, in particular, "OT Position for Review and Acceptance of Spent Fuel Storage and Handling Applications", USNRC (1978) and 1979 Addendum thereto [1].

The new Cask Area storage racks are freestanding and self-supporting. The principal construction materials for the SFP racks are SA240-Type 304L stainless steel sheet and plate stock, and SA564-630 (precipitation hardened stainless steel) for the adjustable support spindles. The only non-stainless material utilized in the rack is the neutron absorber material, which is discussed in Section 3. The racks are designed to the stress limits of, and analyzed in accordance with, Section III, Division 1, Subsection NF of the ASME Boiler and Pressure Vessel (B&PV) Code [2]. The material procurement, analysis, fabrication, and installation of the rack modules conform to 10CFR50 Appendix B requirements.

Sections 2 and 3 of this report provide an abstract of the design and material information on the racks.

Section 4 provides a summary of the methods and results of the criticality evaluations performed for the Cask Area storage racks. The criticality safety analysis requires that the effective neutron multiplication factor (k_{eff}) is less than or equal to 0.95 with the storage racks fully loaded with fuel of the highest permissible reactivity and the pool flooded with unborated water at a temperature corresponding to the highest reactivity. The maximum calculated reactivities include a margin for uncertainty in reactivity calculations, including manufacturing tolerances, and are calculated with a 95% probability at a 95% confidence level. The criticality safety analysis sets the requirements on the neutron absorber panel length and the amount of B^{10} per unit area (i.e., loading density) for the new racks.

Thermal-hydraulic consideration requires that fuel cladding will not fail due to excessive thermal stress, and that the steady state pool bulk temperature will remain within the limits prescribed for the Fuel Cask Storage Pool and Spent Fuel Pool to satisfy the pool structural strength, operational, and regulatory

requirements. The thermal-hydraulic analyses carried out in support of this storage expansion effort are described in Section 5.

Rack module structural analysis requires that the primary stresses in the rack module structure will remain below the ASME B&PV Code (Subsection NF) [2] allowables. Demonstrations of seismic and structural adequacy are presented in Section 6.0. The structural qualification also requires that the subcriticality of the stored fuel will be maintained under all postulated accident scenarios. The structural consequences of these postulated accidents are evaluated and presented in Section 7 of this report.

Section 8 discusses the evaluation of the Fuel Cask Storage Pool and Spent Fuel Pool structures to withstand the new rack loads. The radiological considerations are documented in Section 9.0. Section 10 discusses the salient considerations in the installation of the new racks. Section 11 discusses a cost/benefit and environmental assessment to establish the acceptability of the wet storage expansion option.

All computer programs utilized to perform the analyses documented in this report are benchmarked and verified. Holtec International has utilized these programs in numerous license applications over the past decade.

The analyses presented herein clearly demonstrate that the new racks possess wide margins of safety with respect to all considerations of safety specified in the OT Position Paper [1], namely, nuclear subcriticality, thermal-hydraulic safety, seismic and structural adequacy, radiological compliance, and mechanical integrity.

1.1 References

[1] USNRC, "OT Position for Review and Acceptance of Spent Fuel Storage and Handling Applications, April 14, 1978, and Addendum dated January 18, 1979.

[2] American Society of Mechanical Engineers (ASME), Boiler & Pressure Vessel Code, Section III, 1977 Edition, Subsection NF, and Appendices.

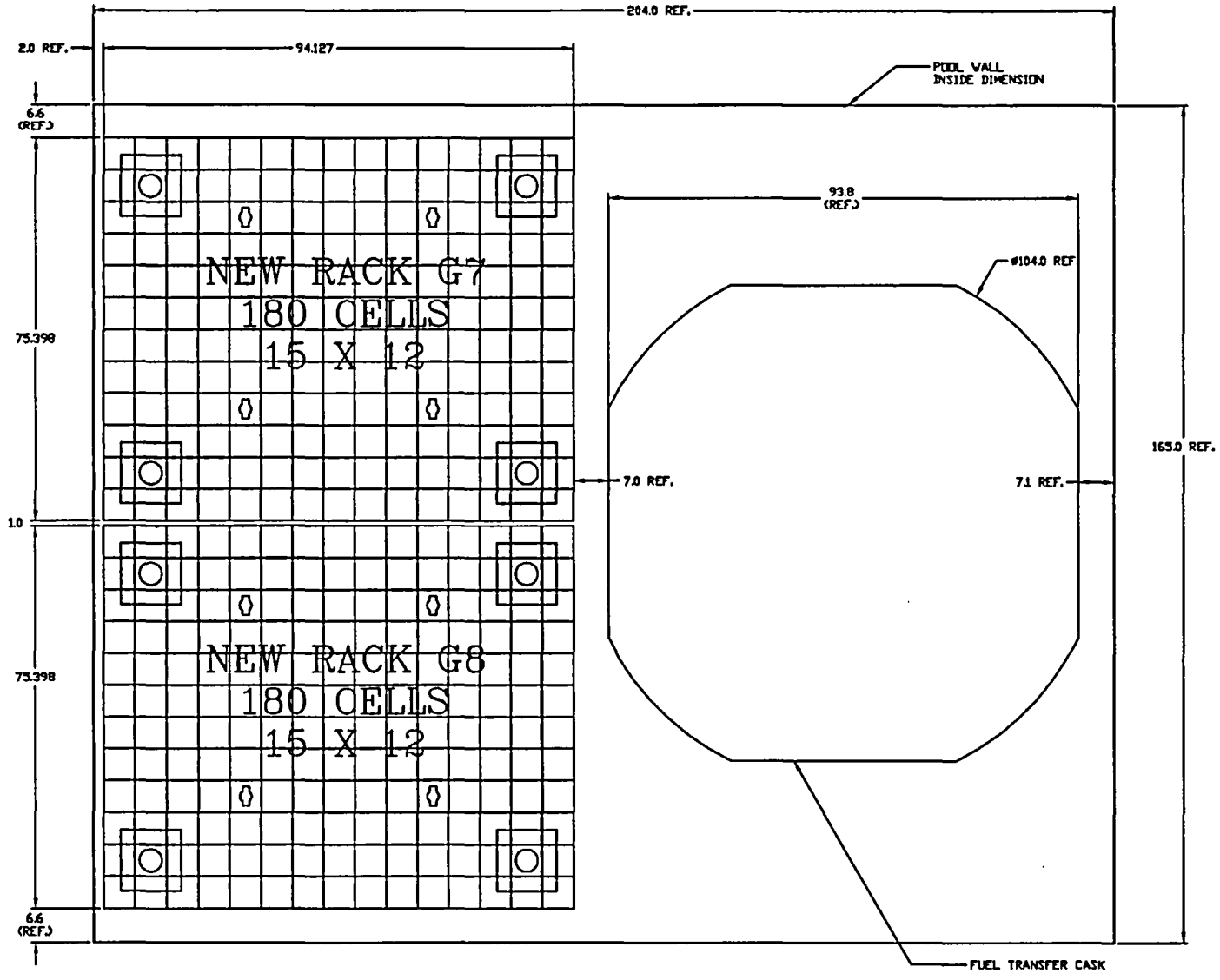

FIGURE 1.1.1; PHASE 1 – FUEL CASK STORAGE POOL RACK LAYOUT

DIMENSIONS ARE NOMINAL VALUES FOR REFERENCE ONLY

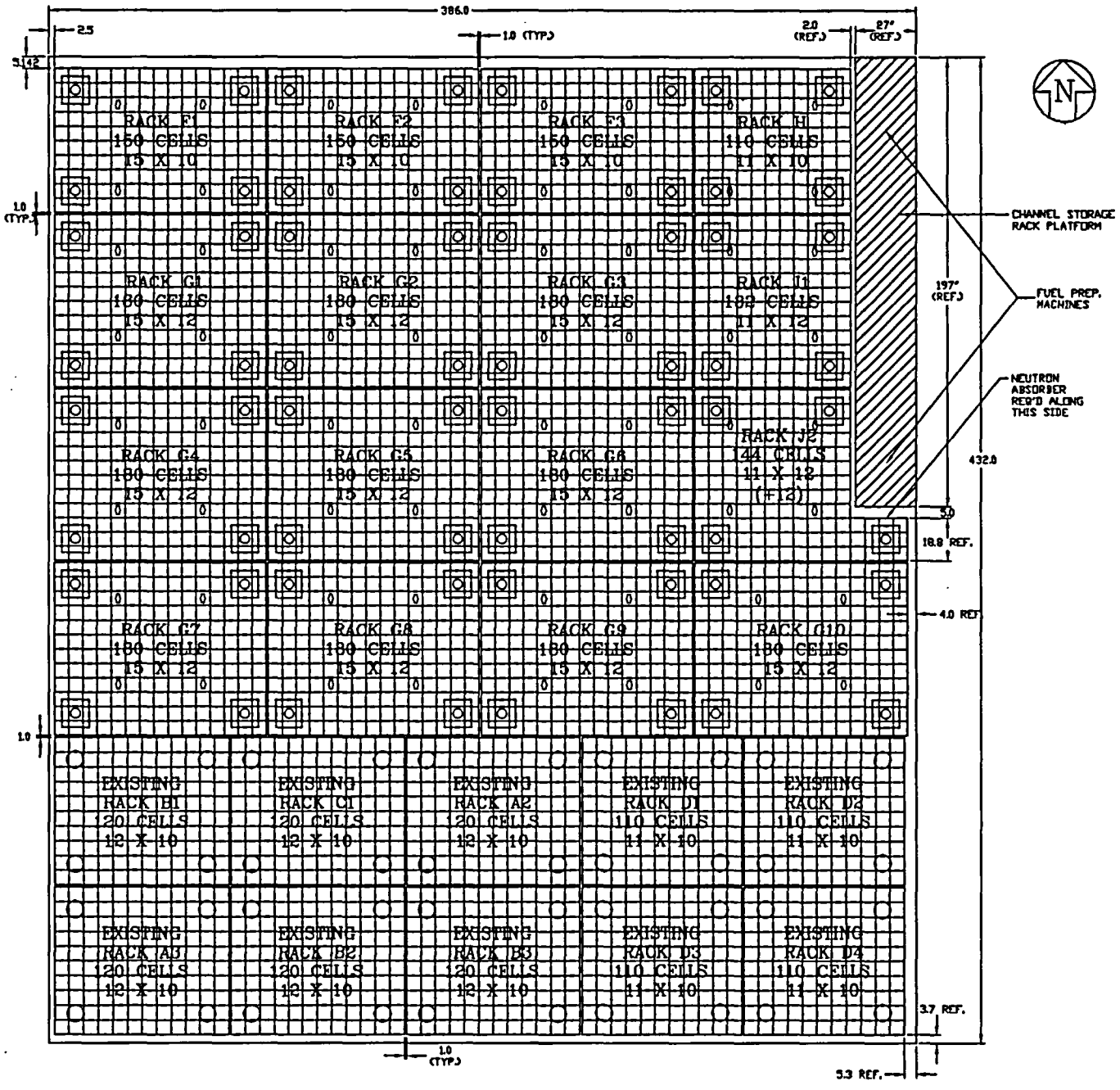

FIGURE 1.1.2; PHASE 2 – SPENT FUEL POOL RACK LAYOUT

H1342

DIMENSIONS ARE NOMINAL VALUES SHOWN FOR REFERENCE ONLY

HI-2033124

G\DRAWINGS\D-FIGURES\1342\REPORT-HI2033124\CHPT_1\FIG_1_1_2

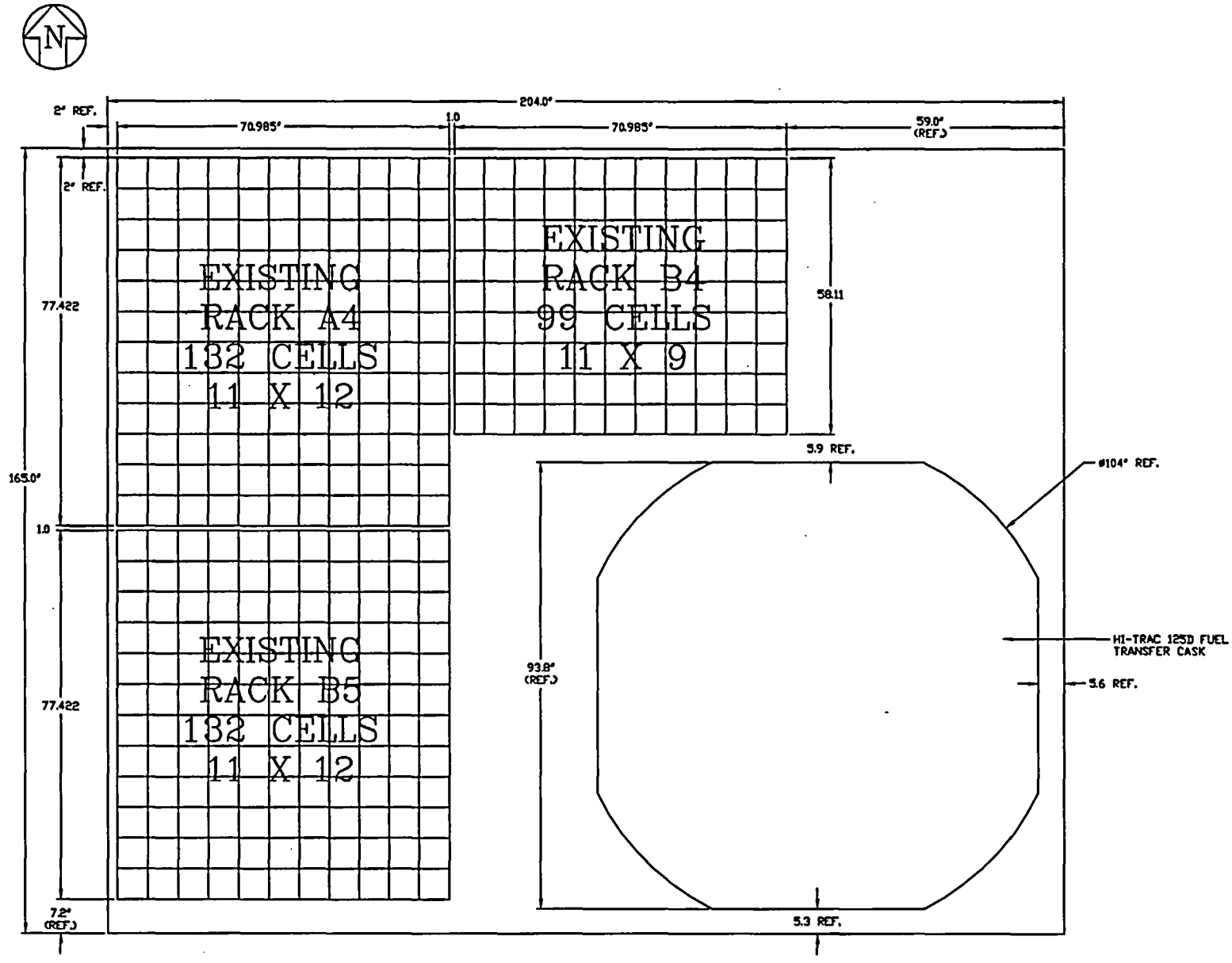

FIGURE 1.1.3; PHASE 2 – FUEL CASK STORAGE POOL RACK LAYOUT

DIMENSIONS ARE NOMINAL VALUES SHOWN FOR REFERENCE ONLY

2.0 STORAGE RACKS DESCRIPTION

2.1 Introduction

The new Clinton Power Station (CPS) fuel storage racks will be freestanding modules, made primarily from Type 304L austenitic stainless steel containing honeycomb storage cells interconnected through longitudinal welds. Neutron absorber panels containing a high areal loading of the boron-10 (B-10) isotope provide appropriate neutron attenuation between adjacent storage cells.

Figure 2.1.1 provides an isometric schematic of a typical Region 2 storage rack module. Data on the cross sectional dimensions, weight and cell count for the rack modules are presented in Table 2.1.1. All of the new rack modules are designed and constructed to have identical configurations, except for the number of storage cells.

The baseplates on all spent fuel rack modules extend approximately 1/2" beyond the rack module periphery wall such that the plate protrusions act to maintain rack-to-rack distances. Each rack is supported by four pedestals, which are remotely height-adjustable. The rack module support pedestals are engineered to accommodate minor level adjustments. Thus, the racks can be made plumb during installation. The cell height and overall height of the racks is chosen to be similar to the existing racks. The similar cell height ensures that the existing fuel grapple can properly engage bundles and provides sufficient access for storage and removal of fuel channels. The overall rack height similarity coupled with the adjustable pedestal heights also ensures that the top of the racks will be approximately co-planar with all other new racks and the existing racks in the pool.

The overall design of the rack modules is similar to those presently in service in the spent fuel pools at many other nuclear plants, among them Hatch and J.A. FitzPatrick. Altogether, over 50 thousand storage cells of this design have been provided by Holtec International to various nuclear plants around the world.

2.2 Summary of Principal Design Criteria

The key design criteria for the new racks are set forth in the USNRC memorandum entitled "OT Position for Review and Acceptance of Spent Fuel Storage and Handling Applications", dated April 14, 1978 as modified by amendment dated January 18, 1979. The individual sections of this report address the specific design bases derived from the above-mentioned "OT Position Paper". The design bases for the new racks are summarized in the following:

a. Disposition: New rack modules are required to be free-standing.

b. Kinematic Stability: Each freestanding module must be kinematically stable (against tipping or overturning) if a seismic event is imposed.

c. Structural Compliance: All primary stresses in the rack modules must satisfy the limits postulated in Section III subsection NF of the ASME B & PV Code.

d. Thermal-Hydraulic Compliance: The spatial average bulk pool temperature is required to remain below 150°F in the wake of a normal partial core offload or a full core offload.

e. Criticality Compliance: The Holtec high-density spent fuel storage racks are designed to assure that the neutron multiplication factor (k_{eff}) is equal or less than 0.95 with the racks fully loaded with fuel of the highest anticipated reactivity and the pool flooded with unborated water at a temperature corresponding to the highest reactivity. The maximum calculated reactivity includes a margin for uncertainty in reactivity calculations and in manufacturing tolerances, statistically combined, giving assurance that the true k_{eff} will be equal to or less than 0.95 with a 95% probability at a 95% confidence level. Reactivity effects of the abnormal and accident conditions have also been evaluated to assure that under credible abnormal and accident conditions, the reactivity will be maintained less than 0.95.

f. Accident Events: In the event of postulated drop events (uncontrolled lowering of a fuel assembly, for instance), it is necessary to demonstrate that the subcritical geometry of the rack structure is not compromised.

The foregoing design bases are further articulated in Sections 4 through 7 of this licensing report.

2.3 Applicable Codes and Standards

The following codes, standards and practices are used as applicable for the design, construction, and assembly of the fuel storage racks. Additional specific references related to detailed analyses are given in each section.

a. Design Codes

(1) American Institute of Steel Construction (AISC) Manual of Steel Construction, 9th Edition, 1989.

(2) American National Standards Institute/ American Nuclear Society ANSI/ANS-57.2-1983, "Design Requirements for Light Water Reactor Spent Fuel Storage Facilities at Nuclear Power Plants" (contains guidelines for fuel rack design).

(3) ASME B&PV Code Section III, 1977 Edition; ASME Section IX, 1977 Edition.

(4) American Society for Nondestructive Testing SNT-TC-1A, June 1980, Recommended Practice for Personnel Qualifications and Certification in Non-destructive Testing.

(5) American Concrete Institute Building Code Requirements for Reinforced Concrete (ACI 318-71).

(6) Code Requirements for Nuclear Safety Related Concrete Structures, ACI 349-76/ACI 349R-76, and ACI 349.1R-80.

(7) ASME Y14.5M, Dimensioning and Tolerancing

(8) ASME B&PV Code, Section II-Parts A and C, 1977 Edition.

(9) ASME B&PV Code NCA3800 - Metallic Material Organization's Quality System Program.

b. Standards of American Society for Testing and Materials (ASTM)

(1) ASTM E165 - Standard Test Method for Liquid Penetrant Examination.

(2) ASTM A240 - Standard Specification for Heat-Resisting Chromium and Chromium-Nickel Stainless Steel Plate, Sheet and Strip for Pressure Vessels.

(3) ASTM A262 - Standard Practices for Detecting Susceptibility to Intergranular Attack in Austenitic Stainless Steel.

(4) ASTM A276 - Standard Specification for Stainless Steel Bars and Shapes.

(5) ASTM A479 - Standard Specification for Stainless Steel Bars and Shapes for use in Boilers and other Pressure Vessels.

(6) ASTM A564 - Standard Specification for Hot-Rolled and Cold-Finished Age-Hardening Stainless Steel Bars and Shapes.

(7) ASTM C750 - Standard Specification for Nuclear-Grade Boron Carbide Powder.

(8) ASTM A380 - Standard Practice for Cleaning, Descaling, and Passivation of Stainless Steel Parts, Equipment and Systems.

(9) ASTM C992 - Standard Specification for Boron-Based Neutron Absorbing Material Systems for Use in Nuclear Spent Fuel Storage Racks.

(10) ASTM E3 - Standard Practice for Preparation of Metallographic Specimens.

(11) ASTM E190 - Standard Test Method for Guided Bend Test for Ductility of Welds.

c. Welding Code:

ASME B&PV Code, Section IX - Welding and Brazing Qualifications, 1977.

d. Quality Assurance, Cleanliness, Packaging, Shipping, Receiving, Storage, and Handling

(1) ANSI N45.2.1 - Cleaning of Fluid Systems and Associated Components during Construction Phase of Nuclear Power Plants - 1973 (R.G. 1.37).

(2) ANSI N45.2.2 - Packaging, Shipping, Receiving, Storage and Handling of Items for Nuclear Power Plants - 1972 (R.G. 1.38).

(3) ANSI N45.2.6 - Qualifications of Inspection, Examination, and Testing Personnel for the Construction Phase of Nuclear Power Plants - 1978. (R.G. 1.58).

(4) ANSI N45.2.8 - Supplementary Quality Assurance Requirements for Installation, Inspection and Testing of Mechanical Equipment and Systems for the Construction Phase of Nuclear Plants - 1975 (R.G. 1.116).

(5) ANSI N45.2.11 - Quality Assurance Requirements for the Design of Nuclear Power Plants - 1974 (R.G. 1.64).

(6) ANSI N45.2.12 - Requirements for Auditing of Quality Assurance Programs for Nuclear Power Plants - 1977 (R.G. 1.144).

(7) ANSI N45.2.13 - Quality Assurance Requirements for Control of Procurement of Items and Services for Nuclear Power Plants - 1976 (R. G. 1.123).

(8) ANSI N45.2.23 - Qualification of Quality Assurance Program Audit Personnel for Nuclear Power Plants - 1978 (R.G. 1.146).

(9) ASME B&PV Code, Section V, Nondestructive Examination, 1977 Edition.

(10) ANSI N16.9-75 - Validation of Calculation Methods for Nuclear Criticality Safety.

(11) ASME NQA-1 – Quality Assurance Program Requirements for Nuclear Facilities.

(12) ASME NQA-2 – Quality Assurance Requirements for Nuclear Power Plants.

e. USNRC Documents

(1) "OT Position for Review and Acceptance of Spent Fuel Storage and Handling Applications," dated April 14, 1978, and the modifications to this document of January 18, 1979.

(2) NUREG 0612, "Control of Heavy Loads at Nuclear Power Plants", USNRC, Washington, D.C., July, 1980.

f. Other ANSI Standards (not listed in the preceding)

(1) ANSI/ANS 8.1 - Nuclear Criticality Safety in Operations with Fissionable Materials Outside Reactors.

(2) ANSI/ANS 8.17 - Criticality Safety Criteria for the Handling, Storage, and Transportation of LWR Fuel Outside Reactors.

(3) ANSI N45.2 - Quality Assurance Program Requirements for Nuclear Power Plants - 1977.

(4) ANSI N45.2.9 - Requirements for Collection, Storage and Maintenance of Quality Assurance Records for Nuclear Power Plants - 1974.

(5) ANSI N45.2.10 - Quality Assurance Terms and Definitions - 1973.

(6) ANSI N14.6 - American National Standard for Special Lifting Devices for Shipping Containers Weighing 10,000 pounds (4500 kg) or more for Nuclear Materials - 1993.

(7) ANSI/ASME N626-3 - Qualification and Duties of Specialized Professional Engineers.

(8) ANSI/ANS- 57.3 – Design Requirements for New Fuel Storage Facilities at Light Water Reactor Plants.

g. Code-of-Federal Regulations (CFR)

(1) 10CFR20 - Standards for Protection Against Radiation.

(2) 10CFR21 - Reporting of Defects and Non-compliance.

(3) 10CFR50 Appendix A - General Design Criteria for Nuclear Power Plants.

(4) 10CFR50 Appendix B - Quality Assurance Criteria for Nuclear Power Plants and Fuel Reprocessing Plants.

(5) 10CFR61 - Licensing Requirements for Land Disposal of Radioactive Waste.

(6) 10CFR71 - Packaging and Transportation of Radioactive Material.

(7) 10CFR100 – Reactor Site Criteria

(8) 10CFR50.68 ""Criticality Accident Requirements"

h. Regulatory Guides (RG)

(1) RG 1.13 - Spent Fuel Storage Facility Design Basis (Revision 2 Proposed).

(2) RG 1.25 - Assumptions Used for Evaluating the Potential Radiological Consequences of a Fuel Handling Accident in the Fuel Handling and Storage Facility for Boiling and Pressurized Water Reactors, Rev. 0 - March, 1972.

(3) RG 1.28 - Quality Assurance Program Requirements - Design and Construction, Rev. 2 - February, 1979 (endorses ANSI N45.2).

(4) RG 1.33 – Quality Assurance Program Requirements.

(5) RG 1.29 - Seismic Design Classification, Rev. 2 - February, 1976.

(6) RG 1.31 - Control of Ferrite Content in Stainless Steel Weld Metal.

(7) RG 1.38 - Quality Assurance Requirements for Packaging, Shipping, Receiving, Storage and Handling of Items for Water-Cooled Nuclear Power Plants, Rev. 2 - May, 1977 (endorses ANSI N45.2.2).

(8) RG 1.44 - Control of the Use of Sensitized Stainless Steel.

(9) RG 1.58 - Qualification of Nuclear Power Plant Inspection, Examination, and Testing Personnel, Rev. 1 - September 1980 (endorses ANSI N45.2.6).

(10) RG 1.60 – Design Response Spectra for Seismic Design of Nuclear Power Plants.

(11) RG 1.61 - Damping Values for Seismic Design of Nuclear Power Plants, Rev. 0, 1973.

(12) RG 1.64 - Quality Assurance Requirements for the Design of Nuclear Power Plants, Rev. 2 - June, 1976 (endorses ANSI N45.2.11).

(13) RG 1.71 - Welder Qualifications for Areas of Limited Accessibility.

(14) RG 1.74 - Quality Assurance Terms and Definitions, Rev. 2 - February, 1974 (endorses ANSI N45.2.10).

(15) RG 1.85 - Materials Code Case Acceptability - ASME Section III, Division 1.

(16) RG 1.88 - Collection, Storage and Maintenance of Nuclear Power Plant Quality Assurance Records, Rev. 2 - October, 1976 (endorses ANSI N45.2.9).

(17) RG 1.92 - Combining Modal Responses and Spatial Components in Seismic Response Analysis, Rev. 1 - February, 1976.

(18) RG 1.116 - Quality Assurance Requirements for Installation, Inspection and Testing of Mechanical Equipment and Systems, Rev. 0-R - May,1977 (endorses ANSI N45.2.8-1975)

(19) RG 1.123 - Quality Assurance Requirements for Control of Procurement of Items and Services for Nuclear Power Plants, Rev. 1 - July, 1977 (endorses ANSI N45.2.13).

(20) RG 1.124 - Service Limits and Loading Combinations for Class 1 Linear-Type Component Supports, Revision 1, January, 1978.

(21) RG 1.144 - Auditing of Quality Assurance Programs for Nuclear Power Plants, Rev.1 - September, 1980 (endorses ANSI N45.2.12-1977)

(22) RG 3.4 - Nuclear Criticality Safety in Operations with Fissionable Materials at Fuels and Materials Facilities.

(23) RG 8.8 - Information Relative to Ensuring that Occupational Radiation Exposures at Nuclear Power Stations will be as Low as Reasonably Achievable (ALARA).

(24) IE Information Notice 83-29 - Fuel Binding Caused by Fuel Rack Deformation.

(25) RG 8.38 - Control of Access to High and Very High Radiation Areas in Nuclear Power Plants, June, 1993.

i. Branch Technical Position

(1) CPB 9.1-1 - Criticality in Fuel Storage Facilities.

j. American Welding Society (AWS) Standards

(1) AWS D1.1 - Structural Welding Code - Steel.

(2) AWS D1.3 - Structure Welding Code - Sheet Steel.

(3) AWS D9.1 - Sheet Metal Welding Code.

(4) AWS A2.4 - Standard Symbols for Welding, Brazing and Nondestructive Examination.

(5) AWS A3.0 - Standard Welding Terms and Definitions.

(6) AWS A5.12 - Specification for Tungsten and Tungsten Alloy Electrodes for Arc-Welding and Cutting

(7) AWS QC1 - Standard for AWS Certification of Welding Inspectors.

(8) AWS 5.4 – Specification for Stainless Steel Electrodes for Shielded Metal Arc Welding.

(9) AWS 5.9 – Specification for Bare Stainless Steel Welding Electrodes and Rods.

2.4 Quality Assurance Program

The governing quality assurance requirements for design and fabrication of the spent fuel racks are stated in 10CFR50 Appendix B. Holtec's Nuclear Quality Assurance program complies with this regulation and is designed to provide a system for the design, analysis and licensing of customized components in accordance with various codes, specifications, and regulatory requirements.

The manufacturing of the racks will be carried out by Holtec's designated manufacturer, U.S. Tool & Die, Inc. (UST&D). The Quality Assurance system enforced on the manufacturer's shop floor shall provide for all controls necessary to fulfill all quality assurance requirements. UST&D has manufactured high-density racks for over 60 nuclear plants around the world. UST&D has been audited by the nuclear industry group Nuclear Procurement Issues Committee (NUPIC), and the Quality Assurance branch of the USNRC Office of Nuclear Material Safety and Safeguards (NMSS) with satisfactory results.

The Quality Assurance System that will be used by Holtec to install the racks is also controlled by the Holtec Nuclear Quality Assurance Manual and by the CPS site-specific requirements.

2.5 Mechanical Design

The CPS rack modules are designed as cellular structures such that each fuel assembly has a square opening with conforming lateral support and a flat horizontal-bearing surface. All of the storage locations are constructed with multiple cooling flow holes to ensure that redundant flow paths for the coolant are available. The basic characteristics of the racks are summarized in Table 2.5.1.

A central objective in the design of the new rack modules is to maximize structural strength while minimizing inertial mass and dynamic response. Accordingly, the rack modules have been designed to simulate multi-flange beam structures resulting in excellent de-tuning characteristics with respect to the applicable seismic events. The next subsection presents an item-by-item description of the rack modules in the context of the fabrication methodology.

2.6 Rack Fabrication

The object of this section is to provide a brief description of the rack module construction activities, which enable an independent appraisal of the adequacy of design. The pertinent methods used in manufacturing the racks may be stated as follows:

1. The rack modules are fabricated in such a manner that the storage cell surfaces, which would come in contact with the fuel assembly, will be free of harmful chemicals and projections (e.g., weld splatter).

2. The component connection sequence and welding processes are selected to reduce fabrication distortions.

3. The fabrication process involves operational sequences that permit immediate accessibility for verification by the inspection staff.

4. The racks are fabricated per the UST&D Appendix B Quality Assurance program, which ensures, and documents, that the fabricated rack modules meet all of the requirements of the design and fabrication documents.

5. The corners of these storage cells are connected to each other using austenitic stainless steel connector elements, which lead to a honeycomb lattice construction. The extent of welding is selected to "detune" the racks from the seismic input motion [1].

2.6.1 Rack Modules

This section describes the constituent elements of the new CPS rack modules in the fabrication sequence. Figure 2.1.1 provides a schematic view of a typical BWR rack.

The rack module manufacturing begins with fabrication of the "box". The boxes are fabricated from two precision formed channels by seam welding in a machine equipped with copper chill bars and pneumatic clamps to minimize distortion due to welding heat input. Figure 2.6.1 shows the box. The minimum

weld seam penetration is 80% of the box metal gage, which is 0.075 inch (14 gage). 3/4 inch diameter holes are punched on at least two sides near the end of the box to provide the redundant flow holes.

Each box constitutes a storage location. Each external box side is equipped with a stainless steel sheathing, which holds one integral neutron absorber sheet (poison material) on each side, except the boxes on the south and west peripheries of each rack, which only have neutron absorber panels on the interior sides. This is because it is only necessary to have neutron absorber panels on one of the two sides of facing racks. The existing racks have neutron absorber panels on all four of the outer sides. The design objective calls for attaching neutron absorber panels tightly on the box surface. This is accomplished by die forming the box sheathings, as shown in Figure 2.6.2. The flanges of the sheathing are attached to the box using intermittent welds and spot welds. The sheathings serve to locate and position the poison sheet accurately, and to preclude its movement under seismic conditions.

Having fabricated the required number of composite box assemblies, they are joined together in a fixture using connector elements in the manner shown in Figure 2.6.3. Figure 2.6.4 shows an elevation view of two storage cells of a BWR rack module. Joining the cells by the connector elements results in a well-defined shear flow path, and essentially makes the box assemblage into a multi-flanged beam-type structure. The "baseplate" is attached to the bottom edge of the boxes. The baseplate is a 5/8 inch thick austenitic stainless steel plate stock which has 3-5/8 inch diameter holes (except at four lift locations, which are modified to accept the lifting rig lug) cut out in a pitch identical to the box pitch. The 3-5/8 inch diameter flow holes are specifically designed to accept the bottom nozzle of the BWR style fuel assembly. The baseplate is attached to the cell assemblage by fillet welding the box edge to the plate.

In the final step, adjustable leg support pedestals (shown in Figure 2.6.5) are welded to the underside of the baseplate. The top (female threaded) portion is made of austenitic steel material. The bottom male threaded part is made of 17:4 Ph series stainless steel to avoid galling problems. All support legs are the adjustable type (Figure 2.6.5), which provide a ± 1/2-inch vertical height adjustment at each leg location for leveling the rack. Each support leg is equipped with a readily accessible socket to enable remote leveling of the rack after its placement in the pool.

Appropriate NDE (nondestructive examination) occurs on all welds including visual examination of sheathing welds, box longitudinal seam welds, box-to-baseplate welds, and box-to-box connection welds; and liquid penetrant examination of support leg welds, in accordance with the design drawings.

2.7 References

[1] Holtec Position Paper WS-110, The Detuned Honeycomb Rack Module, Revision 0 dated November 7, 1996.

Table 2.1.1
Geometric and Physical Data for Storage Racks

RACK I.D.	NO. OF CELLS		MODULE ENVELOPE SIZE		WEIGHT (lbs)	NO. OF CELLS PER RACK
	N-S Direction	E-W Direction	N-S (in.)	E-W (in.)		
F1 thru F3	10	15	62.9	94.1	14,142	150
G1 thru G10	12	15	75.4	94.1	16,737	180
H	10	11	62.9	69.2	10,637	110
J1	12	11	75.4	69.2	12,558	132
J2	12	15	75.4	94.1	13,769	144 †

† A 4 by 9 array of cells has been removed to provide clearance for existing equipment within the pool, as shown in Figure 1.1.2.

Table 2.5.1

MODULE DATA FOR NEW BWR RACKS †

Storage cell inside nominal dimension	6.05 in.
Cell pitch	6.243 in.
Storage cell height (above the baseplate)	168 in.
Baseplate hole size (except for lift and pedestal locations)	3.625 in.
Baseplate thickness	0.625 in.
Support pedestal height	5.5 in. +/- 0.5 in.
Support pedestal type	Remotely adjustable pedestals
Number of support pedestals per rack	4
Number of cell walls containing 0.75" diameter flow holes at base of cell wall	At Least Two Cell Walls
Remote lifting and handling provisions	Yes
Poison material	Metamic
Poison length	152 in.
Poison width	4.75 in.

† All dimensions indicate nominal values unless noted.

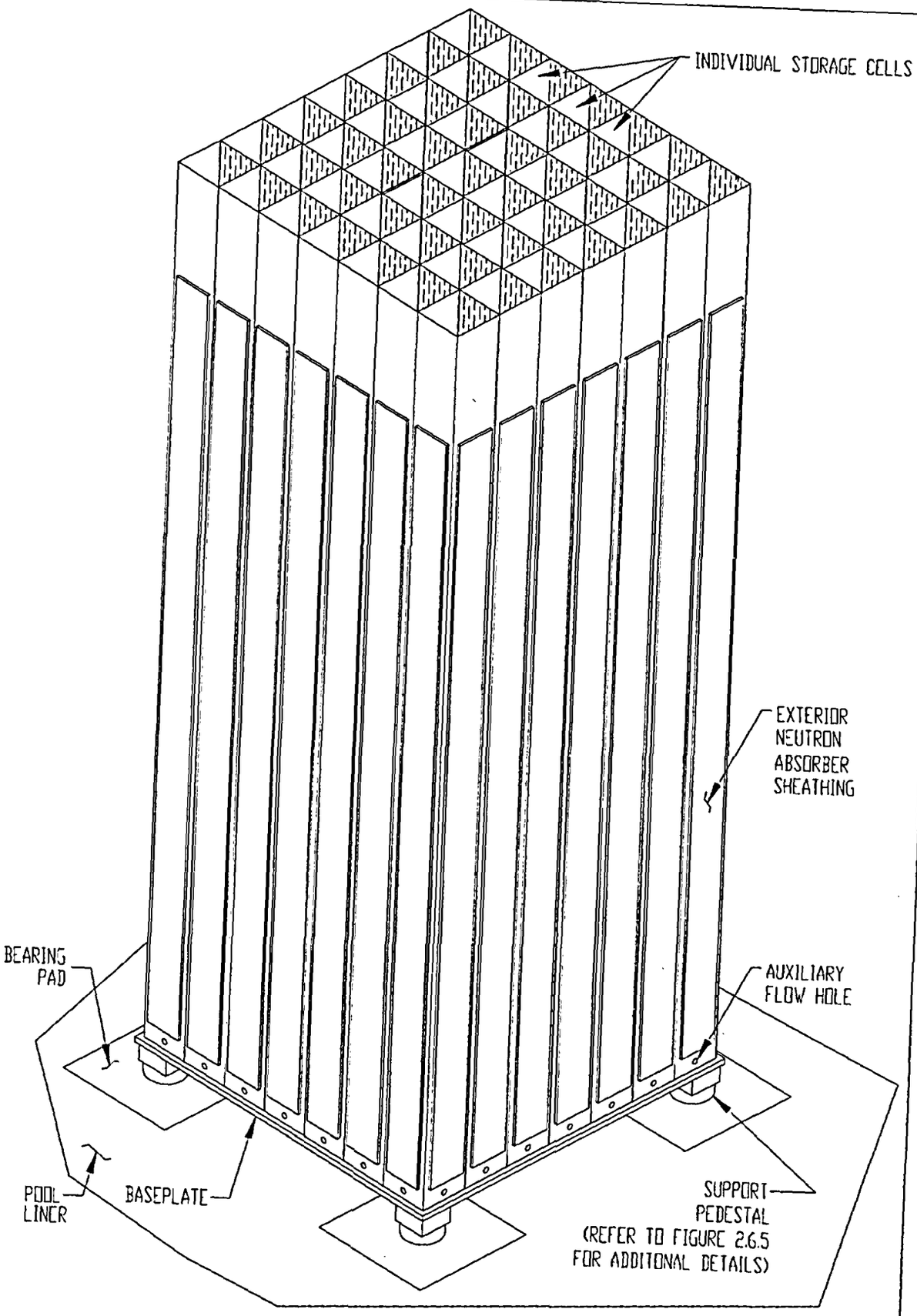

FIGURE 2.1.1; PICTORIAL VIEW OF A TYPICAL BWR RACK MODULE

NOTE: THE NUMBER OF CELLS SHOWN IS NOT INTENDED TO DEPICT ACTUAL RACK SIZES

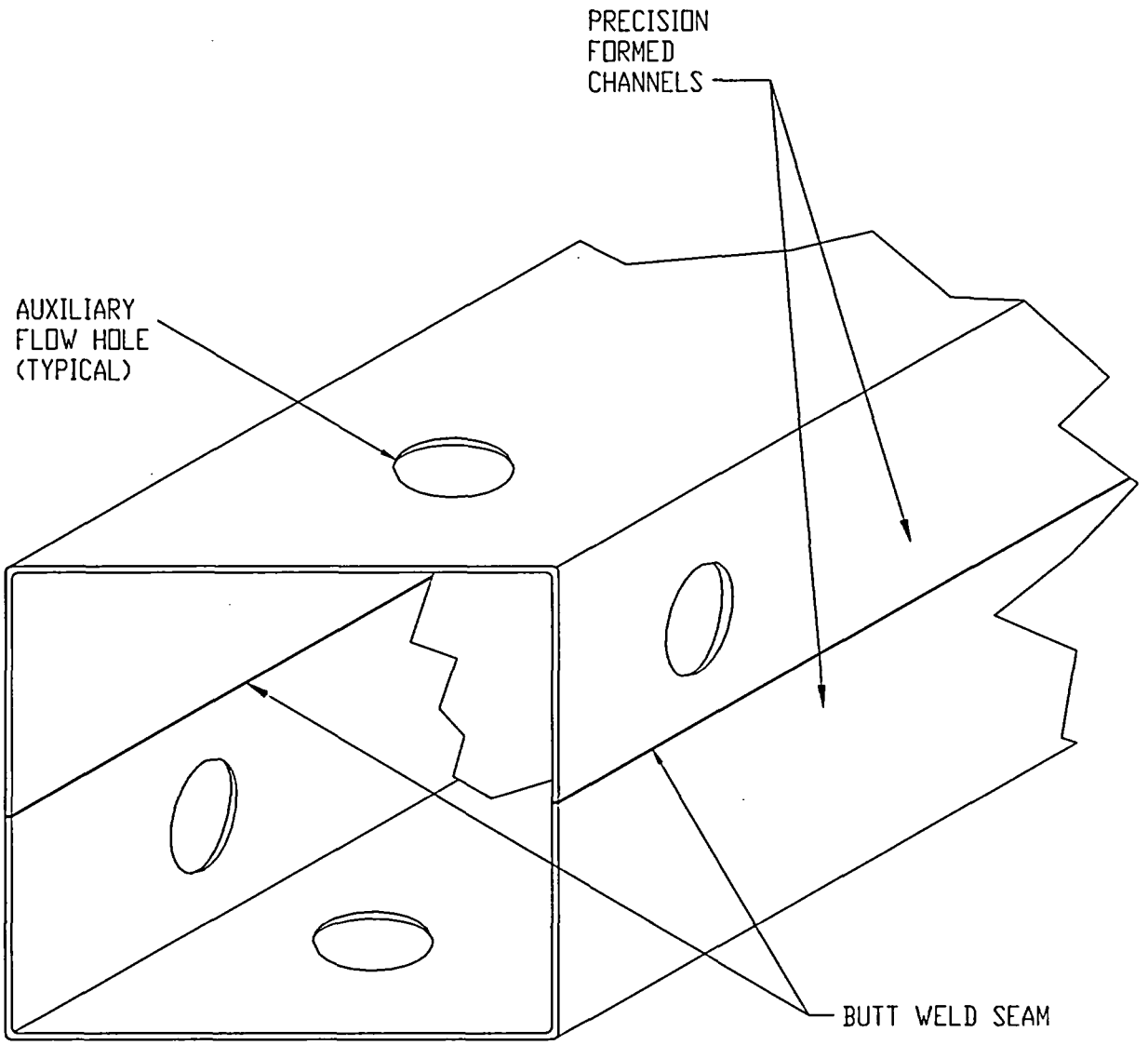

FIGURE 2.6.1; FABRICATED SQUARE CROSS-SECTION CELL BOX

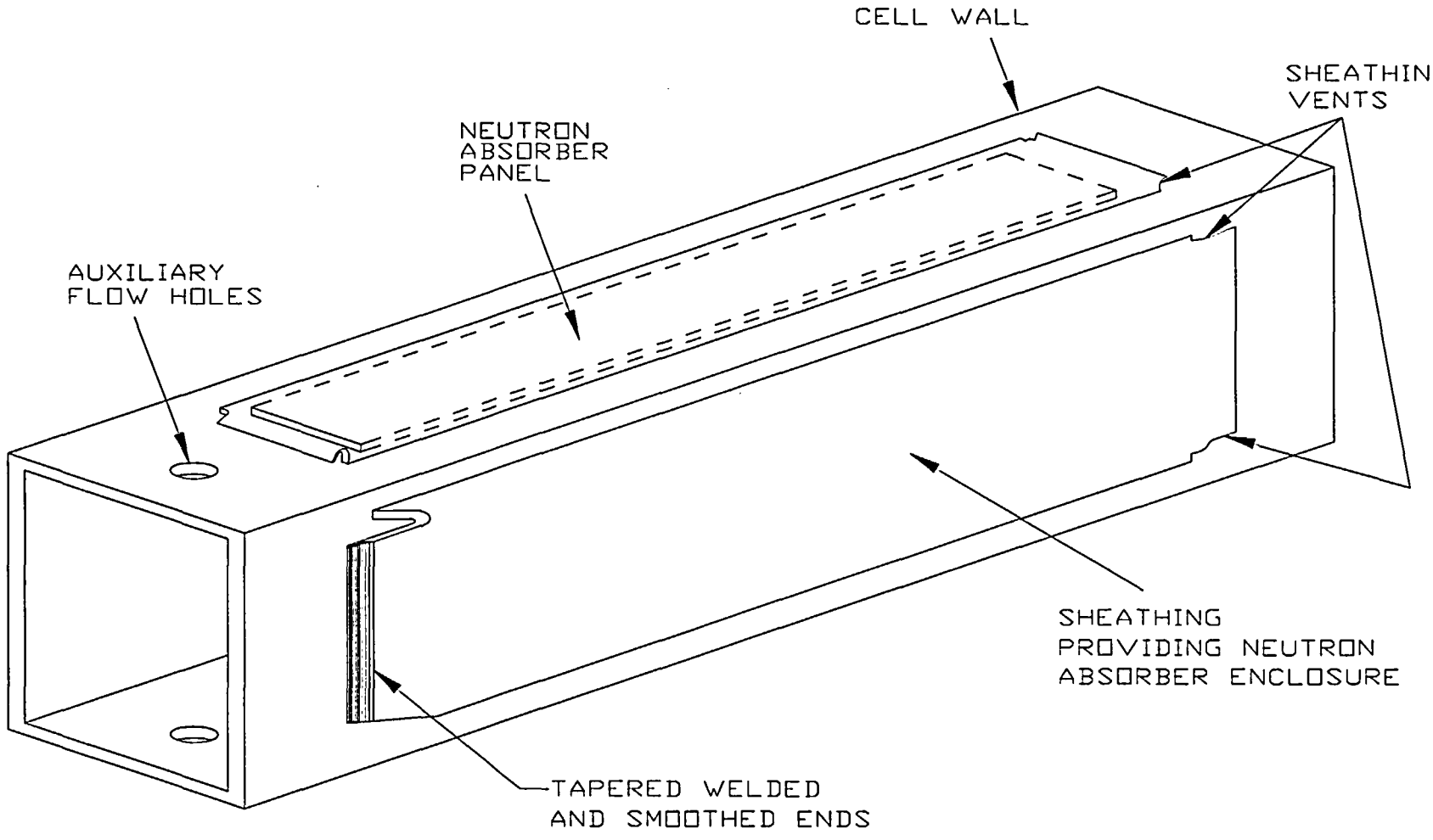

FIGURE 2.6.2; COMPOSITE BOX ASSEMBLY

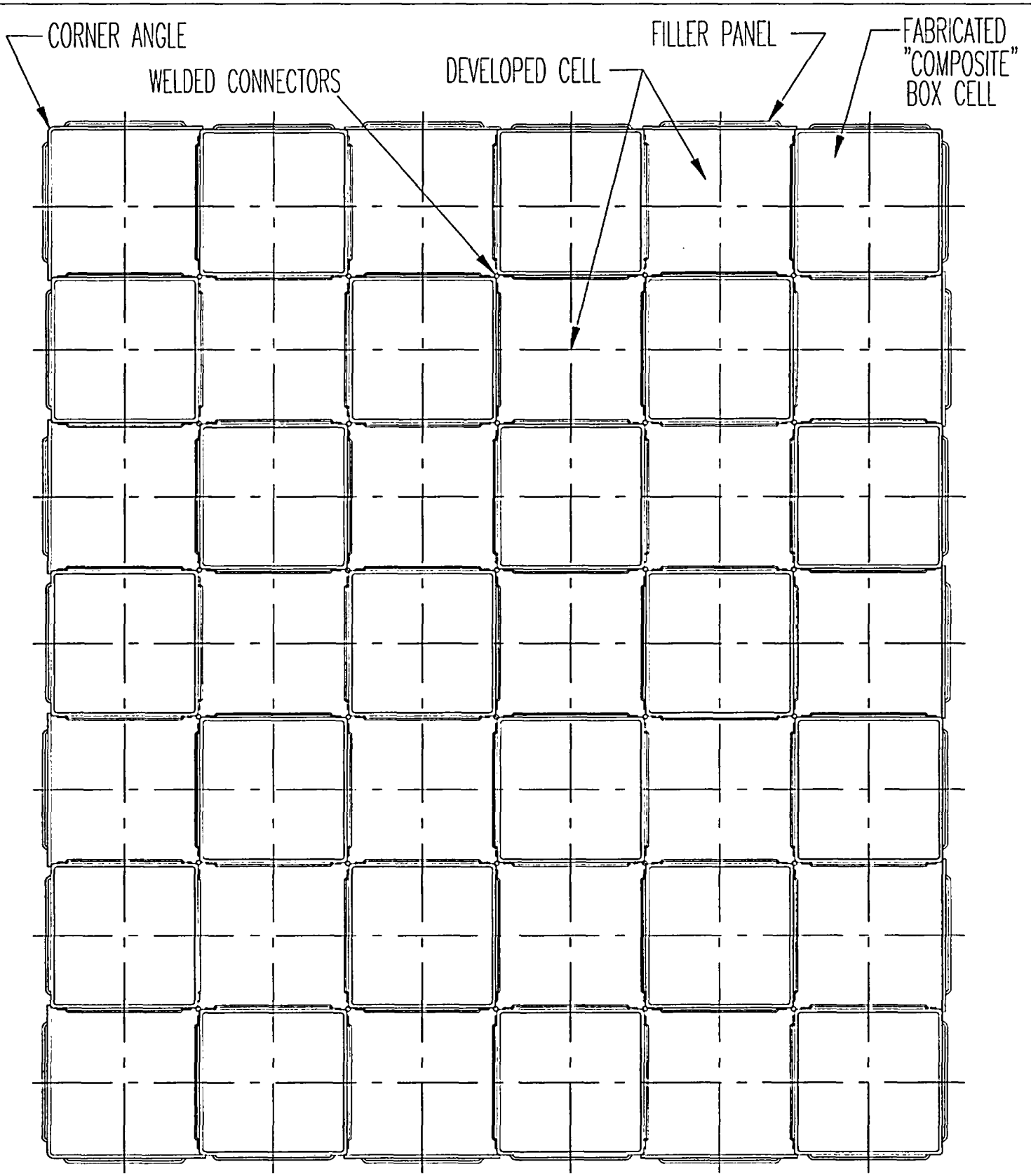

FIGURE 2.6.3; TYPICAL ARRAY OF STORAGE CELLS

NOTE: THE NUMBER OF CELLS SHOWN IS NOT INTENDED TO DEPICT ACTUAL RACK CELLS

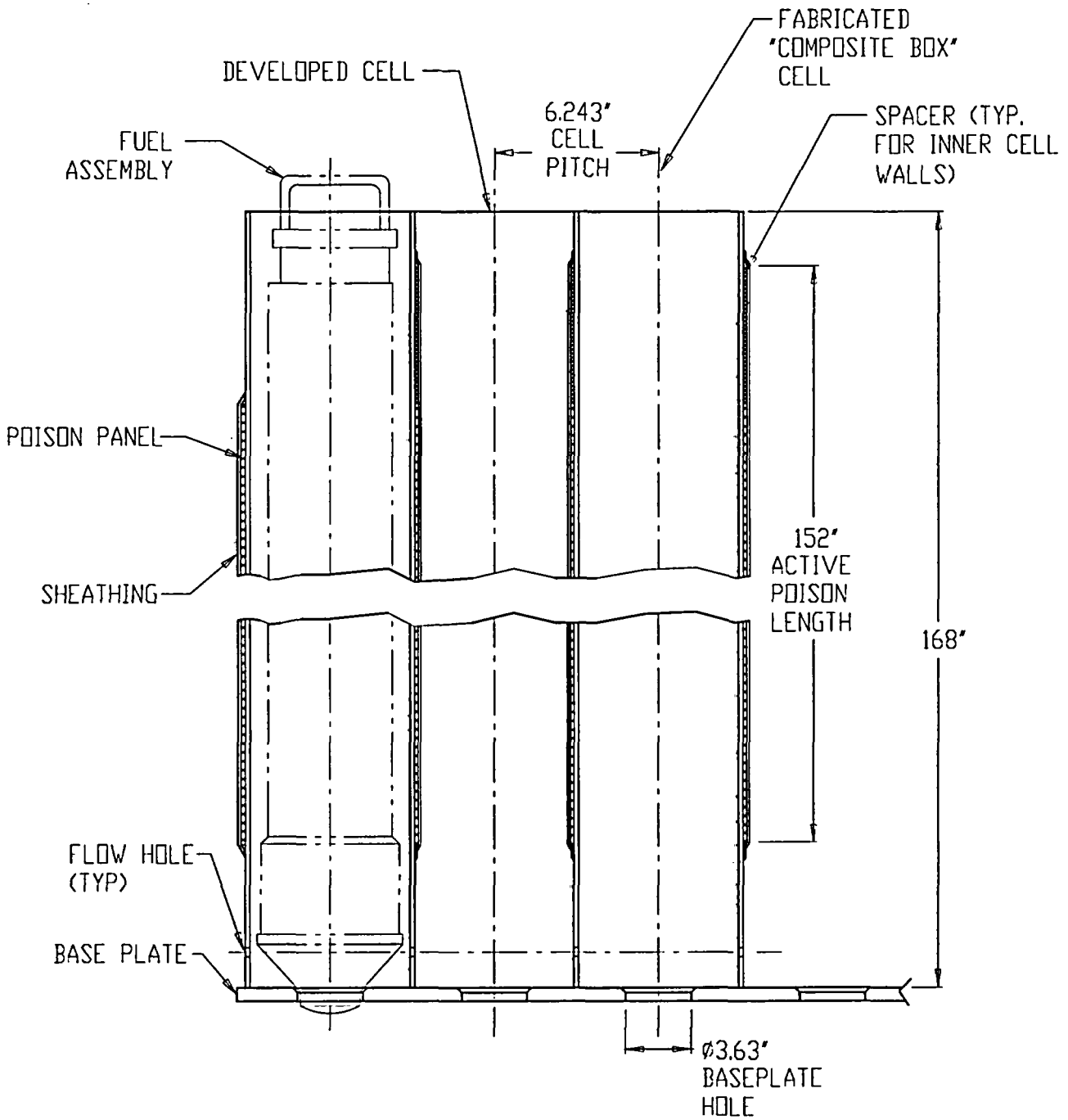

FIGURE 2.6.4: ELEVATION VIEW OF A TYPICAL BWR STORAGE RACK MODULE

NOTE: FUEL ASSEMBLY IS NOT INTENDED TO DEPICT ACTUAL CONFIGURATION

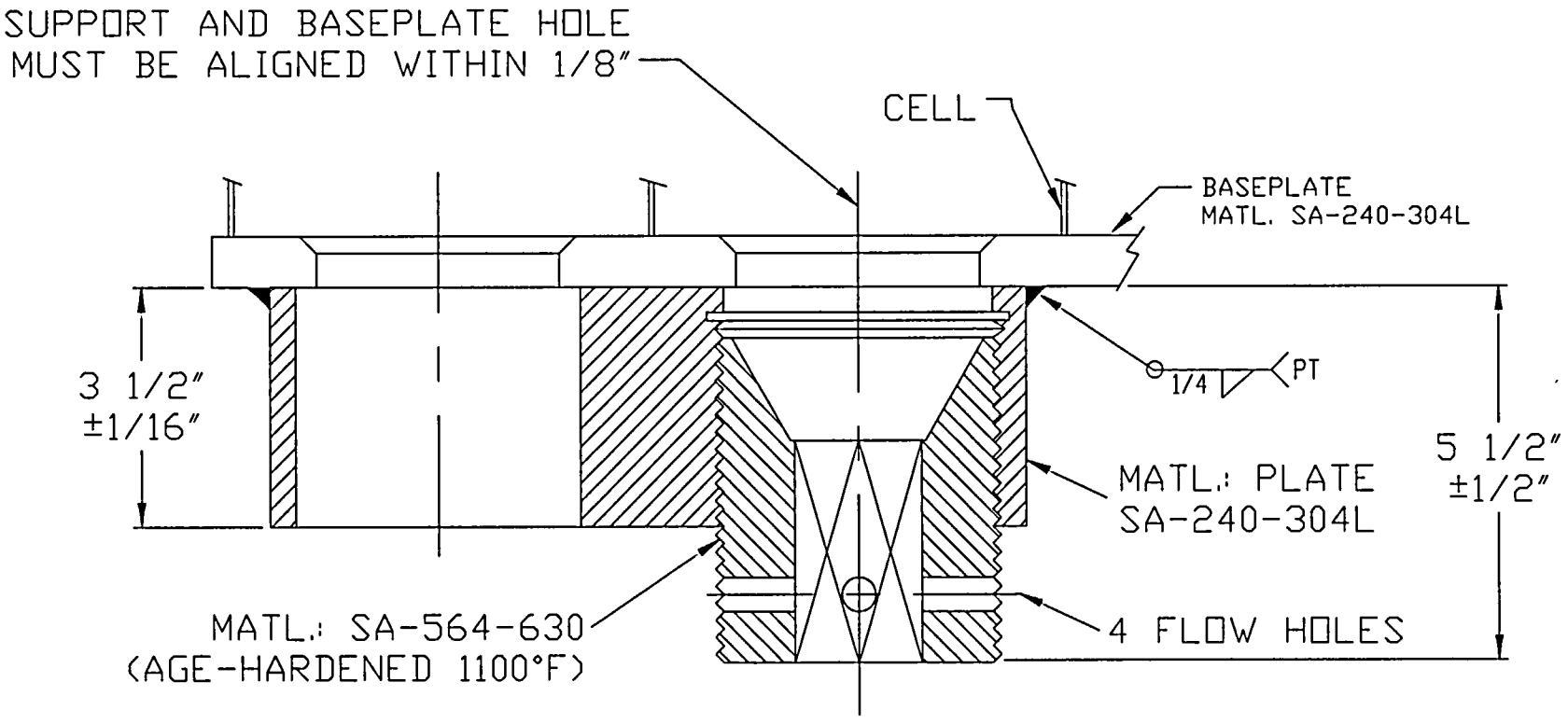

FIGURE 2.6.5; SUPPORT PEDESTALS FOR BWR RACKS

3.0 MATERIAL AND HEAVY LOAD CONSIDERATIONS

3.1 Introduction

A primary consideration in the design of the racks proposed in this amendment request is that the materials introduced in the pool water be of proven durability and compatible with the pool water environment. This section provides a synopsis of the considerations that provide the assurance that the rack structural materials and the neutron absorber panels will perform their intended function for the design life of the fuel racks.

3.2 Structural Materials

The following structural materials will be utilized in the fabrication of the Clinton fuel racks:

a. ASTM A240-304L for all sheet metal stock and baseplate

b. Internally threaded support legs: ASTM A240-304L

c. Externally threaded support spindle: ASTM A564-630 precipitation hardened stainless steel (heat treated to 1100°F)

d. Weld material – austenitic stainless steel

3.3 Neutron Absorbing Material

3.3.1 Metamic™ Neutron Absorber Panels

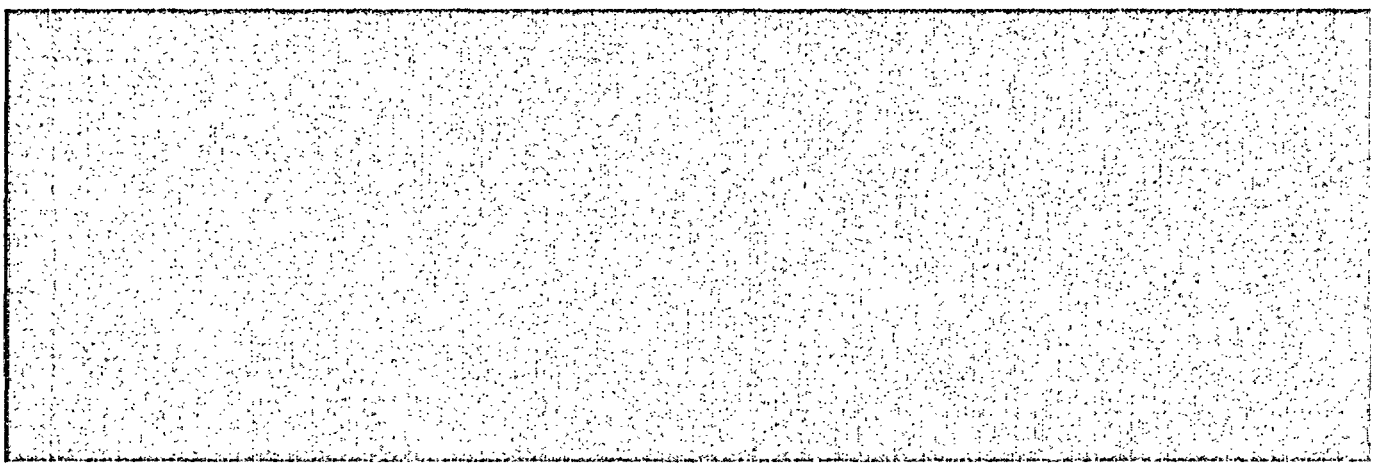

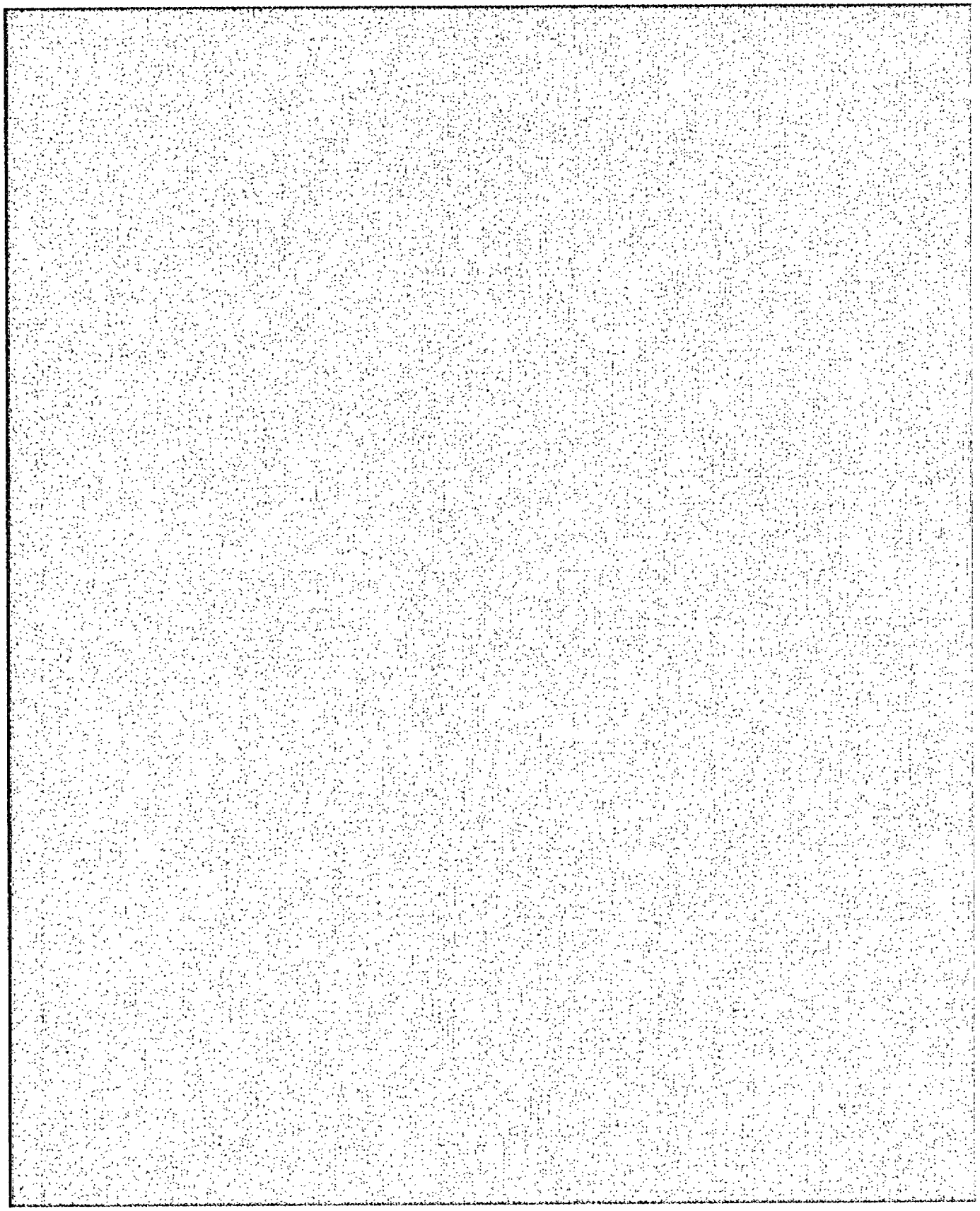

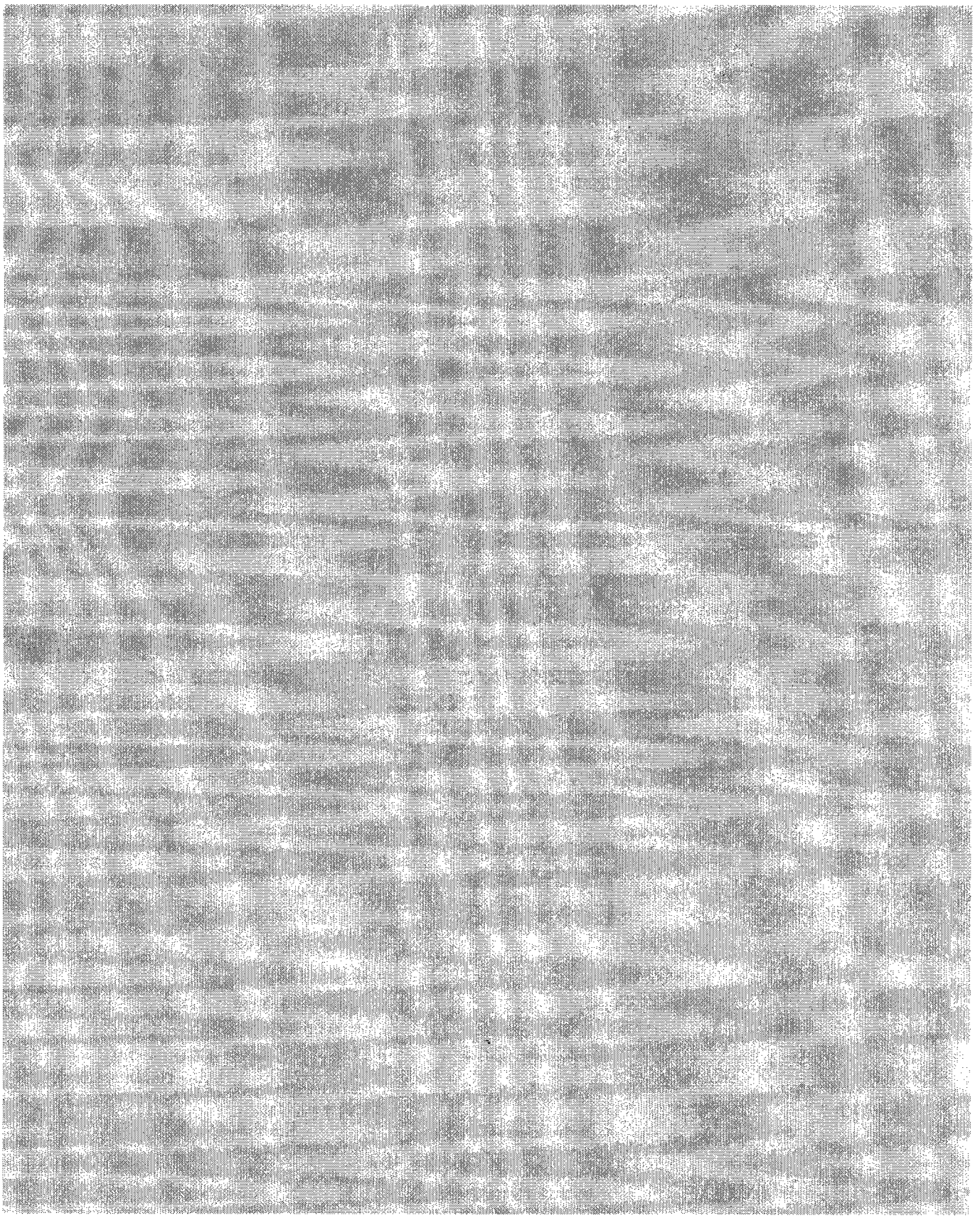

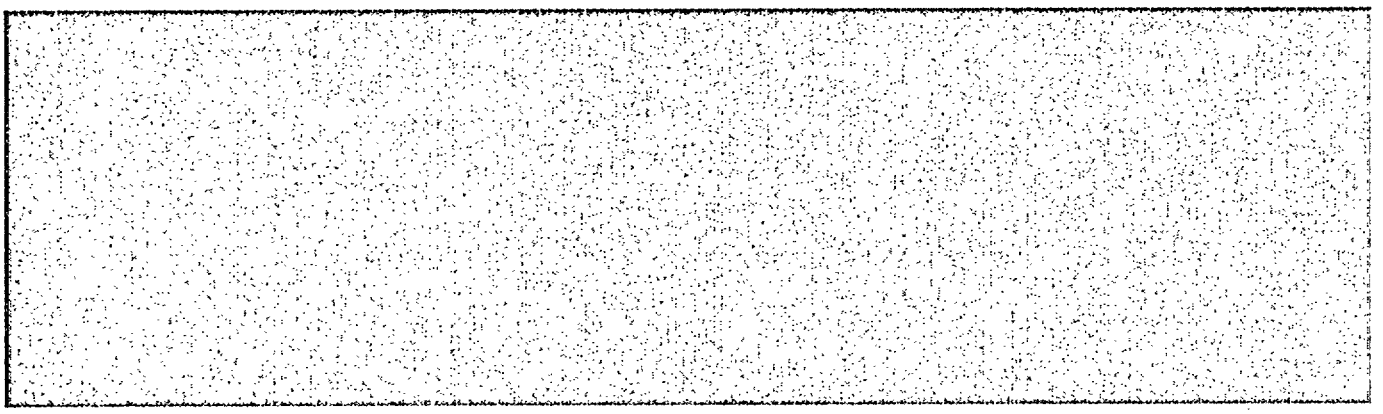

3.4 Compatibility with Environment

All materials used in the construction of the Holtec racks have been determined to be compatible with the Clinton Power Station Spent Fuel Pool and Fuel Cask Storage Pool, and have an established history of in-pool usage. Austenitic stainless steel (304L) is a widely used stainless alloy in nuclear power plants and has a proven in-service performance as the liner material for many fuel pools in the U.S. and abroad. Both of the constituent materials used in the neutron absorber, namely boron carbide and aluminum, are chemically compatible and ideally suited for long-term use in the radiation, thermal and chemical environment of a spent fuel pool.

3.5 Heavy Load Considerations for the Proposed Rack Installations

The Fuel Building Crane will be used for installing the new racks and removing the existing racks. The Fuel Building Crane is designed as Seismic Category I equipment. The capacity of the main hoist is 125 tons. However, the hoist has been derated to a single failure capacity equivalent to 62 tons to comply with NUREG 0612. The Fuel Building Crane is designed for spent fuel cask handling operations. More specifically, it is used to place casks within the Fuel Cask Storage Pool for removal of spent fuel from the plant. Cask drop accidents have been evaluated previously, as discussed within the plant USAR [3.5.1]. The cask drop evaluations will remain valid and will not be compromised by placement of racks

within the Fuel Cask Storage Pool. All fuel will be removed from the Fuel Cask Storage Pool racks before placement of any cask in this vicinity.

The Fuel Building Crane will also be used to lift new and existing racks between the truck bay and the operating deck to enable rack access and egress from the building. However, physical travel limits of the Fuel Building Crane preclude use of the main hook over the east end of the spent fuel pool. Therefore, the Fuel Building Crane cannot be used to install and remove all of the racks within the Spent Fuel Pool during Phase 2 of the project. To overcome this constraint, a low profile temporary crane will be required to install and remove the racks along the east wall. The Fuel Building Crane will be used to lower racks into the pool and place racks within the range of accessibility and to remove racks from the SFP. The temporary crane will be used to lift racks from the pool floor and move the racks horizontally with a limited lift height above the pool floor. The Fuel Building Crane will be used to assemble the temporary crane on the operating deck.

The temporary low profile crane will have a sufficient rated lifting capacity to lift each of the new and old racks, including any additional lifting hardware (i.e., rack lift rig, hoist block, and rigging).

Safe handling of heavy loads by the Fuel Building Crane and temporary crane will be ensured by following the defense in depth approach guidelines of NUREG 0612:

- Defined safe load paths in accordance with approved procedures
- Supervision of heavy load lifts by designated individuals
- Crane operator training and qualification that satisfies the requirements of ANSI/ASME B30.2-1976 [3.5.2]
- Use of lifting devices (slings) that are selected, inspected and maintained in accordance with ANSI B30.9-1971 [3.5.3]
- Inspection, testing and maintenance of cranes in accordance with ANSI/ASME B30.2-1976
- Ensuring the designs of the Fuel Building Crane and the temporary crane meet the requirements of CMAA-70 [3.5.4] and ANSI/ASME B30.2-1976

- Reliability of special lifting devices by application of design safety margins, and periodic inspection and examinations using approved procedures

The salient features of the lifting devices and associated procedures are described as follows:

a. Safe Load Paths and Procedures

Safe load paths will be defined for moving the new rack into the Fuel Building. The racks will be lifted by the main hook of the Fuel Building Crane and enter the Fuel Building operating deck through the opening designed for ingress and egress of spent fuel casks. The rack will enter the building at a location adjacent to the area of placement and will not be carried over any portions of the existing storage racks containing active fuel assemblies. A staging area will be setup on the operating deck as a laydown area for racks. The staging area location also will not require any heavy load to be lifted over the pools or any safety-related equipment.

All phases of rack installation activities will be conducted in accordance with written procedures, which will be reviewed and approved by the owner.

b. Supervision of Lifts

Procedures used during the installation of the racks require supervision of heavy load lifts by a designated individual who is responsible for ensuring procedural compliance and safe lifting practices. Holtec personnel experienced in similar rack installations will supervise the initial installation of the racks.

c. Crane Operator Training

All crew members involved in the use of the lifting and upending equipment will be given training by Holtec International using a videotape-aided instruction course which has been utilized in previous rack installation operations.

d. Lifting Devices Design and Reliability

The Fuel Building Crane is located at the west end of the Fuel Building, where it can access the opening to the truck bay, adjacent laydown area, Fuel Cask Storage Pool, and the west end of the SFP. Physical limitations prevent movement of the hook to the eastern portion of the SFP. The Crane is single failure proof with sufficient capacity to handle all lifts during the reracking process.

The following table determines the maximum lift weight during the installation of the new racks.

Item	Weight (lbs)
Rack	16,737 (max.)
Lift Rig	1,100
Rigging	500
Total Lift	18,337

It is clear, based on the heaviest rack weight to be lifted, that the heaviest load will be well below the 62 ton rating of the Fuel Building Crane main hoist The temporary hoist to be used to maintain the main hoist hook in a dry condition and lift racks into the pool will be selected to provide an adequate load capacity and comply with NUREG-0612.

Remotely engaging lift rigs, meeting all requirements of NUREG-0612, will be used to lift the rack modules. The rack lift rigs consist of four independently loaded traction rods in a lift configuration. The individual lift rods have a safety factor of greater than 10. If one of the rods break, the load will still be supported by at least two rods, which will have a safety factor of more than 5 against ultimate strength. Therefore, the lift rigs comply with the duality feature called for in Section 5.1.6 (3) of NUREG 0612.

The lift rigs have the following attributes:

- The traction rod is designed to prevent loss of its engagement with the rig in the locked position. Moreover, the locked configuration can be directly verified from above the pool water without the aid of an underwater camera.

- The stress analysis of the rig is carried out and the primary stress limits postulated in ANSI N14.6 [3.5.5] are met.

- The rigs are load tested with 300% of the maximum weight to be lifted. The test weight is maintained in the air for 10 minutes. All critical weld joints are liquid penetrant examined to establish the soundness of all critical joints.

e. Crane Maintenance

The Fuel Building Crane is maintained functional per the Clinton Power Station preventive maintenance procedures.

The proposed heavy load lifts will comply with the guidelines of NUREG-0612, which calls for measures to "provide an adequate defense-in-depth for handling of heavy loads near spent fuel...". The NUREG-0612 guidelines cite four major causes of load handling accidents, namely

i. operator errors
ii. rigging failure
iii. lack of adequate inspection
iv. inadequate procedures

The rack installation ensures maximum emphasis on mitigating the potential load drop accidents by implementing measures to eliminate shortcomings in all aspects of the operation including the four aforementioned areas. A summary of the measures specifically planned to deal with the major causes is provided below.

Operator errors: As mentioned above, comprehensive training will be provided to the installation crew. All training shall be in compliance with ANSI B30.2.

Rigging failure: The lifting device designed for handling and installing the new racks has redundancies in the lift legs and lift eyes such that there are four independent load members in the new rack lift rig. Failure of any one load bearing member would not lead to uncontrolled lowering of the load. The rig complies with all provisions of ANSI N14.6-1993, including compliance with the primary stress criteria, load testing at 300% of maximum lift load, and dye examination of critical welds.

The rig designs are similar to the rigs used in the initial racking or the rerack of numerous other plants, such as Hope Creek, Millstone Unit 1, Indian Point Unit Two, Ulchin II, Laguna Verde, J.A. FitzPatrick, and Three Mile Island Unit 1.

Lack of adequate inspection: The designer of the racks has developed a set of inspection points that have been proven to eliminate any incidence of rework or erroneous installation in numerous prior rerack projects. Surveys and measurements are performed on the storage racks prior to and subsequent to placement into the pool to ensure that the as-built dimensions and installed locations are acceptable. Measurements of the pool and floor elevations are also performed to determine actual pool configuration and to allow height adjustments of the pedestals prior to rack installation. These inspections minimize rack manipulation during placement into the pool. Preoperational crane testing will verify proper function of crane interlocks prior to rack movement.

Inadequate procedures: Procedures will be developed to address operations pertaining to the rack installation effort, including, but not limited to, mobilization, rack handling, upending, lifting, installation, verticality, alignment, dummy gage testing, site safety, and ALARA compliance. The procedures will be the successors of the procedures successfully implemented in previous projects.

Table 3.5.1 provides a synopsis of the requirements delineated in NUREG-0612, and its intended compliance.

3.6 References

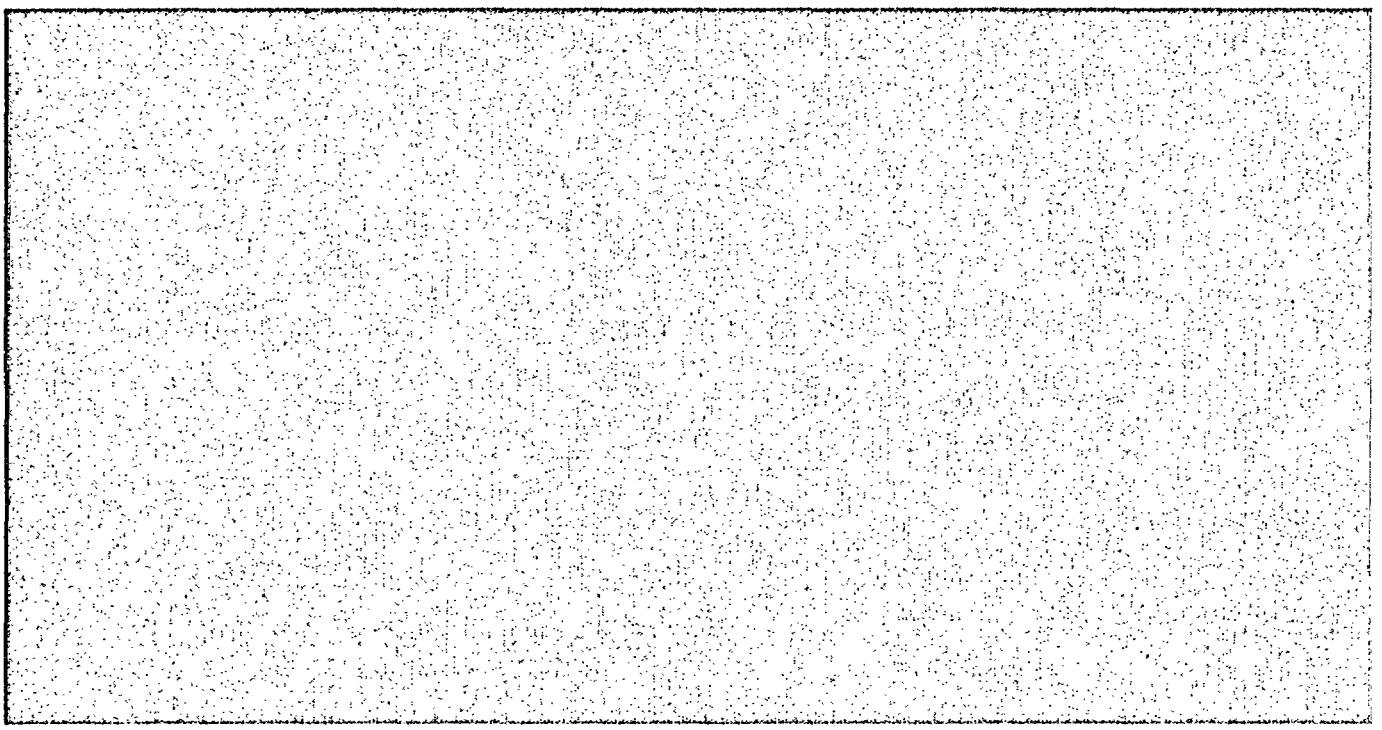

[3.3.7] "Safety Evaluation by the Office of Nuclear Reactor Regulation Related to Holtec International Report HI-2022871 Regarding Use of Metamic in Fuel Pool Applications," Facility Operating License Nos. DPR-51 and NPF-6, Entergy Operations, Inc., Docket No. 50-313 and 50-368, USNRC, June 2003.

[3.3.8] USNRC Docket No. 72-1004, NRC's Safety Evaluation Report on NUHOMS 61BT (2002).

[3.3.9] "METAMIC 6061 + 40% boron Carbide Metal Matrix Composite Test Program for NAC International, Inc.", California Consolidated Technology, Inc. (2001).

[3.3.10] "METAMIC" Qualification Program for Nuclear Fuel Storage Applications, Final Test Results", Report NET 152-03, Prepared for Reynolds Metal Company, Inc. by Northeast Technology Corporation.

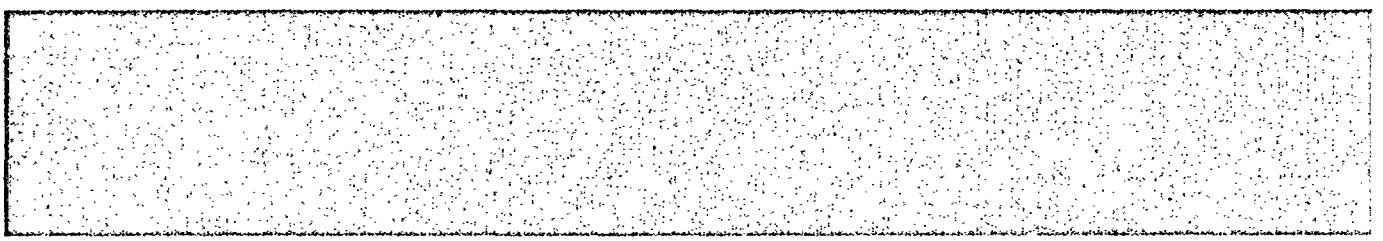

[3.5.1] Clinton Power Station, Updated Safety Analysis Report (USAR), Revision 7.

[3.5.2] ANSI/ASME B30.2, "Overhead and Gantry Cranes, (Top Running Bridge, Single or Multiple Girder, Top Running Trolley Hoist)," American Society of Mechanical Engineers, 1976.

[3.5.3] ANSI B30.9, "Safety Standards for Slings," 1971.

[3.5.4] CMMA Specification 70, "Electrical Overhead Traveling Cranes," Crane Manufacturers Association of America, Inc., 2000.

[3.5.5] ANSI N14.6-1993, Standard for Special Lifting Devices for Shipping Containers Weighing 10000 Pounds or more for Nuclear Materials," American National Standard Institute, Inc., 1978.

[3.5.6] ANSI/ASME B30.20, "Below-the-Hook Lifting Devices," American Society of Mechanical Engineers, 1993.

Table 3.5.1

HEAVY LOAD HANDLING COMPLIANCE MATRIX (NUREG-0612)

	Criterion	Compliance
1.	Are safe load paths defined for the movement of heavy loads to minimize the potential of impact, if dropped, on irradiated fuel?	Yes
2.	Will procedures be developed to cover: identification of required equipment, inspection and acceptance criteria required before movement of load, steps and proper sequence for handling the load, defining the safe load paths, and special precautions?	Yes
3.	Will crane operators be trained and qualified?	Yes
4.	Will special lifting devices meet the guidelines of ANSI 14.6-1993?	Yes
5.	Will non-custom lifting devices be installed and used in accordance with ANSI B30.20 [3.5.6], latest edition?	Yes
6.	Will the cranes be inspected and tested prior to use in rack installation?	Yes
7.	Does the crane meet the requirements of ANSI B30.2-1976 and CMMA-70?	Yes

4.0 CRITICALITY SAFETY EVALUATION

4.1 INTRODUCTION

4.1.1 Purpose

The purpose of the present study is to document the analyses supporting the criticality safety of the Holtec spent fuel storage racks in the Clinton Station. The Holtec high-density spent fuel storage racks for the Clinton Nuclear Power Station are designed to assure that the neutron multiplication factor (k_{eff}) is equal to or less than 0.95 with the racks fully loaded with fuel of the highest anticipated reactivity and the pool flooded with (clean) unborated water at a temperature corresponding to the highest reactivity. The maximum calculated reactivity includes a margin for uncertainty in reactivity calculations and in mechanical tolerances, statistically combined, giving assurance that the true k_{eff} will be less than 0.95 with a 95% probability at a 95% confidence level. Reactivity effects of abnormal and accident conditions are also evaluated to assure that under credible abnormal or accident conditions, the reactivity will be maintained less than 0.95.

The rack design philosophy has been described in a paper by Cummings and Turner [4.1.1]. In this philosophy, the racks are designed to assure a k_{eff} less than 0.95 for fuel of a specified k_∞ in the standard cold core geometry* (SCCG) for a given fuel assembly average enrichment and configuration, without consideration of the gadolinia burnable poison normally used in BWR reactors. The specified assembly configuration, average enrichment and maximum k_∞ (SCCG) define a discharge fuel burnup above which any fuel assembly can be safely stored in the racks. Once the rack design is completed for the specified design basis, credit may be taken for the gadolinia in the assembly and a minimum Gd_2O_3 loading and number of fuel rods with Gd_2O_3 defined that will protect against the storage of any fuel assembly with burnup less than the design basis limit. There is also a limiting enrichment below which any fuel assembly may be safely stored without consideration of the burnup or Gd_2O_3 loading.

- The k_∞ in the standard cold core geometry is defined as the infinite multiplication factor (k_∞) in a 6-inch core lattice at 20°C without void or control rods.

The rack design and criticality analyses utilize Metamic as the neutron absorber material.

The fuel used as the design basis for the racks is a GE-14 (10x10) assembly with an (uniform) initial enrichment of 4.8 % U-235. All fuel assembly types to be stored in the high-density racks were explicitly analyzed to confirm their acceptability for storage.

Applicable codes, standards, and regulations, or pertinent sections thereof, include the following:

- *Code of Federal Regulations*, Title 10, Part 50, Appendix A, General Design Criterion 62, "Prevention of Criticality in Fuel Storage and Handling".
- USNRC Standard Review Plan, NUREG-0800, Section 9.1.2, Spent Fuel Storage.
- USNRC letter of April 14, 1978 to all Power Reactor Licensees - OT Position for Review and Acceptance of Spent Fuel Storage and Handling Applications, including modification letter dated January 18, 1979.
- USNRC Regulatory Guide 1.13, Spent Fuel Storage Facility Design Basis, Rev. 2 (proposed), December 1981.
- ANSI-8.17-1984, Criticality Safety Criteria for the Handling, Storage and Transportation of LWR Fuel Outside Reactors.
- L. Kopp, "Guidance On The Regulatory Requirements For Criticality Analysis Of Fuel Storage At Light-Water Reactor Power Plants", USNRC Internal Memorandum, L. Kopp to Timothy Collins, August 19, 1998.

4.1.2 Design Criteria and Assumptions

To assure the true reactivity will always be less than the calculated reactivity, the following conservative design criteria and assumptions were made.

- The racks are assumed to contain the most reactive fuel authorized to be stored in the facility without any control rods or uncontained burnable poison.
- Moderator is pure, unborated water at a temperature (4°C) within the design basis range corresponding to the highest reactivity.
- Criticality safety analyses are based upon an infinite radial array of storage cells. No credit is taken for radial neutron leakage, except in the assessment of certain abnormal/accident conditions where neutron leakage is inherent. A finite axial length of the design basis fuel assembly is used, with an effectively infinite (30 cm) water reflector top and bottom.*
- Neutron absorption in minor structural members is neglected, i.e., spacer grids are replaced by water.
- An average void content (40 %) in the reactor core was assumed in the depletion calculation.
- No credit is taken for axial blankets of natural or depleted UO_2.
- The neutron absorber material, Metamic, is an alloy of aluminum encapsulating boron-carbide.

* The 30 cm axial reflectors effectively bounds any water and stainless steel (and fittings) that would exist.

4.2 SUMMARY AND CONCLUSIONS

The fuel assembly used as the design basis for the racks is a standard GE 10x10 array (GE-14) of BWR fuel rods containing UO_2 clad in Zircaloy, and assumes uniform initial enrichments of 4.8 wt% U-235. Explicit analyses of all other fuel assembly types (see Table 4-1) were performed to confirm their acceptability for storage in the high-density racks. The effects of calculational and manufacturing tolerances were evaluated and added in determining the maximum k_{eff} in the storage rack.

In BWR fuel, there are a wide variety of designs, including enrichment distribution and gadolinia loading, which often vary in the axial direction. Three different criteria, which bound fuel acceptable for safe storage, are defined as follows.

1. Any fuel with an average enrichment less than or equal to 3.3% U-235, independent of burnup or the gadolinia normally used in BWR fuel, may be safely stored with assurance that the maximum reactivity in the storage rack will be less than the regulatory limit.

2. For fuel assemblies with an average initial enrichment above 3.3% and up to 4.8%, a minimum discharge burnup of 12 MWD/KgU is acceptable. Any fuel equal to or greater than 12 MWD/KgU may be safely stored with assurance that the maximum reactivity in the storage rack will be less than the regulatory limit.

3. A maximum nominal enrichment of 4.8 wt% U-235, with a maximum planar k_{inf} in the standard cold core geometry (SCCG) of 1.33, where the SCCG is defined as the multiplication factor (k_∞) for an infinite array of fuel assemblies on a 6-inch lattice spacing, at 20 °C without voids or control rods. A minimum of 3.0 wt% Gd_2O_3 in at least 6 fuel rods is required to assure a k_∞ (SCCG) less than 1.33 or to assure the criticality safety in storage of fuel with less than 12 MWD/KgU burnup.

Any one of the three criteria is sufficient to determine the acceptability of fuel for safe storage in the spent fuel racks. Based on these criteria, all of the fuel assemblies currently at the Clinton Station are acceptable for storage in the spent fuel racks with assurance that the maximum k_{eff} is below the regulatory limit.

For conservatism, these criteria should be applied to the axial (planar) region of highest reactivity. Each planar region should be separately evaluated to assure that the planar region of highest reactivity is assessed. If fuel vendor calculations are used to determine the k_∞ (SCCG) of the spent fuel, it is suggested that the vendor value be increased by 0.01 Δk to compensate for any difference in vendor calculations and those reported herein.

The basic calculations supporting the criticality safety of the Clinton Station fuel storage racks are summarized in Table 4-2 and Table 4-3.

Abnormal and accident conditions were also evaluated. None of the abnormal or accident conditions that have been identified as credible will result in exceeding the limiting reactivity (k_{eff} of 0.95). The effects on reactivity of credible abnormal and accident conditions are summarized in Table 4-4. The double contingency principle of ANSI N16.1-1975 (and in the principal USNRC guidelines) specifies that it shall require at least two unlikely independent and concurrent events to produce a criticality accident. This principle precludes consideration of the simultaneous occurrence of multiple accident conditions. Other hypothetical events were considered and no credible occurrences or configurations have been identified that might have any adverse effect on the storage rack criticality safety.

4.3 INPUT PARAMETERS

4.3.1 Fuel Assembly Specifications

The design basis fuel assembly is a standard GE-14 assembly with a 10x10 array of BWR fuel rods containing UO_2 clad in Zircaloy (see Table 4-1). The GE-14 fuel exhibits the highest reactivity compared to all other types of fuel design used at the Clinton Power Station.

The other designs evaluated (see Table 4-1), are listed below:

A GE-6 design 8x8 assembly with 62 fuel rods and 2 water rods,
A GE-7 design 8x8 assembly with 62 fuel rods and 2 water rods,
A GE-8 design 8x8 assembly with 62 fuel rods and 2 water rods,
A GE-10 design 8x8 assembly with 60 fuel rods and 1 large water rod.

4.3.2 Storage Rack Cell Specifications

The high-density storage rack cells consist of an egg-crate structure, as is illustrated in Figure 4-1, with fixed neutron absorber material positioned between the fuel assembly storage cells in a [redacted]-inch channel. The neutron absorber material is Metamic, with an areal density of [redacted] [redacted] areal density. This arrangement provides a nominal center-to-center lattice spacing of 6.243 [redacted] inches. Manufacturing tolerances used in evaluating uncertainties in reactivity are indicated in Table 4-5. The 0.075-in. stainless-steel box that defines the fuel assembly storage cell has a nominal inside dimension of 6.05 in. This allows adequate clearance for inserting/removing the fuel assemblies, with or without the Zircaloy flow channel. The neutron absorber panels are 152 inches long, 4.75 inches wide, and [redacted] inches thick. Neutron absorber panels are not needed or used on the exterior walls of modules facing non-fueled regions, i.e., the pool walls where there is insufficient room to mis-load a fuel assembly. Similarly, neutron absorber panels are used on only one exterior surface of the modules that face each other across the small water gap between the modules.

4.4 ANALYTICAL METHODOLOGY

4.4.1 Computer Codes and Benchmarking

In the fuel rack evaluation, criticality analyses of the high-density spent fuel storage racks were performed with the MCNP4a code [4.4.1] (a continuous energy Monte Carlo code developed by the Los Alamos National Laboratory). Independent calculations were made with the CASMO4 code [4.4.2], a two-dimensional multi-group transport theory code.

Benchmark calculations are presented in Appendix 4A and indicate a bias of 0.0009 ± 0.0011 for MCNP4a evaluated at the 95% probability, 95% confidence level [4.4.3][4.4.4]. These benchmark calculations have previously been reviewed and accepted by the USNRC in numerous licensing applications. In the geometric model used in both CASMO4 and MCNP4a calculations, each fuel rod and its cladding were explicitly described and reflecting boundary conditions (zero neutron current) were used at the effective centerline of the neutron absorber and steel plate between storage cells. These boundary conditions have the effect of conservatively creating an infinite array of storage cells in the radial direction. MCNP4a is a 3-dimensional code and the calculations assumed a 30 cm water reflector (effectively infinite) on the top and bottom of the assemblies.

The CASMO4 computer code was used as a means of evaluating small reactivity increments associated with manufacturing tolerances. Depletion calculations were also performed with CASMO4, using the restart option to describe spent fuel in the storage cell.

MCNP4a was used as the primary method of criticality analysis and to assess the reactivity consequences of eccentric fuel positioning and abnormal locations of fuel assemblies.

In the CASMO4a depletion calculations, the assumed fuel and moderator temperatures were 832 K (1038°F) and 560 K (549°F) respectively. A typical average of 40% moderator void is usually assumed in BWR core during depletion calculations. To investigate the sensitivity of the

calculations to void content, an average core void of 45% was also calculated. Results showed an increase in reactivity of 0.0006 Δk, which illustrates the insensitivity to core void.

CASMO4 depletion calculations include three nuclides (Pm-148m and two lumped fission products, 401 and 402) that are not included in the MCNP library. These nuclides amount to 0.0050 Δk at 12 MWD/KgU and are compensated by an equivalent B-10 concentration. A check calculation confirmed the accuracy of this calculational approach.

4.4.2 CASMO4 Validation

The CASMO4 calculations were validated against MCNP4a for the specific fuel assemblies and geometries involved. Comparison calculations are listed in Table 4-6 and Table 4-7. (MCNP4a results are bias corrected and listed at the 95%/95% level)*. These data confirm the CASMO4 calculations, and show that MCNP4a calculations tend to be more conservative than the corresponding CASMO4 calculations.

4.4.3 Calculation of the k_∞ in the SCCG

The k_∞ in the SCCG was calculated (CASMO4) as a function of fuel burnup, evaluated in the storage rack reference design at 4.8 % initial enrichment. Results are shown in Figure 4-2. At the design basis limit of a k_∞ in the SCCG of 1.33, the limiting reactivity in the storage rack at 4°C is 0.9267 (CASMO4) or 0.9285±0.0012 (MCNP4a, uncertainties not included). This is the fundamental design basis of the storage rack. The uncertainties are evaluated separately and the maximum rack k_{eff} is shown in Table 4-3.

Figure 4-4 shows a similar correlation for all of the fuel types considered (calculated without gadolinia) and confirms that the GE-14 assembly type at 4.8% enrichment bounds all other fuel types considered at a k_{inf} (SCCG) of 1.33. The values shown in Figure 4-4 were also evaluated at

* K-factor for one-sided tolerance at 95%/ 95% from NBS Handbook 91 [4] is 1.70.

4.8% enrichment although, in practice, the other assemblies would usually have a significantly lower enrichment.

4.4.4 Gadolinia Effects and Burnup

Once the storage rack design is completed (based on the k_∞ (SCCG)) and the minimum burnup is determined, credit for gadolinia is taken to assure that the design basis reactivity is not exceeded at burnups below the design limit (12 MWD/KgU). Gadolinia (Gd_2O_3) is used in almost all BWR fuel designs as a means of augmenting reactivity control in core operations. Gadolinium has a higher cross-section than U-235 and the reactivity of an assembly generally increases with burnup, reaching a maximum at some point in burnup where the gadolinium is virtually depleted. For fuel of 4.8% average enrichment, Figure 4-3 illustrates the reactivity variation with burnup for several illustrative gadolinia loadings with GE-14 fuel of 4.8% enrichment, evaluated in the spent fuel storage rack. Also shown in Figure 4-3 is the reference calculation without any Gd_2O_3, which define the design basis burnup.

From the data shown in Figure 4-3, it is concluded that all of the cases considered are bounded by the reference design basis burnup curve calculated without any gadolinia. The limiting (minimum) design burnup is 12 MWD/KgU and credit for the gadolinia actually present is taken with fuel of less than 12 MWD/KgU burnup to assure that the regulatory limit on the maximum k_{eff} (0.95) is not exceeded.

4.4.5 Gadolinia Rod Locations

A number of alternative locations of the gadolinia rods were calculated to evaluate the potential effect of rod locations. As part of this investigation, corresponding calculations were made with MCNP4a at zero burnup to compensate for any discrepancy that might exist in the CASMO4 estimates of self-shielding in the strongly absorbing gadolinia-bearing fuel rods. Results of these analyses are shown in Table 4-7 and indicate that the MCNP4a calculations are slightly more conservative (higher reactivity) than the corresponding CASMO4 calculations although the difference is not large. The calculations that are most important are the calculations with 6

gadolinia rods per assembly since 8 Gd_2O_3 rods in an assembly are well below the reference reactivity. A larger number of Gd_2O_3 rods or higher loading of Gd_2O_3 would be even more conservative.

In general, the MCNP4a calculations tend to be slightly more conservative than the corresponding CASMO4 calculations at zero burnup. The design basis MCNP4a calculation gave a calculated k_{eff} of 0.9285 ± 0.0012 (see Table 4-6). For 2 of the cases in Table 4-7, the MCNP4a calculated k_{eff} is higher than that of the reference design. These two cases are the 3.0% and 3.5% Gd_2O_3 loadings (cases 9 and 10 in Table 4-7) where the Gd_2O_3 rods are in close proximity to each other. These two cases suggest the possibility of a small bias in the calculations where Gd_2O_3 rods are close in proximity and mutually shield each other. Cases 9 and10 represent the largest difference between the MCNP4a calculations at zero burnup and the design basis reactivity, amounting to a bias of +0.0030Δk at 3% Gd_2O_3 and 0.0007Δk at 3.5% Gd_2O_3. Although the bias values would apply only to 3.0% and 3.5% Gd_2O_3 in a unique arrangement, for conservatism, the largest bias (+0.0030) is included in the evaluation of the maximum rack reactivity in Table 4-3.

With this correction bias, the data in Table 4-3 and Table 4-7 indicates that for the GE14 fuel at 4.8 % enrichment, a minimum Gd_2O_3 loading of 3 % in 6 rods is required to protect against the possible loading of fuel with less than 12 MWD/KgU burnup.

4.5 CRITICALITY ANALYSES AND TOLERANCE VARIATIONS

4.5.1 Nominal Design Case

4.5.1.1 Enrichment Limit Criterion

One criterion for acceptable storage is an enrichment of 3.3 % (or less), which would not require any credit for gadolinia or burnup. Results of calculations with 3.3% enrichment are summarized in Table 4-2 and confirm that the maximum reactivity is below the regulatory limit. The criterion of an enrichment of 3.3% is therefore acceptable, without any consideration of the Gadolinia normally present in the fuel, or the discharge fuel burnup.

4.5.1.2 Maximum k_{inf} in the Standard Cold Core Geometry

It is conventional practice for the fuel vendor, in developing a specific assembly design, to provide values for k_{inf} in the SCCG for each planar (axial) region of significantly different composition or arrangements. These k_{inf} values are usually provided at 0% void (core inlet), 40% void (core average), and 70% void (exit condition). The 40% core average is the most meaningful since the 0% and 70% void cases would apply only to the ends of the assemblies (small volume and high neutron leakage).

The initial design Gd_2O_3 loading enters into the fuel vendor's calculations of the burnup at which the peak reactivity occurs. At this burnup, the gadolinium is essentially depleted. Consequently, calculations of the reactivity in the storage rack do not need to include gadolinium, but only the average enrichment, burnup and fuel design. Calculations are provided illustrating this fact and correlating the reactivity in the storage rack to the k_{inf} in the SCCG. Figure 4-2 illustrates the variation in reactivity of the storage rack with values of the k_{inf} in the SCCG. The acceptance criterion for safe storage of spent fuel is that the k_{inf} in the SCCG must be equal to or less than 1.33 for the planar region of highest reactivity. Thus, the k_{eff} values in the storage rack are determined by the limiting k_{inf} in the SCCG (1.33).

The design basis fuel assembly is the GE-14. For each of the fuel assembly types considered (listed in Table 4-1), the k_{inf} in the rack for a k_{inf} in the SCCG were calculated and the results are summarized in Figure 4-4. These data confirm that all other fuel assembly types are less reactive and therefore bounded by the GE-14 fuel type, and at an enrichment of 4.8 %. In fact, the other fuel types have average enrichment significantly less than 4.8 % and would therefore exhibit even lower reactivity.

The maximum k_{eff} value, including calculational and manufacturing uncertainties, is listed in Table 4-3. These calculations confirm that, for fuel of 4.8% enrichment or less, the criteria of a maximum k_{inf} of 1.33 in the SCCG will assure compliance with the regulatory guidelines (k_{eff} limit of 0.95).

4.5.1.3 Criteria for Minimum Gadolinia Loading

Gadolinia (Gd_2O_3) is normally used in BWR fuel to augment reactivity control during in-core operation. A very wide variety of Gd_2O_3 loadings are commonly used – often differing in axial (planar) regions. Furthermore, the Gd_2O_3 loadings for fuel of 4.8% average enrichment have not yet been developed. However, it is possible to define criteria for the minimum Gd_2O_3 loadings required to assure that the highest reactivity over burnup is always less than the regulatory limit.

Results of the analysis of a series of cases with various Gd_2O_3 loadings were described earlier (Section 4.4.4 and 4.4.5) and summarized in Figure 4-3, for fuel of 4.8 % initial average enrichment. For fuel of 4.8 % enrichment, a burnup of at least 12 MWD/KgU is required and a burnup lower than 12 MWD/KgU will require credit for Gd_2O_3.

Figure 4-3 shows the effect of Gd_2O_3 concentration for 6 and 8 Gd_2O_3 rods per assembly and indicates that a minimum of 6 Gd_2O_3 rods of at least 3% loading is required. The 6-rod case bounds cases of 8 or more Gd_2O_3 rods per assembly. At enrichments less than 4.8%, the peak reactivity will be even lower, and the criteria of 3 % Gd_2O_3 in at least 6 rods will be even more conservative. Thus, the criterion of a minimum Gadolinia loading (including tolerance on Gd_2O_3 content), evaluated at the axial planar region of the highest reactivity, will assure safe storage of

all fuel assemblies and conformance with the NRC guidelines. For fuel of 3.3 % average enrichment (Table 4-2), no Gd_2O_3 or burnup is necessary and any assembly of 3.3 % enrichment or less may be safely stored in the rack. For enrichments less than or equal to 3.3%, the maximum k_{inf} in the rack is less than 0.95 (including uncertainties and allowances) regardless of gadolinia content or the k_{inf} in the SCCG.

4.5.2 Uncertainties Due to Manufacturing Tolerances

4.5.2.1 Rack Manufacturing Tolerances

The GE-14 assembly was used for the evaluation of incremental reactivity changes due to manufacturing tolerances. The reactivity effects associated with manufacturing tolerances are listed in Table 4-5 and discussed below. Values at 12 MWD/KgU burnup (the approximate burnup for a k_{inf} of 1.33 in the SCCG) were used, although the reactivity uncertainties are nearly insensitive to burnup.

4.5.2.2 Boron-10 Loading Variation

The Metamic absorber panels are nominally [ ]-inch thick, with a design B-10 areal density of [ ]. The manufacturing tolerance limit is [ ] in B-10 content, including both thickness ([ ]) and composition ([ ]) tolerances. This assures that the minimum boron-10 areal density will not be less than [ ] in any location or any panel. Differential CASMO4 calculations provide the incremental reactivity uncertainty shown in Table 4-5.

4.5.2.3 Neutron Absorber Width Tolerance Variation

The reference storage cell design uses a neutron absorber panel width of 4.75 inches. The tolerance on the panel width is [redacted], and the reactivity effect is shown in Table 4-5.

4.5.2.4 Lattice Spacing Variation

The design storage cell lattice spacing is 6.243 inches. Decreasing the lattice spacing (by decreasing the box I.D.) increases reactivity. The manufacturing tolerance is [redacted] and the corresponding uncertainties in reactivity are listed in Table 4-5.

4.5.2.5 Stainless Steel Thickness Tolerances

The nominal thickness of the stainless steel box is 0.075 inches with [redacted] for the steel sheath. The maximum positive reactivity effects of the expected stainless steel thickness tolerance were calculated with CASMO4 and are listed in Table 4-5.

4.5.2.6 Zircaloy Flow Channel

Elimination of the Zircaloy flow channel results in a small decrease in reactivity (see listing below).

Description	With Zr Channel	Without Zr Channel
3.3 % Uniform Enrichment	0.9293	0.9263
4.8 % Uniform Enrichment @ 12 MWD/KgU	0.9267	0.9225

4.5.3 Fuel Tolerances (Enrichment and Density Uncertainties)

CASMO4 calculations of the sensitivity to small changes in fuel enrichment and UO_2 density gave uncertainties in reactivity listed below:

Reactivity Effects of Enrichment and Density Tolerances

Case Description	Tolerance	Reactivity effect, Δk
3.3 % Enrichment	+0.05 % in Enrichment	0.0035
3.3 % Enrichment	0.20 increase in Fuel Density	0.0024
4.8 % Enrichment @ 12 MWD/KgU	+0.05 % in Enrichment	0.0028
4.8 % Enrichment @ 12 MWD/KgU	0.20 increase in Fuel Density	0.0021

4.5.4 Uncertainty in Depletion Calculations

Since critical experiment data with spent fuel is not available for determining the uncertainty in depletion calculations; a conservative allowance for uncertainty in reactivity was assigned based upon the Kopp memorandum (reference 5). In the Clinton racks, the reactivity decrement (from fresh to the design basis burnup) in the absence of gadolinium is 0.0854 Δk. It is assumed that the uncertainty in depletion calculations is less than 5% of the total reactivity decrement or an uncertainty ±0.0043Δk.

4.5.5 Existing Fuel Assemblies at the Clinton Station

Fuel assemblies from cycles 1 through 7 are presently in storage at the Clinton Station. All of these assemblies may be safely stored in the fuel racks in accordance with the acceptance criteria established in this report. Examination of the G.E. fuel design reports reveal that fuels from Cycles 1 through 4 has average enrichments less than 3.3%. In Cycles 5 through 7, the number and loading of the gadolinia rods is well above the minimum required and the fuel assemblies are therefore acceptable for storage.

4.6 ABNORMAL AND ACCIDENT CONDITIONS

4.6.1 Temperature and Water Density Effects

The moderator temperature coefficient of reactivity is negative. Using the minimum temperature of 4 °C (maximum possible water density) therefore assures that the true reactivity will always be lower than the calculated value regardless of the temperature. Temperature effects on reactivity have been calculated and the results are shown in Table 4-8. Introducing voids in the water in the storage cells (to simulate boiling) decreased reactivity, as shown in the table. Boiling at the submerged depth of the racks would occur at approximately 120°C. The only significance of these calculations is to confirm that the temperature and void coefficients of reactivity are negative and the reference temperature of 4 °C is conservative.

4.6.2 Abnormal Location of a Fuel Assembly

It is hypothetically possible to suspend a fuel assembly of the highest allowable reactivity outside and adjacent to the fuel rack, although such an accident condition is highly unlikely. The exterior walls of the rack modules facing the outside (where such an accident condition might be conceivable) are regions of high neutron leakage, which more than compensates for the extra fuel assembly. For comparison to the reference k_{eff}, calculations were performed (MCNP4a) for this condition with an extraneous fuel assembly present. The calculations were performed with the GE-14 fuel assembly. Conservatively, no neutron absorber panels were assumed to be present on the exterior rack wall. With the inherent neutron leakage included, the k_{eff} with an extraneous fuel assembly of the maximum reactivity located outside and adjacent to the fuel rack, is less than the reference k_{eff}. Thus it is concluded that the abnormal location of a fuel assembly will have a negligible reactivity effect (see listing below).

Description	Calculated k_{eff} (Bias and Tolerance not included)
Normal Condition – explicit model without extraneous fuel assembly	0.9258
Accident Condition – with extraneous assembly	0.9229

4.6.3 Eccentric Fuel Assembly Positioning

The fuel assembly is normally located in the center of the storage rack cell with bottom fittings and spacers that mechanically restrict lateral movement of the fuel assemblies. Nevertheless, calculations were performed with the fuel assembly moved into the corner of the storage rack cell (four-assembly cluster at closest approach) to investigate the effect on reactivity. Two cases were considered: (1) fuel of 3.3% enrichment and (2) fuel of 4.8% burned to 12 MWD/KgU was used. These (MCNP4a) calculations (see below) resulted in a small negative reactivity effect. Thus, the nominal case, with the fuel assembly positioned in the center of the storage cell, yields the higher reactivity.

Fuel Assembly	Reference k_{inf}	Eccentric k_{inf}
GE-14 @ 3.3 % Enrichment	0.9266	0.9191
GE-14 @ 4.8 % burned to 12 MWD/KgU	0.9258	0.9192

4.6.4 Dropped Fuel Assembly

For a drop on top of the rack, the fuel assembly will come to rest horizontally on top of the rack with a minimum separation distance from the active fuel region of more than 12 inches, which is sufficient to preclude neutron coupling (i.e., an effectively infinite separation). Maximum expected deformation under seismic or accident conditions will not reduce this spacing to less than 12 inches.

It is conceivable that a dropped assembly might penetrate a storage cell in a vertical position, impacting and causing local deformation of the base plate. The maximum expected local deformation is about 2 inches, with smaller deformations in the eight immediately adjacent cells. Conservative calculations, using a bounding deviation of 2.5 inches of exposed fuel in all cells everywhere, showed that the k_{eff} of the rack was increased only slightly and the maximum k_{eff} would remain less than 0.95.

Description	Calculated k_{eff} (bias and uncertainties not added)
Normal Condition	0.9258 ± 0.0002
Accident Condition – with 2.5 inches of exposed fuel	0.9259 ± 0.0002

These values are within the expected statistical variation of MCNP4a calculations and confirm that a dropped fuel assembly will not have an adverse effect on reactivity and the maximum k_{eff} will remain below the regulatory limit.

4.6.5 Fuel Rack Lateral Movement

Neutron absorber panels are installed in the rack wall along one side of the water gap between adjacent racks. With this configuration, the maximum reactivity of the storage rack is not dependent upon the water-gap spacing between modules. Thus, misalignment of the racks or seismically induced movement will not affect the maximum reactivity of the rack.

4.7 REFERENCES

[4.1.1] K. Cummings and S. E. Turner, "Design of Wet Storage racks for Spent BWR Fuel", Proceedings of the Topical Meeting on Practical Implementation of Nuclear Criticality Safety, November 2001, ANS Meeting – Reno, Nevada.

[4.4.1] J.F. Briesmeister, Ed., "MCNP- A General Purpose Monte Carlo N-Particle Transport Code, Version 4A", Los Alamos National Laboratory, LA-12625-M (1993).

[4.4.2] A. Ahlin and M. Edenius, "CASMO - A Fast Transport Theory Depletion Code for LWR Analysis," ANS Transactions, Vol. 26, p. 604, 1977.

M. Edenius, et al., "CASMO4, A Fuel Assembly Burnup Program, Users Manual", Studsvik Report SOA/95/1, Studsvik Report (proprietary).

[4.4.3] M.G. Natrella, Experimental Statistics, National Bureau of Standards, Handbook 91, August 1963.

[4.4.4] L.I. Kopp, "Guidance on the Regulatory Requirements for Criticality Analysis of Fuel Storage at Light Water Reactor Plants", USNRC memorandum, Kopp to Collins, August 1998.

Table 4-1

FUEL ASSEMBLY DESIGN SPECIFICATIONS USED IN THE ANALYSES

FUEL ROD DATA	GE-6	GE-7	GE-8	GE-10	GE-14
Cladding outside diameter, in.					
Cladding inside diameter, in.					
Cladding material					
Pellet diameter, in.					
Enrichment (design basis)					
UO_2 density (stack), g/cc UO_2					
WATER ROD DATA					
Number of water rods					
Inside diameter, inch					
Outside diameter					
Material					
FUEL ASSEMBLY DATA					
Fuel rod array					
Number of fuel rods					
Fuel rod pitch, inch					
Fuel channel, material					
Inside dimension, inch					
Channel Thickness, inch					

The Shaded Areas are Proprietary to GE Company

Table 4-2

SUMMARY OF CRITICALITY SAFETY ANALYSES
FOR FUEL OF 3.3 % ENRICHMENT W/OUT Gd_2O_3 OR BURNUP

Reference Fuel Type	GE-14
Temperature assumed for analysis	20 °C
Fuel Enrichment (average)	3.3%
Gd_2O_3 loading %	N/A
MCNP4a Calculated k_{eff}	0.9266
Calculational bias, Δk	0.0009
Temperature Correction to 4 °C, Δk	0.0025
Allowance for Gd_2O_3 rod location	N/A
Reference k_{eff}	0.9300
Uncertainties	
Removal of flow channel	negative
Eccentric assembly location	negative
Uncertainty in bias	±0.0011
Tolerances (Table 4-5)	± 0.0073
Uncertainty in Depletion calculations	N/A
MCNP Statistics	± 0.0007
Total Uncertainties	± 0.0074
Maximum Reactivity	0.9374
Regulatory Limit	0.95

Table 4-3

SUMMARY OF CRITICALITY SAFETY ANALYSES AT DESIGN BASIS ENRICHMENT AND BURNUP

Reference Fuel Type	GE-14
Temperature assumed for analysis	20°C
Initial Fuel Enrichment (average)	4.8
Maximum k_{inf} in SCCG	1.33
Design basis Burnup, MWD/KgU	12
Calculated k_{eff}	0.9258
Calculated bias	0.0009
Temperature correction to 4 °C	0.0018
Allowance for Gd_2O_3 rod location	0.0030
Reference k_{eff}	0.9315
UNCERTAINTIES	
Removal of flow channel	negative
Eccentric assembly location	negligible
Uncertainty in bias	±0.0011
Tolerances (Table 4-5)	± 0.0069
Uncertainty in Depletion calculations	± 0.0043
MCNP Statistics	± 0.0003
Total Uncertainty	±0.0082
MAXIMUM REACTIVITY	0.9397 **
Regulatory Limit	0.95

** For an average core void of 45%, the maximum k_{eff} would increase to 0.9403.

Table 4-4

REACTIVITY EFFECTS OF ABNORMAL AND ACCIDENT CONDITIONS

Accident/Abnormal Condition	Reactivity Effect
Temperature increase	Negative (Table 4-8)
Void (boiling)	Negative (Table 4-8)
Assembly dropped on top of rack	Negligible
Misplacement of a fuel assembly	Negligible
Seismic Movement	Negligible

Table 4-5

REACTIVITY UNCERTAINTIES DUE TO
MANUFACTURING TOLERANCES

Quantity	Nominal Value	Tolerance	Reactivity Effects of Manufacturing Tolerances @ 3.3 % E @ 0 MWD/KgU	Reactivity Effects of Manufacturing Tolerances 4.8 % E @ 12 MWD/KgU
CASMO Case Number				
B-10 Loading - Metamic	[redacted]	[redacted]	±0.0046	±0.0045
Metamic Width	4.75 inches		± 0.0025	±0.0024
Lattice spacing (Box I.D.)	6.243 inches		±0.0024	±0.0028
SS thickness	0.075 [redacted]	±10%	±0.0008	±0.0008
Fuel enrichment	[redacted]	[redacted]	±0.0035	±0.0028
Fuel density			±0.0024	±0.0021
Statistical combination of tolerance uncertainties			±0.0073	±0.0069

Table 4-6 COMPARISON OF CASMO4 AND MCNP4a CALCULATIONS

Case Description	MCNP4a		CASMO4
	Calculated	Corrected	
1.) Uniform 3.3 % Enrichment, no Gadolinia	0.9292	0.9326±0.0012 (1)	0.9293
2.) 4.8 % E Fuel at 12 MWD/KgU, no Gadolinia	0.9260	0.9287±0.0012 (2),(3)	0.9267

(1) With bias (0.0009) and temperature correction (0.0025Δk) to 4°C.
(2) With bias (0.0009) and temperature correction (0.0018Δk) to 4°C.
(3) 0.9285 ± 0.0012 with axial leakage (Design Basis)

Table 4-7 Reactivity Effects of Gd_2O_3 Rod Locations

	MCNP4a (1)	CASMO4
Case Description	**k_∞**	**k_∞**
Nominal GE Locations		
1) 6 GD Rods of 3% Gd_2O_3	0.9235±0.0013	0.9230
2) 6 GD Rods of 3.5% Gd_2O_3	0.9211±0.0013	0.9211
3) 6 GD Rods of 4% Gd_2O_3	0.9199±0.0013	0.9194
4) 8 GD Rods of 3% Gd_2O_3	0.8917±0.0013	0.8958
5) 8 GD Rods of 3.5% Gd_2O_3	0.8887±0.0013	0.8933
6) 8 GD Rods of 4% Gd_2O_3	0.8865±0.0013	0.8911
Alternate Configurations		
7) 6 GD Rods of 3.5% Gd_2O_3	0.9247±0.0013	0.9234
8) 6 GD Rods of 3.5% Gd_2O_3	0.9263±0.0013	0.9249
9) 6 GD Rods of 3.5% Gd_2O_3	0.9292±0.0013	0.9283
10) 8 GD Rods of 3.5% Gd_2O_3	0.9315±0.0013	0.9300

(1) With bias (0.0009) and temperature correction (0.0018Δk) to 4°C

Table 4-8

EFFECT OF TEMPERATURE AND VOID ON CALCULATED REACTIVITY OF THE STORAGE RACK

Case	Incremental Reactivity Change, Δk	
	GE-14 @ 3.3 % E, 0 Burnup	GE-14 4.8 %E @ 12 MWD/KgU
4°C (39°F)	Reference	Reference
20° (68°F)	-0.0025	-0.0018
40°C (122°F)	-0.0062	-0.0047
80°C (176°F)	-0.0146	-0.0116
100°C (212°F)	-0.0196	-0.0157
120°C (248°F)	-0.0249	-0.0200
120°C + 20% void	-0.0450	-0.0405

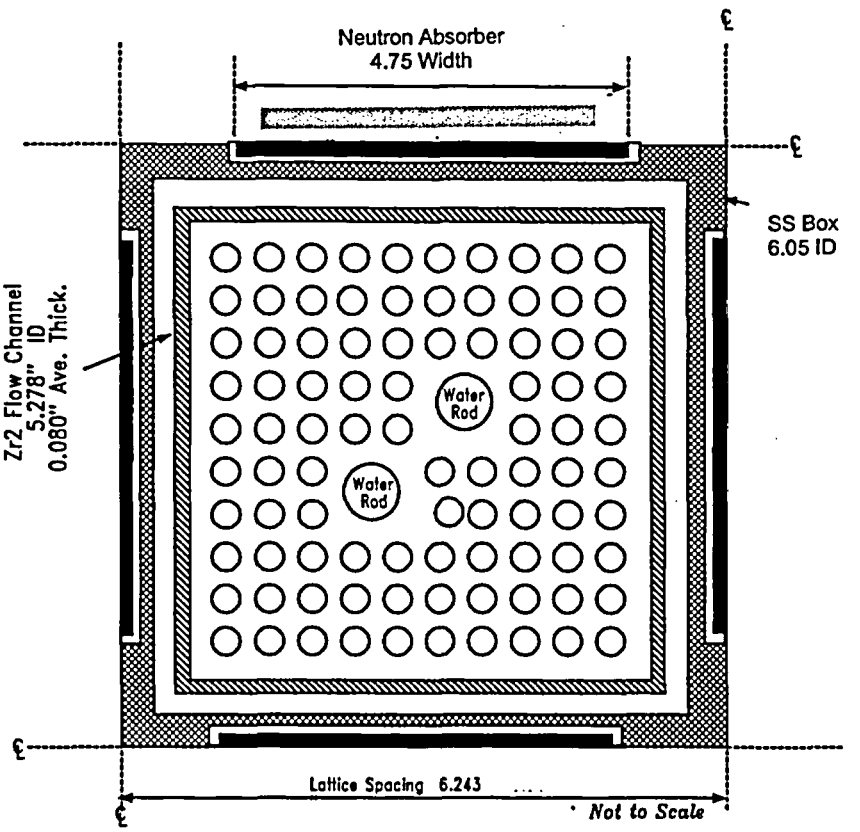

(GE-14 Assembly Illustrated)

Figure 4-1 Storage Cell Calculational Model

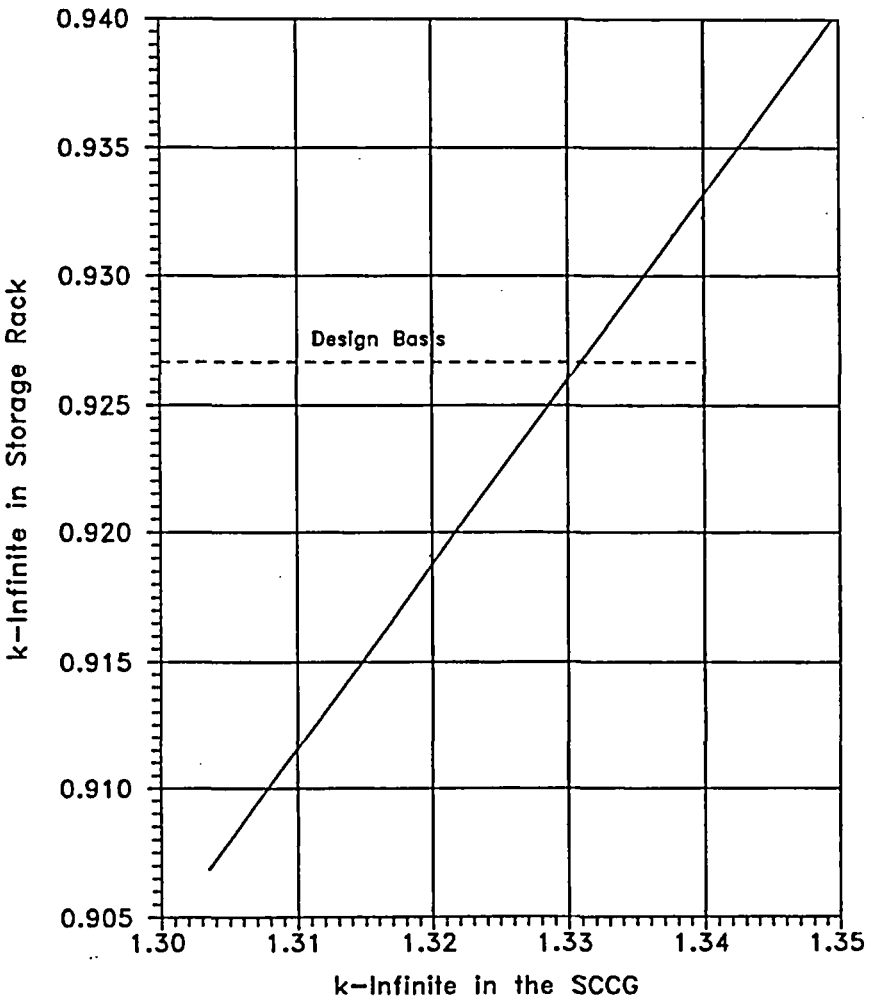

Fig. 4-2 Correlation Between k-Infinite in the SCCG and k-Infinite in the Storage Rack

(Note: Bias and Uncertainties not Included)

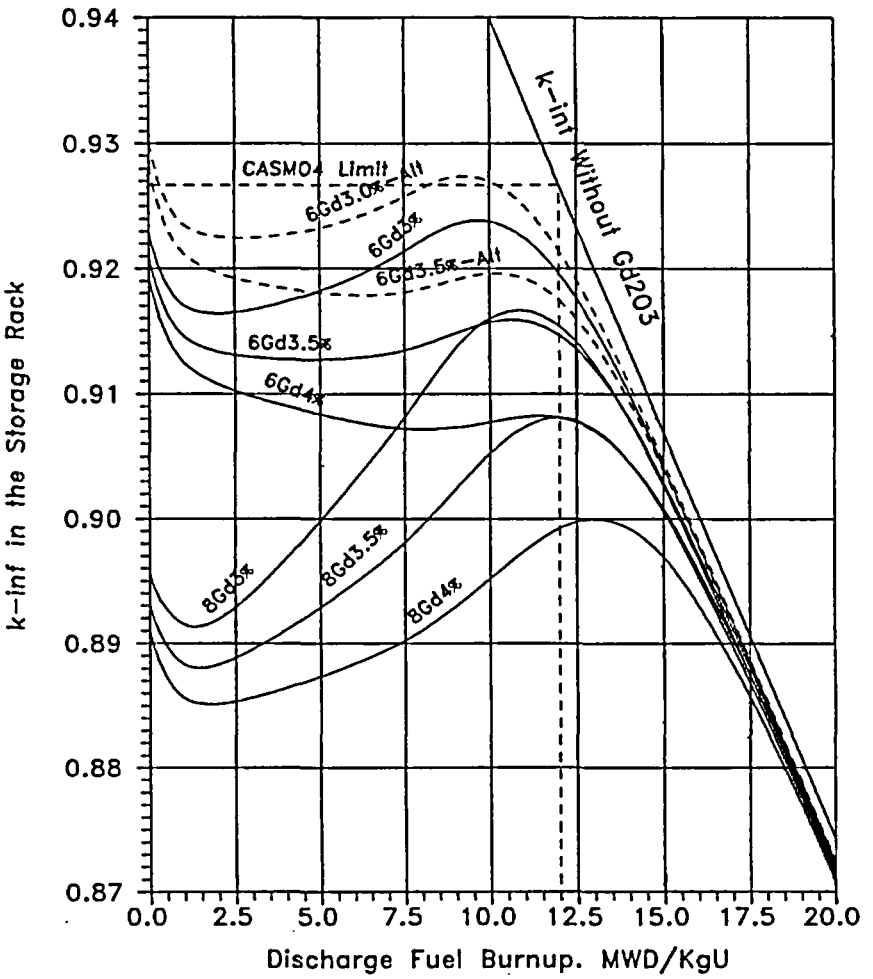

Fig. 4–3 Variation in Rack Reactivity with Burnup for 4.8% Fuel with Gd_2O_3

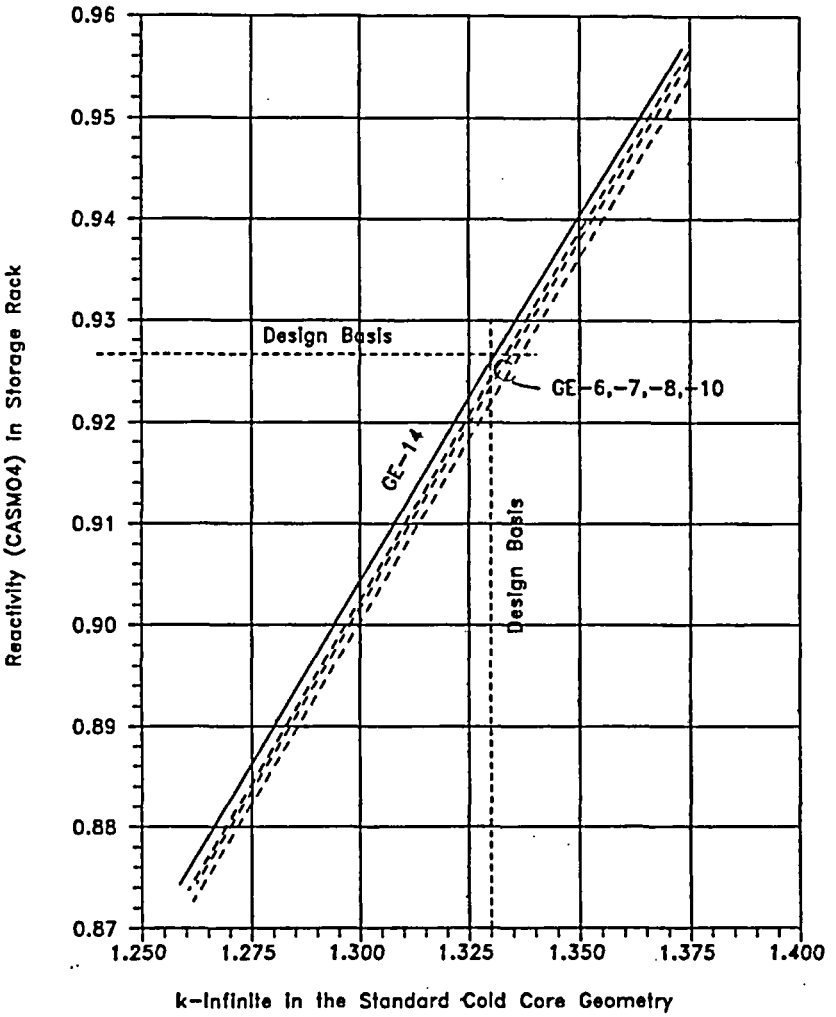

Fig. 4-4 Correlation of Reactivity in Rack and k-infinite in the SCCG for Fuel of Various Designs

APPENDIX 4A: BENCHMARK CALCULATIONS

(Total of 26 Pages Including This Page)

Note: This appendix was taken from a different report.
Hence, the next page is labeled "Appendix 4A, Page 1".

APPENDIX 4A: BENCHMARK CALCULATIONS

4A.1 INTRODUCTION AND SUMMARY

Benchmark calculations have been made on selected critical experiments, chosen, in so far as possible, to bound the range of variables in the rack designs. Two independent methods of analysis were used, differing in cross section libraries and in the treatment of the cross sections. MCNP4a [4A.1] is a continuous energy Monte Carlo code and KENO5a [4A.2] uses group-dependent cross sections. For the KENO5a analyses reported here, the 238-group library was chosen, processed through the NITAWL-II [4A.2] program to create a working library and to account for resonance self-shielding in uranium-238 (Nordheim integral treatment). The 238 group library was chosen to avoid or minimize the errors† (trends) that have been reported (e.g., [4A.3 through 4A.5]) for calculations with collapsed cross section sets.

In rack designs, the three most significant parameters affecting criticality are (1) the fuel enrichment, (2) the ^{10}B loading in the neutron absorber, and (3) the lattice spacing (or water-gap thickness if a flux-trap design is used). Other parameters, within the normal range of rack and fuel designs, have a smaller effect, but are also included in the analyses.

Table 4A.1 summarizes results of the benchmark calculations for all cases selected and analyzed, as referenced in the table. The effect of the major variables are discussed in subsequent sections below. It is important to note that there is obviously considerable overlap in parameters since it is not possible to vary a single parameter and maintain criticality; some other parameter or parameters must be concurrently varied to maintain criticality.

One possible way of representing the data is through a spectrum index that incorporates all of the variations in parameters. KENO5a computes and prints the "energy of the average lethargy causing fission" (EALF). In MCNP4a, by utilizing the tally option with the identical 238-group energy structure as in KENO5a, the number of fissions in each group may be collected and the EALF determined (post-processing).

---

† Small but observable trends (errors) have been reported for calculations with the 27-group and 44-group collapsed libraries. These errors are probably due to the use of a single collapsing spectrum when the spectrum should be different for the various cases analyzed, as evidenced by the spectrum indices.

Figures 4A.1 and 4A.2 show the calculated k_{eff} for the benchmark critical experiments as a function of the EALF for MCNP4a and KENO5a, respectively (UO_2 fuel only). The scatter in the data (even for comparatively minor variation in critical parameters) represents experimental error† in performing the critical experiments within each laboratory, as well as between the various testing laboratories. The B&W critical experiments show a larger experimental error than the PNL criticals. This would be expected since the B&W criticals encompass a greater range of critical parameters than the PNL criticals.

Linear regression analysis of the data in Figures 4A.1 and 4A.2 show that there are no trends, as evidenced by very low values of the correlation coefficient (0.13 for MCNP4a and 0.21 for KENO5a). The total bias (systematic error, or mean of the deviation from a k_{eff} of exactly 1.000) for the two methods of analysis are shown in the table below.

Calculational Bias of MCNP4a and KENO5a	
MCNP4a	0.0009±0.0011
KENO5a	0.0030±0.0012

The bias and standard error of the bias were derived directly from the calculated k_{eff} values in Table 4A.1 using the following equations††, with the standard error multiplied by the one-sided K-factor for 95% probability at the 95% confidence level from NBS Handbook 91 [4A.18] (for the number of cases analyzed, the K-factor is ~2.05 or slightly more than 2).

$$\bar{k} = \frac{1}{n} \sum_{i}^{n} k_i \qquad (4A.1)$$

† A classical example of experimental error is the corrected enrichment in the PNL experiments, first as an addendum to the initial report and, secondly, by revised values in subsequent reports for the same fuel rods.

†† These equations may be found in any standard text on statistics, for example, reference [4A.6] (or the MCNP4a manual) and is the same methodology used in MCNP4a and in KENO5a.

$$\sigma_{\bar{k}}^2 = \frac{\sum_{i=1}^{n} k_i^2 - (\sum_{i=1}^{n} k_i)^2 / n}{n\,(n-1)} \qquad (4A.2)$$

$$Bias = (1 - \bar{k}) \pm K\,\sigma_{\bar{k}} \qquad (4A.3)$$

where k_i are the calculated reactivities of n critical experiments; $\sigma_{\bar{k}}$ is the unbiased estimator of the standard deviation of the mean (also called the standard error of the bias (mean)); K is the one-sided multiplier for 95% probability at the 95% confidence level (NBS Handbook 91 [4A.18]).

Formula 4.A.3 is based on the methodology of the National Bureau of Standards (now NIST) and is used to calculate the values presented on page 4.A-2. The first portion of the equation, (1- $\bar{k}$), is the actual bias which is added to the MCNP4a and KENO5a results. The second term, $K\sigma_{\bar{k}}$, is the uncertainty or standard error associated with the bias. The K values used were obtained from the National Bureau of Standards Handbook 91 and are for one-sided statistical tolerance limits for 95% probability at the 95% confidence level. The actual K values for the 56 critical experiments evaluated with MCNP4a and the 53 critical experiments evaluated with KENO5a are 2.04 and 2.05, respectively.

The bias values are used to evaluate the maximum k_{eff} values for the rack designs. KENO5a has a slightly larger systematic error than MCNP4a, but both result in greater precision than published data [4A.3 through 4A.5] would indicate for collapsed cross section sets in KENO5a (SCALE) calculations.

4A.2 Effect of Enrichment

The benchmark critical experiments include those with enrichments ranging from 2.46 w/o to 5.74 w/o and therefore span the enrichment range for rack designs. Figures 4A.3 and 4A.4 show the calculated k_{eff} values (Table 4A.1) as a function of the fuel enrichment reported for the critical experiments. Linear regression analyses for these data confirms that there are no trends, as indicated by low values of the correlation coefficients (0.03 for MCNP4a and 0.38 for KENO5a). Thus, there are no corrections to the bias for the various enrichments.

As further confirmation of the absence of any trends with enrichment, a typical configuration was calculated with both MCNP4a and KENO5a for various enrichments. The cross-comparison of calculations with codes of comparable sophistication is suggested in Reg. Guide 3.41. Results of this comparison, shown in Table 4A.2 and Figure 4A.5, confirm no significant difference in the calculated values of k_{eff} for the two independent codes as evidenced by the 45° slope of the curve. Since it is very unlikely that two independent methods of analysis would be subject to the same error, this comparison is considered confirmation of the absence of an enrichment effect (trend) in the bias.

4A.3 Effect of ^{10}B Loading

Several laboratories have performed critical experiments with a variety of thin absorber panels similar to the Boral panels in the rack designs. Of these critical experiments, those performed by B&W are the most representative of the rack designs. PNL has also made some measurements with absorber plates, but, with one exception (a flux-trap experiment), the reactivity worth of the absorbers in the PNL tests is very low and any significant errors that might exist in the treatment of strong thin absorbers could not be revealed.

Table 4A.3 lists the subset of experiments using thin neutron absorbers (from Table 4A.1) and shows the reactivity worth (Δk) of the absorber.[†]

No trends with reactivity worth of the absorber are evident, although based on the calculations shown in Table 4A.3, some of the B&W critical experiments seem to have unusually large experimental errors. B&W made an effort to report some of their experimental errors. Other laboratories did not evaluate their experimental errors.

To further confirm the absence of a significant trend with ^{10}B concentration in the absorber, a cross-comparison was made with MCNP4a and KENO5a (as suggested in Reg. Guide 3.41). Results are shown in Figure 4A.6 and Table 4A.4 for a typical geometry. These data substantiate the absence of any error (trend) in either of the two codes for the conditions analyzed (data points fall on a 45° line, within an expected 95% probability limit).

[†] The reactivity worth of the absorber panels was determined by repeating the calculation with the absorber analytically removed and calculating the incremental (Δk) change in reactivity due to the absorber.

4A.4 Miscellaneous and Minor Parameters

4A.4.1 Reflector Material and Spacings

PNL has performed a number of critical experiments with thick steel and lead reflectors.[†] Analysis of these critical experiments are listed in Table 4A.5 (subset of data in Table 4A.1). There appears to be a small tendency toward overprediction of k_{eff} at the lower spacing, although there are an insufficient number of data points in each series to allow a quantitative determination of any trends. The tendency toward overprediction at close spacing means that the rack calculations may be slightly more conservative than otherwise.

4A.4.2 Fuel Pellet Diameter and Lattice Pitch

The critical experiments selected for analysis cover a range of fuel pellet diameters from 0.311 to 0.444 inches, and lattice spacings from 0.476 to 1.00 inches. In the rack designs, the fuel pellet diameters range from 0.303 to 0.3805 inches O.D. (0.496 to 0.580 inch lattice spacing) for PWR fuel and from 0.3224 to 0.494 inches O.D. (0.488 to 0.740 inch lattice spacing) for BWR fuel. Thus, the critical experiments analyzed provide a reasonable representation of power reactor fuel. Based on the data in Table 4A.1, there does not appear to be any observable trend with either fuel pellet diameter or lattice pitch, at least over the range of the critical experiments applicable to rack designs.

4A.4.3 Soluble Boron Concentration Effects

Various soluble boron concentrations were used in the B&W series of critical experiments and in one PNL experiment, with boron concentrations ranging up to 2550 ppm. Results of MCNP4a (and one KENO5a) calculations are shown in Table 4A.6. Analyses of the very high boron concentration experiments (> 1300 ppm) show a tendency to slightly overpredict reactivity for the three experiments exceeding 1300 ppm. In turn, this would suggest that the evaluation of the racks with higher soluble boron concentrations could be slightly conservative.

---

† Parallel experiments with a depleted uranium reflector were also performed but not included in the present analysis since they are not pertinent to the Holtec rack design.

4A.5 MOX Fuel

The number of critical experiments with PuO_2 bearing fuel (MOX) is more limited than for UO_2 fuel. However, a number of MOX critical experiments have been analyzed and the results are shown in Table 4A.7. Results of these analyses are generally above a k_{eff} of 1.00, indicating that when Pu is present, both MCNP4a and KENO5a overpredict the reactivity. This may indicate that calculation for MOX fuel will be expected to be conservative, especially with MCNP4a. It may be noted that for the larger lattice spacings, the KENO5a calculated reactivities are below 1.00, suggesting that a small trend may exist with KENO5a. It is also possible that the overprediction in k_{eff} for both codes may be due to a small inadequacy in the determination of the Pu-241 decay and Am-241 growth. This possibility is supported by the consistency in calculated k_{eff} over a wide range of the spectral index (energy of the average lethargy causing fission).

4A.6 References

[4A.1] J.F. Briesmeister, Ed., "MCNP4a - A General Monte Carlo N-Particle Transport Code, Version 4A; Los Alamos National Laboratory, LA-12625-M (1993).

[4A.2] SCALE 4.3, "A Modular Code System for Performing Standardized Computer Analyses for Licensing Evaluation", NUREG-0200 (ORNL-NUREG-CSD-2/U2/R5, Revision 5, Oak Ridge National Laboratory, September 1995.

[4A.3] M.D. DeHart and S.M. Bowman, "Validation of the SCALE Broad Structure 44-G Group ENDF/B-Y Cross-Section Library for Use in Criticality Safety Analyses", NUREG/CR-6102 (ORNL/TM-12460) Oak Ridge National Laboratory, September 1994.

[4A.4] W.C. Jordan et al., "Validation of KENOV.a", CSD/TM-238, Martin Marietta Energy Systems, Inc., Oak Ridge National Laboratory, December 1986.

[4A.5] O.W. Hermann et al., "Validation of the Scale System for PWR Spent Fuel Isotopic Composition Analysis", ORNL-TM-12667, Oak Ridge National Laboratory, undated.

[4A.6] R.J. Larsen and M.L. Marx, An Introduction to Mathematical Statistics and its Applications, Prentice-Hall, 1986.

[4A.7] M.N. Baldwin et al., Critical Experiments Supporting Close Proximity Water Storage of Power Reactor Fuel, BAW-1484-7, Babcock and Wilcox Company, July 1979.

[4A.8] G.S. Hoovier et al., Critical Experiments Supporting Underwater Storage of Tightly Packed Configurations of Spent Fuel Pins, BAW-1645-4, Babcock & Wilcox Company, November 1991.

[4A.9] L.W. Newman et al., Urania Gadolinia: Nuclear Model Development and Critical Experiment Benchmark, BAW-1810, Babcock and Wilcox Company, April 1984.

[4A.10] J.C. Manaranche et al., "Dissolution and Storage Experimental Program with 4.75 w/o Enriched Uranium-Oxide Rods," Trans. Am. Nucl. Soc. 33: 362-364 (1979).

[4A.11] S.R. Bierman and E.D. Clayton, Criticality Experiments with Subcritical Clusters of 2.35 w/o and 4.31 w/o ^{235}U Enriched UO_2 Rods in Water with Steel Reflecting Walls, PNL-3602, Battelle Pacific Northwest Laboratory, April 1981.

[4A.12] S.R. Bierman et al., Criticality Experiments with Subcritical Clusters of 2.35 w/o and 4.31 w/o ^{235}U Enriched UO_2 Rods in Water with Uranium or Lead Reflecting Walls, PNL-3926, Battelle Pacific Northwest Laboratory, December, 1981.

[4A.13] S.R. Bierman et al., Critical Separation Between Subcritical Clusters of 4.31 w/o ^{235}U Enriched UO_2 Rods in Water with Fixed Neutron Poisons, PNL-2615, Battelle Pacific Northwest Laboratory, October 1977.

[4A.14] S.R. Bierman, Criticality Experiments with Neutron Flux Traps Containing Voids, PNL-7167, Battelle Pacific Northwest Laboratory, April 1990.

[4A.15] B.M. Durst et al., Critical Experiments with 4.31 wt % ^{235}U Enriched UO_2 Rods in Highly Borated Water Lattices, PNL-4267, Battelle Pacific Northwest Laboratory, August 1982.

[4A.16] S.R. Bierman, Criticality Experiments with Fast Test Reactor Fuel Pins in Organic Moderator, PNL-5803, Battelle Pacific Northwest Laboratory, December 1981.

[4A.17] E.G. Taylor et al., Saxton Plutonium Program Critical Experiments for the Saxton Partial Plutonium Core, WCAP-3385-54, Westinghouse Electric Corp., Atomic Power Division, December 1965.

[4A.18] M.G. Natrella, Experimental Statistics, National Bureau of Standards, Handbook 91, August 1963.

Table 4A.1

Summary of Criticality Benchmark Calculations

				Calculated k_{eff}		EALF † (eV)	
	Reference	Identification	Enrich.	MCNP4a	KENO5a	MCNP4a	KENO5a
1	B&W-1484 (4A.7)	Core I	2.46	0.9964 ± 0.0010	0.9898± 0.0006	0.1759	0.1753
2	B&W-1484 (4A.7)	Core II	2.46	1.0008 ± 0.0011	1.0015 ± 0.0005	0.2553	0.2446
3	B&W-1484 (4A.7)	Core III	2.46	1.0010 ± 0.0012	1.0005 ± 0.0005	0.1999	0.1939
4	B&W-1484 (4A.7)	Core IX	2.46	0.9956 ± 0.0012	0.9901 ± 0.0006	0.1422	0.1426
5	B&W-1484 (4A.7)	Core X	2.46	0.9980 ± 0.0014	0.9922 ± 0.0006	0.1513	0.1499
6	B&W-1484 (4A.7)	Core XI	2.46	0.9978 ± 0.0012	1.0005 ± 0.0005	0.2031	0.1947
7	B&W-1484 (4A.7)	Core XII	2.46	0.9988 ± 0.0011	0.9978 ± 0.0006	0.1718	0.1662
8	B&W-1484 (4A.7)	Core XIII	2.46	1.0020 ± 0.0010	0.9952 ± 0.0006	0.1988	0.1965
9	B&W-1484 (4A.7)	Core XIV	2.46	0.9953 ± 0.0011	0.9928 ± 0.0006	0.2022	0.1986
10	B&W-1484 (4A.7)	Core XV ††	2.46	0.9910 ± 0.0011	0.9909 ± 0.0006	0.2092	0.2014
11	B&W-1484 (4A.7)	Core XVI ††	2.46	0.9935 ± 0.0010	0.9889 ± 0.0006	0.1757	0.1713
12	B&W-1484 (4A.7)	Core XVII	2.46	0.9962 ± 0.0012	0.9942 ± 0.0005	0.2083	0.2021
13	B&W-1484 (4A.7)	Core XVIII	2.46	1.0036 ± 0.0012	0.9931 ± 0.0006	0.1705	0.1708

Table 4A.1

Summary of Criticality Benchmark Calculations

	Reference	Identification	Enrich.	Calculated k_{eff}		EALF † (eV)	
				MCNP4a	KENO5a	MCNP4a	KENO5a
14	B&W-1484 (4A.7)	Core XIX	2.46	0.9961 ± 0.0012	0.9971 ± 0.0005	0.2103	0.2011
15	B&W-1484 (4A.7)	Core XX	2.46	1.0008 ± 0.0011	0.9932 ± 0.0006	0.1724	0.1701
16	B&W-1484 (4A.7)	Core XXI	2.46	0.9994 ± 0.0010	0.9918 ± 0.0006	0.1544	0.1536
17	B&W-1645 (4A.8)	S-type Fuel, w/886 ppm B	2.46	0.9970 ± 0.0010	0.9924 ± 0.0006	1.4475	1.4680
18	B&W-1645 (4A.8)	S-type Fuel, w/746 ppm B	2.46	0.9990 ± 0.0010	0.9913 ± 0.0006	1.5463	1.5660
19	B&W-1645 (4A.8)	SO-type Fuel, w/1156 ppm B	2.46	0.9972 ± 0.0009	0.9949 ± 0.0005	0.4241	0.4331
20	B&W-1810 (4A.9)	Case 1 1337 ppm B	2.46	1.0023 ± 0.0010	NC	0.1531	NC
21	B&W-1810 (4A.9)	Case 12 1899 ppm B	2.46/4.02	1.0060 ± 0.0009	NC	0.4493	NC
22	French (4A.10)	Water Moderator 0 gap	4.75	0.9966 ± 0.0013	NC	0.2172	NC
23	French (4A.10)	Water Moderator 2.5 cm gap	4.75	0.9952 ± 0.0012	NC	0.1778	NC
24	French (4A.10)	Water Moderator 5 cm gap	4.75	0.9943 ± 0.0010	NC	0.1677	NC
25	French (4A.10)	Water Moderator 10 cm gap	4.75	0.9979 ± 0.0010	NC	0.1736	NC
26	PNL-3602 (4A.11)	Steel Reflector, 0 separation	2.35	NC	1.0004 ± 0.0006	NC	0.1018

Table 4A.1

Summary of Criticality Benchmark Calculations

	Reference	Identification	Enrich.	Calculated k_{eff}		EALF † (eV)	
				MCNP4a	KENO5a	MCNP4a	KENO5a
27	PNL-3602 (4A.11)	Steel Reflector, 1.321 cm sepn.	2.35	0.9980 ± 0.0009	0.9992 ± 0.0006	0.1000	0.0909
28	PNL-3602 (4A.11)	Steel Reflector, 2.616 cm sepn	2.35	0.9968 ± 0.0009	0.9964 ± 0.0006	0.0981	0.0975
29	PNL-3602 (4A.11)	Steel Reflector, 3.912 cm sepn.	2.35	0.9974 ± 0.0010	0.9980 ± 0.0006	0.0976	0.0970
30	PNL-3602 (4A.11)	Steel Reflector, infinite sepn.	2.35	0.9962 ± 0.0008	0.9939 ± 0.0006	0.0973	0.0968
31	PNL-3602 (4A.11)	Steel Reflector, 0 cm sepn.	4.306	NC	1.0003 ± 0.0007	NC	0.3282
32	PNL-3602 (4A.11)	Steel Reflector, 1.321 cm sepn.	4.306	0.9997 ± 0.0010	1.0012 ± 0.0007	0.3016	0.3039
33	PNL-3602 (4A.11)	Steel Reflector, 2.616 cm sepn.	4.306	0.9994 ± 0.0012	0.9974 ± 0.0007	0.2911	0.2927
34	PNL-3602 (4A.11)	Steel Reflector, 5.405 cm sepn.	4.306	0.9969 ± 0.0011	0.9951 ± 0.0007	0.2828	0.2860
35	PNL-3602 (4A.11)	Steel Reflector, Infinite sepn. ††	4.306	0.9910 ± 0.0020	0.9947 ± 0.0007	0.2851	0.2864
36	PNL-3602 (4A.11)	Steel Reflector, with Boral Sheets	4.306	0.9941 ± 0.0011	0.9970 ± 0.0007	0.3135	0.3150
37	PNL-3926 (4A.12)	Lead Reflector, 0 cm sepn.	4.306	NC	1.0003 ± 0.0007	NC	0.3159
38	PNL-3926 (4A.12)	Lead Reflector, 0.55 cm sepn.	4.306	1.0025 ± 0.0011	0.9997 ± 0.0007	0.3030	0.3044
39	PNL-3926 (4A.12)	Lead Reflector, 1.956 cm sepn.	4.306	1.0000 ± 0.0012	0.9985 ± 0.0007	0.2883	0.2930

Table 4A.1

Summary of Criticality Benchmark Calculations

	Reference	Identification	Enrich.	Calculated k_{eff}		EALF † (eV)	
				MCNP4a	KENO5a	MCNP4a	KENO5a
40	PNL-3926 (4A.12)	Lead Reflector, 5.405 cm sepn.	4.306	0.9971 ± 0.0012	0.9946 ± 0.0007	0.2831	0.2854
41	PNL-2615 (4A.13)	Experiment 004/032 - no absorber	4.306	0.9925 ± 0.0012	0.9950 ± 0.0007	0.1155	0.1159
42	PNL-2615 (4A.13)	Experiment 030 - Zr plates	4.306	NC	0.9971 ± 0.0007	NC	0.1154
43	PNL-2615 (4A.13)	Experiment 013 - Steel plates	4.306	NC	0.9965 ± 0.0007	NC	0.1164
44	PNL-2615 (4A.13)	Experiment 014 - Steel plates	4.306	NC	0.9972 ± 0.0007	NC	0.1164
45	PNL-2615 (4A.13)	Exp. 009 1.05% Boron-Steel plates	4.306	0.9982 ± 0.0010	0.9981 ± 0.0007	0.1172	0.1162
46	PNL-2615 (4A.13)	Exp. 012 1.62% Boron-Steel plates	4.306	0.9996 ± 0.0012	0.9982 ± 0.0007	0.1161	0.1173
47	PNL-2615 (4A.13)	Exp. 031 - Boral plates	4.306	0.9994 ± 0.0012	0.9969 ± 0.0007	0.1165	0.1171
48	PNL-7167 (4A.14)	Experiment 214R - with flux trap	4.306	0.9991 ± 0.0011	0.9956 ± 0.0007	0.3722	0.3812
49	PNL-7167 (4A.14)	Experiment 214V3 - with flux trap	4.306	0.9969 ± 0.0011	0.9963 ± 0.0007	0.3742	0.3826
50	PNL-4267 (4A.15)	Case 173 - 0 ppm B	4.306	0.9974 ± 0.0012	NC	0.2893	NC
51	PNL-4267 (4A.15)	Case 177 - 2550 ppm B	4.306	1.0057 ± 0.0010	NC	0.5509	NC
52	PNL-5803 (4A.16)	MOX Fuel - Type 3.2 Exp. 21	20% Pu	1.0041 ± 0.0011	1.0046 ± 0.0006	0.9171	0.8868

Table 4A.1

Summary of Criticality Benchmark Calculations

	Reference	Identification	Enrich.	Calculated k_{eff}		EALF† (eV)	
				MCNP4a	KENO5a	MCNP4a	KENO5a
53	PNL-5803 (4A.16)	MOX Fuel - Type 3.2 Exp. 43	20% Pu	1.0058 ± 0.0012	1.0036 ± 0.0006	0.2968	0.2944
54	PNL-5803 (4A.16)	MOX Fuel - Type 3.2 Exp. 13	20% Pu	1.0083 ± 0.0011	0.9989 ± 0.0006	0.1665	0.1706
55	PNL-5803 (4A.16)	MOX Fuel - Type 3.2 Exp. 32	20% Pu	1.0079 ± 0.0011	0.9966 ± 0.0006	0.1139	0.1165
56	WCAP-3385 (4A.17)	Saxton Case 52 PuO2 0.52" pitch	6.6% Pu	0.9996 ± 0.0011	1.0005 ± 0.0006	0.8665	0.8417
57	WCAP-3385 (4A.17)	Saxton Case 52 U 0.52" pitch	5.74	1.0000 ± 0.0010	0.9956 ± 0.0007	0.4476	0.4580
58	WCAP-3385 (4A.17)	Saxton Case 56 PuO2 0.56" pitch	6.6% Pu	1.0036 ± 0.0011	1.0047 ± 0.0006	0.5289	0.5197
59	WCAP-3385 (4A.17)	Saxton Case 56 borated PuO2	6.6% Pu	1.0008 ± 0.0010	NC	0.6389	NC
60	WCAP-3385 (4A.17)	Saxton Case 56 U 0.56" pitch	5.74	0.9994 ± 0.0011	0.9967 ± 0.0007	0.2923	0.2954
61	WCAP-3385 (4A.17)	Saxton Case 79 PuO2 0.79" pitch	6.6% Pu	1.0063 ± 0.0011	1.0133 ± 0.0006	0.1520	0.1555
62	WCAP-3385 (4A.17)	Saxton Case 79 U 0.79" pitch	5.74	1.0039 ± 0.0011	1.0008 ± 0.0006	0.1036	0.1047

Notes: NC stands for not calculated.

† EALF is the energy of the average lethargy causing fission.

†† These experimental results appear to be statistical outliers (>3σ) suggesting the possibility of unusually large experimental error. Although they could justifiably be excluded, for conservatism, they were retained in determining the calculational basis.

Table 4A.2

COMPARISON OF MCNP4a AND KENO5a CALCULATED REACTIVITIES[†] FOR VARIOUS ENRICHMENTS

Enrichment	Calculated $k_{eff} \pm 1\sigma$	
	MCNP4a	KENO5a
3.0	0.8465 ± 0.0011	0.8478 ± 0.0004
3.5	0.8820 ± 0.0011	0.8841 ± 0.0004
3.75	0.9019 ± 0.0011	0.8987 ± 0.0004
4.0	0.9132 ± 0.0010	0.9140 ± 0.0004
4.2	0.9276 ± 0.0011	0.9237 ± 0.0004
4.5	0.9400 ± 0.0011	0.9388 ± 0.0004

† Based on the GE 8x8R fuel assembly.

Table 4A.3

MCNP4a CALCULATED REACTIVITIES FOR
CRITICAL EXPERIMENTS WITH NEUTRON ABSORBERS

Ref.	Experiment		Δk Worth of Absorber	MCNP4a Calculated k_{eff}	EALF † (eV)
4A.13	PNL-2615	Boral Sheet	0.0139	0.9994±0.0012	0.1165
4A.7	B&W-1484	Core XX	0.0165	1.0008±0.0011	0.1724
4A.13	PNL-2615	1.62% Boron-steel	0.0165	0.9996±0.0012	0.1161
4A.7	B&W-1484	Core XIX	0.0202	0.9961±0.0012	0.2103
4A.7	B&W-1484	Core XXI	0.0243	0.9994±0.0010	0.1544
4A.7	B&W-1484	Core XVII	0.0519	0.9962±0.0012	0.2083
4A.11	PNL-3602	Boral Sheet	0.0708	0.9941±0.0011	0.3135
4A.7	B&W-1484	Core XV	0.0786	0.9910±0.0011	0.2092
4A.7	B&W-1484	Core XVI	0.0845	0.9935±0.0010	0.1757
4A.7	B&W-1484	Core XIV	0.1575	0.9953±0.0011	0.2022
4A.7	B&W-1484	Core XIII	0.1738	1.0020±0.0011	0.1988
4A.14	PNL-7167	Expt 214R flux trap	0.1931	0.9991±0.0011	0.3722

†EALF is the energy of the average lethargy causing fission.

Table 4A.4

COMPARISON OF MCNP4a AND KENO5a
CALCULATED REACTIVITIES† FOR VARIOUS ^{10}B LOADINGS

^{10}B, g/cm^2	Calculated $k_{eff} \pm 1\sigma$	
	MCNP4a	KENO5a
0.005	1.0381 ± 0.0012	1.0340 ± 0.0004
0.010	0.9960 ± 0.0010	0.9941 ± 0.0004
0.015	0.9727 ± 0.0009	0.9713 ± 0.0004
0.020	0.9541 ± 0.0012	0.9560 ± 0.0004
0.025	0.9433 ± 0.0011	0.9428 ± 0.0004
0.03	0.9325 ± 0.0011	0.9338 ± 0.0004
0.035	0.9234 ± 0.0011	0.9251 ± 0.0004
0.04	0.9173 ± 0.0011	0.9179 ± 0.0004

† Based on a 4.5% enriched GE 8x8R fuel assembly.

Table 4A.5

CALCULATIONS FOR CRITICAL EXPERIMENTS WITH THICK LEAD AND STEEL REFLECTORS†

Ref.	Case	E, wt%	Separation, cm	MCNP4a k_{eff}	KENO5a k_{eff}
4A.11	Steel Reflector	2.35	1.321	0.9980±0.0009	0.9992±0.0006
		2.35	2.616	0.9968±0.0009	0.9964±0.0006
		2.35	3.912	0.9974±0.0010	0.9980±0.0006
		2.35	∞	0.9962±0.0008	0.9939±0.0006
4A.11	Steel Reflector	4.306	1.321	0.9997±0.0010	1.0012±0.0007
		4.306	2.616	0.9994±0.0012	0.9974±0.0007
		4.306	3.405	0.9969±0.0011	0.9951±0.0007
		4.306	∞	0.9910±0.0020	0.9947±0.0007
4A.12	Lead Reflector	4.306	0.55	1.0025±0.0011	0.9997±0.0007
		4.306	1.956	1.0000±0.0012	0.9985±0.0007
		4.306	5.405	0.9971±0.0012	0.9946±0.0007

† Arranged in order of increasing reflector-fuel spacing.

Table 4A.6

CALCULATIONS FOR CRITICAL EXPERIMENTS WITH VARIOUS SOLUBLE BORON CONCENTRATIONS

Reference	Experiment	Boron Concentration, ppm	Calculated k_{eff}	
			MCNP4a	KENO5a
4A.15	PNL-4267	0	0.9974 ± 0.0012	-
4A.8	B&W-1645	886	0.9970 ± 0.0010	0.9924 ± 0.0006
4A.9	B&W-1810	1337	1.0023 ± 0.0010	-
4A.9	B&W-1810	1899	1.0060 ± 0.0009	-
4A.15	PNL-4267	2550	1.0057 ± 0.0010	-

Table 4A.7

CALCULATIONS FOR CRITICAL EXPERIMENTS WITH MOX FUEL

Reference	Case†	MCNP4a		KENO5a	
		k_{eff}	EALF††	k_{eff}	EALF††
PNL-5803 [4A.16]	MOX Fuel - Exp. No. 21	1.0041±0.0011	0.9171	1.0046±0.0006	0.8868
	MOX Fuel - Exp. No. 43	1.0058±0.0012	0.2968	1.0036±0.0006	0.2944
	MOX Fuel - Exp. No. 13	1.0083±0.0011	0.1665	0.9989±0.0006	0.1706
	MOX Fuel - Exp. No. 32	1.0079±0.0011	0.1139	0.9966±0.0006	0.1165
WCAP-3385-54 [4A.17]	Saxton @ 0.52" pitch	0.9996±0.0011	0.8665	1.0005±0.0006	0.8417
	Saxton @ 0.56" pitch	1.0036±0.0011	0.5289	1.0047±0.0006	0.5197
	Saxton @ 0.56" pitch borated	1.0008±0.0010	0.6389	NC	NC
	Saxton @ 0.79" pitch	1.0063±0.0011	0.1520	1.0133±0.0006	0.1555

Note: NC stands for not calculated

† Arranged in order of increasing lattice spacing.

†† EALF is the energy of the average lethargy causing fission.

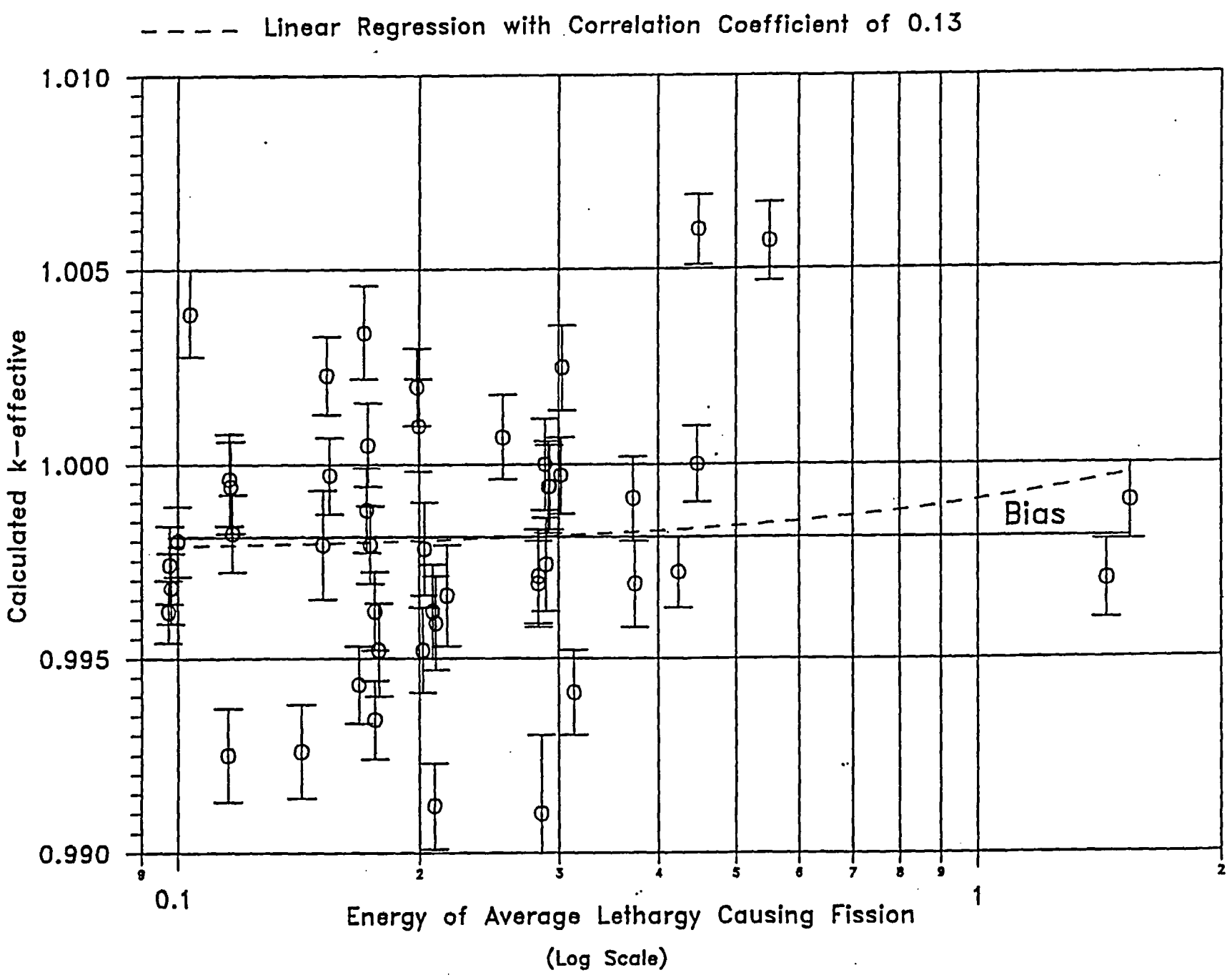

FIGURE 4A.1 MCNP CALCULATED k-eff VALUES for VARIOUS VALUES OF THE SPECTRAL INDEX

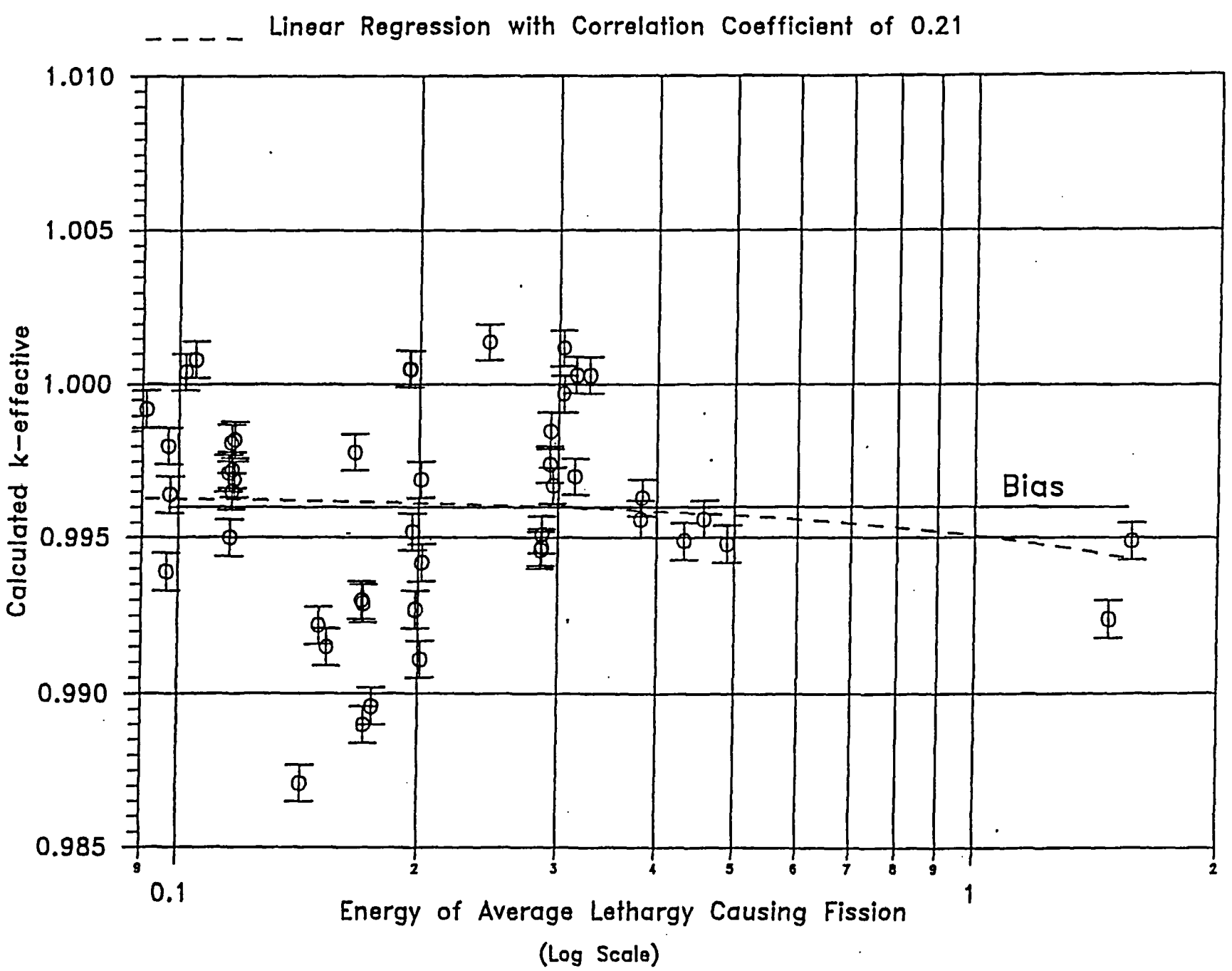

FIGURE 4A.2 KENO5a CALCULATED k-eff VALUES FOR VARIOUS VALUES OF THE SPECTRAL INDEX

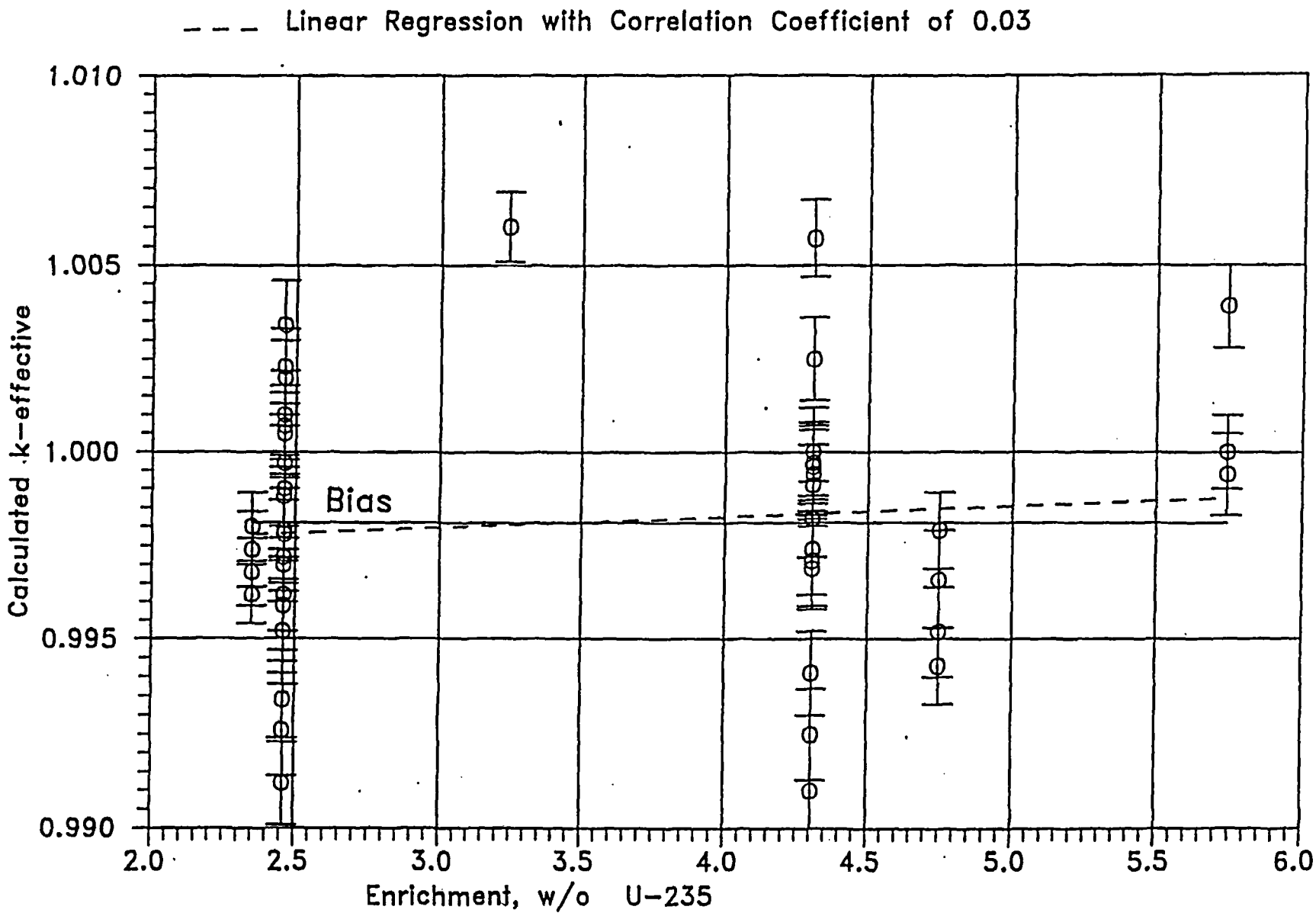

FIGURE 4A.3 MCNP CALCULATED k-eff VALUES AT VARIOUS U-235 ENRICHMENTS

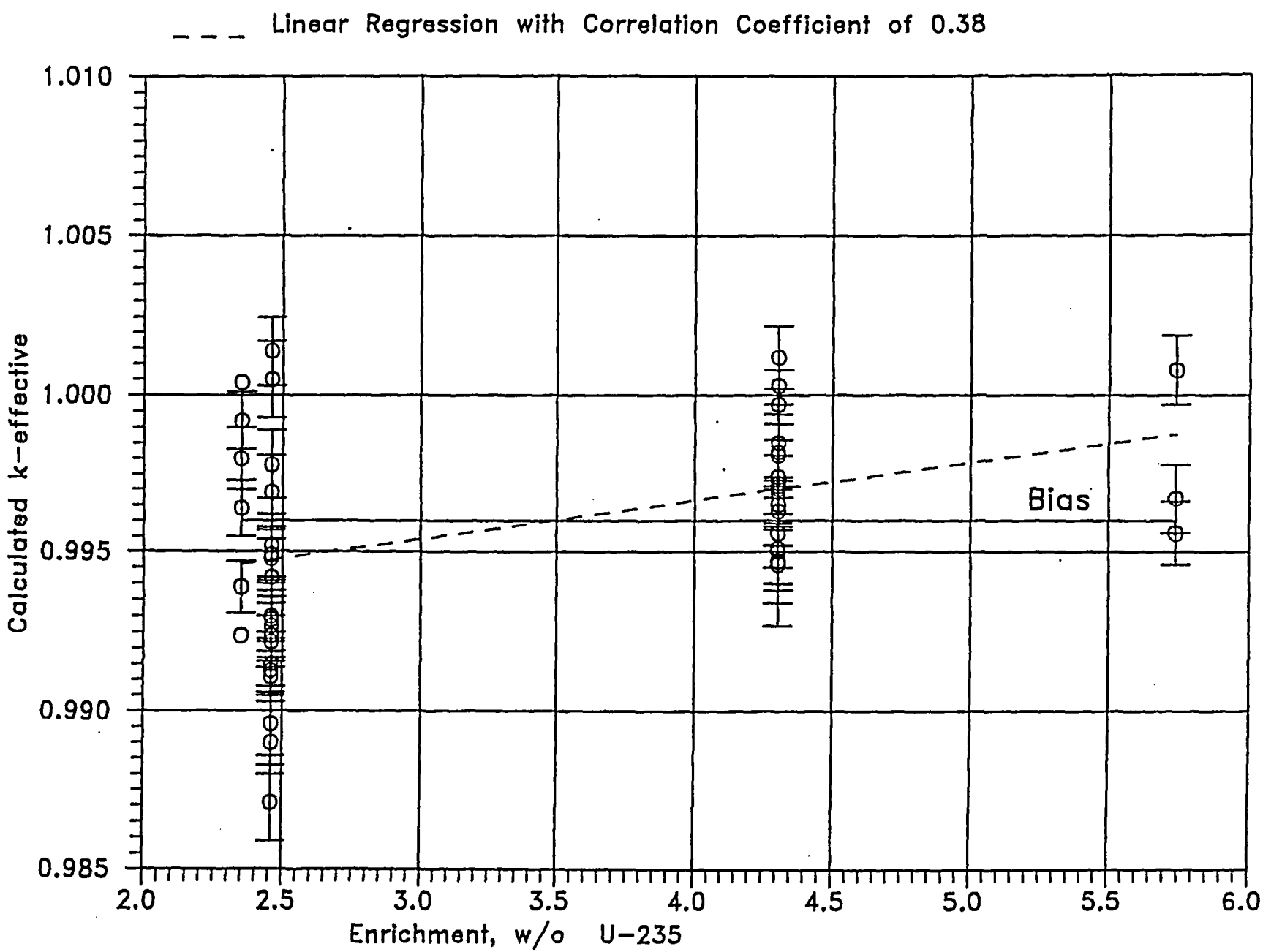

FIGURE 4A.4. KENO CALCULATED k-eff VALUES AT VARIOUS U-235 ENRICHMENTS

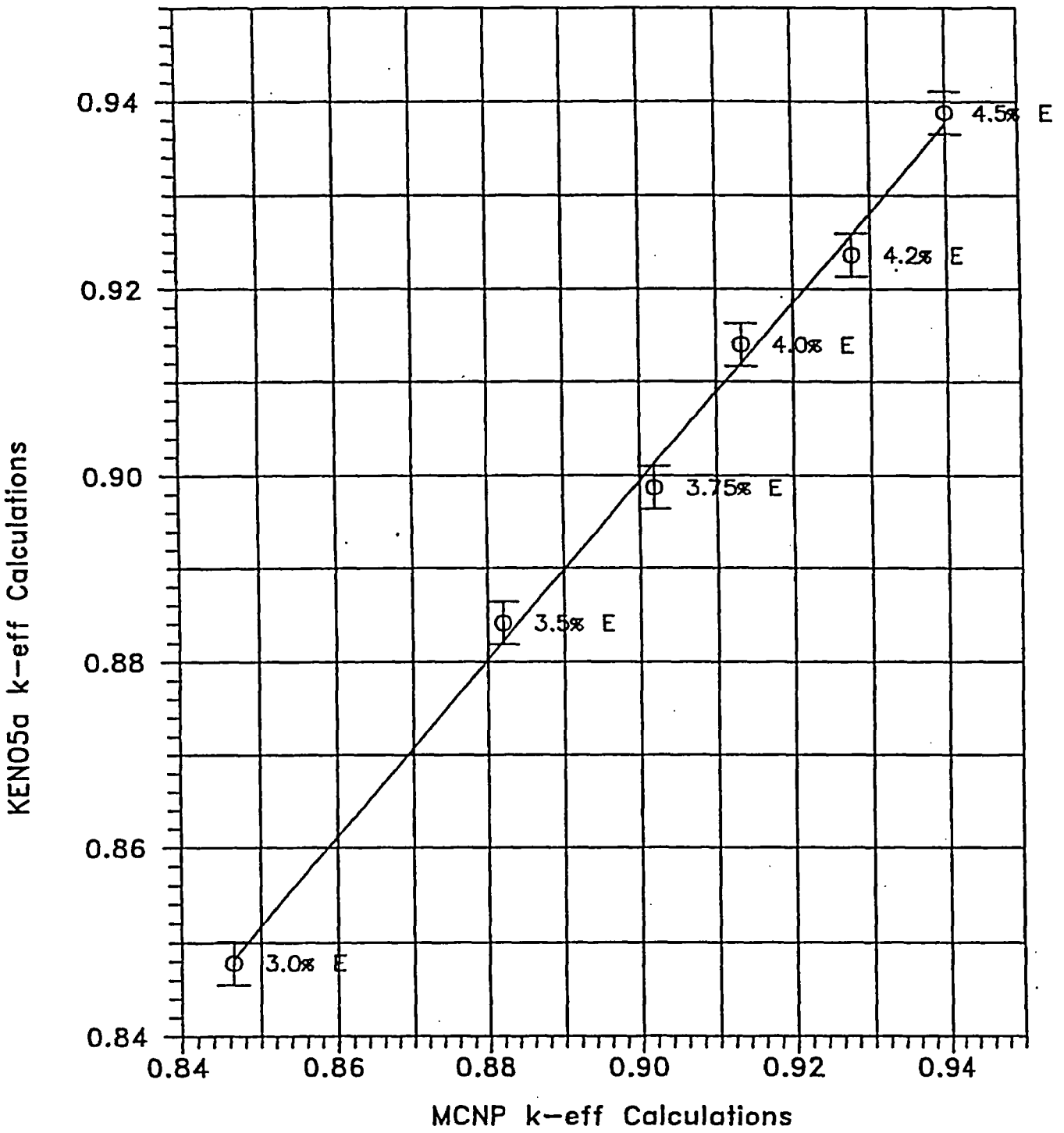

FIGURE 4A.5 COMPARISON OF MCNP AND KENO5A CALCULATIONS FOR VARIOUS FUEL ENRICHMENTS

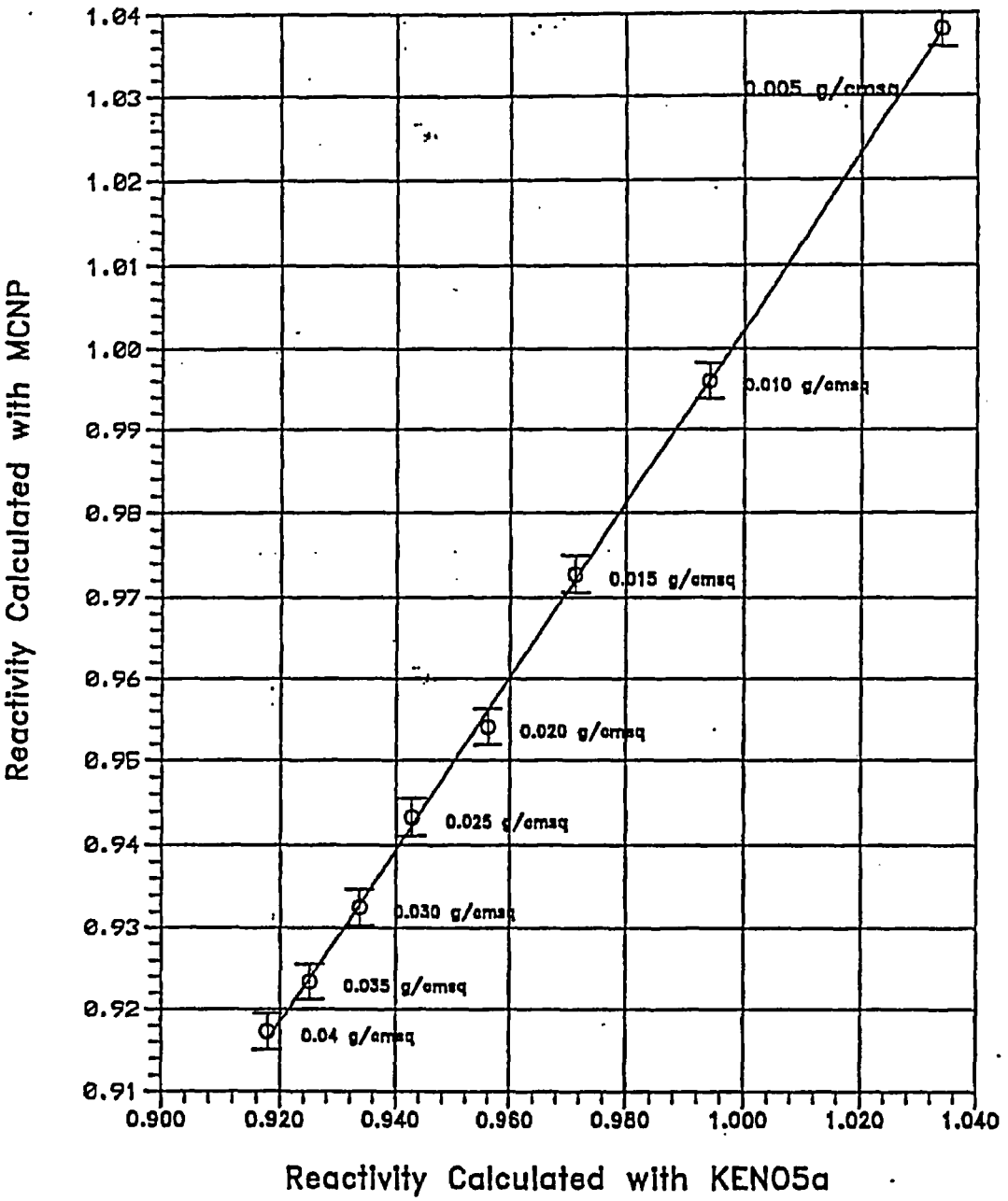

FIGURE 4A.6 : COMPARISON OF MCNP AND KENO5a CALCULATIONS FOR VARIOUS BORON-10 AREAL DENSITIES

5.0 THERMAL-HYDRAULIC EVALUATION

5.1 Introduction

The storage capacity at Clinton Power Station (CPS) is proposed to be expanded by adding racks to the open spaces in the Cask Storage Pool (CSP) and re-racking of the Spent Fuel Pool (SFP) with high density storage racks. To ensure the thermal-hydraulic adequacy of the expanded storage configuration it must be demonstrated that the Spent Nuclear Fuel (SNF) in the SFP and CSP racks is adequately cooled.

This section provides a summary of the methods, models, analyses and numerical results to demonstrate the CPS spent fuel pool meets the thermal-hydraulic requirements for safe storage of SNF set forth in Sub-section 5.2 herein. Similar thermal-hydraulic analyses have been used in spent fuel pool licensing at many nuclear plants worldwide (see Table 5.1.1 for a partial list). Specifically, the following analyses are required:

1. Calculation of the SNF decay heat. The decay heat contributions from both previously stored fuels and freshly discharged fuels must be considered.

2. Determination of the SFP bulk thermal response versus time in accordance with each discharge scenario.

3. Calculation of time-to-boil during a postulated loss of forced cooling event for each discharge scenario.

4. Rigorous Computational Fluid Dynamics (CFD) based study to conservatively quantify the peak local water temperature in the fuel storage cells.

5. Determination of the maximum fuel clad temperature.

The CPS thermal-hydraulic evaluation is presented in the following.

5.2 Acceptance Criteria

Applicable codes, standards and regulations include the following:

a. NUREG-0800, Standard Review Plan, Section 9.1.3.

b. USNRC OT Position Paper for Review and Acceptance of Spent Fuel Storage and Handling Application, 4/78 [5.1.1].

The design of the rack modules must ensure that fuel assemblies are adequately cooled by natural circulation of water. For this purpose bounding discharge scenarios are defined and evaluated. The storage of SNF in the SFP and CSP fuel racks is evaluated for two cases: Case I for Normal (end of cycle) fuel batch discharge and Case II for Abnormal (full core) discharge. The case description and acceptance criteria are:

1. Under a Normal discharge scenario (Case I), a batch of 312 bundles is transferred to the SFP after 24 months of reactor operation. The SFP is cooled with one Spent Fuel Pool Cooling System (SFPCS) train operating with component cooling water (CCW) at 105°F. The bulk pool water temperature shall be limited to 140°F and water in the rack cells in a sub-cooled condition.

2. Under an Abnormal discharge scenario (Case II) a full core (624 bundles) is transferred to the SFP after 24 months of reactor operation. The SFP is cooled with one SFPCS train operating with component cooling water (CCW) at 105°F. The bulk pool water temperature shall be limited to 150°F and water in the rack cells in a sub-cooled condition.

5.3 Assumptions and Inputs

5.3.1 Assumptions

The Clinton thermal-hydraulic analysis embeds an array of assumptions to render a conservative portrayal of spent fuel pool temperatures. A numbered list of assumptions are provided in the following:

Bulk Pool Temperature Analyses

1. Heat loss by the conduction through pool walls is neglected.
2. The thermal capacity of the SFP is computed on the water volume above fuel. This assumption neglects thermal capacity of fuel, cladding, racks metal and water in the racks resulting in faster computed heat-up rate, higher pool temperatures and shorter times-to-boil.
3. As an added measure of conservatism, thermal inertia of water in the upper containment pool and cask storage pool are neglected.
4. The decay heat load contribution of previously discharged fuel assemblies is assumed constant during all discharge scenarios.
5. All refueling batches discharged previously and freshly discharged fuels are assumed to be at a bounding 43000 MWD/MTU burnup. This maximizes the decay heat load associated with all fuels stored in the SFP.
6. For minimizing the cooling time of old fuel, a short (18 month) cycle is assumed for previously discharged fuel batches.
7. The maximum SFP building temperature is assumed for evaporative heat loss calculations. This conservatively minimizes credit for evaporative cooling.
8. All of the radioactive decay energy is assumed to heat the fuel pool water, including that from gamma radiation. This conservatively maximizes heat input to the SFPCS, yielding conservative bulk temperatures.

9. For time-to-boil calculations a loss of forced cooling is assumed to occur at the instant of maximum bulk SFP temperature for each discharge scenario. This conservatively minimizes the time-to-boil.

Local Temperature Analyses

1. Passive heat losses (i.e., conduction through walls and slab) are neglected.
2. Calculations employ conservative bounding hydraulic resistances of fuel. This understates natural circulation cooling and maximizes water temperatures.
3. Downcomer flow between rack modules is neglected. This conservatively minimizes natural circulation flow.
4. The peripheral downcomer area is understated in the CFD modeling. This conservatively maximized the downcomer flow resistance.
5. The hottest fuel assemblies are assumed to be located together at the center of the spent fuel pool, conservatively maximizing the local decay heat generation rates.
6. An additional heat transfer resistance (0.005 (hr×ft^2×°F)/Btu) is conservatively assumed to the outside of the fuel rods to maximize clad temperatures.
7. For peak-clad temperature calculations the maximum local water temperature (at the fuel rack cell exit) and peak heat flux (typically near the mid-height of the active fuel region) are assumed to occur co-incidentally. The superposition of these two maximum values conservatively maximizes the computed fuel clad temperatures.

5.3.2 Design Data

Bulk Pool Analysis

The principal input data employed to determine the maximum bulk temperature of CPS fuel pools is summarized in Table 5.3.1. To maximize decay heat, a bounding burnup, maximum uranium weight and minimum fuel enrichment reported in Table 5.3.1 are assumed for all fuel discharged in the CPS pool. The cumulative decay heat load from old fuel batches is

determined using ORIGEN 2 [5.3.2], as incorporated in Holtec's QA validated computer program DECOR [5.3.1], for a sufficient number of discharged batches to fill the racks in the SFP and CSP up to a reserve of one normal batch.

Local Temperature Analysis

The principal inputs for local analysis, namely the racks construction data and fuel bundle data are presented in Tables 5.3.2 and 5.3.3.

5.4 Bulk Pool Analysis Methodology

This analysis is performed to determine bulk temperature of water and decay heat profiles under postulated discharge scenarios. The mathematical formulation for this analysis can be explained with reference to the simplified heat exchanger alignment shown in Figure 5.4.1. Referring to the Spent Fuel Pool Cooling System (SFPCS), the governing differential equation for bulk pool temperature can be written by utilizing conservation of energy as:

$$C \times \frac{dT}{d\tau} = P_{cons} + Q(\tau) - Q_{HX}(T) - Q_{EVAP}(T, T_A) + Q_p - Q_w$$

where:

C	thermal capacity of water in the pool, $Btu/^{\circ}F$
P_{CONS}	heat generation rate from previous discharges, Btu/hr
$Q(\tau)$	heat generation rate from recently discharged fuel as a function of time, Btu/hr
$Q_{HX}(T)$	heat removed by the SFP heat exchangers, Btu/hr
$Q_{EVAP}(T, T_A)$	evaporative heat loss, Btu/hr
Q_p	pump heat, Btu/hr
Q_w	heat loss from pool walls, Btu/hr (conservatively neglected)

T bulk pool temperature, $^{\circ}F$

T_A fuel building ambient temperature, $^{\circ}F$

In bulk pool thermal-hydraulics, it is recognized that pump heat (Q_p) is very small in comparison with pool decay heat (about 2 orders of magnitude smaller). As a result it's effect on pool temperatures is negligible. Accordingly, the contribution of pump heat to fuel pool energy input is ignored in the evaluation.

The heat removed by the SFP heat exchangers, $Q_{HX}(T)$ is defined by the following equation:

$$Q_{HX}(T) = W_C \cdot c_C \cdot p \cdot (T - T_C)$$

where:

W_C coolant flow rate, $^{lb}/_{hr}$

c_C coolant specific heat, $^{Btu}/_{lb \cdot ^{\circ}F}$

p temperature effectiveness of heat exchanger

T bulk pool temperature, $^{\circ}F$

T_C coolant inlet water temperature, $^{\circ}F$

The equation used to determine the temperature effectiveness, p of the SFPCS heat exchanger is as follows:

$$p = \frac{T_{C,o} - T_{C,i}}{T_P - T_{C,i}}$$

where:

$T_{C,i}$ coolant inlet water temperature, $^{\circ}F$

$T_{C,o}$ coolant outlet water temperature, $^{\circ}F$

T_P SFP water temperature at heat exchanger inlet, $^{\circ}F$

The temperature effectiveness, p is determined from the SFP heat exchanger specifications.

The SFP decay heat contribution from all previously stored fuels is held constant during the entire analysis because its decrease with decay time after shutdown is conservatively neglected. The decay heat generation, $Q(\tau)$ of the freshly discharged fuel decays exponentially with elapsed time after reactor shutdown. The evaporative heat loss, $Q_{EVAP}(T,T_A)$ is a nonlinear function of pool temperature, T and ambient temperature, T_A, and includes heat loss from the pool surface by natural convection and radiation. The evaporation heat loss is a function of rate of moisture generation from the pool surface which is obtained using a proprietary Holtec correlation [5.4.1]. For a conservative assessment of evaporation cooling of the fuel pool, the ambient temperature is assumed to be at it's design (i.e. maximum) temperature and relative humidity is 100%.

The Holtec's QA validated BULKTEM computer program [5.4.2] is used to numerically solve the bulk pool thermal hydraulic equations described in the foregoing. Inputs to the BULKTEM computer program include the coolant flow rate and temperature, the temperature effectiveness of SFP cooling heat exchanger, the discharge batch transfer time from reactor to SFP, in-core exposure times, the average assembly operating power, "old" fuels decay heat contribution, SFP thermal capacity, initial SFP water temperature, SFP surface area, and ambient temperature in fuel building. Outputs from BULKTEM include the bulk water temperature, evaporative cooling loss and net decay heat – all as functions of time.

5.4.1 Time-To-Boil Calculation

This analysis is used to determine the time it takes for pool water to reach boiling temperature in case all forced cooling trains become unavailable. Clearly, the most critical instant of loss-of-cooling is when the SFP pool water temperature has reached its maximum value. The following governing differential equation can be derived from the differential

thermal response equation defined in Section 5.4 without including the SFPCS heat rejection term.

$$C \times \frac{dT}{d\tau} = P_{cons} + Q(\tau) - Q_{EVAP}(T, T_A)$$

where:

C	is thermal capacity of the pool, $Btu/^{\circ}F$
P_{CONS}	is heat generation rate from "old" fuel, Btu/hr
$Q(\tau)$	is heat generation rate from recently discharged fuel as a function of time, Btu/hr
$Q_{EVAP}(T,T_A)$	is evaporative heat loss, Btu/hr
T	is bulk pool temperature, $^{\circ}F$
T_A	is fuel building ambient temperature, $^{\circ}F$

The Holtec QA validated TBOIL computer program [5.4.3] is used to numerically integrate the foregoing equation and time-to-boil, boil-off rate, and pool water depth versus time profile obtained.

5.4.2 Bulk Pool Temperature Results

As required by Sub-section 5.2, the maximum bulk pool temperature analyses are performed for the two cases, namely Case I (Normal) and Case II (Abnormal) discharge scenarios. As stated previously in Sub-section 5.3.2, for decay heat inputs the bulk pool evaluations use bounding assumptions for fuel burnup, uranium weight and enrichment. The time dependent bulk pool temperature profiles are presented in Figures 5.4.2 and 5.4.3. The time dependent pool decay heat profiles are presented in Figures 5.4.4 and 5.4.5.

The results of the maximum bulk pool temperature analyses are summarized in Table 5.4.1. The results of the analysis confirm that the bulk pool water temperatures are below the prescribed limits set forth in Section 5.2 (140°F (Normal), 150°F (Abnormal)).

5.4.3 Time-to-Boil Results

Under a loss of all forced pool cooling, the pool water temperature will rise to reach the boiling temperature of water (~212°F). The time to reach boiling temperature will be the shortest when the loss of forced cooling occurs coincident with the maximum bulk pool temperature. Although the probability of a loss-of-cooling event coinciding with the instant when the pool water has reached its peak value is extremely remote, the calculations are performed under this scenario to obtain a bounding result. The results with the additional proviso that no makeup water is added to the pool are summarized in Table 5.4.2. The water depth profiles in the SFP as a function of time after loss of cooling are presented in Figure 5.4.6 and 5.4.7.

5.5 Local Analysis Methodology

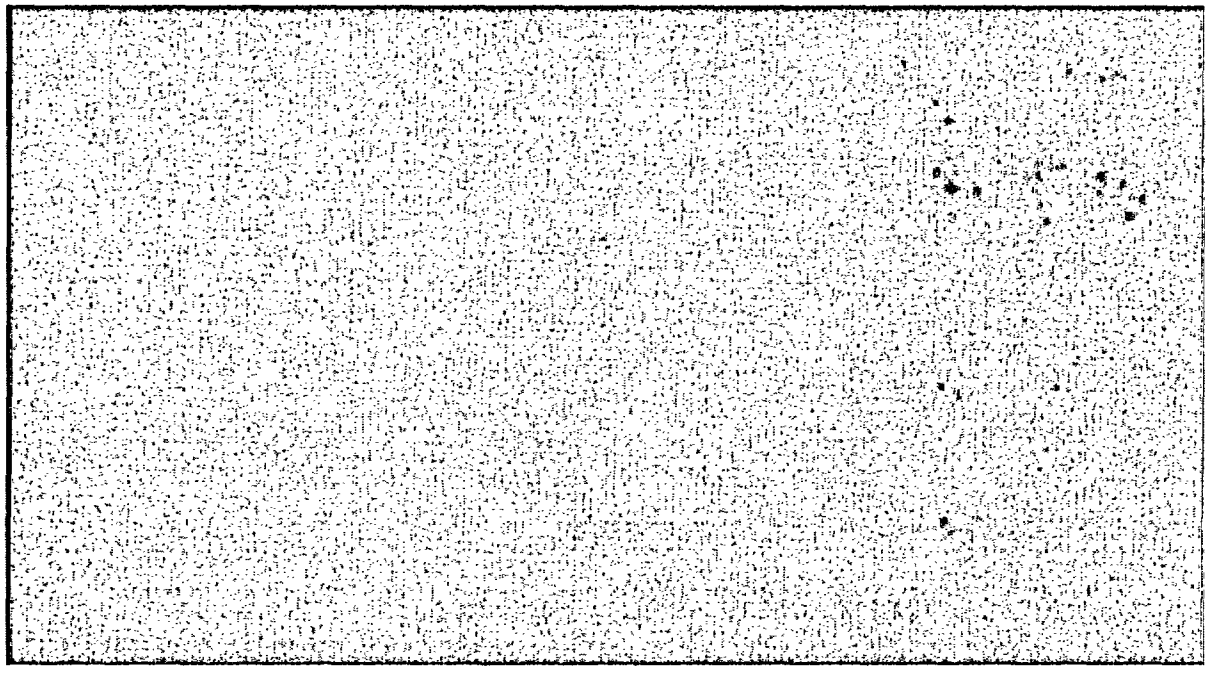

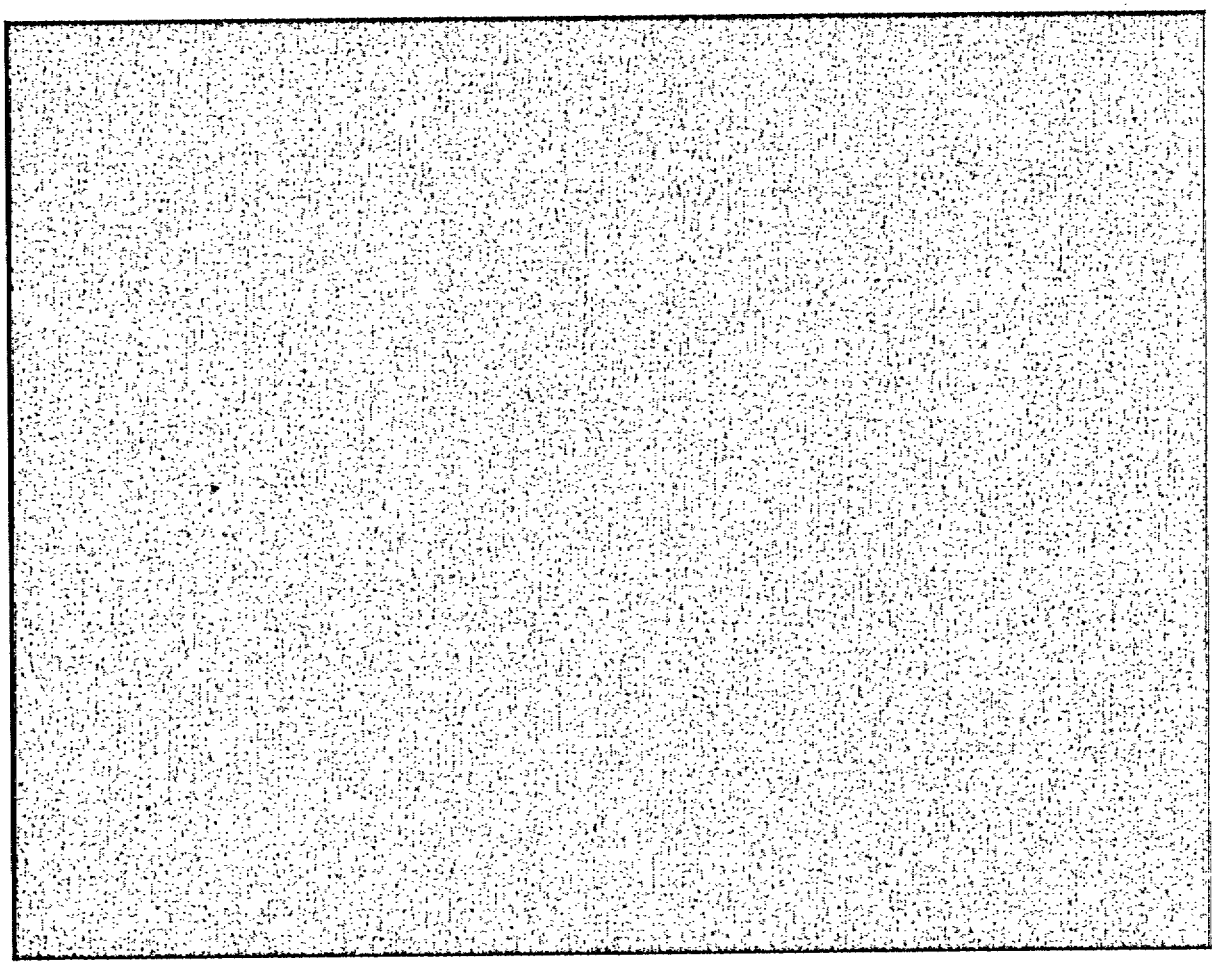

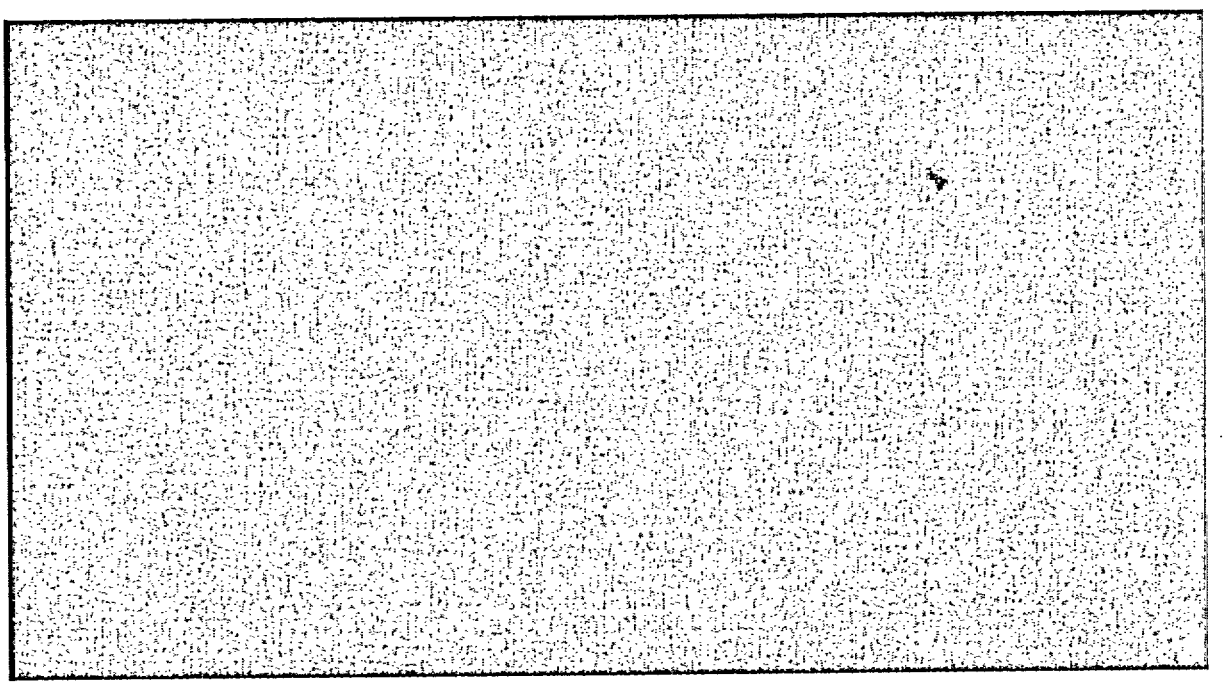

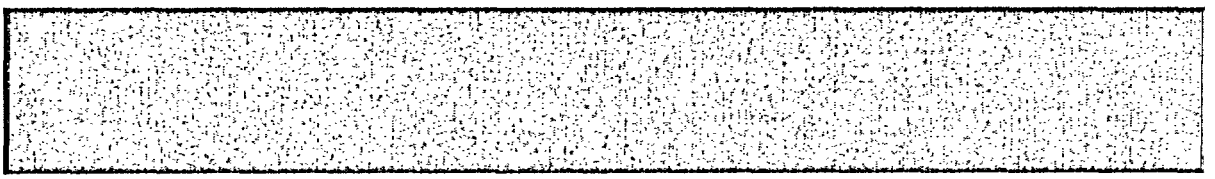

5.5.1 Peak Clad Temperature Calculation

Having determined the maximum local water temperature, the peak clad temperature is determined by a procedure described next. The maximum specific decay power of a single fuel assembly among the freshly discharged batch of assemblies (Q_A) can be given by:

$$Q_A = Q_{average} \times f_r$$

where:

f_r is radial peaking factor

$Q_{average}$ is average fuel assembly decay power

A fuel rod can produce f_z times the average heat emission rate over a small length, where f_z is the axial peaking factor. The axial heat distribution in a rod is generally a maximum in the central region, and tapers off at its two extremities. Thus, peak cladding heat flux per unit heat transfer area of fuel assembly is given by the equation:

$$q_{peak} = \frac{Q_A \times f_z}{A_{rod}}$$

where :

A_{rod} is the cladding external heat transfer area in the active fuel length region of a single fuel assembly, ft^2

Within each fuel assembly sub-channel, water is continuously heated by the cladding as it moves axially upwards from bottom to top under laminar flow conditions. Rohsenow and Hartnett [5.5.4] report Nusselt-number (Nu) based on the heat transfer correlation for laminar flow in a heated channel. Nu is defined as follows:

$$Nu = \frac{h_c}{k_{water}} \times D_h = 4.364$$

where:

k_{water} is the water thermal conductivity, $Btu/hr \cdot ft \cdot °F$

h_c is laminar flow convective heat transfer coefficient, $Btu/hr \cdot ft^2 \cdot °F$

D_h is sub-channel hydraulic diameter, ft

Solving for h_c, we obtain:

$$h_c = 4.364 \times \frac{k_{water}}{D_h}$$

In order to introduce some additional margin in the analysis, we assume that the fuel cladding has an additional conservatively assumed crud deposit resistance, R_{crud} (equal to 0.005 [$hr \cdot ft^2 \cdot °F/Btu$]), covering the cladding. Therefore, the overall heat transfer coefficient U, considering a crud deposit resistance R_{crud} , is defined by the following:

$$U = \frac{1}{\left(\frac{1}{h_c} + R_{crud}\right)}$$

Thus, the temperature difference, ΔT_c between the fuel cladding and the local water is computed by the following:

$$\Delta T_c = \frac{q_{peak}}{U}$$

Finally, the maximum fuel rod temperature is defined by the following:

$$T_{clad} = T_{loc} + \Delta T_c$$

where:

T_{clad} is the maximum fuel clad temperature

T_{loc} is the maximum local water temperature

5.5.2 Local Analysis Results

As discussed in Section 5.5 a CFD model of the CPS fuel storage pools is constructed for the two discharge scenarios (Case I and Case II) on the FLUENT computer program. From this model, local water temperatures in the fuel storage racks are obtained co-incident with the maximum bulk pool temperature. In Figures 5.5.2 and 5.5.3, planar temperature contours in the hot fuel region are shown for the Case I and Case II discharge scenarios. The maximum local water temperature results (T_{loc}) and maximum clad-to-water temperature differentials (ΔT_c) are provided in Table 5.5.1. For conservatism, the axial locations of maximum T_{loc} and ΔT_c are assumed to be co-incident and an upperbound to the peak cladding temperature obtained by adding T_{loc} and ΔT_c. The results are provided in Table 5.5.1. At any depth within a fuel pool, the local pressure can be calculated by adding the water head pressure and atmospheric pressure as shown below:

$$P_h = P_{atm} + \frac{h\rho g}{144 g_c}$$

where P_{atm} is atmosphere pressure (14.7 psi), P_h is local pressure (psi), h is depth below water surface (ft), ρ is water density at a globally bounding water temperature of 170°F (60.8 lbm/ft^3 [5.5.5]), g is gravitational acceleration (32.2 ft/s^2) and g_c is universal constant (32.2 lbm-ft/(s^2-lb)). At a depth of 23 feet (distance from surface of pool to the top of racks), the local pressure is:

$$P_h = 14.7 + \frac{23 * 60.8 * 32.2}{144 * 32.2} = 24.41 \cdot psi$$

From steam tables [5.5.5] the water saturation temperature (T_{sat}) at P_h is obtained as 238.7°F. The maximum local temperatures reported in Table 5.5.1 are below T_{sat}. The local analysis results are in compliance with the sub-cooled water requirement (Section 5.2).

5.6 References

[5.1.1] "OT Position Paper for Review and Acceptance of Spent Fuel Storage and Handling Applications", April 14, 1978.

[5.3.1] "QA Documentation of DECOR", Holtec Report HI-971734, Rev. 0.

[5.3.2] A.G. Croff, "ORIGEN2 – A Revised and Updated Version of the Oak Ridge Isotope and generation depletion Code," ORNL-5621, Oak Ridge National Laboratory, 1980.

[5.4.1] "An Improved Correlation for Evaporation from Spent Fuel Pools", Holtec Report HI-971664, Rev. 0.

[5.4.2] "QA Documentation for BULKTEM", Holtec Report HI-951391, Rev. 1.

[5.4.3] "QA Documentation of Computer Program TBOIL", Holtec Report HI-92832, Rev. 5.

[5.5.1] Batchelor, G.K., "An Introduction to Fluid Dynamics", Cambridge University Press, 1967.

[5.5.2] "Documentation and Validation of FLUENT Versions 4.48 and 4.56"†, Holtec Report HI-981921, Rev. 1.

[5.5.3] Launder, B.E., and Spalding, D.B., "Lectures in Mathematical Models of Turbulence", Academic Press, London, 1972.

[5.5.4] Rohsenow, W.M. and J.P. Hartnett, "Handbook of Heat Transfer", McGraw Hill Book Company, NY, (1973).

[5.5.5] Balzhiser, R.E. & Samuels, M.R., "Engineering Thermodynamics", Prentice Hall, Inc. (1977).

† FLUENT version 4.56 is employed in the CFD analyses.

Table 5.1.1 PARTIAL LISTING OF RERACK APPLICATIONS USING SIMILAR METHODS OF THERMAL-HYDRAULIC ANALYSIS	
PLANT	DOCKET NO.
Enrico Fermi Unit 2	USNRC 50-341
Quad Cities 1 and 2	USNRC 50-254, 50-265
Rancho Seco	USNRC 50-312
Grand Gulf Unit 1	USNRC 50-416
Oyster Creek	USNRC 50-219
Pilgrim	USNRC 50-293
V.C. Summer	USNRC 50-395
Diablo Canyon Units 1 and 2	USNRC 50-275, 50-455
Byron Units 1 and 2	USNRC 50-454, 50-455
Braidwood Units 1 and 2	USNRC 50-456, 50-457
Vogtle Unit 2	USNRC 50-425
St. Lucie Unit 1	USNRC 50-425
Millstone Point Unit 1	USNRC 50-245
D.C. Cook Units 1 and 2	USNRC 50-315, 50-316
Indian Point Unit 2	USNRC 50-247
Three Mile Island Unit 1	USNRC 50-289
J.A. FitzPatrick	USNRC 50-333
Shearon Harris Unit 2	USNRC 50-401
Hope Creek	USNRC 50-354
Kuosheng Units 1 and 2	Taiwan Power Company

Table 5.1.1 (Contd .) PARTIAL LISTING OF RERACK APPLICATIONS USING SIMILAR METHODS OF THERMAL-HYDRAULIC ANALYSIS	
Ulchin Unit 2	Korea Electric Power Corporation
Laguna Verde Units 1 and 2	Comision Federal de Electricidad
Zion Station Units 1 and 2	USNRC 50-295, 50-304
Sequoyah	USNRC 50-327, 50-328
La Salle Unit One	USNRC 50-373
Duane Arnold	USNRC 50-331
Chin Shan Units 1 and 2	Taiwan Power Company
Fort Calhoun	USNRC 50-285
Nine Mile Point Unit One	USNRC 50-220
Beaver Valley Unit One	USNRC 50-334
Limerick Unit 2	USNRC 50-353
Ulchin Unit 1	Korea Electric Power orporation
J.A. Fitzpatrick	USNRC 50-333
Callaway	USNRC 50-483
Byron/Braidwood	USNRC 50-454, 50-455, 50-567. 50-457
Wolf Creek	USNRC 50-482
Plant Hatch Units 1 & 2	USNRC 50-321, 50-366
Harris Pools C and D	USNRC 50-401
Waterford 3	USNRC 50-382
Turkey Point	USNRC 50-250, 50-251

Table 5.3.1 INPUTS FOR BULK POOL ANALYSIS	
INPUT DATA	VALUE
SFP Exchanger Flow Rates	4150 gpm (Shell) 4150 gpm (Tube)
SFP Exchanger Design Inlet Temperatures	105°F (Shell) 120°F (Tube)
SFP Exchanger Heat Duty	19.7×10^6 Btu/hr
Water Height Above SNF	23 ft (min)
Reactor Thermal Power	3543 MW
Reactor Core Size	624 bundles
Fuel Building Temperature	104°F
In-core Hold Time	24 hr
Fuel Transfer Rate	7/hr first 160 bundles followed by 4/hr
Normal Batch Size	312
Cycle Length‡	24 months
Uranium Weight	180.17 Kg (max)
Enrichment	3.53% (min)
Burnup	43000 MWD/MTU
Pool Width	386 in
Pool Length	432 in
Number of fuel cells	3796 (SFP) 363 (CSP)

‡ For minimizing the cooling time of old fuel an 18 month cycle is assumed for previously discharged fuel batches.

Table 5.3.2 INPUTS FOR LOCAL ANALYSIS	
INPUT DATA	VALUE
Racks Height	175.625 in
Bottom Plenum	7 in
Cell Length	168 in
Cell Pitch	6.243 in
Cell Opening	6.05 in
Pedestal flow holes	Four ½ in dia.
Radial Peaking Factor	1.2
Axial Peaking Factor	1.7
Transfer Canal Opening	4 ft
Transfer Canal Length	15 ft

Table 5.3.3 FUEL BUNDLE DATA			
Parameter	GE6,GE7B,GE8B	GE10	GE14
Rods Array Size	8x8	8x8	10x10
Fuel Rod OD (in)	0.483	0.483	0.404
Pitch (in)	0.636	0.64	0.51
Number of Fuel Rods	62	60	92
Active Fuel Length	150	150	150
Channel ID	5.215	5.278	5.278

Table 5.4.1
SUMMARY OF BULK POOL TEMPERATURE RESULTS

Discharge Scenario	Max. Bulk SFP Temp (°F)	Coincident Time After Shutdown (hrs)	Coincident Decay Heat (Btu/hr)	Coincident Evaporation Heat Loss (Btu/hr)
Case I	125.83	87	27.7×10^6	0.402×10^6
Case II	134.95	164	40.0×10^6	0.637×10^6

Table 5.4.2
SUMMARY OF TIME-TO-BOIL ANALYSIS RESULTS

Discharge Scenario	Time-to-Boil (hrs)	Time-to-Top of Rack (hrs)	Max. Water Loss (gpm)
Case I	5.35	61.16	59.49
Case II	3.25	41.90	85.90

Table 5.5.1 RESULTS OF LOCAL TEMPERATURE ANALYSIS		
Discharge Scenario	Parameter	$^{\circ}F$
Case I	Maximum Local Water Temperature (T_{loc})	158.1
	Maximum Clad-to-Water Temperature Differential (ΔT_c)	54.3
	Maximum Clad Temperature (T_{clad})	212.4
Case II	Maximum Local Water Temperature (T_{loc})	164.1
	Maximum Clad-to-Water Temperature Differential (ΔT_c)	41.9
	Maximum Clad Temperature (T_{clad})	206.0

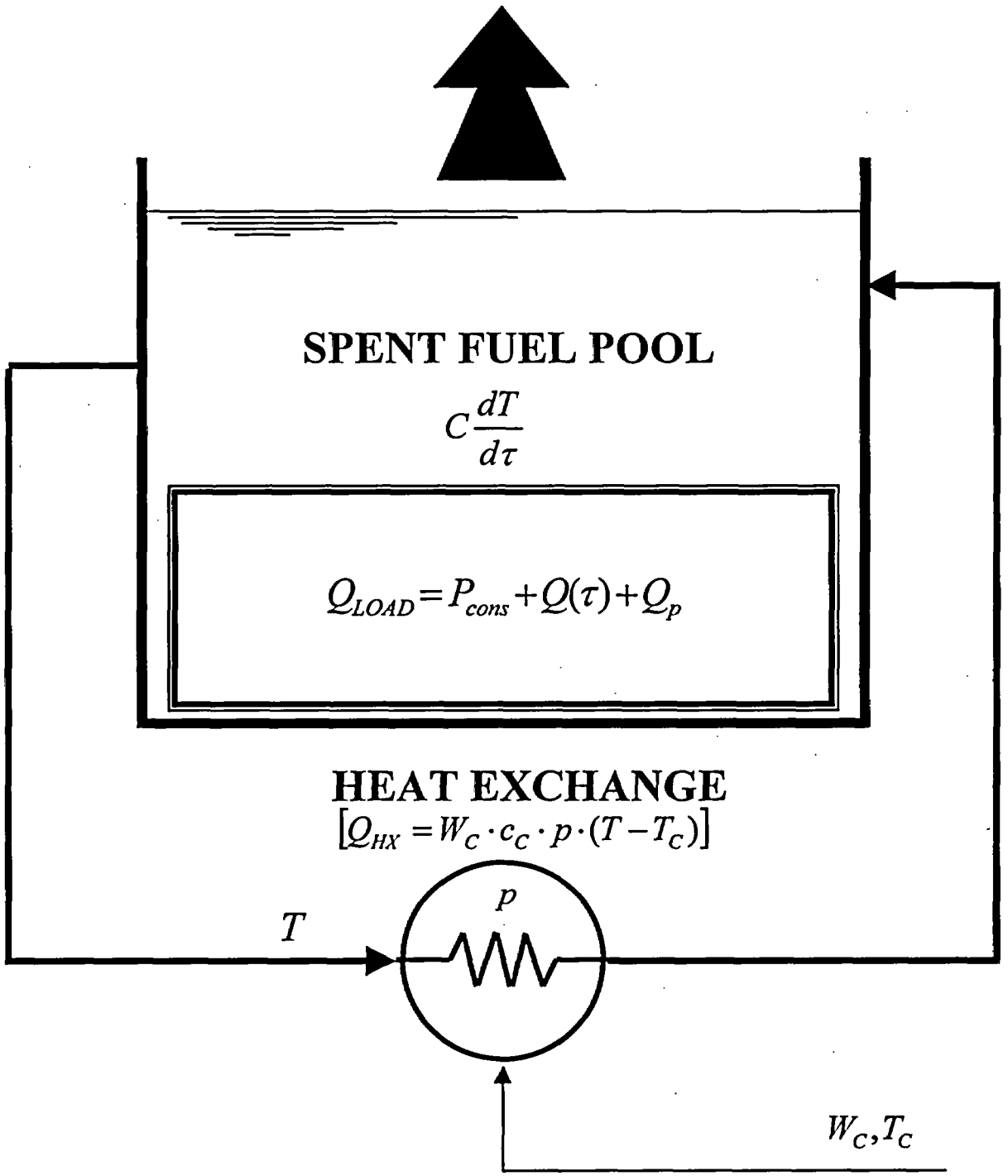

Figure 5.4.1: Spent Fuel Pool Cooling Model

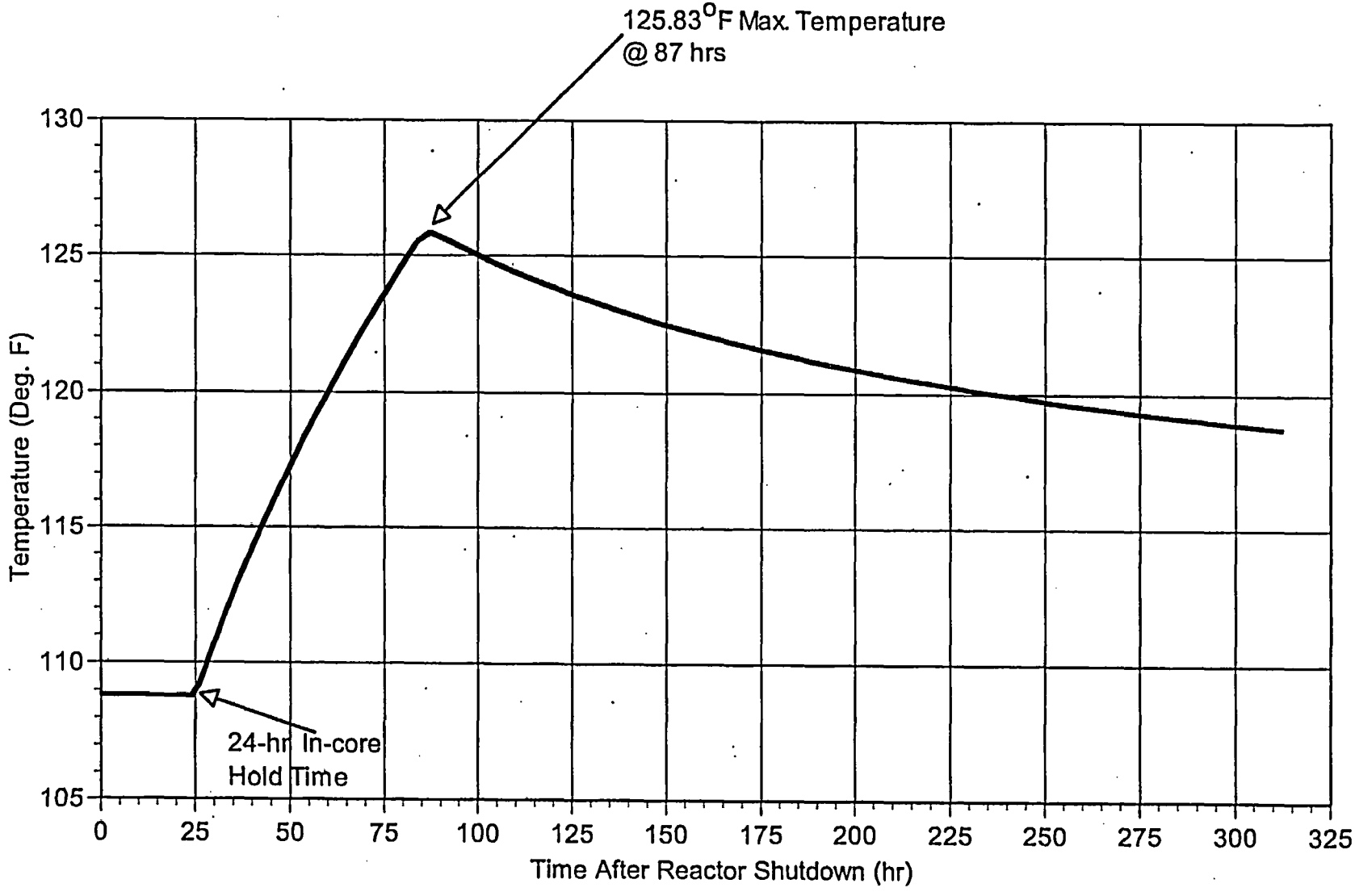

FIGURE 5.4.2: NORMAL DISCHARGE SCENARIO BULK POOL TEMPERATURE PLOT

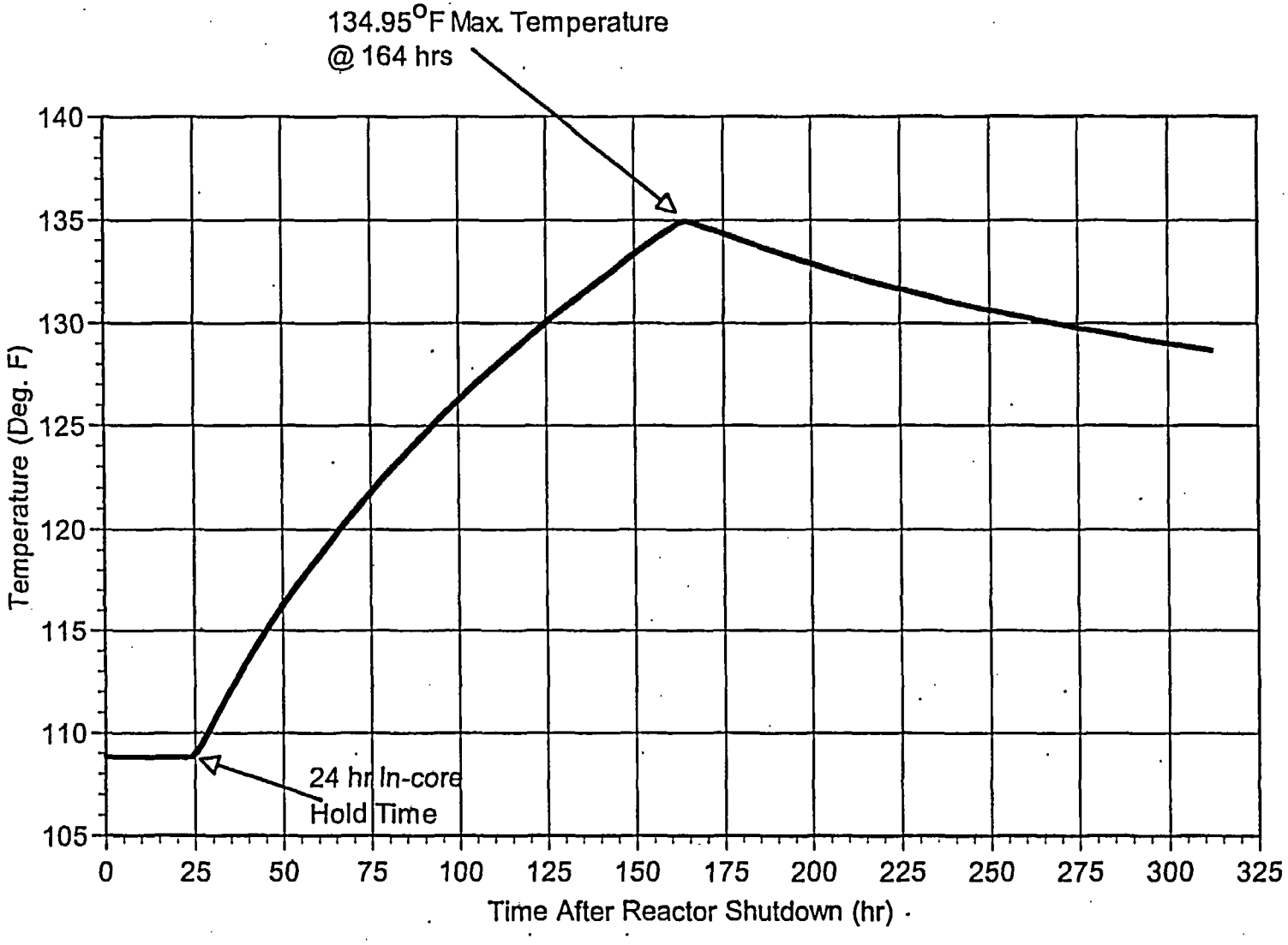

FIGURE 5.4.3: FULL CORE DISCHARGE SCENARIO BULK POOL TEMPERATURE PLOT

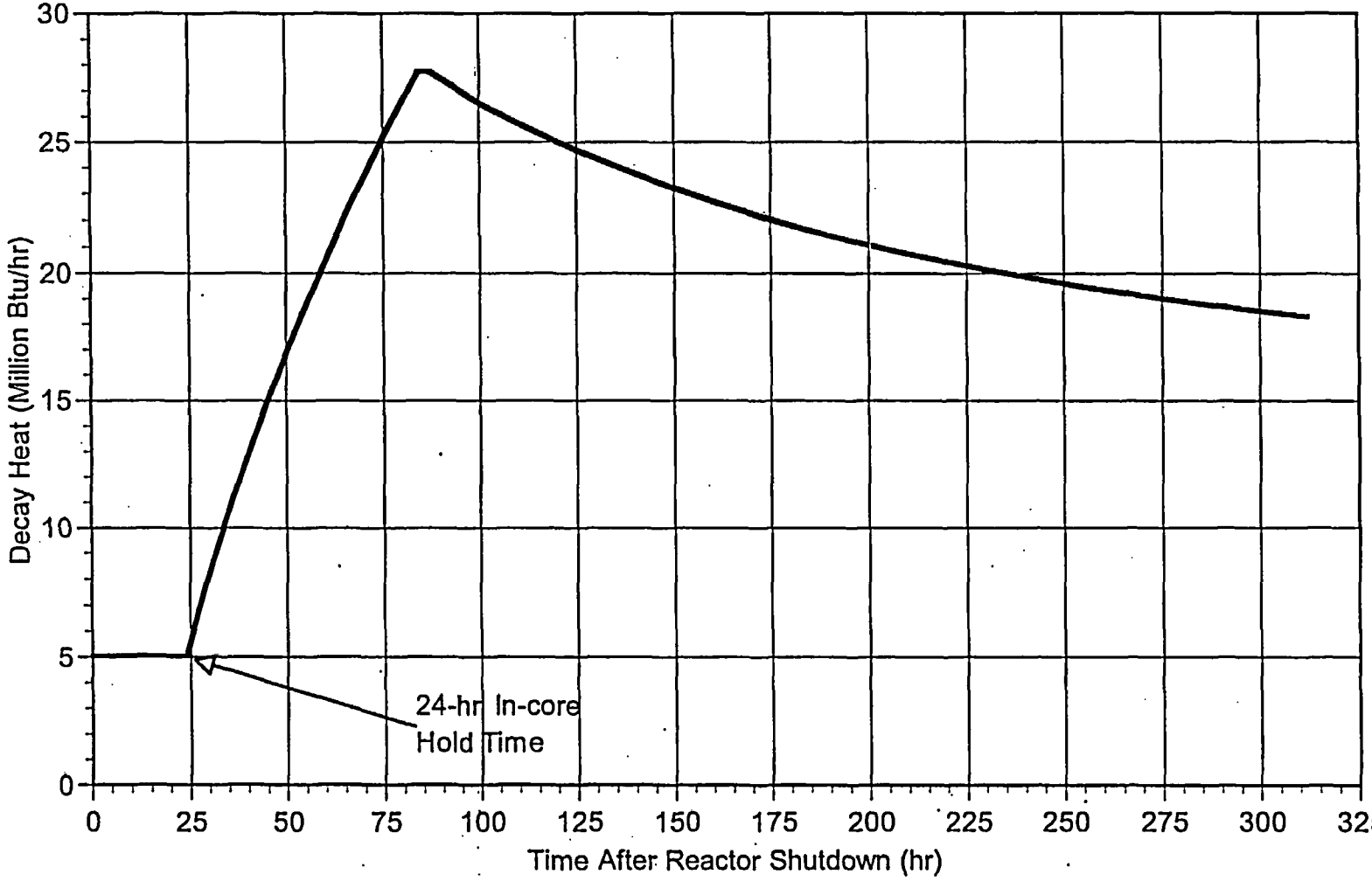

FIGURE 5.4.4: NORMAL DISCHARGE SCENARIO FUEL POOL DECAY HEAT PLOT

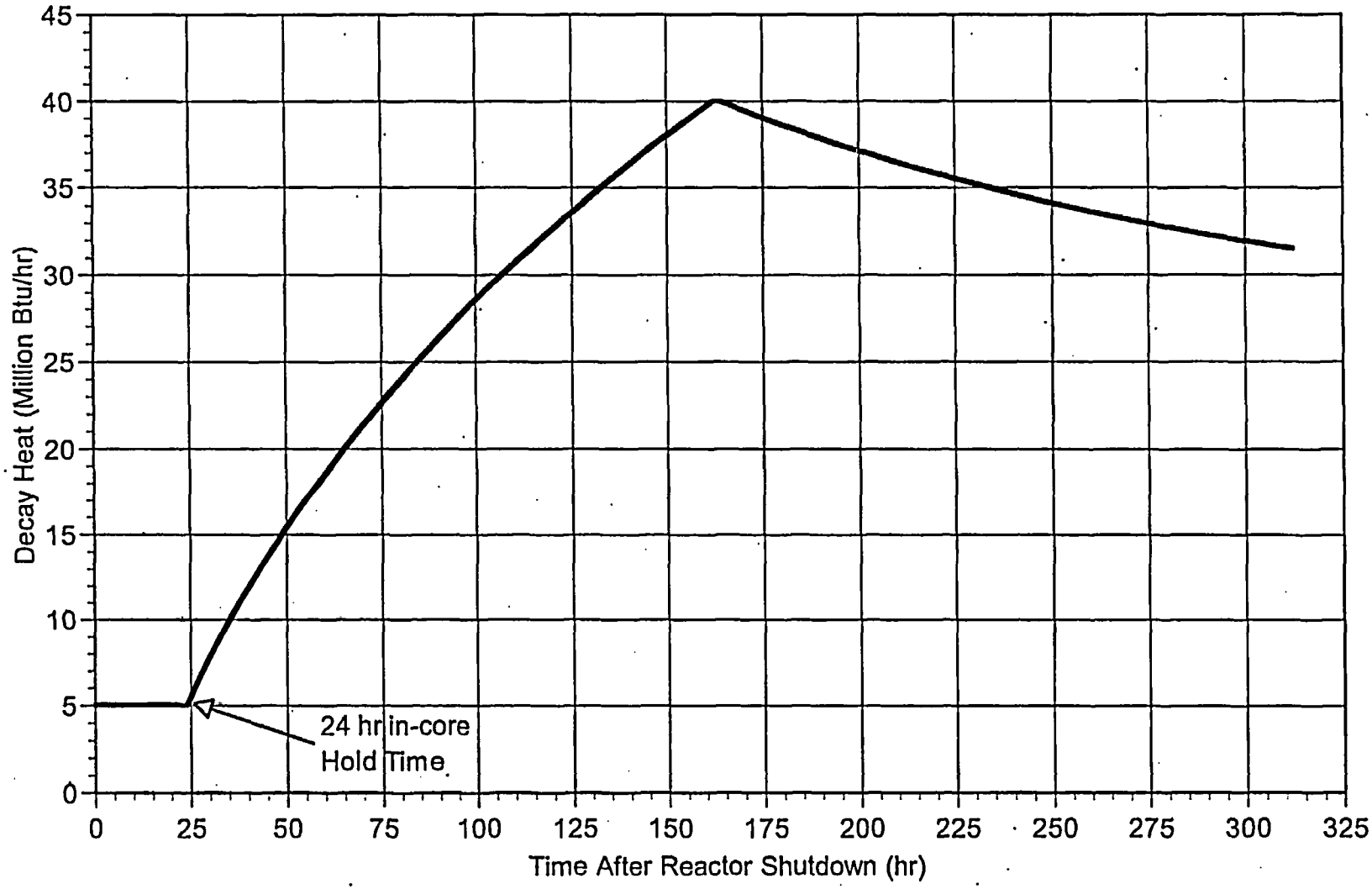

FIGURE 5.4.5: FULL CORE DISCHARGE SCENARIO POOL DECAY HEAT PLOT

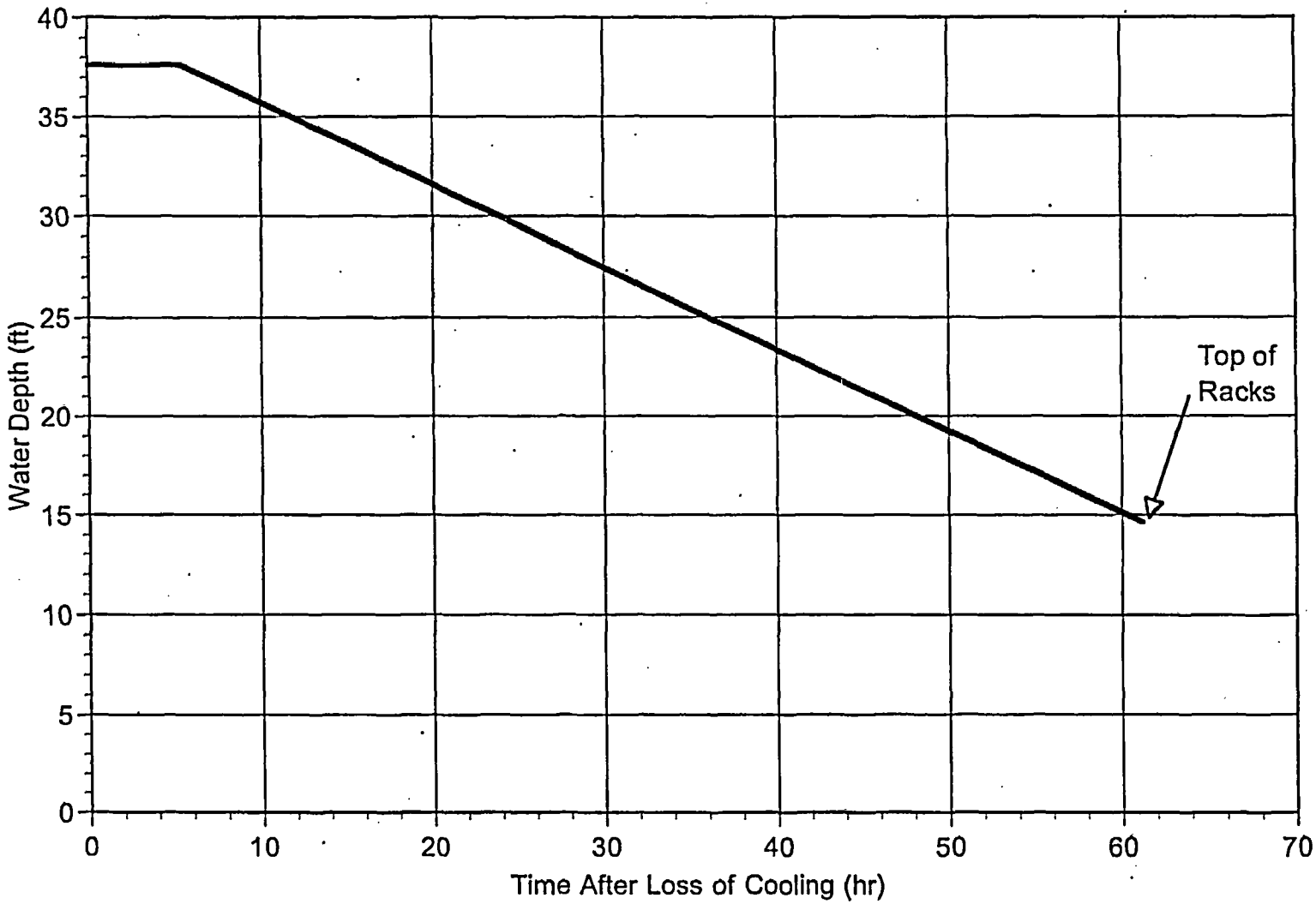

FIGURE 5.4.6: WATER DEPTH PLOT IN A LOSS OF COOLING EVENT (CASE I)

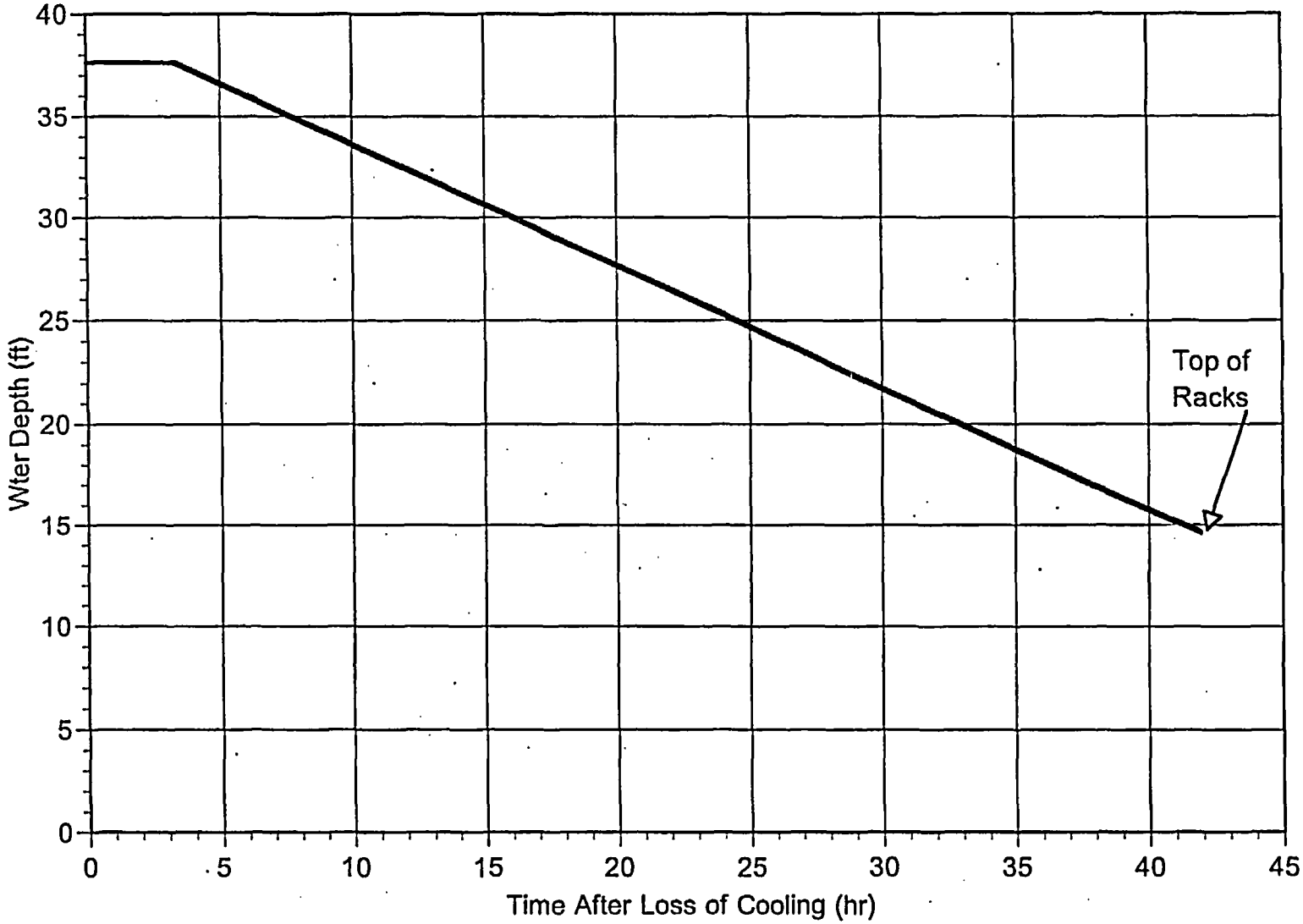

FIGURE 5.4.7: WATER DEPTH PLOT IN A LOSS OF COOLING EVENT (CASE II)

Figure 5.5.1

Proprietary Figure

Figure 5.5.2

Proprietary Figure

Figure 5.5.3

Proprietary Figure

6.0 STRUCTURAL/SEISMIC CONSIDERATIONS

6.1 Introduction

This section considers the structural adequacy of the new Spent Fuel Pool (SFP) maximum density spent fuel racks under all loadings postulated for normal, seismic, and accident conditions at the Clinton Power Station (CPS). New racks will be placed in both the SFP and the Fuel Cask Storage Pool in two phases, as discussed in Section 1.0. The module layouts for both phases are illustrated in Figures 1.1.1 thru 1.1.3.

In order to evaluate interim configurations encountered during periods wherein the full complement of racks is not yet installed, additional single rack evaluations are performed. During the structural evaluation of the racks, the input parameters affecting the dynamic rack response are varied to determine the set of characteristics resulting in greatest displacement at the top of the racks for both the Operating Basis Earthquake (OBE) and the Safe Shutdown Earthquake (SSE). Following this determination, single rack analyses with increased earthquake excitation are performed for those cases to conservatively establish the overturning safety factor of the racks.

The analyses undertaken to confirm the structural integrity of the racks, are performed in compliance with the USNRC Standard Review Plan (SRP) [6.1.1] and the OT Position Paper [6.1.2]. An abstract of the methodology, modeling assumptions, key results, and summary of the parametric evaluation is presented. Delineation of the relevant criteria is discussed in the text associated with each analysis.

6.2 Overview of Rack Structural Analysis Methodology

The response of a free-standing rack module to seismic inputs is highly nonlinear and involves a complex combination of motions (sliding, rocking, twisting, and turning), resulting in potential impacts and friction effects. Some of the unique attributes of the rack dynamic behavior include a large fraction of the total structural mass in a confined rattling motion, friction support of rack pedestals against lateral motion, and large fluid coupling effects due to deep submergence and independent motion of closely spaced adjacent structures.

Linear methods, such as modal analysis and response spectrum techniques, cannot accurately simulate the structural response of such a highly nonlinear structure to seismic excitation. An accurate simulation is obtained only by direct integration of the nonlinear equations of motion with the three pool slab acceleration time-histories applied as the forcing functions acting simultaneously.

Whole Pool Multi-Rack (WPMR) analysis is the vehicle utilized in this project to simulate the dynamic behavior of the complex storage rack structures. The following sections provide the basis for this selection and discussion on the development of the methodology.

6.2.1 Background of Analysis Methodology

Reliable assessment of the stress field and kinematic behavior of the rack modules calls for a conservative dynamic model incorporating all *key attributes* of the actual structure. This means that the model must feature the ability to execute the concurrent motion forms compatible with the free-standing installation of the modules.

The model must possess the capability to effect momentum transfers which occur due to rattling of fuel assemblies inside storage cells and the capability to simulate lift-off and subsequent impact of support pedestals with the pool liner (or bearing pad). The contribution of the water mass in the interstitial spaces around the rack modules and within the storage cells must be

modeled in an accurate manner, since erring in quantification of fluid coupling on either side of the actual value is no guarantee of conservatism.

The Coulomb friction coefficient at the pedestal-to-pool liner (or bearing pad) interface may lie in a rather wide range and a conservative value of friction cannot be prescribed *a priori*. In fact, a perusal of results of rack dynamic analyses in numerous dockets (Table 6.2.1) indicates that an upper bound value of the coefficient of friction often maximizes the computed rack displacements as well as the corresponding elastostatic stresses.

In short, there are a large number of parameters with potential influence on the rack kinematics. The comprehensive structural evaluation must deal with all of these without sacrificing conservatism.

The three-dimensional single rack dynamic model introduced by Holtec International in the Enrico Fermi Unit 2 rack project (ca. 1980) and used in some 50 rerack projects since that time (Table 6.2.1) addresses most of the abovementioned array of parameters. The details of this methodology are also published in the permanent literature [6.2.1]. Despite the versatility of the 3-D seismic model, the accuracy of the single rack simulations has been suspect due to one key element; namely, hydrodynamic participation of water around the racks. During dynamic rack motion, hydraulic energy is either drawn from or added to the moving rack, modifying its submerged motion in a significant manner. Therefore, the dynamics of one rack affects the motion of all others in the pool.

A dynamic simulation, which treats only one rack, or a small grouping of racks, is intrinsically inadequate to predict the motion of rack modules with any quantifiable level of accuracy. Three-dimensional Whole Pool Multi-Rack analyses carried out on several previous plants demonstrate that single rack simulations under predict rack displacement during seismic responses [6.2.2].

Briefly, the 3-D rack model dynamic simulation, involving one or more spent fuel racks, handles the array of variables as follows:

Interface Coefficient of Friction Parametric runs are made with upper bound and lower bound values of the coefficient of friction. The limiting values are based on experimental data which have been found to be bounded by the values 0.2 and 0.8. Simulations are also performed with the array of pedestals having randomly chosen coefficients of friction in a Gaussian distribution with a mean of 0.5 and lower and upper limits of 0.2 and 0.8, respectively. In the fuel rack simulations, the Coulomb friction interface between rack support pedestal and liner is simulated by piecewise linear (friction) elements. These elements function only when the pedestal is physically in contact with the pool liner or bearing pad.

Rack Beam Behavior Rack elasticity, relative to the rack base, is included in the model by introducing linear springs to represent the elastic bending action, twisting, and extensions.

Impact Phenomena Compression-only gap elements are used to provide for opening and closing of interfaces such as the pedestal-to-bearing pad interface, and the fuel assembly-to-cell wall interface. These interface gaps are modeled using nonlinear spring elements. The term "nonlinear spring" is a generic term used to denote the mathematical representation of the condition where a restoring force is not linearly proportional to displacement.

Fuel Loading Scenarios The fuel assemblies are conservatively assumed to rattle in unison which obviously exaggerates the contribution of impact against the cell wall.

Fluid Coupling Holtec International extended Fritz's classical two-body fluid coupling model to multiple bodies and utilized it to perform the first two-dimensional multi-rack analysis (Diablo Canyon, ca. 1987). Subsequently, laboratory experiments were conducted to validate the multi-rack fluid coupling theory. This technology was incorporated in the computer code DYNARACK [6.2.4] which handles simultaneous simulation of all racks in the pool as a Whole Pool Multi-Rack 3-D analysis. This development was first utilized in Chinshan, Oyster Creek, and Harris plants [6.2.1, 6.2.3] and, subsequently, in numerous other rerack projects. The

WPMR analyses have corroborated the accuracy of the single rack 3-D solutions in predicting the maximum structural stresses, and also serve to improve predictions of rack kinematics.

For closely spaced racks, demonstration of kinematic compliance is verified by including all modules in one comprehensive simulation using a WPMR model. In WPMR analysis, all rack modules in the pool are modeled and evaluated simultaneously and the coupling effect due to this multi-body motion is included in the analysis. Due to the superiority of this technique in predicting the dynamic behavior of closely spaced submerged storage racks, the Whole Pool Multi-Rack analysis methodology is used to evaluate the configurations of the storage racks subsequent to the completion of the reracking process, as shown in Figures 1.1.1 through 1.1.3. Additional, more conservative, single rack analyses are performed to confirm kinematic stability under the most adverse conditions such as fuel loading eccentricities and interim reracking configurations.

6.3 Description of Racks

The racks in the SFP and the Fuel Cask Storage Pool are analyzed as follows:

RACK WEIGHT DATA

Rack #/Module I.D.	Cells/Module	Array Size	Empty Rack Dry Weight (lbs)
1-3/F1-F3	150	15x10	14,142
4/H	110	11x10	10,637
5-7,9-11,13-16/G1-G10	180	15x12	16,737
8/J1	132	11x12	12,558
12/J2	144	15x12	13,769
17-19,22-24/B1-B3,A2-A3,C1	120	12x10	14,467
20,21,25,26/D1-D4	110	11x10	13,381
CP1,CP3/A4,B5	132	11x12	15,761
CP2/B4	99	11x9	12,190

For the purpose of analytical modeling, the racks in all cases addressed are numbered. Rack #1 is in the northwest corner of either the SFP or Fuel Cask Storage Pool. The numbering progresses west to east, continuing with the west most rack in the next row to the south, etc.. Thus for the SFP case module H, in the northeast corner, is Rack #4 and module D4 in the southeast corner is Rack #26. In Fuel Cask Storage Pool cases, modules G7 and G8 are Rack #1 and Rack #2, respectively, in Phase 1. In Phase 2, referring to Figure 1.1.3, the existing rack identities of CP1 thru CP3 are given above.

Rack material is defined in Table 6.3.1.

The cartesian coordinate system utilized within the rack dynamic model has the following nomenclature:

x = Horizontal axis along plant East
y = Horizontal axis along plant North
z = Vertical axis upward from the rack base

6.4 Synthetic Time-Histories

The synthetic time-histories in three orthogonal directions (N-S, E-W, and vertical) are generated in accordance with the provisions of SRP Section 3.7.1 [6.1.1]. In order to prepare an acceptable set of acceleration time-histories, Holtec International's proprietary code GENEQ [6.4.1] is utilized.

A preferred criterion for the synthetic time-histories in SRP 3.7.1 calls for both the response spectrum and the power spectral density corresponding to the generated acceleration time-history to envelope their target (design basis) counterparts with only finite enveloping infractions. The time-histories for the pools have been generated to satisfy this preferred criterion. The seismic files also satisfy the requirements of statistical independence mandated by SRP 3.7.1.

Figures 6.4.1 through 6.4.3 provide plots of the time-history accelerograms which were generated over a 20 second duration for the SSE event. Figures 6.4.4 through 6.4.6 provide plots of the time-history accelerograms which were generated over a 20 second duration for the OBE event. These artificial time-histories are used in all non-linear dynamic simulations of the racks.

Results of the correlation function of the three time-histories are given in Table 6.4.1. Absolute values of the correlation coefficients are shown to be less than 0.15, indicating that the desired statistical independence of the three data sets has been met.

6.5 WPMR Methodology

Recognizing that the analytical work effort must deal with both stress and displacement criteria, the sequence of model development and analysis steps that are undertaken are summarized in the following:

a. Prepare 3-D dynamic models suitable for a time-history analysis of the new maximum density racks. These models include the assemblage of all rack modules in each pool. Include all fluid coupling interactions and mechanical coupling appropriate to performing an accurate non-linear simulation. This 3-D simulation is referred to as a Whole Pool Multi-Rack model.

b. Perform 3-D dynamic analyses on various physical conditions (such as coefficient of friction and extent of cells containing fuel assemblies). Archive appropriate displacement and load outputs from the dynamic model for post-processing.

c. Perform stress analysis of high stress areas for the limiting case of all the rack dynamic analyses. Demonstrate compliance with ASME Code Section III, Subsection NF limits on stress and displacement.

6.5.1 Model Details for Spent Fuel Racks

The dynamic modeling of the rack structure is prepared with special consideration of all nonlinearities and parametric variations. Particulars of modeling details and assumptions for the Whole Pool Multi-Rack analysis of racks are given in the following:

6.5.1.1 Assumptions

a. The fuel rack structure motion is captured by modeling the rack as a 12 degree-of-freedom structure. Movement of the rack cross-section at any height is described by six degrees-of-freedom of the rack base and six degrees-of-freedom at the rack top. In this manner, the response of the module, relative to the base-plate, is captured in the dynamic analyses once suitable springs are introduced to couple the rack degrees-of-freedom and simulate rack stiffness.

b. Rattling fuel assemblies within the rack are modeled by five lumped masses located at H, .75H, .5H, .25H, and at the rack base (H is the rack height measured

above the base-plate). Each lumped fuel mass has two horizontal displacement degrees-of-freedom. Vertical motion of the fuel assembly mass is assumed equal to rack vertical motion at the base-plate level. The centroid of each fuel assembly mass can be located off-center, relative to the rack structure centroid at that level, to simulate a partially loaded rack.

c. Seismic motion of a fuel rack is characterized by random rattling of fuel assemblies in their individual storage locations. All fuel assemblies are assumed to move in-phase within a rack. This exaggerates computed dynamic loading on the rack structure and, therefore, yields conservative results.

d. Fluid coupling between the rack and fuel assemblies, and between the rack and wall, is simulated by appropriate inertial coupling in the system kinetic energy. Inclusion of these effects uses the methods of [6.5.2, 6.5.3] for rack/assembly coupling and for rack-to-rack coupling.

e. Fluid damping and form drag are conservatively neglected.

f. Sloshing is found to be negligible at the top of the rack and is, therefore, neglected in the analysis of the rack.

g. Potential impacts between the cell walls of the new racks and the contained fuel assemblies are accounted for by appropriate compression-only gap elements between the masses involved. The possible incidence of rack-to-wall or rack-to-rack impact is simulated by gap elements at the top and bottom of the rack in two horizontal directions. Bottom gap elements are located at the base-plate elevation. The initial gaps reflect the presence of baseplate extensions, and the rack stiffnesses are chosen to simulate local structural detail.

h. Pedestals are modeled by gap elements in the vertical direction and as "rigid links" for transferring horizontal stress. The base of each pedestal support is linked to the pool liner (or bearing pad) by two friction springs. The spring rate for the friction springs includes any lateral elasticity of the pedestals. Local pedestal vertical spring stiffness accounts for floor elasticity and for local rack elasticity just above the pedestal.

i. Rattling of fuel assemblies inside the storage locations causes the gap between fuel assemblies and cell wall to change from a maximum of twice the nominal gap to a theoretical zero gap. Fluid coupling coefficients are based on the nominal gap in order to provide a conservative measure of fluid resistance to gap closure.

j. The model for the rack is considered supported, at the base level, on four pedestals modeled as non-linear compression only gap spring elements and eight piecewise linear friction spring elements. These elements are properly located

with respect to the centerline of the rack beam, and allow for arbitrary rocking and sliding motions.

6.5.1.2 Element Details

Figure 6.5.1 shows a schematic of the dynamic model of a single rack. The schematic depicts many of the characteristics of the model including all of the degrees-of-freedom and some of the spring restraint elements.

Table 6.5.1 provides a complete listing of each of the 22 degrees-of-freedom for a rack model. Six translational and six rotational degrees-of-freedom (three of each type on each end) describe the motion of the rack structure. Rattling fuel mass motions (shown at nodes 1^*, 2^*, 3^*, 4^*, and 5^* in Figure 6.5.1) are described by ten horizontal translational degrees-of-freedom (two at each of the five fuel masses). The vertical fuel mass motion is assumed (and modeled) to be the same as that of the rack baseplate.

Figure 6.5.2 depicts the fuel to rack impact springs (used to develop potential impact loads between the fuel assembly mass and rack cell inner walls) in a schematic isometric. Only one of the five fuel masses is shown in this figure. Four compression only springs, acting in the horizontal direction, are provided at each fuel mass.

Figure 6.5.3 provides a 2-D schematic elevation of the storage rack model, discussed in more detail in Section 6.5.3. This view shows the vertical location of the five storage masses and some of the support pedestal spring members.

Figure 6.5.4 shows the modeling technique and degrees-of-freedom associated with rack elasticity. In each bending plane a shear and bending spring simulate elastic effects [6.5.4]. Linear elastic springs coupling rack vertical and torsional degrees-of-freedom are also included in the model.

Figure 6.5.5 depicts the inter-rack impact springs (used to develop potential impact loads between racks or between rack and wall).

6.5.2 Fluid Coupling Effect

In its simplest form, the so-called "fluid coupling effect" [6.5.2, 6.5.3] can be explained by considering the proximate motion of two bodies under water. If one body (mass m_1) vibrates adjacent to a second body (mass m_2), and both bodies are submerged in frictionless fluid, then Newton's equations of motion for the two bodies are:

$(m_1 + M_{11})A_1 + M_{12}A_2 =$ applied forces on mass $m_1 + O(X_1^2)$

$M_{21} A_1 + (m_2 + M_{22}) A_2 =$ applied forces on mass $m_2 + O(X_2^2)$

A_1 and A_2 denote absolute accelerations of masses m_1 and m_2, respectively, and the notation $O(X^2)$ denotes nonlinear terms.

M_{11}, M_{12}, M_{21}, and M_{22} are fluid coupling coefficients which depend on body shape, relative disposition, etc. Fritz [6.5.3] gives data for M_{ij} for various body shapes and arrangements. The fluid adds mass to the body (M_{11} to mass m_1), and an inertial force proportional to acceleration of the adjacent body (mass m_2). Thus, acceleration of one body affects the force field on another. This force field is a function of inter-body gap, reaching large values for small gaps. Lateral motion of a fuel assembly inside a storage location encounters this effect. For example, fluid coupling behavior will be experienced between nodes 2 and 2* in Figure 6.5.1. The rack analysis also contains inertial fluid coupling terms, which model the effect of fluid in the gaps between adjacent racks.

Terms modeling the effects of fluid flowing between adjacent racks in a single rack analysis suffer from the inaccuracies described earlier. These terms are usually computed assuming that all racks adjacent to the rack being analyzed are vibrating in-phase or 180° out of phase. The WPMR analyses do not require any assumptions with regard to phase.

Rack-to-rack gap elements have initial gaps set to 100% of the physical gap between the racks or between outermost racks and the adjacent pool walls.

6.5.2.1 Multi-Body Fluid Coupling Phenomena

During the seismic event, all racks in the pool are subject to the input excitation simultaneously. The motion of each free-standing module would be autonomous and independent of others as long as they did not impact each other and no water were present in the pool. While the scenario of inter-rack impact is not a common occurrence and depends on rack spacing, the effect of water (the so-called fluid coupling effect) is a universal factor. As noted in Ref. [6.5.2, 6.5.4], the fluid forces can reach rather large values in closely spaced rack geometries. It is, therefore, essential that the contribution of the fluid forces be included in a comprehensive manner. This is possible only if all racks in the pool are *allowed* to execute 3-D motion in the mathematical model. For this reason, single rack or even multi-rack models involving only a portion of the racks in the pool, are inherently inaccurate. The Whole Pool Multi-Rack model removes this intrinsic limitation of the rack dynamic models by simulating the 3-D motion of all modules simultaneously. The fluid coupling effect, therefore, encompasses interaction between *every* set of racks in the pool, i.e., the motion of one rack produces fluid forces on all other racks and on the pool walls. Stated more formally, both near-field and far-field fluid coupling effects are included in the analysis.

The derivation of the fluid coupling matrix [6.5.5] relies on the classical inviscid fluid mechanics principles, namely the principle of continuity and Kelvin's recirculation theorem. The derivation of the fluid coupling matrix has been verified by an extensive set of shake table experiments [6.5.5].

6.5.3 Stiffness Element Details

Three element types are used in the rack models. Type 1 are linear elastic elements used to represent the beam-like behavior of the integrated rack cell matrix. Type 2 elements are the piece-wise linear friction springs used to develop the appropriate forces between the rack pedestals and the supporting bearing pads. Type 3 elements are non-linear gap elements, which model gap closures and subsequent impact loadings i.e., between fuel assemblies and the storage cell inner walls, and rack outer periphery spaces.

If the simulation model is restricted to two dimensions (one horizontal motion plus one vertical motion, for example), for the purposes of model clarification only, then Figure 6.5.3 describes the configuration. This simpler model is used to elaborate on the various stiffness modeling elements.

Type 3 gap elements modeling impacts between fuel assemblies and racks have local stiffness K_i in Figure 6.5.3. Support pedestal spring rates K_S are modeled by type 3 gap elements. Local compliance of the concrete floor is included in K_S. The type 2 friction elements are shown in Figure 6.5.3 as K_f. The spring elements depicted in Figure 6.5.4 represent linear type 1 elements.

Friction at support/liner interface is modeled by the piecewise linear friction springs with suitably large stiffness K_f up to the limiting lateral load μN, where N is the current compression load at the interface between support and liner. At every time-step during transient analysis, the current value of N (either zero if the pedestal has lifted off the liner/bearing pad, or a compressive finite value) is computed.

The gap element K_S, modeling the effective compression stiffness of the structure in the vicinity of the support, includes stiffness of the pedestal, local stiffness of the underlying pool slab, and local stiffness of the rack cellular structure above the pedestal.

The previous discussion is limited to a 2-D model solely for simplicity. Actual analyses incorporate 3-D motions.

6.5.4 Coefficients of Friction

To eliminate the last significant element of uncertainty in rack dynamic analyses, multiple simulations are performed to adjust the friction coefficient ascribed to the support pedestal/pool bearing pad interface. These friction coefficients are chosen consistent with the two bounding extremes from Rabinowicz's data [6.5.1]. Simulations are also performed by imposing intermediate value friction coefficients, both 0.5 and those developed by a random number generator with Gaussian normal distribution characteristics. The assigned values are then held

constant during the entire simulation in order to obtain reproducible results.† Thus, in this manner, the WPMR analysis results are brought closer to the realistic structural conditions.

The coefficient of friction (μ) between the pedestal supports and the pool floor is indeterminate. According to Rabinowicz [6.5.1], results of 199 tests performed on austenitic stainless steel plates submerged in water show a mean value of μ to be 0.503 with standard deviation of 0.125. Upper and lower bounds (based on twice standard deviation) are 0.753 and 0.253, respectively. Analyses are therefore performed for coefficient of friction values of 0.2 (lower limit), 0.5 and 0.8 (upper limit), as well as for random friction values clustered about a mean of 0.5. The bounding values of μ = 0.2 and 0.8 have been found to envelope the upper limit of module response in previous rerack projects.

6.5.5 Governing Equations of Motion

Using the structural model discussed in the foregoing, equations of motion corresponding to each degree-of-freedom are obtained using Lagrange's Formulation [6.5.4]. The system kinetic energy includes contributions from solid structures and from trapped and surrounding fluid. The final system of equations obtained have the matrix form:

$$[M]\left[\frac{d^2 q}{d t^2}\right] = [Q] + [G]$$

where:

[M] - total mass matrix (including structural and fluid mass contributions). The size of this matrix will be 22n x22n for a WPMR analysis (n = number of racks in the model).

† It is noted that DYNARACK has the capability to change the coefficient of friction at any pedestal at each instant of contact based on a random reading of the computer clock cycle. However, exercising this option would yield results that could not be reproduced. Therefore, the random choice of coefficients is made only once per run.

q - the nodal displacement vector relative to the pool slab displacement (the term with q indicates the second derivative with respect to time, i.e., acceleration)

[G] - a vector dependent on the given ground acceleration

[Q] - a vector dependent on the spring forces (linear and nonlinear) and the coupling between degrees-of-freedom

The above column vectors have length 22n. The equations can be rewritten as follows:

$$\left[\frac{d^2q}{dt^2}\right] = [M]^{-1}[Q] + [M]^{-1}[G]$$

This equation set is mass uncoupled, displacement coupled at each instant in time. The numerical solution uses a central difference scheme built into the proprietary computer program DYNARACK [6.2.4].

6.6 Structural Evaluation of Spent Fuel Rack Design

6.6.1 Kinematic and Stress Acceptance Criteria

There are two sets of criteria to be satisfied by the rack modules:

a. Kinematic Criteria

An isolated fuel rack situated in the middle of the storage cavity is most vulnerable to overturning because such a rack would be hydrodynamically uncoupled from any adjacent structures. Therefore, to assess the margin against overturning, a single rack module is evaluated. Section IV(6) of Reference [6.1.2]

refers to the SRP for safety factors against rack overturning. According to SRP Section 3.8.5.II-5 [6.1.1], the minimum required safety margins under the OBE and SSE events are 1.5 and 1.1, respectively. In order to ensure that these safety factors are met, the simulations resulting in the highest top of rack displacements were re-performed with an earthquake excitation multiplier of, conservatively, 1.5 for both OBE and SSE. The maximum rotations of the rack (about the two principal axes) are obtained from a post processing of the rack time history response output. The ratio of the rotation required to produce incipient tipping in either principal plane to the actual maximum rotation in that plane from the time history solution is the margin of safety. Since the factors of safety are conservatively embedded in the earthquake multipliers, meeting the acceptance criteria is established by the ratio described above being greater than 1.0.

b. Stress Limit Criteria

Stress limits must not be exceeded under the postulated load combinations provided herein.

6.6.2 Stress Limit Evaluations

The stress limits presented below apply to the rack structure and are derived from the ASME Code, Section III, Subsection NF, 2001 [6.6.1] for the new racks, and 1977 [6.6.3] for existing racks. Parameters and terminology are in accordance with the ASME Code. Material properties are obtained from the ASME Code Appendices [6.6.2], and are listed in Table 6.3.1.

(i) Normal Conditions (Level A)

a. Allowable stress in tension on a net section is:

$F_t = 0.6\ S_y$

Where, S_y = yield stress at temperature, and F_t is equivalent to primary membrane stress.

b. Allowable stress in shear on a net section is:

$F_v = 0.4\ S_y$

c. Allowable stress in compression on a net section is:

$$F_a = S_y\left(.47 - \frac{kl}{444\ r}\right)$$

where kl/r for the main rack body is based on the full height and cross section of the honeycomb region and does not exceed 120 for all sections.

l = unsupported length of component

k = length coefficient which gives influence of boundary conditions. The following values are appropriate for the described end conditions:

1 (simple support both ends)

2 (cantilever beam)

½ (clamped at both ends)

r = radius of gyration of component

d. Maximum allowable bending stress at the outermost fiber of a net section, due to flexure about one plane of symmetry is:

$F_b = 0.60\ S_y$ (equivalent to primary bending)

e. Combined bending and compression on a net section satisfies:

$$\frac{f_a}{F_a} + \frac{C_{mx}\ f_{bx}}{D_x\ F_{bx}} + \frac{C_{my}\ f_{by}}{D_y\ F_{by}} < 1$$

where:

f_a = Direct compressive stress in the section

f_{bx} = Maximum bending stress along x-axis

f_{by} = Maximum bending stress along y-axis

C_{mx} = 0.85

C_{my} = 0.85

D_x = $1 - (f_a/F'_{ex})$

D_y = $1 - (f_a/F'_{ey})$

$F'_{ex,ey}$ = $(\pi^2\ E)/(2.15\ (kl/r)^2_{x,y})$

E = Young's Modulus

and subscripts x,y reflect the particular bending plane.

f. Combined flexure and compression (or tension) on a net section:

$$\frac{f_a}{0.6S_y} + \frac{f_{bx}}{F_{bx}} + \frac{f_{by}}{F_{by}} < 1.0$$

The above requirements are to be met for both direct tension or compression.

g. Welds

Allowable maximum shear stress on the net section of a weld is given by:

$F_w = 0.3\ S_u$

where S_u is the weld material ultimate strength at temperature. For fillet weld legs in contact with base metal, the shear stress on the gross section is limited to $0.4S_y$, where S_y is the base material yield strength at temperature.

h. Bearing

Allowable maximum stress for bearing on a contact area is given by:

$F_p = 0.9\ S_u$

(ii) Level B Service Limits (Upset Conditions, including OBE)

Section NF-3321 (ASME Section III, Subsection NF [6.6.1]) states that, for the Level B condition, the allowable stresses for those given above in (i) may be increased by a factor of 1.33.

(iii) Level D Service Limits (including SSE)

Section F-1334 (ASME Section III, Appendix F [6.6.2]), states that limits for the Level D condition are the smaller of 2 or $1.167S_u/S_y$ times the corresponding limits for the Level A condition if $S_u > 1.2S_y$, or 1.4 if S_u less than or equal $1.2S_y$ except for requirements specifically listed below. S_u ,S_y are the ultimate strength and yield strength at the

specified rack design temperature. Examination of material properties for 304L stainless demonstrates that 1.2 times the yield strength is less than the ultimate strength. Therefore, the Level D stress limits are double the correponding Level A limits.

Exceptions to the above general multiplier are the following:

a) Stresses in shear shall not exceed the lesser of $0.72S_y$ or $0.42S_u$. In the case of the Austenitic Stainless material used here, $0.72S_y$ governs.

b) Axial Compression Loads shall be limited to 2/3 of the calculated buckling load.

c) Combined Axial Compression and Bending - The equations for Level A conditions shall apply except that:

F_a = 0.667 x Buckling Load/ Gross Section Area,
and the terms F'_{ex} and F'_{ey} may be increased by the factor 1.65.

d) For welds, the Level D allowable maximum weld stress is not specified in Appendix F of the ASME Code. An appropriate limit for weld throat stress is conservatively set here as:

$F_w = (0.3\ S_u)$ x factor

where:

factor = (Level D shear stress limit)/(Level A shear stress limit)

6.6.3 Dimensionless Stress Factors

For convenience, the stress results are in dimensionless form. Dimensionless stress factors are defined as the ratio of the actual developed stress to the specified limiting stress value. The limiting value of each stress factor is 1.0. Stress factors are determined as follows:

R_1 = Ratio of direct tensile or compressive stress on a net section to its allowable value (note pedestals only resist compression)

R_2 = Ratio of gross shear on a net section in the x-direction to its allowable value

R_3 = Ratio of maximum x-axis bending stress to its allowable value for the section

R_4 = Ratio of maximum y-axis bending stress to its allowable value for the section

R_5 = Combined flexure and compressive factor (as defined in the foregoing)

R_6 = Combined flexure and tension (or compression) factor (as defined in the foregoing)

R_7 = Ratio of gross shear on a net section in the y-direction to its allowable value

6.6.4 Loads and Loading Combinations for Spent Fuel Racks

The applicable loads and their combinations, which must be considered in the seismic analysis of rack modules, are excerpted from the OT Position [6.1.3] and SRP, Section 3.8.4 [6.1.2]. The load combinations considered are identified below:

Loading Combination	Service Level
$D + L$ $D + L + T_o$ $D + L + T_o + E$	Level A
$D + L + T_a + E$ $D + L + T_o + P_f$	Level B
$D + L + T_a + E'$ $D + L + T_o + F_d$	Level D The functional capability of the fuel racks must be demonstrated. This load case is discussed in Section 7.0.

Where:

- D = Dead weight-induced loads (including fuel assembly weight)
- L = Live Load (not applicable for the fuel rack, since there are no moving objects in the rack load path)
- P_f = Upward force on the racks caused by postulated stuck fuel assembly
- F_d = Impact force from accidental drop of the heaviest load from the maximum possible height.
- E = Operating Basis Earthquake (OBE)
- E' = Safe Shutdown Earthquake (SSE)
- T_o = Differential temperature induced loads (normal operating or shutdown condition based on the most critical transient or steady state condition)
- T_a = Differential temperature induced loads (the highest temperature associated with the postulated abnormal design conditions)

T_a and T_o produce local thermal stresses. The worst thermal stress field in a fuel rack is obtained when an isolated storage location has a fuel assembly generating heat at maximum postulated rate and surrounding storage locations contain no fuel. Heated water makes unobstructed contact with the inside of the storage walls, thereby producing maximum possible temperature difference between adjacent cells. Secondary stresses produced are limited to the body of the rack; that is, support pedestals do not experience secondary (thermal) stresses.

6.7 Parametric Simulations

The multiple rack models employ the fluid coupling effects for all racks in the pool, as discussed above, and these simulations are referred to as WPMR evaluations. In addition, single rack models are also developed for additional study of the effect of various parameters on rack displacement. The models are described as follows:

(I) Whole Pool Multi Rack Model Three models are develop for WPMR analysis. For the phase 1 case, two racks and the fuel transfer cask are present in the Fuel Cask Storage Pool. For phase 2, an array of twenty-six racks in the SFP and three racks in the Fuel Cask Storage Pool are modeled. In these cases, proper interface fluid gaps and a coefficient of friction at the support interface locations with the bearing pad generated by a Gaussian distribution random number generator with 0.5 as the mean and 0.15 standard deviation are implemented. The response to both SSE and OBE seismic excitation is determined.

(II) Single Rack Models : Two models are employed for studying the structural behavior of a single rack. A model is developed for the largest rack and another for the rack with the maximum aspect ratio (defined as the rack exhibiting the maximum ratio of the height to the smaller of the length or width). In both these models, the rack is modeled as fully loaded (to act as a baseline), half loaded (east-west, north-south and diagonally) and nearly empty. The coefficient of friction between male pedestal and bearing pad is taken as one of four possibilities: 0.2, 0.5, 0.8 or as selected by a Gaussian random number generator as introduced in the prior section. For these models, either in phase or opposed phase motion is assumed. The in phase case is implemented by assuming that the maximum actual water gaps that exist between the racks and the four walls of the SFP surround the single rack, in the same north-east-south-west orientation. This reflects the behavior that would occur if all the racks moved in unison. For the opposed phase case, one-half

the actual gap is attributed to each rack side. All single rack cases in the study are done for both SSE and OBE excitation.

(III) Single Rack Overturning Check Model This model is developed to study the potential for rack overturning. The SSE case which had the maximum displacement in the study is run, subjected to 1.5 times the SSE excitation and the OBE case which had the maximum displacement is run, subjected to 1.5 times the OBE excitation.

The Whole Pool and Single Rack simulations listed on the following tables have been performed to investigate the structural integrity of the rack arrays.

LIST OF WPMR SIMULATIONS			
Case	Load Case	COF	Event
1	Fuel Cask Storage Pool Phase 1 All Racks	Random	SSE
2	Fuel Cask Storage Pool Phase 1 All Racks	Random	OBE
3	SFP - All Racks Fully Loaded	Random	SSE
4	SFP - All Racks Fully Loaded	Random	OBE
5	Fuel Cask Storage Pool Phase 2 All Racks	Random	SSE
6	Fuel Cask Storage Pool Phase 2 All Racks	Random	OBE

LIST OF SINGLE RACK SIMULATIONS				
Case	Motion	Load Case	COF	Event
1	IN PHASE	Largest Rack Fully Loaded	Random	SSE
2	IN PHASE	Largest Rack Fully Loaded	0.2	SSE
3	IN PHASE	Largest Rack Fully Loaded	0.5	SSE
4	IN PHASE	Largest Rack Fully Loaded	0.8	SSE
5	IN PHASE	Largest Rack Half Loaded (E-W)	Random	SSE
6	IN PHASE	Largest Rack Half Loaded (E-W)	0.2	SSE
7	IN PHASE	Largest Rack Half Loaded (E-W)	0.5	SSE
8	IN PHASE	Largest Rack Half Loaded (E-W)	0.8	SSE
9	IN PHASE	Largest Rack Half Loaded (N-S)	Random	SSE
10	IN PHASE	Largest Rack Half Loaded (N-S)	0.2	SSE

LIST OF SINGLE RACK SIMULATIONS				
Case	Motion	Load Case	COF	Event
11	IN PHASE	Largest Rack Half Loaded (N-S)	0.5	SSE
12	IN PHASE	Largest Rack Half Loaded (N-S)	0.8	SSE
13	IN PHASE	Largest Rack Half Loaded (Diag)	Random	SSE
14	IN PHASE	Largest Rack Half Loaded (Diag)	0.2	SSE
15	IN PHASE	Largest Rack Half Loaded (Diag)	0.5	SSE
16	IN PHASE	Largest Rack Half Loaded (Diag)	0.8	SSE
17	IN PHASE	Largest Rack Nearly Empty	Random	SSE
18	IN PHASE	Largest Rack Nearly Empty	0.2	SSE
19	IN PHASE	Largest Rack Nearly Empty	0.5	SSE
20	IN PHASE	Largest Rack Nearly Empty	0.8	SSE
21	OPPOSED	Largest Rack Fully Loaded	Random	SSE
22	OPPOSED	Largest Rack Fully Loaded	0.2	SSE
23	OPPOSED	Largest Rack Fully Loaded	0.5	SSE
24	OPPOSED	Largest Rack Fully Loaded	0.8	SSE
25	OPPOSED	Largest Rack Half Loaded (E-W)	Random	SSE
26	OPPOSED	Largest Rack Half Loaded (E-W)	0.2	SSE
27	OPPOSED	Largest Rack Half Loaded (E-W)	0.5	SSE
28	OPPOSED	Largest Rack Half Loaded (E-W)	0.8	SSE
29	OPPOSED	Largest Rack Half Loaded (N-S)	Random	SSE
30	OPPOSED	Largest Rack Half Loaded (N-S)	0.2	SSE
31	OPPOSED	Largest Rack Half Loaded (N-S)	0.5	SSE
32	OPPOSED	Largest Rack Half Loaded (N-S)	0.8	SSE
33	OPPOSED	Largest Rack Half Loaded (Diag)	Random	SSE
34	OPPOSED	Largest Rack Half Loaded (Diag)	0.2	SSE
35	OPPOSED	Largest Rack Half Loaded (Diag)	0.5	SSE
36	OPPOSED	Largest Rack Half Loaded (Diag)	0.8	SSE
37	OPPOSED	Largest Rack Nearly Empty	Random	SSE
38	OPPOSED	Largest Rack Nearly Empty	0.2	SSE
39	OPPOSED	Largest Rack Nearly Empty	0.5	SSE

LIST OF SINGLE RACK SIMULATIONS				
Case	Motion	Load Case	COF	Event
40	OPPOSED	Largest Rack Nearly Empty	0.8	SSE
41	IN PHASE	Largest Rack Fully Loaded	Random	OBE
42	IN PHASE	Largest Rack Fully Loaded	0.2	OBE
43	IN PHASE	Largest Rack Fully Loaded	0.5	OBE
44	IN PHASE	Largest Rack Fully Loaded	0.8	OBE
45	IN PHASE	Largest Rack Half Loaded (E-W)	Random	OBE
46	IN PHASE	Largest Rack Half Loaded (E-W)	0.2	OBE
47	IN PHASE	Largest Rack Half Loaded (E-W)	0.5	OBE
48	IN PHASE	Largest Rack Half Loaded (E-W)	0.8	OBE
49	IN PHASE	Largest Rack Half Loaded (N-S)	Random	OBE
50	IN PHASE	Largest Rack Half Loaded (N-S)	0.2	OBE
51	IN PHASE	Largest Rack Half Loaded (N-S)	0.5	OBE
52	IN PHASE	Largest Rack Half Loaded (N-S)	0.8	OBE
53	IN PHASE	Largest Rack Half Loaded (Diag)	Random	OBE
54	IN PHASE	Largest Rack Half Loaded (Diag)	0.2	OBE
55	IN PHASE	Largest Rack Half Loaded (Diag)	0.5	OBE
56	IN PHASE	Largest Rack Half Loaded (Diag)	0.8	OBE
57	IN PHASE	Largest Rack Nearly Empty	Random	OBE
58	IN PHASE	Largest Rack Nearly Empty	0.2	OBE
59	IN PHASE	Largest Rack Nearly Empty	0.5	OBE
60	IN PHASE	Largest Rack Nearly Empty	0.8	OBE
61	OPPOSED	Largest Rack Fully Loaded	Random	OBE
62	OPPOSED	Largest Rack Fully Loaded	0.2	OBE
63	OPPOSED	Largest Rack Fully Loaded	0.5	OBE
64	OPPOSED	Largest Rack Fully Loaded	0.8	OBE
65	OPPOSED	Largest Rack Half Loaded (E-W)	Random	OBE
66	OPPOSED	Largest Rack Half Loaded (E-W)	0.2	OBE
67	OPPOSED	Largest Rack Half Loaded (E-W)	0.5	OBE
68	OPPOSED	Largest Rack Half Loaded (E-W)	0.8	OBE

LIST OF SINGLE RACK SIMULATIONS				
Case	Motion	Load Case	COF	Event
69	OPPOSED	Largest Rack Half Loaded (N-S)	Random	OBE
70	OPPOSED	Largest Rack Half Loaded (N-S)	0.2	OBE
71	OPPOSED	Largest Rack Half Loaded (N-S)	0.5	OBE
72	OPPOSED	Largest Rack Half Loaded (N-S)	0.8	OBE
73	OPPOSED	Largest Rack Half Loaded (Diag)	Random	OBE
74	OPPOSED	Largest Rack Half Loaded (Diag)	0.2	OBE
75	OPPOSED	Largest Rack Half Loaded (Diag)	0.5	OBE
76	OPPOSED	Largest Rack Half Loaded (Diag)	0.8	OBE
77	OPPOSED	Largest Rack Nearly Empty	Random	OBE
78	OPPOSED	Largest Rack Nearly Empty	0.2	OBE
79	OPPOSED	Largest Rack Nearly Empty	0.5	OBE
80	OPPOSED	Largest Rack Nearly Empty	0.8	OBE
81	IN PHASE	Aspect Rack Fully Loaded	Random	SSE
82	IN PHASE	Aspect Rack Fully Loaded	0.2	SSE
83	IN PHASE	Aspect Rack Fully Loaded	0.5	SSE
84	IN PHASE	Aspect Rack Fully Loaded	0.8	SSE
85	IN PHASE	Aspect Rack Half Loaded (E-W)	Random	SSE
86	IN PHASE	Aspect Rack Half Loaded (E-W)	0.2	SSE
87	IN PHASE	Aspect Rack Half Loaded (E-W)	0.5	SSE
88	IN PHASE	Aspect Rack Half Loaded (E-W)	0.8	SSE
89	IN PHASE	Aspect Rack Half Loaded (N-S)	Random	SSE
90	IN PHASE	Aspect Rack Half Loaded (N-S)	0.2	SSE
91	IN PHASE	Aspect Rack Half Loaded (N-S)	0.5	SSE
92	IN PHASE	Aspect Rack Half Loaded (N-S)	0.8	SSE
93	IN PHASE	Aspect Rack Half Loaded (Diag)	Random	SSE
94	IN PHASE	Aspect Rack Half Loaded (Diag)	0.2	SSE
95	IN PHASE	Aspect Rack Half Loaded (Diag)	0.5	SSE
96	IN PHASE	Aspect Rack Half Loaded (Diag)	0.8	SSE
97	IN PHASE	Aspect Rack Nearly Empty	Random	SSE

LIST OF SINGLE RACK SIMULATIONS				
Case	Motion	Load Case	COF	Event
98	IN PHASE	Aspect Rack Nearly Empty	0.2	SSE
99	IN PHASE	Aspect Rack Nearly Empty	0.5	SSE
100	IN PHASE	Aspect Rack Nearly Empty	0.8	SSE
101	OPPOSED	Aspect Rack Fully Loaded	Random	SSE
102	OPPOSED	Aspect Rack Fully Loaded	0.2	SSE
103	OPPOSED	Aspect Rack Fully Loaded	0.5	SSE
104	OPPOSED	Aspect Rack Fully Loaded	0.8	SSE
105	OPPOSED	Aspect Rack Half Loaded (E-W)	Random	SSE
106	OPPOSED	Aspect Rack Half Loaded (E-W)	0.2	SSE
107	OPPOSED	Aspect Rack Half Loaded (E-W)	0.5	SSE
108	OPPOSED	Aspect Rack Half Loaded (E-W)	0.8	SSE
109	OPPOSED	Aspect Rack Half Loaded (N-S)	Random	SSE
110	OPPOSED	Aspect Rack Half Loaded (N-S)	0.2	SSE
111	OPPOSED	Aspect Rack Half Loaded (N-S)	0.5	SSE
112	OPPOSED	Aspect Rack Half Loaded (N-S)	0.8	SSE
113	OPPOSED	Aspect Rack Half Loaded (Diag)	Random	SSE
114	OPPOSED	Aspect Rack Half Loaded (Diag)	0.2	SSE
115	OPPOSED	Aspect Rack Half Loaded (Diag)	0.5	SSE
116	OPPOSED	Aspect Rack Half Loaded (Diag)	0.8	SSE
117	OPPOSED	Aspect Rack Nearly Empty	Random	SSE
118	OPPOSED	Aspect Rack Nearly Empty	0.2	SSE
119	OPPOSED	Aspect Rack Nearly Empty	0.5	SSE
120	OPPOSED	Aspect Rack Nearly Empty	0.8	SSE
121	IN PHASE	Aspect Rack Fully Loaded	Random	OBE
122	IN PHASE	Aspect Rack Fully Loaded	0.2	OBE
123	IN PHASE	Aspect Rack Fully Loaded	0.5	OBE
124	IN PHASE	Aspect Rack Fully Loaded	0.8	OBE
125	IN PHASE	Aspect Rack Half Loaded (E-W)	Random	OBE
126	IN PHASE	Aspect Rack Half Loaded (E-W)	0.2	OBE

LIST OF SINGLE RACK SIMULATIONS				
Case	Motion	Load Case	COF	Event
127	IN PHASE	Aspect Rack Half Loaded (E-W)	0.5	OBE
128	IN PHASE	Aspect Rack Half Loaded (E-W)	0.8	OBE
129	IN PHASE	Aspect Rack Half Loaded (N-S)	Random	OBE
130	IN PHASE	Aspect Rack Half Loaded (N-S)	0.2	OBE
131	IN PHASE	Aspect Rack Half Loaded (N-S)	0.5	OBE
132	IN PHASE	Aspect Rack Half Loaded (N-S)	0.8	OBE
133	IN PHASE	Aspect Rack Half Loaded (Diag)	Random	OBE
134	IN PHASE	Aspect Rack Half Loaded (Diag)	0.2	OBE
135	IN PHASE	Aspect Rack Half Loaded (Diag)	0.5	OBE
136	IN PHASE	Aspect Rack Half Loaded (Diag)	0.8	OBE
137	IN PHASE	Aspect Rack Nearly Empty	Random	OBE
138	IN PHASE	Aspect Rack Nearly Empty	0.2	OBE
139	IN PHASE	Aspect Rack Nearly Empty	0.5	OBE
140	IN PHASE	Aspect Rack Nearly Empty	0.8	OBE
141	OPPOSED	Aspect Rack Fully Loaded	Random	OBE
142	OPPOSED	Aspect Rack Fully Loaded	0.2	OBE
143	OPPOSED	Aspect Rack Fully Loaded	0.5	OBE
144	OPPOSED	Aspect Rack Fully Loaded	0.8	OBE
145	OPPOSED	Aspect Rack Half Loaded (E-W)	Random	OBE
146	OPPOSED	Aspect Rack Half Loaded (E-W)	0.2	OBE
147	OPPOSED	Aspect Rack Half Loaded (E-W)	0.5	OBE
148	OPPOSED	Aspect Rack Half Loaded (E-W)	0.8	OBE
149	OPPOSED	Aspect Rack Half Loaded (N-S)	Random	OBE
150	OPPOSED	Aspect Rack Half Loaded (N-S)	0.2	OBE
151	OPPOSED	Aspect Rack Half Loaded (N-S)	0.5	OBE
152	OPPOSED	Aspect Rack Half Loaded (N-S)	0.8	OBE
153	OPPOSED	Aspect Rack Half Loaded (Diag)	Random	OBE
154	OPPOSED	Aspect Rack Half Loaded (Diag)	0.2	OBE
155	OPPOSED	Aspect Rack Half Loaded (Diag)	0.5	OBE

LIST OF SINGLE RACK SIMULATIONS				
Case	Motion	Load Case	COF	Event
156	OPPOSED	Aspect Rack Half Loaded (Diag)	0.8	OBE
157	OPPOSED	Aspect Rack Nearly Empty	Random	OBE
158	OPPOSED	Aspect Rack Nearly Empty	0.2	OBE
159	OPPOSED	Aspect Rack Nearly Empty	0.5	OBE
160	OPPOSED	Aspect Rack Nearly Empty	0.8	OBE
161	IN PHASE	Largest Rack Half Loaded (Diag)	0.5	1.1xSSE
162	IN PHASE	Largest Rack Fully Loaded	0.2	1.5xOBE

where Random = Gaussian distribution with a mean coeff. of friction of 0.5. (upper and lower limits of 0.8 and 0.2, respectively) and

COF = Coefficient of Friction

6.8 Time History Simulation Results

The results from the DYNARACK runs may be seen in the raw data output files. However, due to the huge quantity of output data, a post-processor is used to scan for worst case conditions and develop the stress factors discussed in subsection 6.6.3. Further reduction in this bulk of information is provided in this section by extracting the worst case values from the parameters of interest; namely displacements, support pedestal forces, impact loads, and stress factors. This section also summarizes additional analyses performed to develop and evaluate structural member stresses which are not determined by the post processor.

6.8.1 Rack Displacements

The maximum rack displacements are obtained from the time histories of the motion of the upper and lower four corners of each rack in each of the simulations. The maximum absolute value of displacement in the two horizontal directions, relative to the pool slab, is determined by the post-processor for each rack, at the top and bottom corners. The maximum displacement in either direction reported from the WPMR analyses occurred at the top of module B4 in the Phase 2 Fuel Cask Storage Pool configuration. The maximum displacement is 2.276 inches for the SSE scenario and 0.336 inches for the OBE scenario. The maximum displacement in either direction reported from the single rack analyses is 0.8686" from simulation 104, which was performed for module F1.

To assess the kinematic stability safety margin, the maximum displacement single rack cases were run again, using 1.5 times the SSE excitation and 1.5 times the OBE excitation, respectively. These are single rack cases 161 and 162. The maximum displacements from these runs was still less than the displacement results from the WPMR runs. Therefore, the bounding displacement result of 2.276 inches is obtained from the WPMR scenario. The result for module B4 from WPMR case 5 is used to compute the safety factor against overturning. It was shown to be more than 22, which far exceeds the acceptance criteria of 1.0.

6.8.2 Pedestal Vertical Forces

The maximum vertical pedestal force obtained in the WPMR simulations was 138,000 lbf for module G9, one of the 15 x 12 racks in the Phase 1 Fuel Cask Storage Pool SSE simulation. The maximum vertical pedestal force obtained in the OBE simulation was 81,200 lbf for module G1, another 15 x 12 rack, in the SFP simulation.

6.8.3 Pedestal Friction Forces

The maximum interface shear force value in any direction bounding all pedestals in all simulations is 51,500 lbf for module G8 in the Phase 1 Fuel Cask Storage Pool SSE case.

6.8.4 Rack Impact Loads

A freestanding rack, by definition, is a structure subject to potential impacts during a seismic event. Impacts arise, in some instances, from localized impacts between the racks, or between a peripheral rack and the pool wall and from rattling of the fuel assemblies in the storage rack locations. The following sections discuss the bounding values of these impact loads.

6.8.4.1 Impacts External to the Rack

Gap elements track the potential for rack-to-rack or rack-to-pool wall impacts. The result of each gap spring element in terms of impact force is printed in a list format in the output file produced by the DYNARACK program. The lists from each simulation are scanned for non-zero values. A non-zero value indicates an impact and vice versa. Naturally impacts are expected between racks which are initially in contact at the baseplates. These include all new racks which are designed for installation in contact with a neighboring new rack and for impact loads resulting from seismic events. Impacts also occur at the top elevation as well. The maximum rack impact is between modules A4 and B4 (both existing modules) in the Fuel Cask Storage Pool Phase 2 case, with impact of 35,160 lbf at the top of the north end of their interface and 27,250 lbf at the south. The impact site is at the top of the rack which would be above the tops of any stored fuel assemblies. It has been determined that there is no permanent deformation of the rack material

from this impact, with the rack returning to its normal configuration when the impact load is removed. Fuel configuration and poison areas remain unaffected. Therefore these impacts are acceptable.

6.8.4.2 Impacts Internal to the Rack

A review of all simulations performed allows determination of the maximum instantaneous impact load between fuel assembly and fuel cell wall at any modeled impact site. The maximum fuel/cell wall impact loads occur in the SFP WPMR analyses in module D3 and are 815 lbf in the SSE case and 380 lbf for the OBE case. The cell wall integrity under the 815 lbf impact load has been evaluated and shown to remain intact with no permanent damage.

The permissible lateral load on an irradiated spent fuel assembly has been studied by the Lawrence Livermore National Laboratory. The LLNL report [6.8.1] states that "...for the most vulnerable fuel assembly, axial buckling varies from 82g's at initial storage to 95g's after 20 years' storage. In a side drop, no yielding is expected below 63g's at initial storage to 74g's after 20 years' [dry] storage". The most significant load on the fuel assembly arises from rattling during the seismic event.

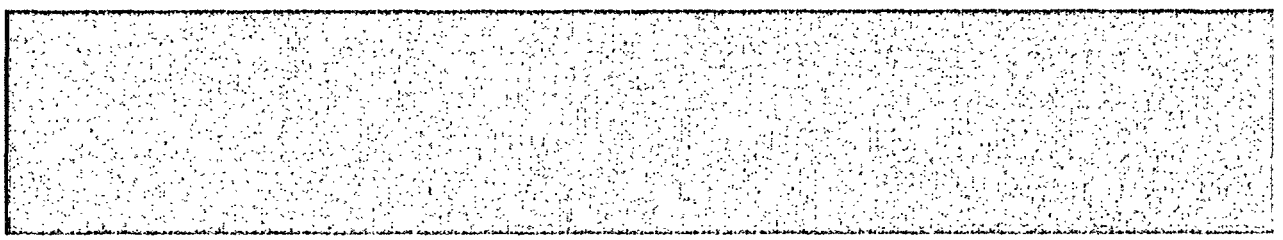

a = permissible lateral acceleration in g's (a = 63)

Therefore, the limiting lateral load, F_e = 12,600 lbs

The maximum fuel-to-storage cell rattling force from the WPMR runs is 815 lbs. Therefore, the nominal factor of safety against fuel failure is computed to be more than 15.

6.9 Rack Structural Evaluation

6.9.1 Rack Stress Factors

The time history results from the DYNARACK solver provide the pedestal normal and lateral interface forces, which may be converted to the limiting bending moment and shear force at the bottom baseplate-pedestal interface. In particular, maximum values for the previously defined stress factors are determined for every pedestal in the array of racks. With this information available, the structural integrity of the pedestal can be assessed and reported. The net section maximum (in time) bending moments and shear forces can also be determined at the bottom baseplate-rack cellular structure interface for each spent fuel rack in the pool. Using these forces and moments, the maximum stress in the limiting rack cell (box) can be evaluated.

The stress factor results for male and female pedestals, and for the entire spent fuel rack cellular cross-section just above the bottom casting has been determined. These factors are reported for every rack in each simulation, and for each pedestal in every rack. These locations are the most heavily loaded net sections in the structure so that satisfaction of the stress factor criteria at these locations ensures that the overall structural criteria set forth in Section 6.6 are met.

An evaluation of the stress factors for all of the WPMR simulations performed leads to the conclusion that all stress factors, as defined in Section 6.6.3, are less than the mandated limit of 1.0 for the load cases examined. All of the maximum stress factors occurred at the base of the rack cell walls under the WPMR scenarios. For the new racks, the bounding stress factor was determined to be 0.243 (R6) for the Phase 2 SFP OBE simulation, occurring in module H. The maximum calculated SSE stress factor for the new racks occurred during the Phase 2 SFP simulation and was 0.167 (R6) for module J1. For the existing racks, the bounding stress factor was determined to be 0.303 (R6) for the Phase 2 Fuel Cask Storage Pool OBE simulation, occurring in the cell region of module A4. The maximum calculated SSE stress factor for the existing racks was 0.210 (R6) for module B4. Relevant stress factors are for cell wall stresses above the baseplate, since these control over the pedestal stress factors. The values for all other

defined stress factors are archived and show that the requirements of Section 6.6 are indeed satisfied for the load levels considered for every limiting location in every rack in the array.

6.9.2 Pedestal Thread Shear Stress

The maximum thread engagement stresses under faulted conditions for every pedestal for every rack in the WPMR simulations run was 8,268 psi for the Fuel Cask Storage Pool Phase 1 SSE run and 4,865 psi for the SFP OBE run. By ASME code section NF-3321, the Level A allowable stress is $0.4*F_y = 0.4(25,000) = 10,000$ psi. Referring to section 6.6.4, for Level B (OBE), the allowable is increased by the factor 1.33 from table NF-3523(b), resulting in an allowable stress of 13,300 psi, which exceeds both calculated stresses.

6.9.3 Local Stresses Due to Impacts

Impact loads at the pedestal base produce stresses in the pedestal for which explicit stress limits are prescribed in the Code. However, impact loads on the cellular region of the racks, as discussed in subsection 6.8.4.2 above, produce stresses which attenuate rapidly away from the loaded region. This behavior is characteristic of secondary stresses.

Even though limits on secondary stresses are not prescribed in the Code for class 3 NF structures, evaluations are made to ensure that the localized impacts do not lead to plastic deformations in the storage cells which affect the sub-criticality of the stored fuel array.

a. Impact Loading Between Fuel Assembly and Cell Wall

Local cell wall integrity is conservatively estimated from peak impact loads. Plastic analysis is used to obtain the limiting impact load which would lead to gross permanent deformation. As shown in Table 6.9.1, the limiting impact load (of 2,826 lbf, including a safety factor of 2.0) is much greater than the highest calculated impact load value (of 815 lbf, see subsection 6.8.4.2) obtained from any of the rack analyses. Therefore, fuel impacts do not represent a significant concern with respect to fuel rack cell deformation.

b. Impacts Between Adjacent Racks

As may be seen from subsection 6.8.4.1, the storage racks will impact each other at a few locations during seismic events. Since the loading produces distributed stresses shown to be less than the yield stress, local deformation will be negligible. The impact loading will be distributed over a large area (a significant portion of the entire face width of the rack of about 58 inches). The resulting compressive stress from the highest combined impact load of 62,410 lbs distributed over 10 cell walls is 17,336 psi, which is less than the cell wall material yield strength of 21,300 psi. Therefore, any deformation will not affect the configuration of the stored fuel.

6.9.4 Assessment of Rack Fatigue Margin

Deeply submerged high density spent fuel storage racks arrayed in close proximity to each other in a free-standing configuration behave primarily as a nonlinear cantilevered structure when subjected to 3-D seismic excitations. In addition to the pulsations in the vertical load at each pedestal, lateral friction forces at the pedestal/ bearing pad interface, which help prevent or mitigate lateral sliding of the rack, also exert a time-varying moment in the baseplate region of the rack. The friction-induced lateral forces act simultaneously in x and y directions with the requirement that their vectorial sum does not exceed μV, where μ is the limiting interface coefficient of friction and V is the concomitant vertical thrust on the bearing pad (at the *given* time instant). As the vertical thrust at a pedestal location changes, so does the maximum friction force, F, that the interface can exert. In other words, the lateral force at the pedestal/bearing pad interface, F, is given by

$$F \leq \mu N(\tau)$$

where N (vertical thrust) is the time-varying function of τ. F does not always equal μN; rather, μN is the maximum value it can attain at any time; the actual value, of course, is determined by the dynamic equilibrium of the rack structure.

In summary, the horizontal friction force at the pedestal/bearing pad interface is a function of time; its magnitude and direction of action varies during the earthquake event.

The time-varying lateral (horizontal) and vertical forces on the extremities of the support pedestals produce stresses at the root of the pedestals in the manner of an end-loaded cantilever. The stress field in the cellular region of the rack is quite complex, with its maximum values located in the region closest to the pedestal. The maximum magnitude of the stresses depends on the severity of the pedestal end loads and on the geometry of the pedestal/rack baseplate region.

Alternating stresses in metals produce metal fatigue if the amplitude of the stress cycles is sufficiently large. In high density racks designed for sites with moderate to high postulated seismic action, the stress intensity amplitudes frequently reach values above the material endurance limit, leading to expenditure of the fatigue "usage" reserve in the material.

Because the locations of maximum stress (viz., the pedestal/rack baseplate junction) and the close placement of racks, a post-earthquake inspection of the high stressed regions in the racks is not feasible. Therefore, the racks must be engineered to withstand multiple earthquakes without reliance of nondestructive inspections for post-earthquake integrity assessment. The fatigue life evaluation of racks is an integral aspect of a sound design.

The time-history method of analysis, deployed in this report, provides the means to obtain a complete cycle history of the stress intensities in the highly stressed regions of the rack. Having determined the amplitude of the stress intensity cycles and their number, the cumulative damage factor, U, can be determined using the classical Miner's rule:

$$U = \Sigma \frac{n_i}{N_i}$$

where n_i is the number of stress intensity cycles of amplitude σ_i, and N_i is the permissible number of cycles corresponding to σ_i from the ASME fatigue curve for the material of construction. U must be less than or equal to 1.0.

To evaluate the cumulative damage factor, a finite element model of a portion of the spent fuel rack in the vicinity of a support pedestal is constructed in sufficient detail to provide an accurate assessment of stress intensities. The finite element solutions for unit pedestal loads in three orthogonal directions are combined to establish the maximum value of stress intensity as a function of the three unit pedestal loads. Using the archived results of the spent fuel rack dynamic analyses (pedestal load histories versus time) enables a time-history of stress intensity to be established at the most limiting location. This permits establishing a set of alternating stress intensity ranges versus cycles. Following ASME Code guidelines for computing U, it is found that U =0.104 due to the combined effects of one SSE and twenty OBE events. This is well below the ASME Code limit of 1.0.

6.9.5 Weld Stresses

Weld locations subjected to significant seismic loading are at the bottom of the rack at the baseplate-to-cell connection, at the top of the pedestal support at the baseplate connection, and at cell-to-cell connections. Bounding values of resultant loads are used to qualify the connections.

a. Baseplate-to-Rack Cell Welds

For Level A or B conditions, Ref. [6.6.1] permits an allowable weld stress of $\tau = .3\ S_u$ = 19,860 psi (multiplied by 1.33 for Level B). As stated in subsection 6.6.2, the allowable may be increased for Level D by an amplification factor which is equal to 1.8 (= $.72S_y/.4S_y$). The allowable stress increase factor of 1.8 greatly exceeds the ratio of maximum SSE to OBE stresses. Therefore, Level B becomes the governing condition.

Weld dimensionless stress factors are produced through the use of a simple conversion (ratio) factor applied to the corresponding stress factor in the adjacent rack material. Addressing the new racks, the *RATIO*, 2.079, is developed from the differences in material thickness and length versus weld throat dimension and length:

RATIO = [redacted]

The highest predicted weld stress for OBE is calculated from the highest cell wall (above the baseplate) R6 value, 0.243, (corresponding to the same simulation as reported in subsection 6.9.1) as follows:

R6 * [(0.6) Fy] * *RATIO* = 0.243 * [0.6 * 21300] * 2.079 = 6,456 psi

This value is less than the Level B allowable weld stress value, which is 1.33 x 19,860 = 26,414 psi. Therefore, all weld stresses between the baseplate and cell wall base are acceptable.

b. Baseplate-to-Pedestal Welds

The weld between baseplate and support pedestal is checked using finite element analysis to determine that the maximum stress is 8,767 psi under a Level D event. This calculated stress value can be shown to be acceptable by comparing to the normal stress allowable of 19,860 psi.

c. Cell-to-Cell Welds

Cell-to-cell connections are by a series of connecting welds along the cell height. Stresses in storage cell to cell welds develop due to fuel assembly impacts with the cell wall. These weld stresses are conservatively calculated by assuming that fuel assemblies in adjacent cells are moving out of phase with one another so that impact loads in two adjacent cells are in opposite directions; this tends to separate the two cells from each other at the weld.

Table 6.9.1 gives the computed results for the maximum allowable load that can be transferred by these welds based on the available weld area. The upper bound on the applied load transferred is also given in Table 6.9.1. This upper bound value is conservatively obtained by applying the bounding rack-to-fuel impact load from any simulation in two orthogonal directions simultaneously, and multiplying the result by 2 to account for the simultaneous impact of two assemblies in adjacent cells moving in opposing directions. An equilibrium analysis at the connection then yields the upper bound load to be transferred. As shown in Table 6.9.1, the calculated stress of 4,031 psi is below the allowable stress of 8,520 psi.

6.9.6 Bearing Pad Analysis

To protect the pool slab from highly localized dynamic loadings, bearing pads are placed between the pedestal base and the slab. Fuel rack pedestals impact on these bearing pads during a seismic event and pedestal loading is transferred to the liner. Bearing pad dimensions are set to ensure that the average pressure on the slab surface due to a static load plus a dynamic impact load does not exceed the American Concrete Institute, ACI-349 [6.9.1] limit on bearing pressures. Section 10.17 of [6.9.2] gives the design bearing strength as

$$f_b = \phi\,(.85\,f_c')\,\in$$

where $\phi = .7$ and f_c' is the specified concrete strength for the spent fuel pool. $\epsilon = 1$ except when the supporting surface is wider on all sides than the loaded area. In that case, $\epsilon = (A_2/A_1)^{.5}$, but not more than 2. A_1 is the actual loaded area, and A_2 is an area greater than A_1 and is defined in [6.9.2]. Using a value of $\epsilon > 2$ includes credit for the confining effect of the surrounding concrete. It is noted that this criterion is in conformance with the ultimate strength primary design methodology of the American Concrete Institute in use since 1971. For CPS, $f_c' = 3{,}500$ psi and the allowable static bearing pressure is $f_b = 4{,}165$ psi, assuming full concrete confinement. This allowable bearing pressure is utilized because concrete confinement is not compromised in the leak chase region due to the large slab dimensions in both lateral and thickness directions (therefore the supporting area A_2 below the slab surface is much larger than the loaded area A_1 at the bearing pad/slab interface).. The primary objective of the bearing pad analysis is to show that this primarily compressive component remains in the elastic range.

The analyses are performed with ANSYS using finite element models, which place a bearing pad over two perpendicular leak chases. For conservatism the pedestal is centered at the intersection of these two leak chases that produces maximum stress. This configuration is selected with the intent of bounding all other possible bearing pad/pool floor interfaces. The analysis applies the maximum total vertical pedestal load from results for all bearing pads, scanned from the time-history solution from the SSE simulation. The maximum vertical pedestal load over a leak chase (which is modeled to remove a 2" wide strip of concrete from under the bearing pad) is taken to be 140 kips on a 12" x 12" bearing pad.

The bearing pads in the SFP will be 1.5" thick. All bearing pads will be made from austenitic stainless steel plate stock. Bearing pad models were prepared to evaluate all possible configurations. Figure 6.9.1 provides an isometric of the controlling ANSYS finite element model (leak chase condition). The model permits the bearing pad to deform and lose contact with the liner, if the conditions of elastostatics so dictate. Figure 6.9.1 shows the bearing pad and underlying leak chases located within the supporting concrete. The slab is modeled as an elastic foundation. The average pressure at the pad to liner interface is computed and compared against the above-mentioned limit. Calculations show that the average pressure at the slab / liner

interface is 3,500 psi, which is well below the allowable value of 4,165 psi, providing a factor of safety of 1.19. The stress distribution in the bearing pad is also evaluated, with the results shown in Figure 6.9.2 (top and bottom views). The peak stress in the bearing pad during a Level D event is 27,964 psi. ASME Section III, Appendix F, Section 1334.10 states that bearing stresses need not be evaluated for Level D conditions. Nevertheless, an appropriate stress limit may be considered by maintaining the increase factor of two above normal condition allowables, as discussed earlier. The material yield strength of 25,000 psi at 200°F then provides an allowable stress of 2*0.9Sy (i.e., 45,000 psi) producing a factor of safety against yield of about 1.61. A similar evaluation performed for Level B conditions shows that the Level D controls. Therefore, the bearing pad design devised for the CPS SFP is deemed appropriate for the prescribed loadings.

6.10 Level A Evaluation

The Level A condition is not a governing condition for spent fuel racks since the general level of imposed loading is far less than Level B or D loading. The stress allowable for Level B loading is only approximately 1/3 greater than the corresponding Level A stress allowable. The ratio of the loading increase from Level A to B loading far exceeds this 1/3 value. Therefore Level A is acceptable by comparison.

6.11 Hydrodynamic Loads on Pool Walls

The hydrodynamic pressures that develop between adjacent racks and the pool walls can be developed from the archived results produced by the WPMR analysis. Of the racks next to the SFP walls, the one that resulted in the maximum displacement generates the maximum hydrodynamic load on its adjacent wall. Time dependent hydrodynamic pressures are determined for subsequent analysis as discussed in Section 8.0.

6.12 Local Stress Considerations

This section presents the results of evaluations for the possibility of cell wall buckling and the secondary stresses produced by temperature effects.

6.12.1 Cell Wall Buckling

The allowable local buckling stresses in the fuel cell walls are obtained by using classical plate buckling analysis using a model as shown in Figure 6.12.1. The evaluation for cell wall buckling is based on the applied stress being uniform along the entire length of the cell wall. In the actual fuel rack, the compressive stress comes from consideration of overall bending of the rack structures during a seismic event, and as such is negligible at the rack top, and maximum at the rack bottom.

The critical buckling stress is determined to be 22,580 psi. The computed compressive stress in the cell wall, based on the R5 stress factor, is 4,090 psi. Therefore, there is a large margin of safety against local cell wall buckling.

6.12.2 Analysis of Welded Joints in the Racks

Cell-to-cell welded joints are examined under the loading conditions arising from thermal effects due to an isolated hot cell in this subsection. This secondary stress condition is evaluated alone and not combined with primary stresses from other load conditions.

A thermal gradient between cells will develop when an isolated storage location contains a fuel assembly emitting maximum postulated heat, while surrounding locations are empty. We obtain a conservative estimate of weld stresses along the length of an isolated hot cell by considering a beam strip uniformly heated by 75°F, and restrained from growth along one long edge. This temperature rise is based on thermal-hydraulic evaluations discussed in Section 5.0, which show that a conservative upper bound for the difference between local cell maximum temperatures and

the bulk temperature in the pool is less than this value. The analyzed configuration is shown in Figure 6.12.2.

Using shear beam theory, as discussed in Holtec generic calculation HI-89330 [6.9.3], and subjecting the strip to a uniform temperature rise $\Delta T = 75°F$, we can calculate an estimate of the maximum value of the average shear stress in the strip. The strip is subjected to the following boundary conditions.

a. Displacement $U_x(x,y) = 0$ at $x = 0$, at $y = H$, all x.

b. Average force M_x, acting on the cross section $Ht = 0$ at $x = l$, all y.

The final result for wall shear stress, maximum at $x = l$, is found to be given as

$$\tau_{max} = \frac{E\alpha\Delta T}{0.931}$$

where $E = 27.6 \times 10^6$ psi, $\alpha = 9.5 \times 10^{-6}$ in/in °F and $\Delta T = 75°F$.

Therefore, we obtain an estimate of maximum weld shear stress in an isolated hot cell, due to thermal gradient, as

$$\tau_{max} = 21{,}122 \text{ psi}$$

Since this is a secondary thermal stress, we use the allowable shear stress criteria for faulted conditions ($0.42*S_u$=27,804 psi) as a guide to indicate that this maximum shear is acceptable. Therefore, there is a margin of safety of 24% against cell wall shear failure due to secondary thermal stresses from cell wall growth under the worst case hot cell conditions.

6.13 References

[6.1.1] USNRC NUREG-0800, Standard Review Plan, June 1987.

[6.1.2] (USNRC Office of Technology) "OT Position for Review and Acceptance of Spent Fuel Storage and Handling Applications", dated April 14, 1978, and January 18, 1979 amendment thereto.

[6.2.1] Soler, A.I. and Singh, K.P., "Seismic Responses of Free Standing Fuel Rack Constructions to 3-D Motions", Nuclear Engineering and Design, Vol. 80, pp. 315-329 (1984).

[6.2.2] Soler, A.I. and Singh, K.P., "Some Results from Simultaneous Seismic Simulations of All Racks in a Fuel Pool", INNM Spent Fuel Management Seminar X, January, 1993.

[6.2.3] Singh, K.P. and Soler, A.I., "Seismic Qualification of Free Standing Nuclear Fuel Storage Racks - the Chin Shan Experience, Nuclear Engineering International, UK (March 1991).

[6.2.4] Holtec Proprietary Report HI-961465 - WPMR Analysis User Manual for Pre&Post Processors & Solver, August, 1997.

[6.4.1] Holtec Proprietary Report HI-89364 - Verification and User's Manual for Computer Code GENEQ, January, 1990.

[6.5.1] Rabinowicz, E., "Friction Coefficients of Water Lubricated Stainless Steels for a Spent Fuel Rack Facility," MIT, a report for Boston Edison Company, 1976.

[6.5.2] Singh, K.P. and Soler, A.I., "Dynamic Coupling in a Closely Spaced Two-Body System Vibrating in Liquid Medium: The Case of Fuel Racks," 3rd International Conference on Nuclear Power Safety, Keswick, England, May 1982.

[6.5.3] Fritz, R.J., "The Effects of Liquids on the Dynamic Motions of Immersed Solids," Journal of Engineering for Industry, Trans. of the ASME, February 1972, pp 167-172.

[6.5.4] Levy, S. and Wilkinson, J.P.D., "The Component Element Method in Dynamics with Application to Earthquake and Vehicle Engineering," McGraw Hill, 1976.

[6.5.5] Paul, B., "Fluid Coupling in Fuel Racks: Correlation of Theory and Experiment", (Proprietary), NUSCO/Holtec Report HI-88243.

[6.6.1] ASME Boiler & Pressure Vessel Code, Section III, Subsection NF, 2001 Edition up to and including 2003 Addenda.

[6.6.2] ASME Boiler & Pressure Vessel Code, Section III, Appendices, 2001 Edition up to and including 2003 Addenda.

[6.6.3] ASME Boiler & Pressure Vessel Code, Section III, Subsection NF, 1977 Edition.

[6.8.1] Chun, R., Witte, M. and Schwartz, M., "Dynamic Impact Effects on Spent Fuel Assemblies," UCID-21246, Lawrence Livermore National Laboratory, October 1987.

[6.9.1] ACI 349-76, Code Requirements for Nuclear Safety Related Concrete Structures, American Concrete Institute, Detroit, Michigan, 1976.

[6.9.2] ACI 318-71, Building Code requirements for Structural Concrete," American Concrete Institute, Detroit, Michigan, 1971.

[6.9.3] Holtec report HI-89330, Rev. 1, "A Seismic Analysis of High Density Fuel Racks; Part III: Structural Design Calculations - Theory."

Table 6.2.1

PARTIAL LISTING OF FUEL RACK APPLICATIONS USING DYNARACK

PLANT	DOCKET NUMBER(s)	YEAR
Enrico Fermi Unit 2	USNRC 50-341	1980
Quad Cities 1 & 2	USNRC 50-254, 50-265	1981
Rancho Seco	USNRC 50-312	1982
Grand Gulf Unit 1	USNRC 50-416	1984
Oyster Creek	USNRC 50-219	1984
Pilgrim	USNRC 50-293	1985
V.C. Summer	USNRC 50-395	1984
Diablo Canyon Units 1 & 2	USNRC 50-275, 50-323	1986
Byron Units 1 & 2	USNRC 50-454, 50-455	1987
Braidwood Units 1 & 2	USNRC 50-456, 50-457	1987
Vogtle Unit 2	USNRC 50-425	1988
St. Lucie Unit 1	USNRC 50-335	1987
Millstone Point Unit 1	USNRC 50-245	1989
Chinshan	Taiwan Power	1988
D.C. Cook Units 1 & 2	USNRC 50-315, 50-316	1992
Indian Point Unit 2	USNRC 50-247	1990
Three Mile Island Unit 1	USNRC 50-289	1991
James A. FitzPatrick	USNRC 50-333	1990
Shearon Harris Unit 2	USNRC 50-401	1991
Hope Creek	USNRC 50-354	1990
Kuosheng Units 1 & 2	Taiwan Power Company	1990

Table 6.2.1

PARTIAL LISTING OF FUEL RACK APPLICATIONS USING DYNARACK

PLANT	DOCKET NUMBER(s)	YEAR
Ulchin Unit 2	Korea Electric Power Co.	1990
Laguna Verde Units 1 & 2	Comision Federal de Electricidad	1991
Zion Station Units 1 & 2	USNRC 50-295, 50-304	1992
Sequoyah	USNRC 50-327, 50-328	1992
LaSalle Unit 1	USNRC 50-373	1992
Duane Arnold Energy Center	USNRC 50-331	1992
Fort Calhoun	USNRC 50-285	1992
Nine Mile Point Unit 1	USNRC 50-220	1993
Beaver Valley Unit 1	USNRC 50-334	1992
Salem Units 1 & 2	USNRC 50-272, 50-311	1993
Limerick	USNRC 50-352, 50-353	1994
Ulchin Unit 1	KINS	1995
Yonggwang Units 1 & 2	KINS	1996
Kori-4	KINS	1996
Connecticut Yankee	USNRC 50-213	1996
Angra Unit 1	Brazil	1996
Sizewell B	United Kingdom	1996
Waterford 3	USNRC 50-382	1997
J.A. Fitzpatrick	USNRC 50-333	1998
Callaway	USNRC 50-483	1998

Table 6.2.1

PARTIAL LISTING OF FUEL RACK APPLICATIONS USING DYNARACK

PLANT	DOCKET NUMBER(s)	YEAR
Nine Mile Unit 1	USNRC 50-220	1998
Chin Shan	Taiwan Power Company	1998
Vermont Yankee	USNRC 50-271	1998
Millstone 3	USNRC 50-423	1998
Byron/Braidwood	USNRC 50-454, 50-455, 50-567, 50-457	1999
Wolf Creek	USNRC 50-482	1999
Plant Hatch Units 1 & 2	USNRC 50-321, 50-366	1999
Harris Pools C and D	USNRC 50-401	1999
Davis-Besse	USNRC 50-346	1999
Enrico Fermi Unit 2	USNRC 50-341	2000
Kewaunee	USNRC 50-305	2001
V.C. Summer	USNRC 50-395	2001
St. Lucie	USNRC 50-335, 50-389	2002
Turkey Point	USNRC 50-250, 251	2002

Table 6.3.1 RACK MATERIAL DATA (200°F) (ASME - Section II, Part D)			
Stainless Steel Material	Young's Modulus E (psi)	Yield Strength S_y (psi)	Ultimate Strength S_u (psi)
SA240, Type 304L (cell boxes)	27.6×10^6	21,300	66,200
SUPPORT MATERIAL DATA (200°F)			
SA240, Type 304L (upper part of support feet & Bearing Pads)	27.6×10^6	21,300	66,200
SA-564-630 (lower part of support feet; age hardened at 1100°F)	28.5×10^6	106,300	140,000

Table 6.4.1 TIME-HISTORY STATISTICAL CORRELATION RESULTS	
OBE	
Data1 to Data2	0.078
Data1 to Data3	0.003
Data2 to Data3	0.008
SSE	
Data1 to Data2	0.083
Data1 to Data3	0.007
Data2 to Data3	0.005

Data1 corresponds to the time-history acceleration values along the X axis (South)

Data2 corresponds to the time-history acceleration values along the Y axis (East)

Data3 corresponds to the time-history acceleration values along the Z axis (Vertical)

Table 6.5.1

Degrees-of-freedom

LOCATION (Node)	DISPLACEMENT			ROTATION		
	U_x	U_y	U_z	θ_x	θ_y	θ_z
1	p_1	p_2	p_3	q_4	q_5	q_6
2	p_7	p_8	p_9	q_{10}	q_{11}	q_{12}
Node 1 is assumed to be attached to the rack at the bottom most point. Node 2 is assumed to be attached to the rack at the top most point. Refer to Figure 6.5.1 for node identification.						
2*	P_{13}	p_{14}				
3*	p_{15}	p_{16}				
4*	p_{17}	p_{18}				
5*	p_{19}	p_{20}				
1*	p_{21}	p_{22}				

where the relative displacement variables q_i are defined as:

$p_i = q_i(t) + U_x(t)$ $\quad i = 1,7,13,15,17,19,21$

$= q_i(t) + U_y(t)$ $\quad i = 2,8,14,16,18,20,22$

$= q_i(t) + U_z(t)$ $\quad i = 3,9$

$= q_i(t)$ $\quad i = 4,5,6,10,11,12$

p_i denotes absolute displacement (or rotation) with respect to inertial space

q_i denotes relative displacement (or rotation) with respect to the floor slab

* denotes fuel mass nodes

U(t) are the three known earthquake displacements

Table 6.9.1

COMPARISON OF BOUNDING CALCULATED LOADS/STRESSES VS. CODE ALLOWABLES

AT IMPACT LOCATIONS AND AT WELDS

	SSE* or OBE[†]	
Item/Location	Calculated	Allowable
Fuel assembly/cell wall impact, lbf.	815	2,826[††]
Rack/baseplate weld, psi	6,456	26,414
Female pedestal/baseplate weld, psi *	8,767*	35,748*
Cell/cell welds, psi, based on impact loads	4,031[†††]	8,520

[†] Loads and allowables given are for the more limiting of OBE or SSE (When applicable to SSE case, it is denoted by an asterisk, *).

[††] Based on the limit load for a cell wall. The allowable load on the fuel assembly itself may be less than this value (see discussion in Section 6.8.4.3), but is greater than 815 lbs.

[†††] Based on the base metal stresses adjacent to weld placements resulting from the maximum shear flow developed between two adjacent cells.

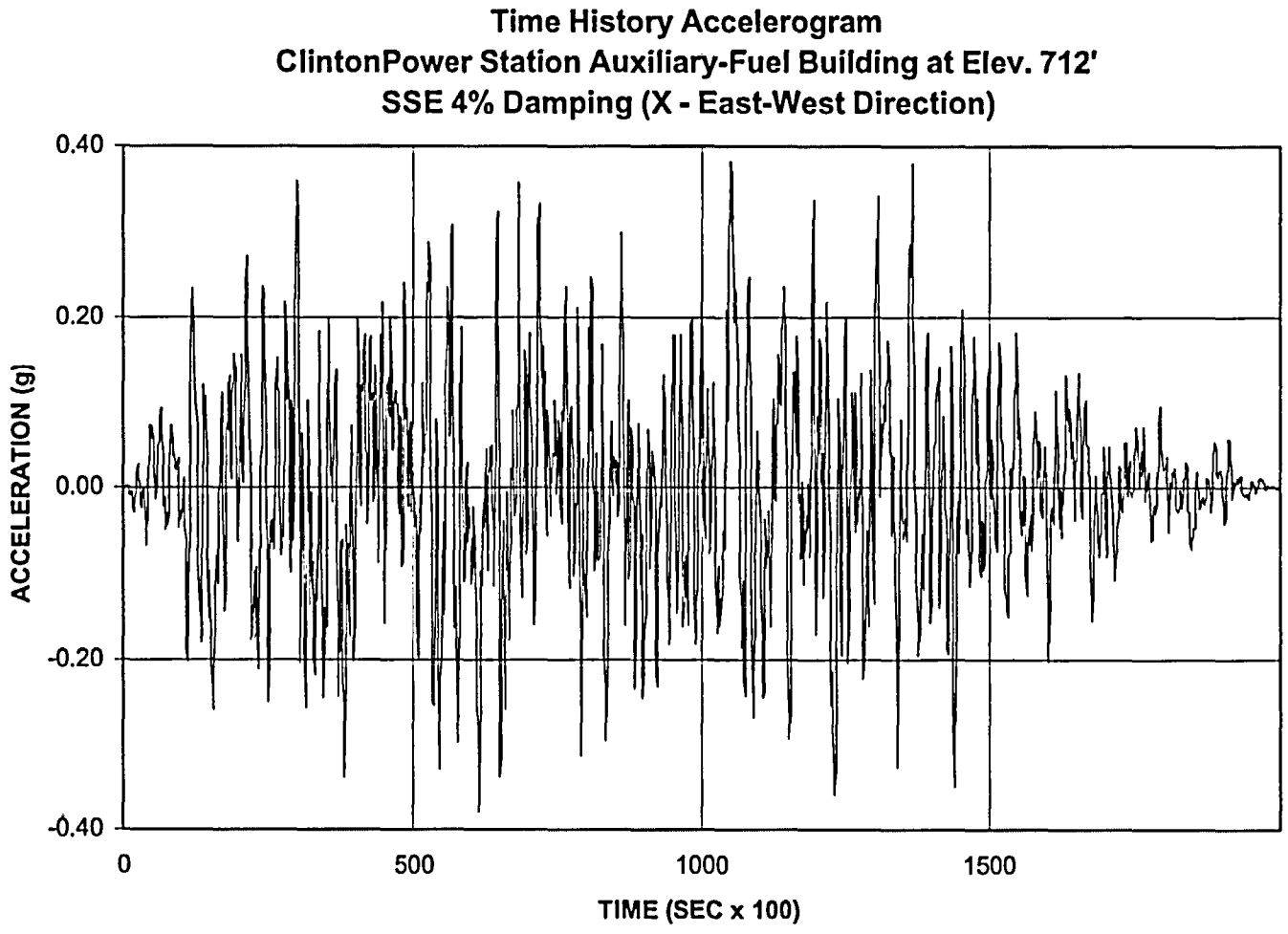
Time History Accelerogram
ClintonPower Station Auxiliary-Fuel Building at Elev. 712'
SSE 4% Damping (X - East-West Direction)
0.40
0.20
0.00
-0.20
-0.40
ACCELERATION (g)
0
500
1000
1500
TIME (SEC x 100)

Figure 6.4.1

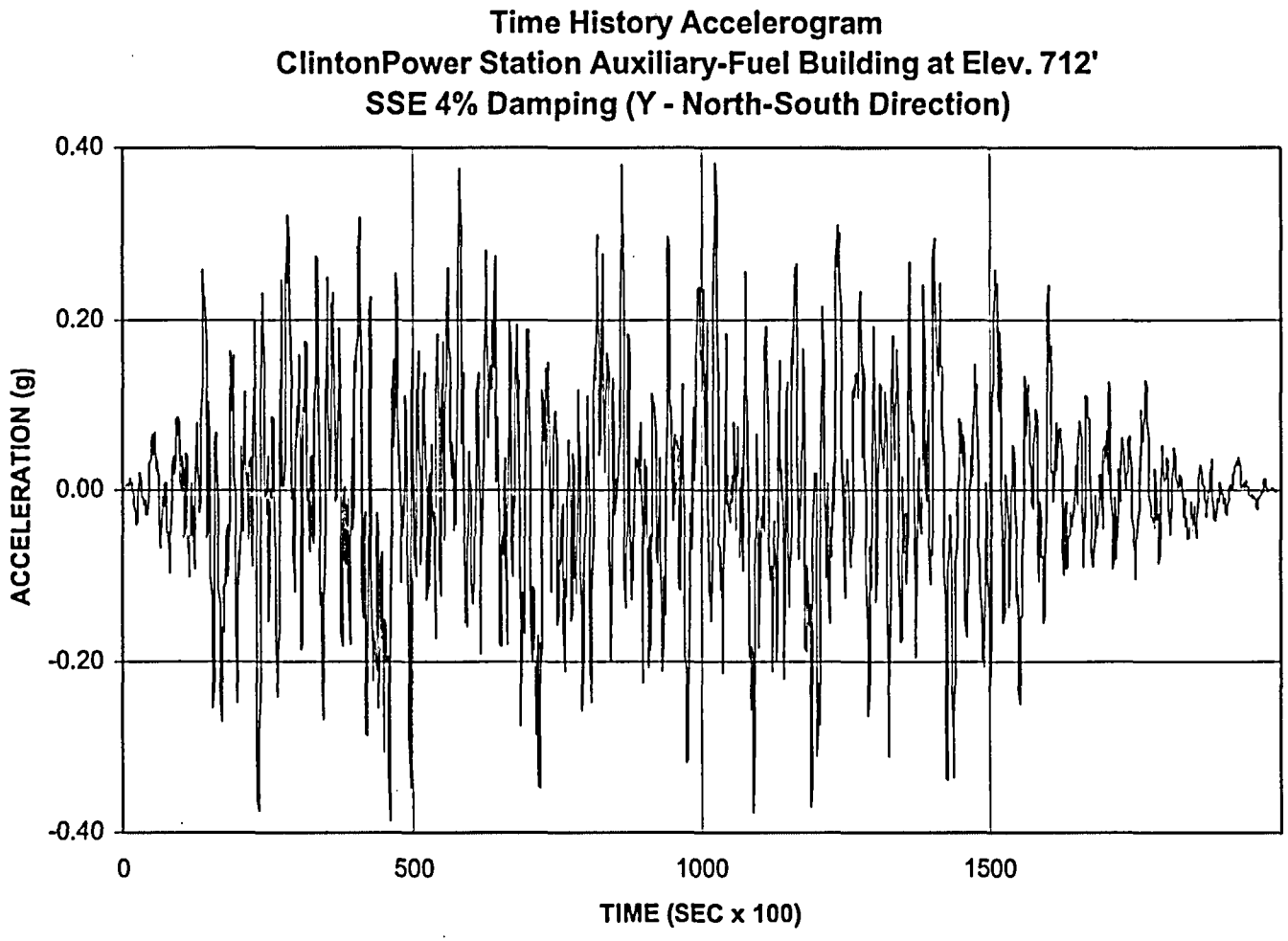

Figure 6.4.2

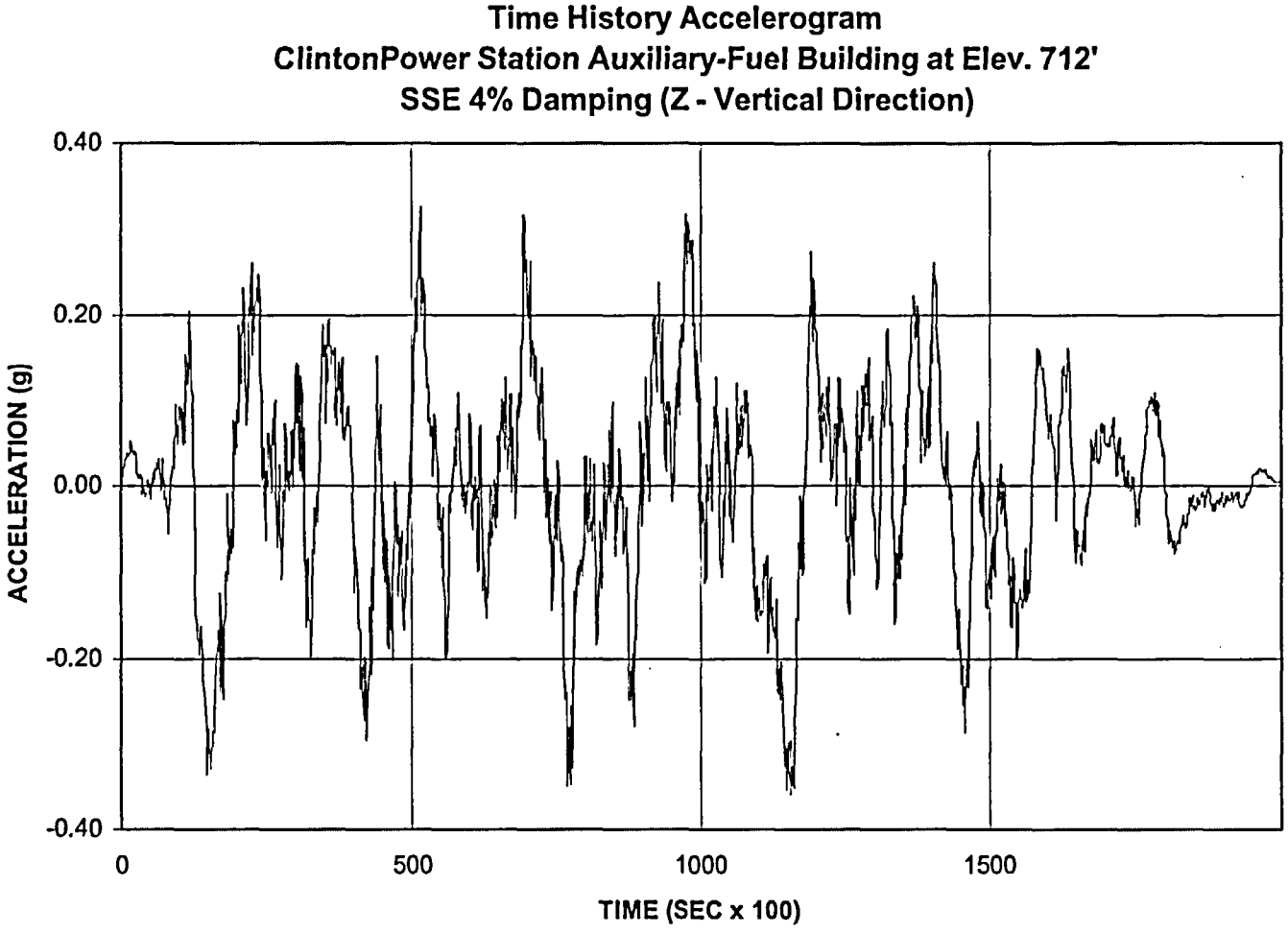

Figure 6.4.3

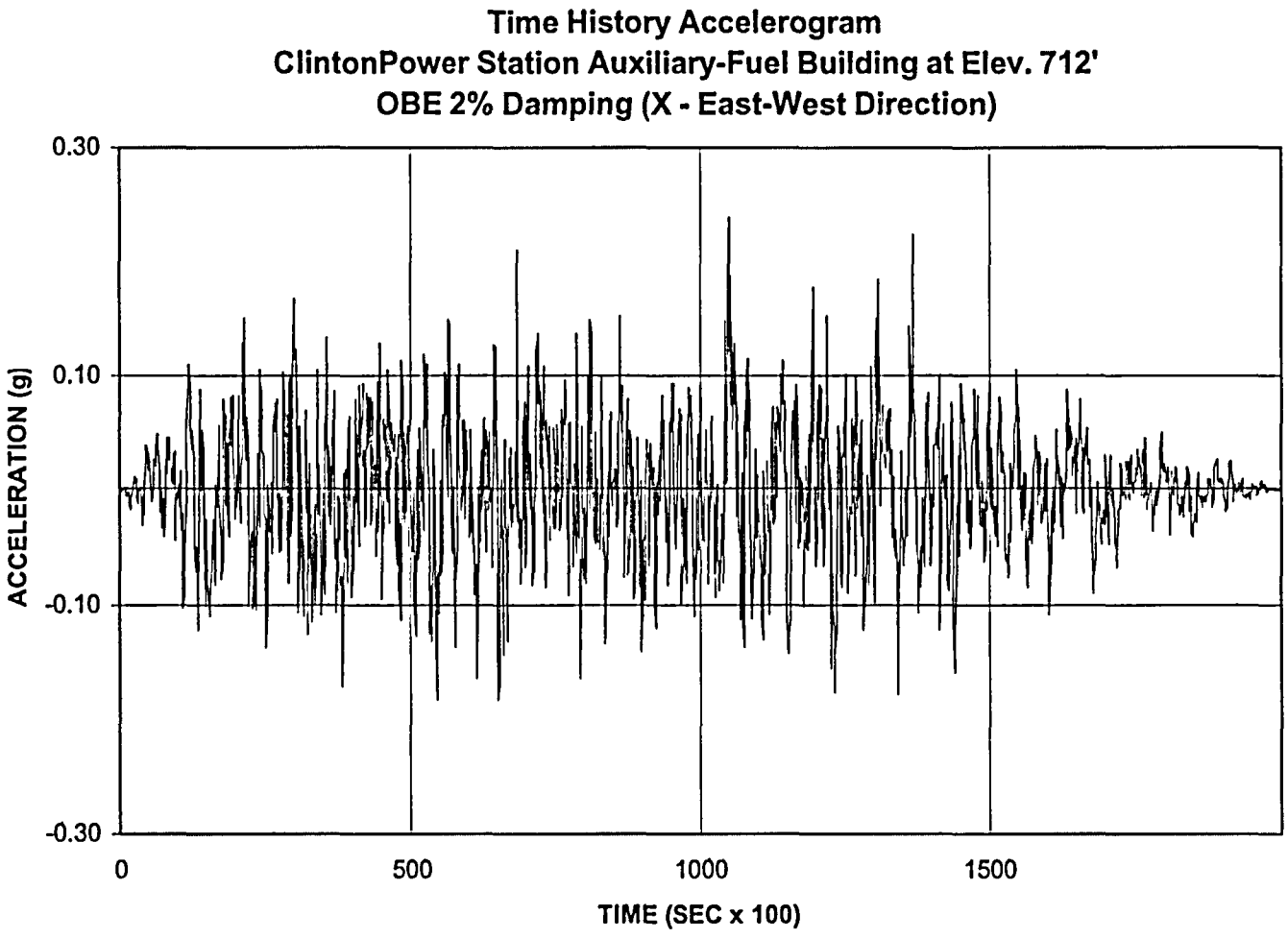

Figure 6.4.4

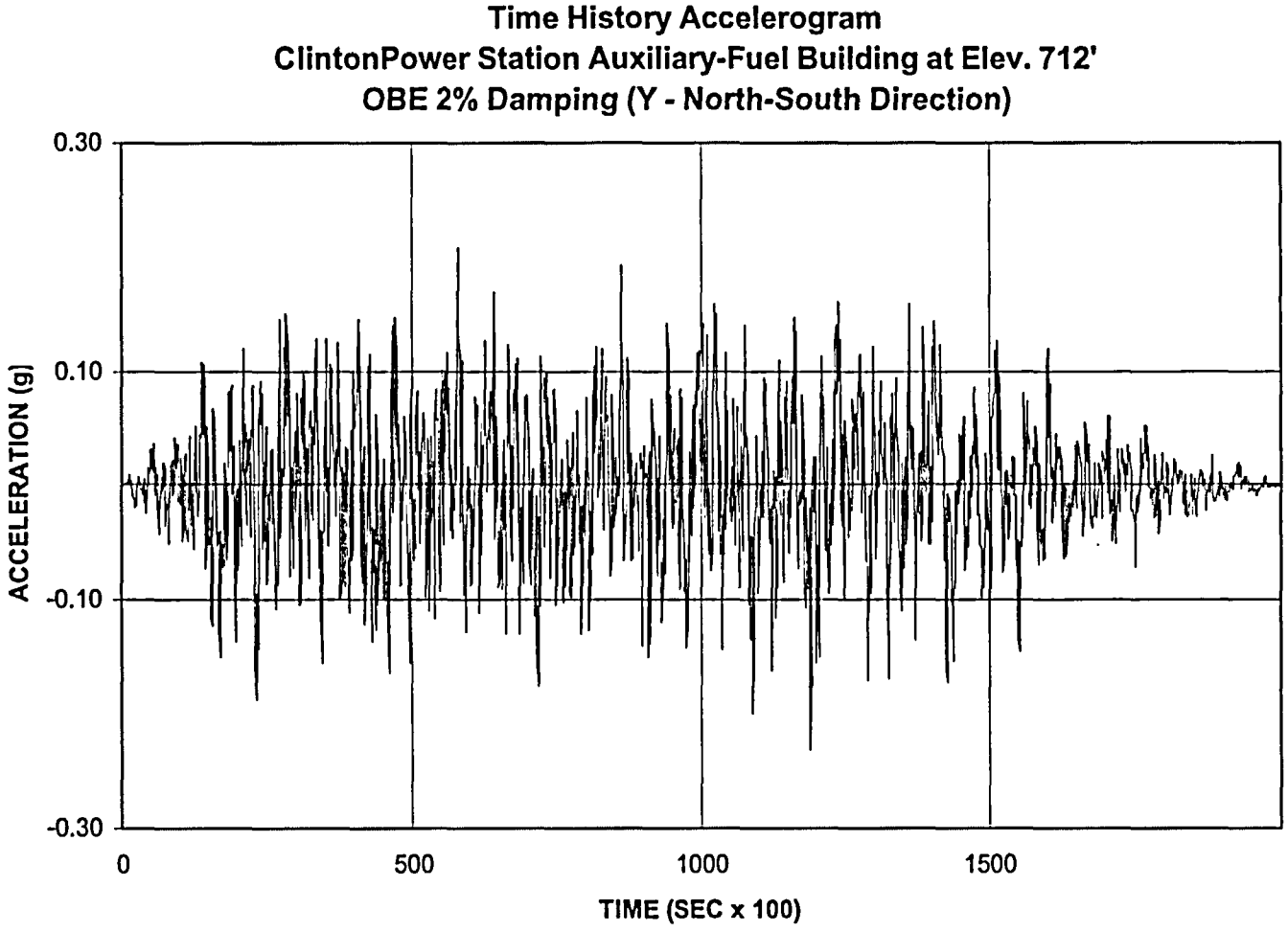

Figure 6.4.5

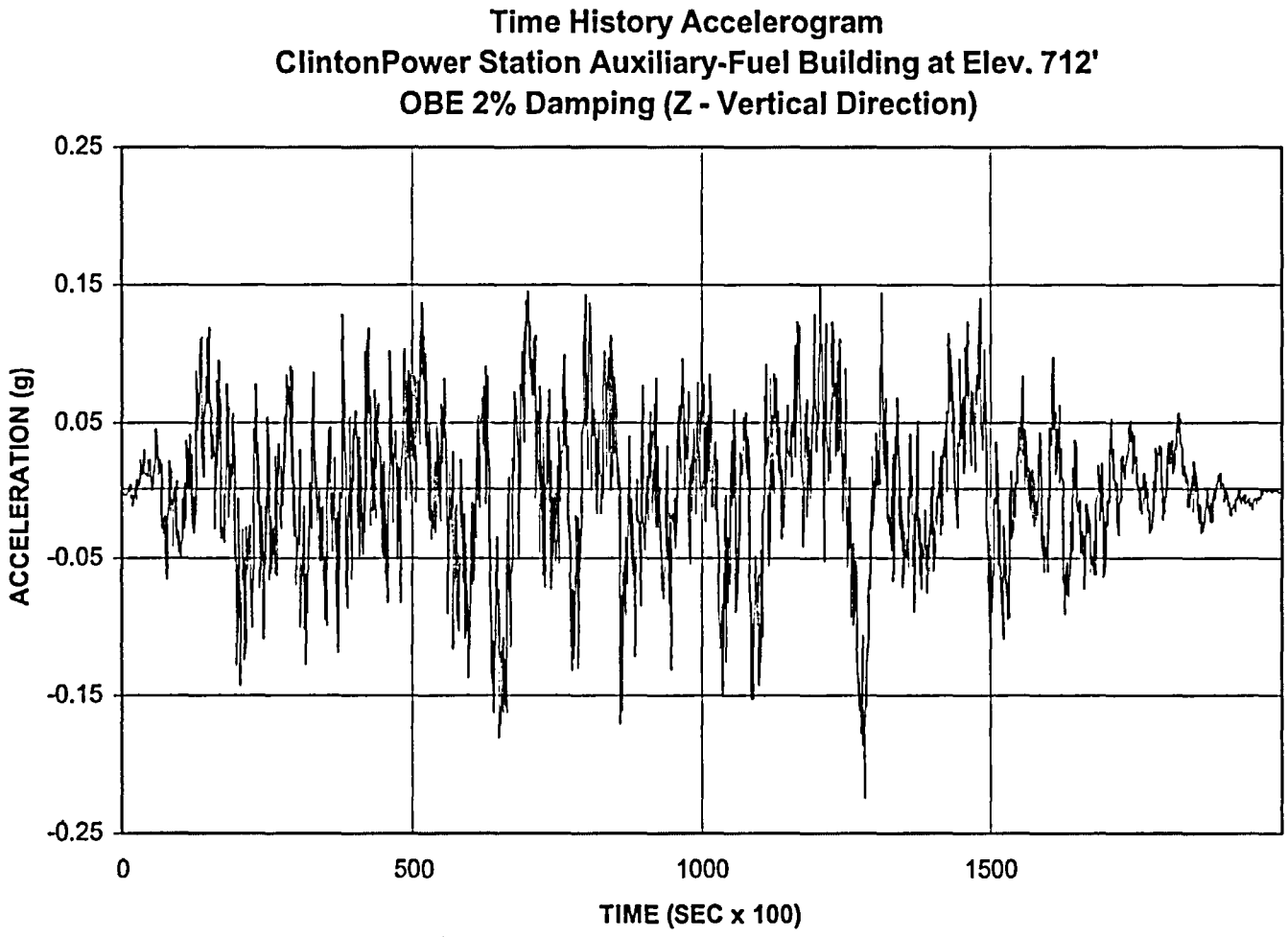

Figure 6.4.6

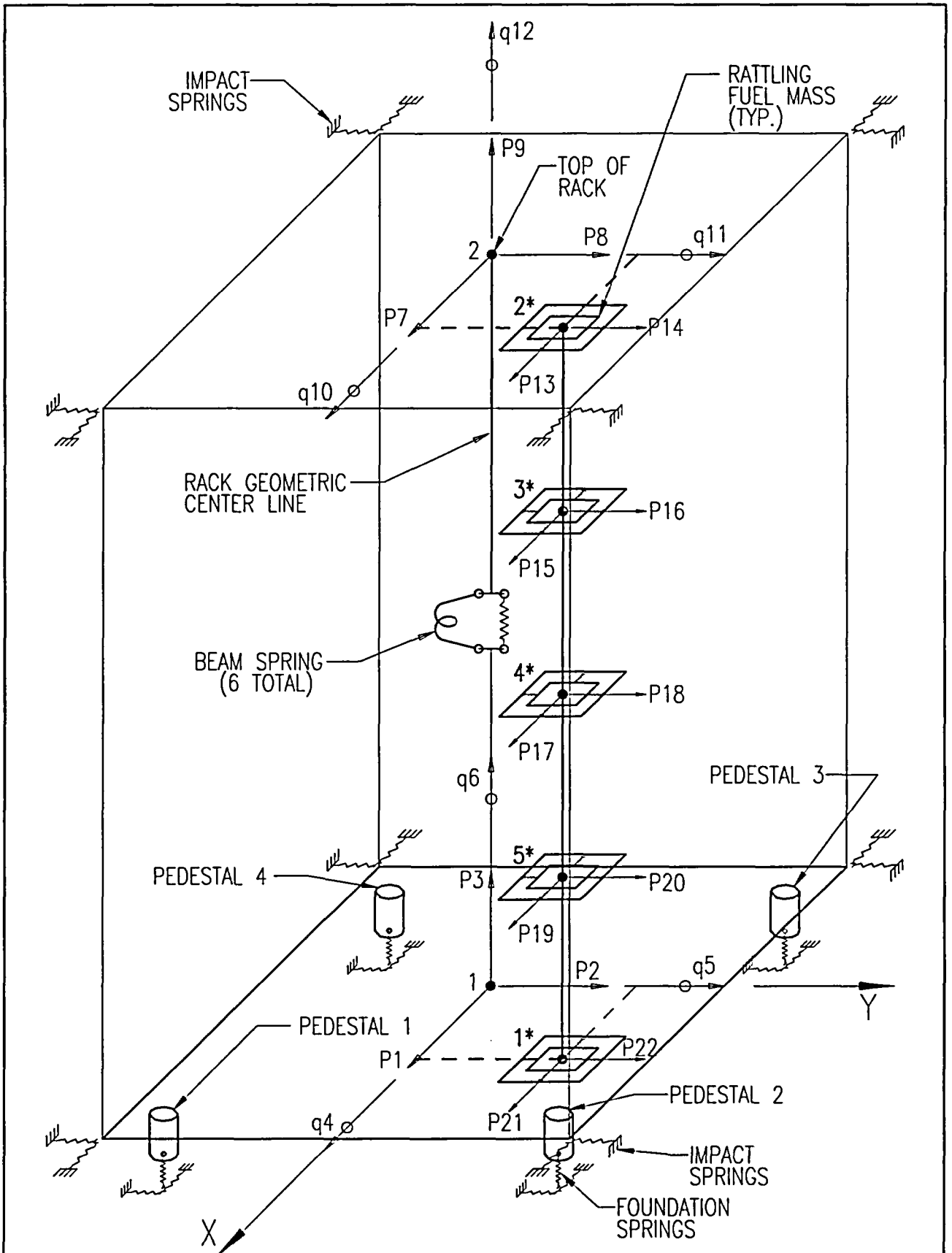

FIGURE 6.5.1; SCHEMATIC OF THE DYNAMIC MODEL OF A SINGLE RACK MODULE USED IN DYNARACK

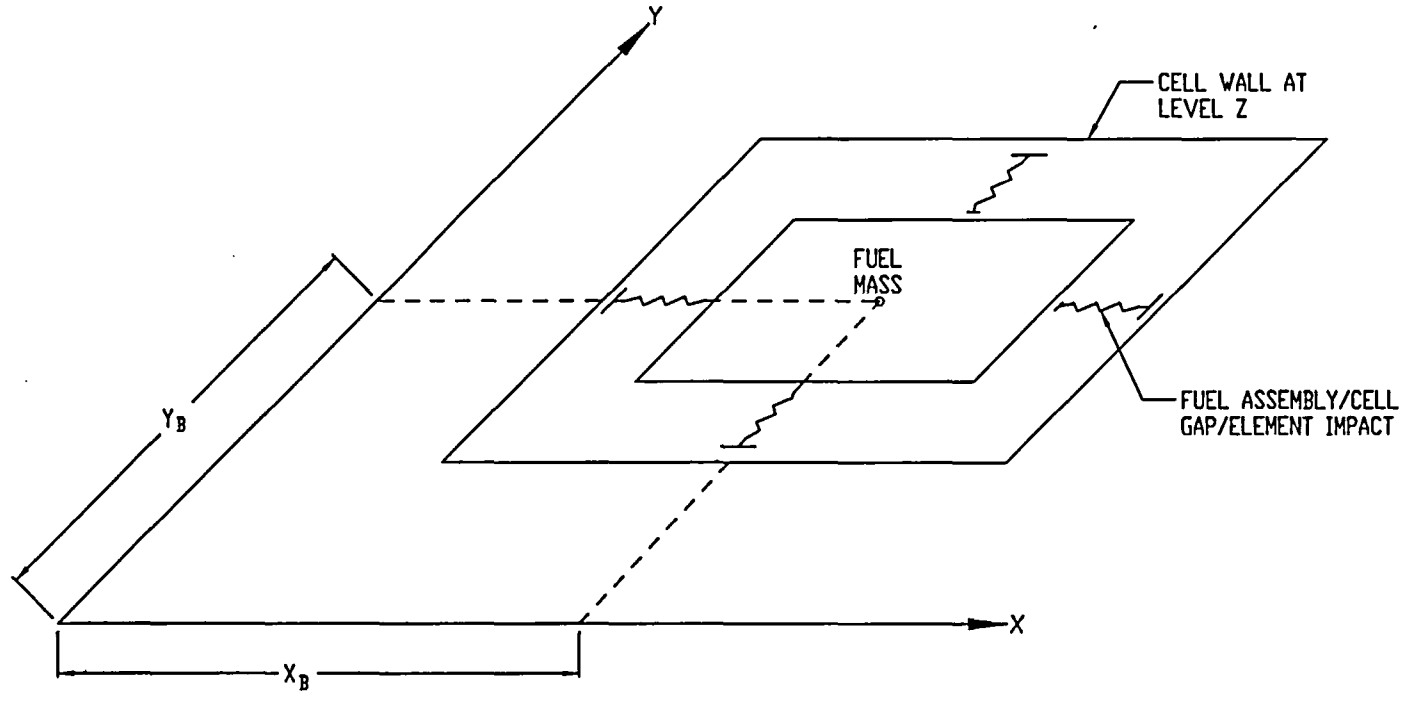

FIGURE 6.5.2; FUEL-TO-RACK GAP/IMPACT ELEMENTS AT LEVEL OF RATTLING MASS

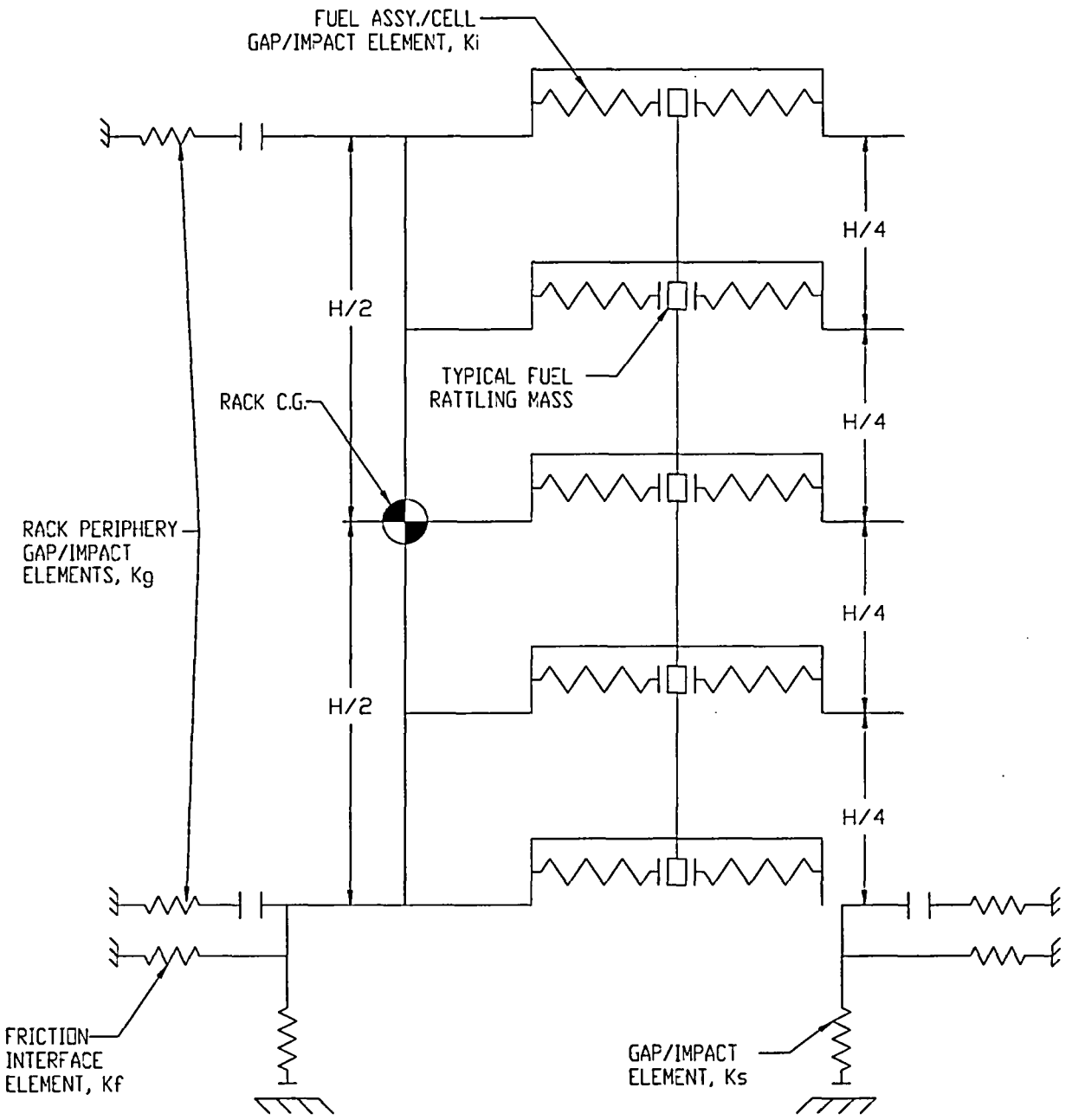

FIGURE 6.5.3; TWO DIMENSIONAL VIEW OF THE SPRING–MASS SIMULATION

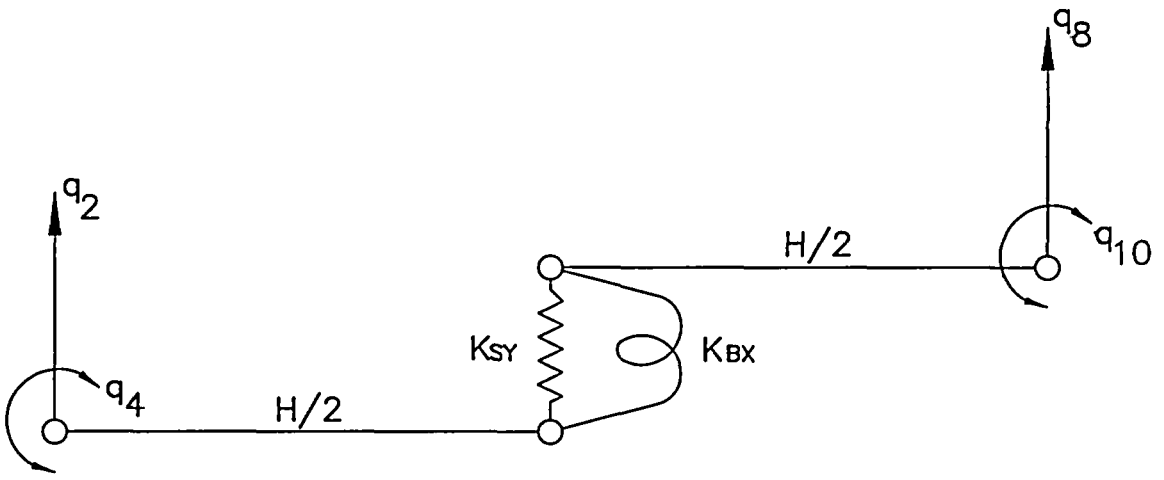

FOR Y–Z PLANE BENDING

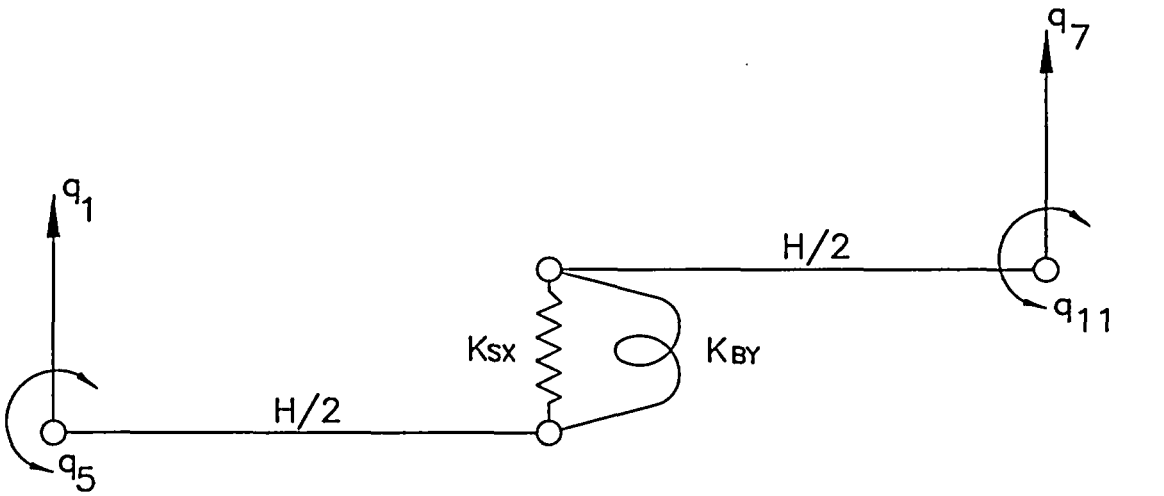

FOR X–Z PLANE BENDING

FIGURE 6.5.4; RACK DEGREES–OF–FREEDOM
WITH SHEAR AND BENDING SPRINGS

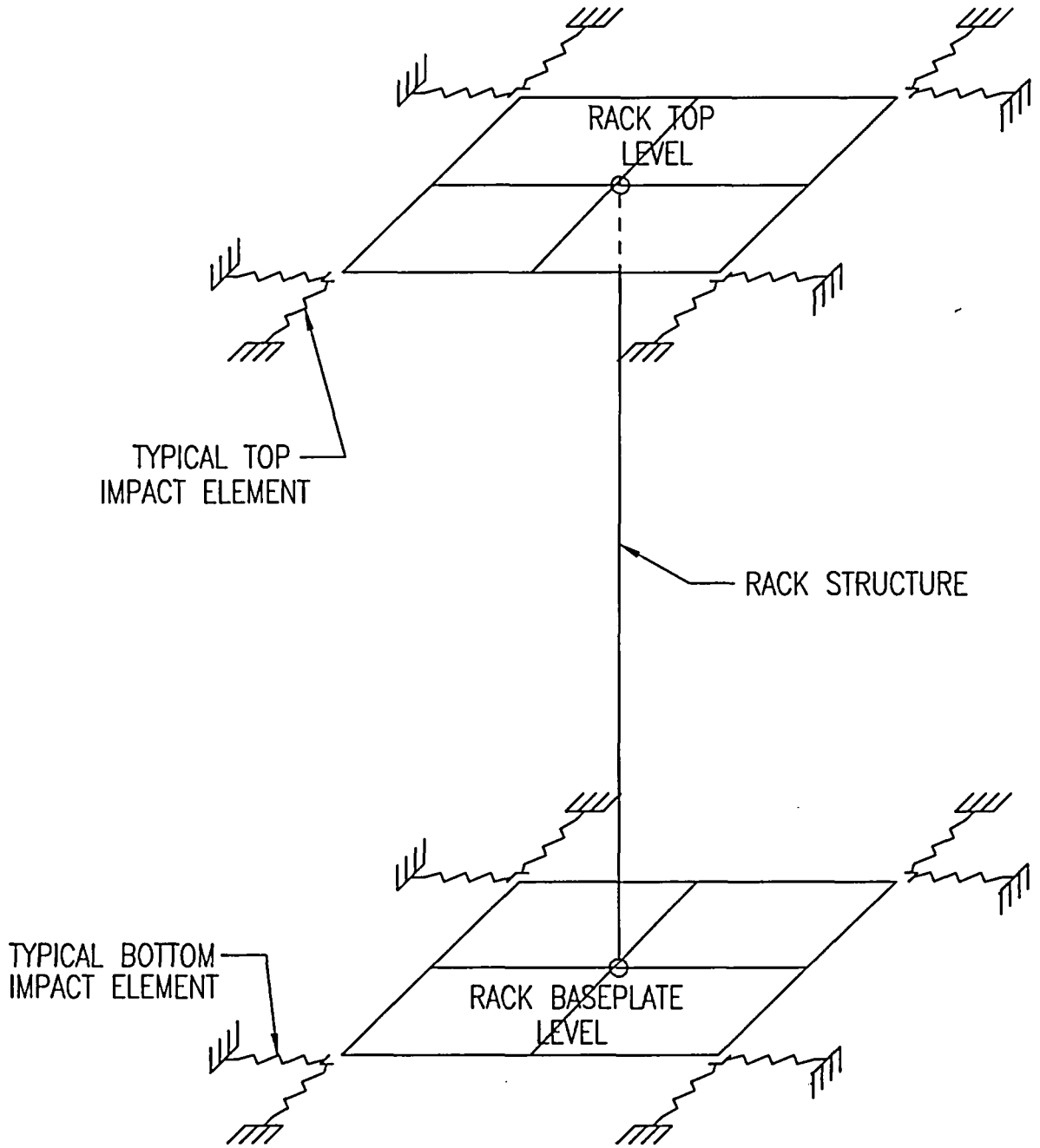

FIGURE 6.5.5; RACK PERIPHERY GAP/IMPACT ELEMENTS

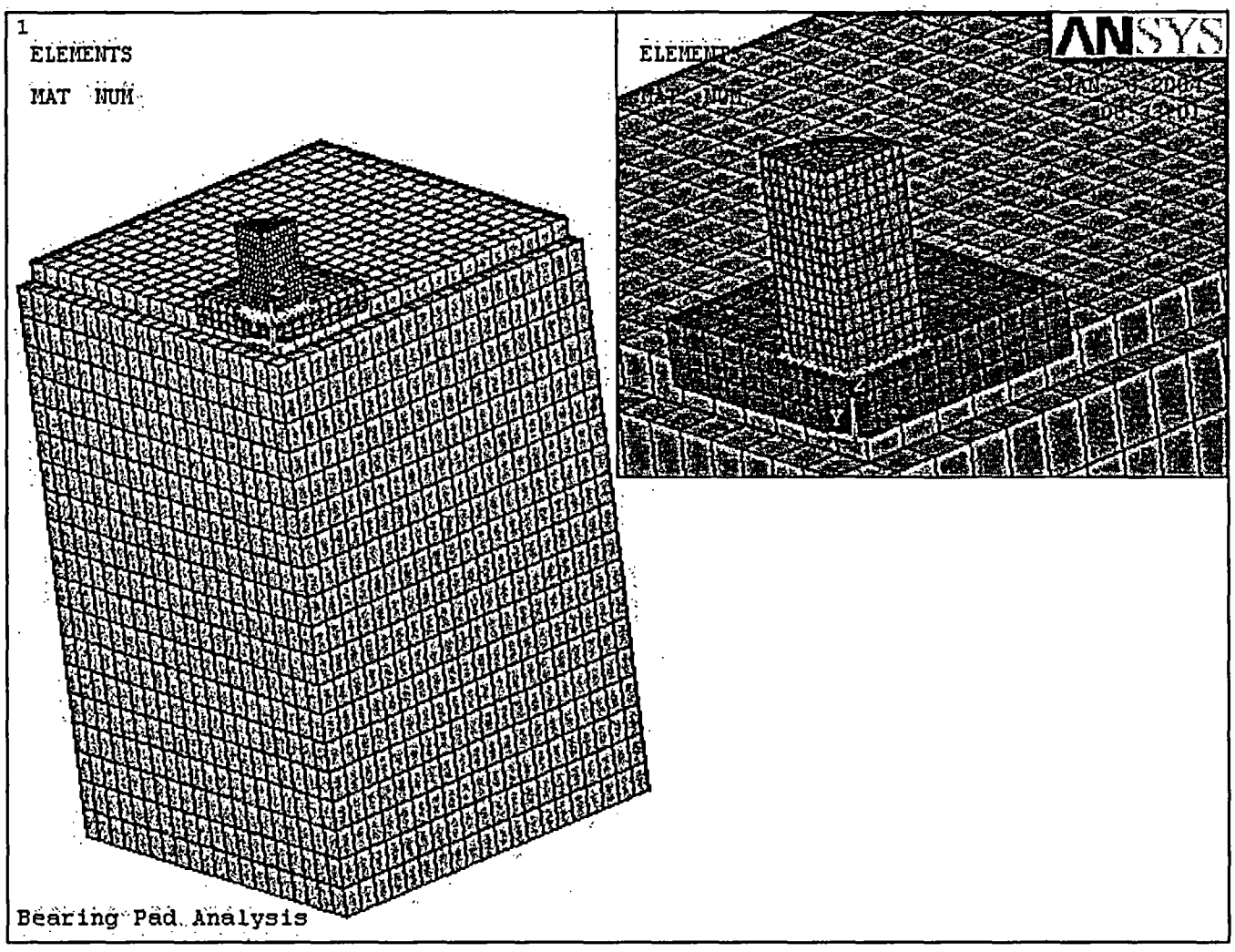

Figure 6.9.1 Isometric of ANSYS Model

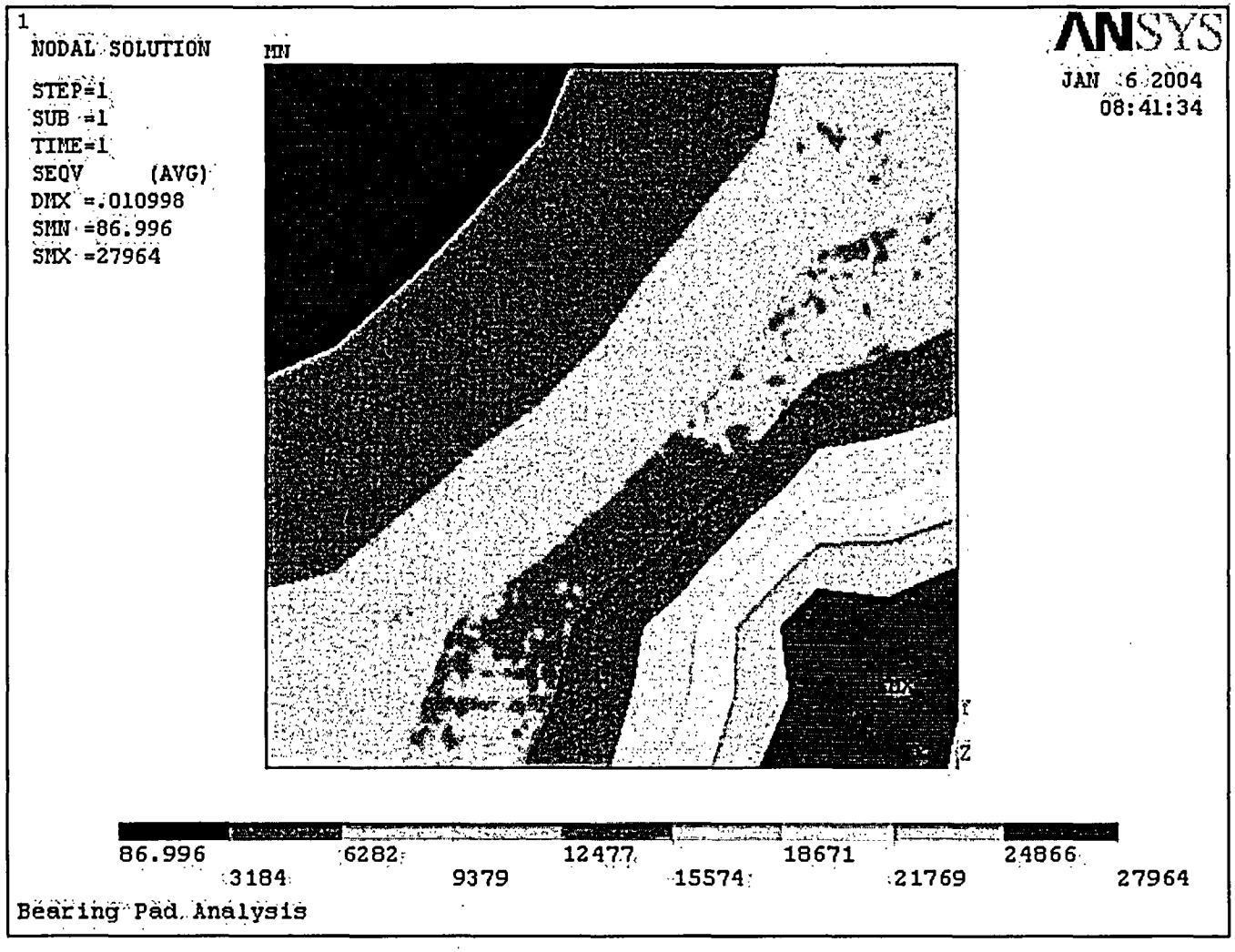

Figure 6.9.2 Stress Distribution in Bearing Pad

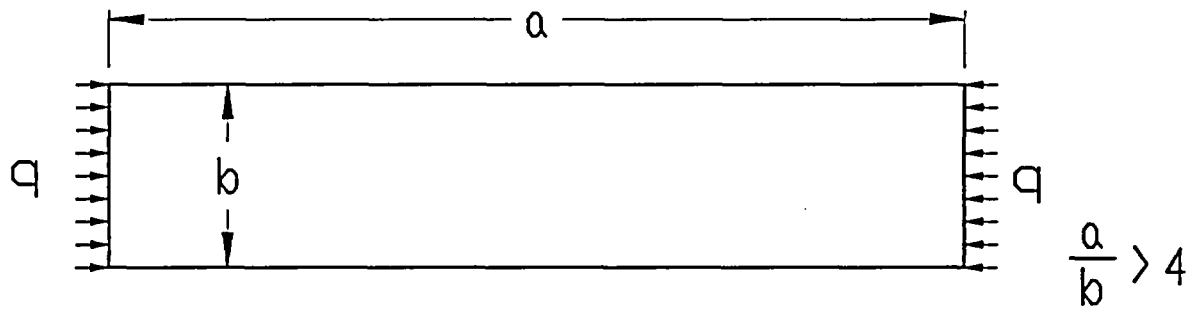

FIGURE 6.12.1; LOADING ON RACK WALL

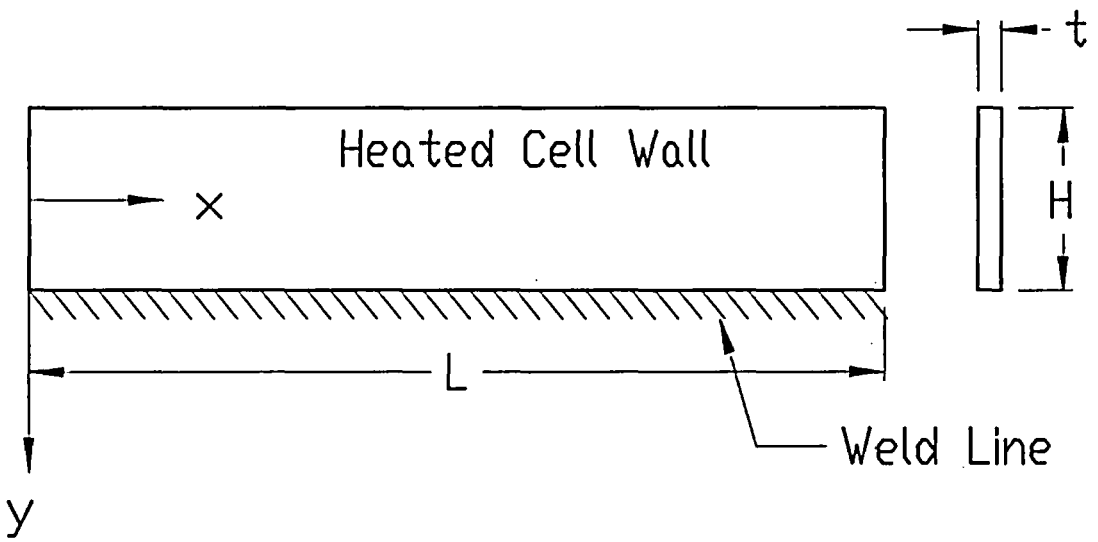

FIGURE 6.12.2; WELDED JOINT IN RACK

7.0 MECHANICAL ACCIDENTS

7.1 Introduction

The USNRC OT position paper [7.1.1] specifies that the design of the rack must ensure the functional integrity of the spent fuel racks and the pool under all credible fuel assembly drop events. This chapter contains synopses of the analyses carried out to demonstrate the regulatory compliance of the proposed racks under postulated accidental drop events germane to the Clinton Power Station Unit 1 spent fuel pool and cask storage pool.

The proposed change does not alter assumptions or results under the current licensing basis on the potential fuel damage due to mechanical accidents.

7.2 Description of Mechanical Accidents

Analyses are performed to evaluate the damage to the new racks and the pool liner subsequent to a fuel assembly impact under various drop scenarios. Two categories of accidental drop events are considered.

In the so-called "shallow" drop event, a fuel assembly, along with the portion of handling tool, which is severable in the case of a single element failure, is assumed to drop vertically and hit the top of a rack cell and subsequently the fuel assembly stored in the cell. Inasmuch as the new racks are of honeycomb construction, the deformation produced by the impact is expected to be confined to the region of collision. However, the "depth" of damage to the affected cell walls must be demonstrated to remain limited to the portion of the cell above the top of the "active fuel region", which is essentially the elevation of the top of the neutron absorber. Stated in quantitative terms, this criterion implies that the plastic deformation of the cell walls should not extend more than 12 inches (downwards) from the top. In order to utilize an upper bound of kinetic energy at impact, the free-fall height is conservatively assumed to be 6 feet [7.2.1].

It is readily apparent from the description of the rack modules in Section 3 that the impact resistance of a rack at its periphery is considerably less than its interior. Accordingly, the limiting shallow drop

scenario, which would produce maximum cell wall deformation, consists of the case where the fuel assembly impacts the peripheral wall of a cell on the periphery of the rack. Furthermore, the dropped fuel assembly can only achieve first contact with the top of the rack at this location because of the orientation of the fuel assembly handle that sticks out of the top of rack. Other impact sites would require the falling fuel assembly to impact the stored fuel assembly handle first. These other impact scenarios would tend to reduce the damage to the rack and are, thus, not considered here, since the goal is to maximize penetration depth to compare against the acceptance criteria. Figure 7.2.1 depicts the finite element model used to evaluate this scenario.

The second class of fuel drop event postulates that the impactor falls through an empty storage cell impacting the fuel assembly support surface (i.e., rack baseplate). This so-called "deep" drop event threatens the structural integrity of the baseplate. If the baseplate is pierced or sufficiently deformed to allow the fuel assembly to impact the liner, then the liner integrity is at risk and water could leak from the pool. The deformed baseplate may also lead to an abnormal condition of the enriched zone of fuel assembly outside the "poisoned" space of the fuel rack. To preclude damage to the pool liner and to avoid the potential of an abnormal fuel storage configuration in the aftermath of a deep drop event, it is required that the baseplate remain unpierced, the baseplate not impact the liner, and that the maximum lowering of the baseplate is shown to be acceptable by the criticality evaluations (see Section 4 for further discussion).

The deep drop event can be classified into two scenarios, namely, a drop in an interior cell away from the support pedestal, as shown in Figure 7.2.2, and a drop through a cell located above a support leg, as shown in Figure 7.2.3. In deep drop scenario 1, the fuel assembly impacts the baseplate away from the support pedestal, where it is more flexible. A gross severing or large deflection of the baseplate leading to a secondary impact with the pool liner is unacceptable. In deep drop scenario 2, the baseplate is buttressed by the support pedestal and presents a hardened impact surface, resulting in a high load. The principal design objective is to ensure that the support pedestal does not tear the liner that overlays the reinforced concrete pool slab.

A review of the proposed cask storage pool layouts (shown in Figures 1.1.1 and 1.1.3) indicates that a transfer cask may be placed adjacent to the storage racks. However, administrative controls will ensure

that all fuel will be removed from the Cask Loading Pool prior to any casks being moved over this area. Controls will be implemented via the plant change package prepared to support the physical modifications. The plant change package will ensure that cask movement and/or fuel movement procedures are modified as necessary to preclude fuel storage in racks located within Cask Loading Pool during fuel cask movement in the vicinity of the Cask Loading Pool. Therefore, there is no need to evaluate any new cask drop scenarios for this fuel storage expansion project.

7.3 Incident Impact Velocity

7.4 Mathematical Model

In the first step of the solution process, the velocity of the dropped object (impactor) is computed for the condition of underwater free fall in the manner of the formulation presented in the above section. Table 7.4.1 contains the computed velocities for the various drop events.

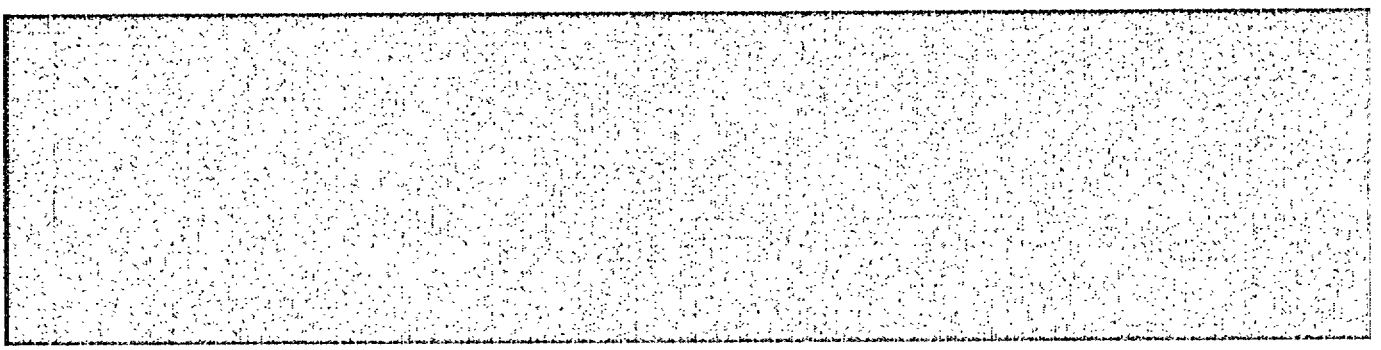

[redacted]. The physical properties of material types undergoing deformation in the postulated impact events are summarized in Table 7.4.2.

7.5 Results

7.5.1 Shallow Drop Event

For the shallow drop event, the dynamic analysis shows that the top of the impacted region undergoes localized plastic deformation. Figure 7.5.1 shows an isometric view of the post-impact geometry of the rack. The maximum depth of plastic deformation is limited to 4.75 inches, which is less than the design limit of 12 inches. Therefore, the damage does not extend into the active fuel region of any stored fuel.

7.5.2 Deep Drop Events

The deep drop through an interior cell does produce some deformation of the baseplate with local severing of the baseplate/cell wall welds. Figure 7.5.2 shows the deformed baseplate configuration. The fuel assembly support surface is lowered by a maximum of 2.6 inches, which is much less than the gap (5.4 inches) between the fuel bottom and the pool liner. The deformation of the baseplate has been determined to be acceptable with respect to lowering the fuel seating position and the resulting criticality consequences, as discussed in Chapter 4.0.

The deep drop event, wherein the impact region is located directly above the support pedestal, is found to produce a maximum plastic strain of 0.0863 in the liner, which is much smaller than the failure strain of the liner material, as shown in Figure 7.5.3. Finally, the concrete slab is found to experience very limited local damage as shown by the predicted cracks and the effective strain distribution in Figure 7.5.4. Since the pool floor can maintain its overall integrity and the liner is not breached in the drop event, there will be no abrupt or uncontrollable loss of water from the pool.

7.6 Conclusion

The drop events postulated for the Clinton Power Station spent fuel/cask storage pools were analyzed and found to produce localized damage within the design limits for the racks. The shallow drop event is found to produce some localized plastic deformation in the top of the storage cell, but the region of permanent strain is limited to the portion of the rack structure situated above the top of the active fuel region. The analysis of the deep drop event at cell locations selected to maximize baseplate deformation indicates that the downward displacement of the baseplate is limited to 2.6 inches, which ensures that fuel will remain in a subcritical condition. The deep drop case analyzed for the scenario to produce maximum pedestal force indicates that the pedestal axial load precludes liner damage and prevents a breach in the integrity of the concrete floor slab. Therefore, there will be no uncontrollable loss of pool water inventory. In conclusion, the new Holtec high-density spent fuel racks for the Clinton Power Station spent fuel/cask storage pools possess acceptable margins of safety under the postulated mechanical accidents.

7.7 References for Chapter 7.0

[7.1.1] "OT Position for Review and Acceptance of Spent Fuel Storage and Handling Applications," dated April 14, 1978, and addendum dated 1979.

[7.2.1] Clinton Power Station USAR, Revision 10.

Table 7.4.1

IMPACT EVENT DATA

Case	Impactor Weight (lb)	Impactor Type	Drop Height (in)	Impact Velocity (in/sec)
1. Shallow drop event	614 (fuel, wet weight) 450 (tool, dry weight)	Fuel assembly & handling tool	72	205.7
2. Deep drop event scenario 1 (away from pedestal)	614 (fuel, wet weight) 450 (tool, dry weight)	Fuel assembly & handling tool	240	343.6
3. Deep drop event scenario 2 (above pedestal)	614 (fuel, wet weight) 450 (tool, dry weight)	Fuel assembly & handling tool	240	299.9

Table 7.4.2

MATERIAL DEFINITION

Material Name	Material Type	Density (pcf)	Elastic Modulus (psi)	Stress		Strain	
				First Yield (psi)	Failure (psi)	Elastic	Failure
Stainless Steel	SA240-304L	501	2.787e+07	2.315e+04	6.810e+04	8.306e-04	3.800e-01
Carbon Steel	SA564-630	490	2.86e+07	1.092e+05	1.400e+05	3.818e-03	1.400e-01
Concrete	f'_c=3,500 psi	140	3.372e+06	--	--	--	--

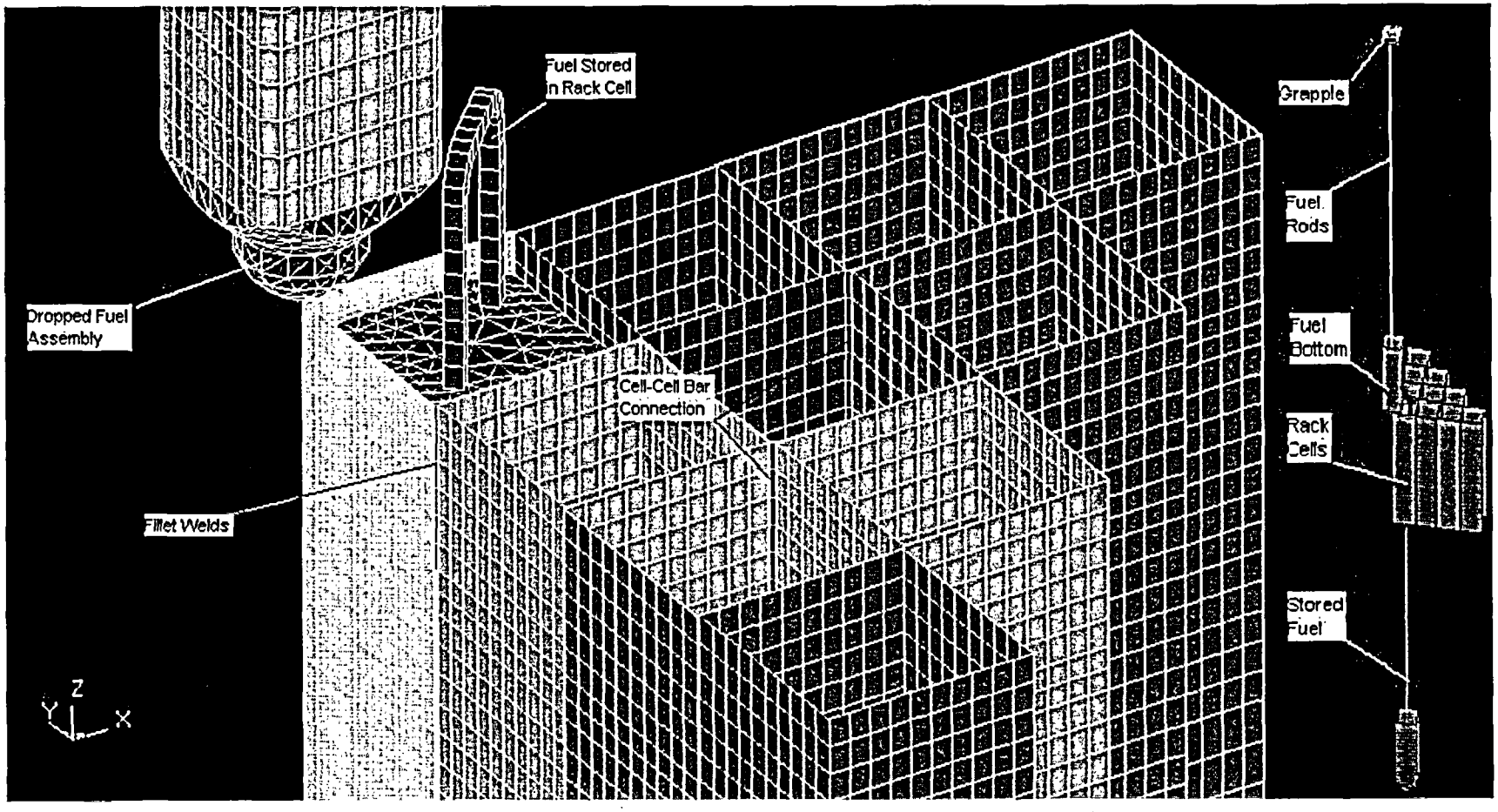

Fig. 7.2.1 Finite Element Model of the "shallow" drop event

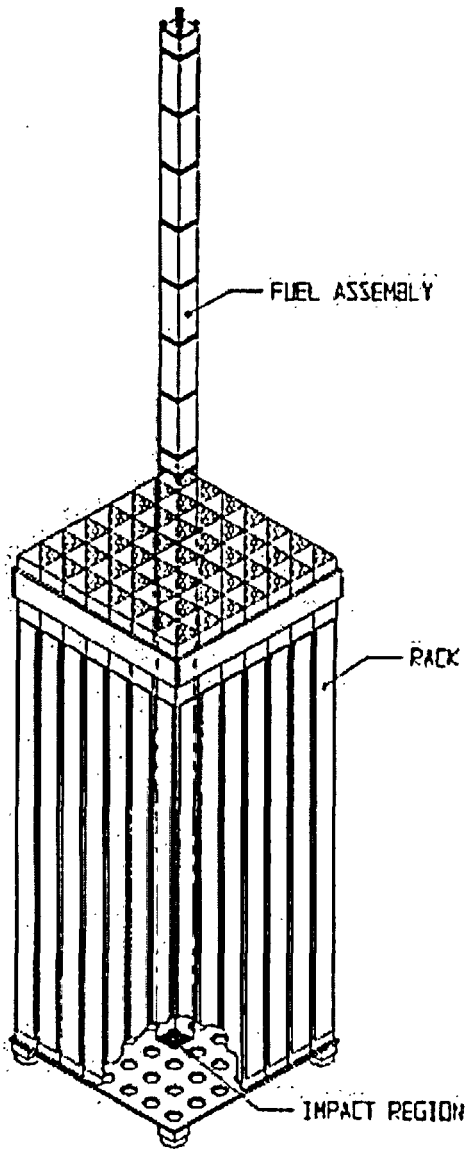

Fig. 7.2.2 Schematics of the "deep" drop scenario 1

Note: This figure is primarily provided to indicate the impact zone for this scenario. The configuration of the rack is not intended to be accurate.

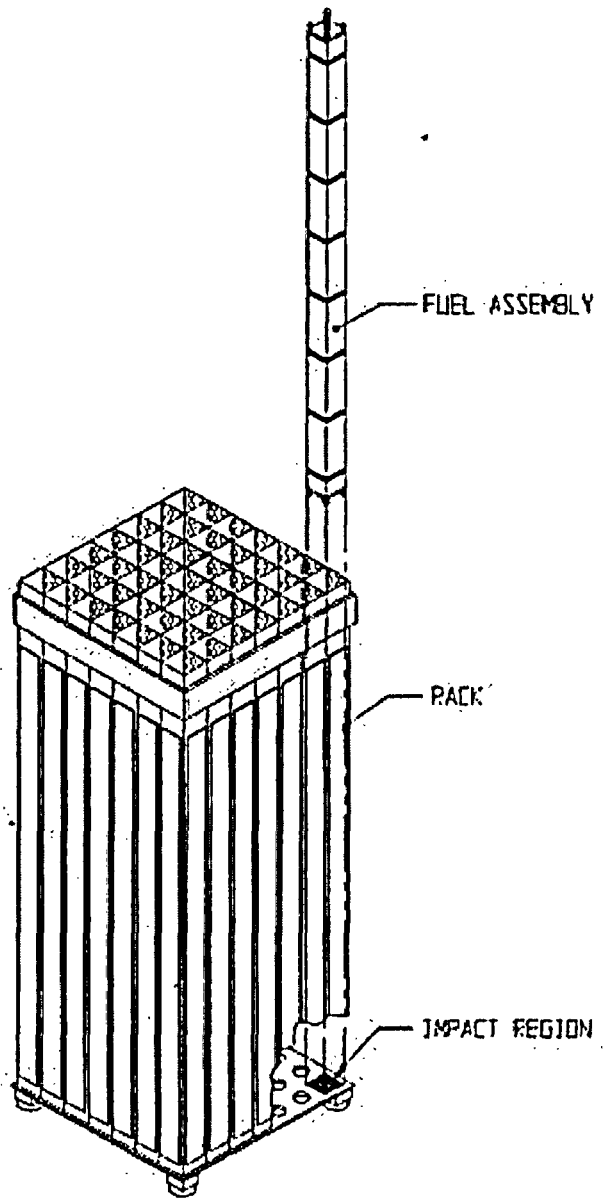

Fig. 7.2.3 Schematics of the "deep" drop scenario 2

Note: This figure is primarily provided to indicate the impact zone for this scenario. The configuration of the rack is not intended to be accurate.

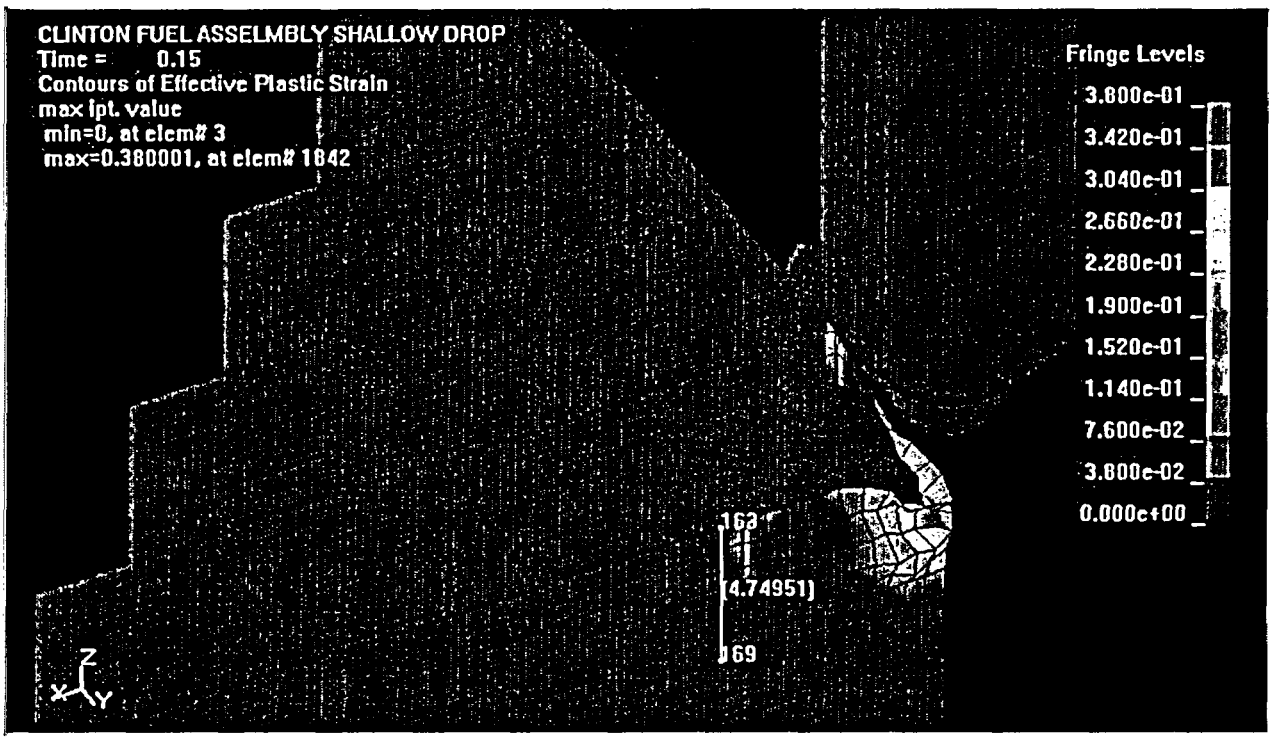

Fig. 7.5.1 "Shallow" Drop: Maximum Plastic Strain

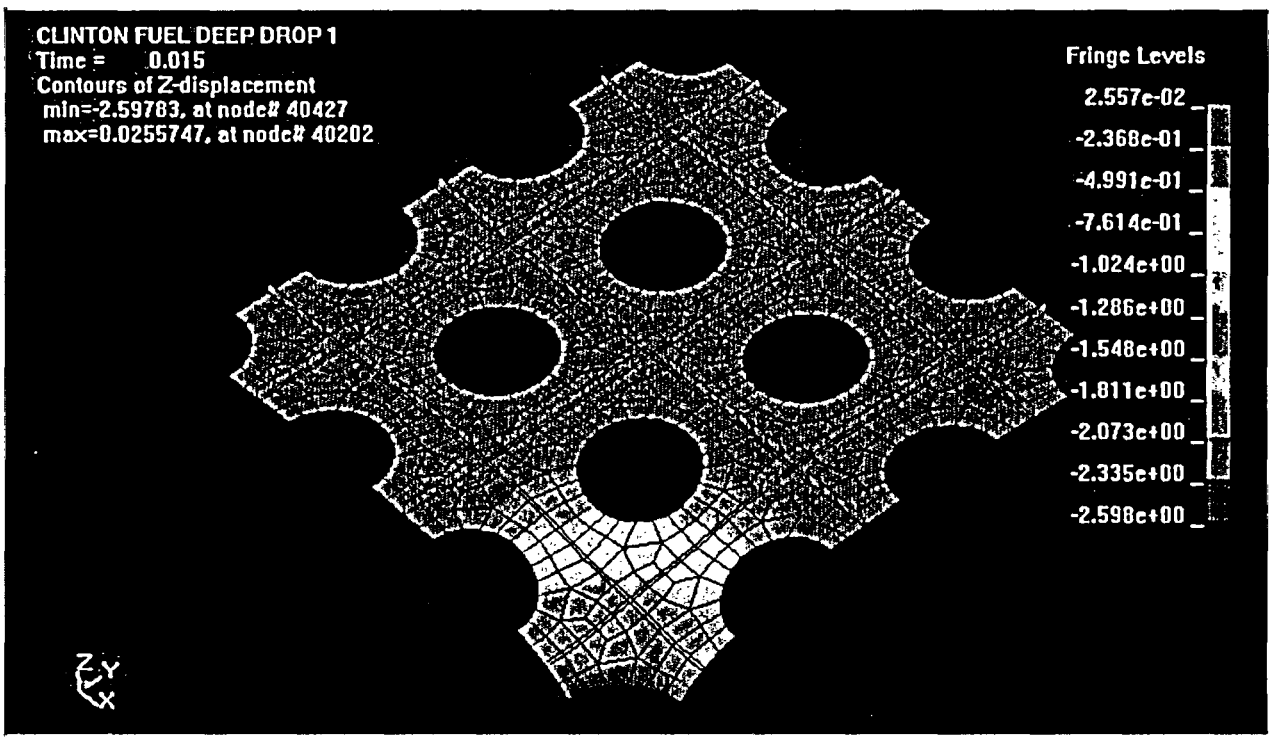

Fig. 7.5.2 "Deep" Drop Scenario 1: Maximum Vertical Displacement

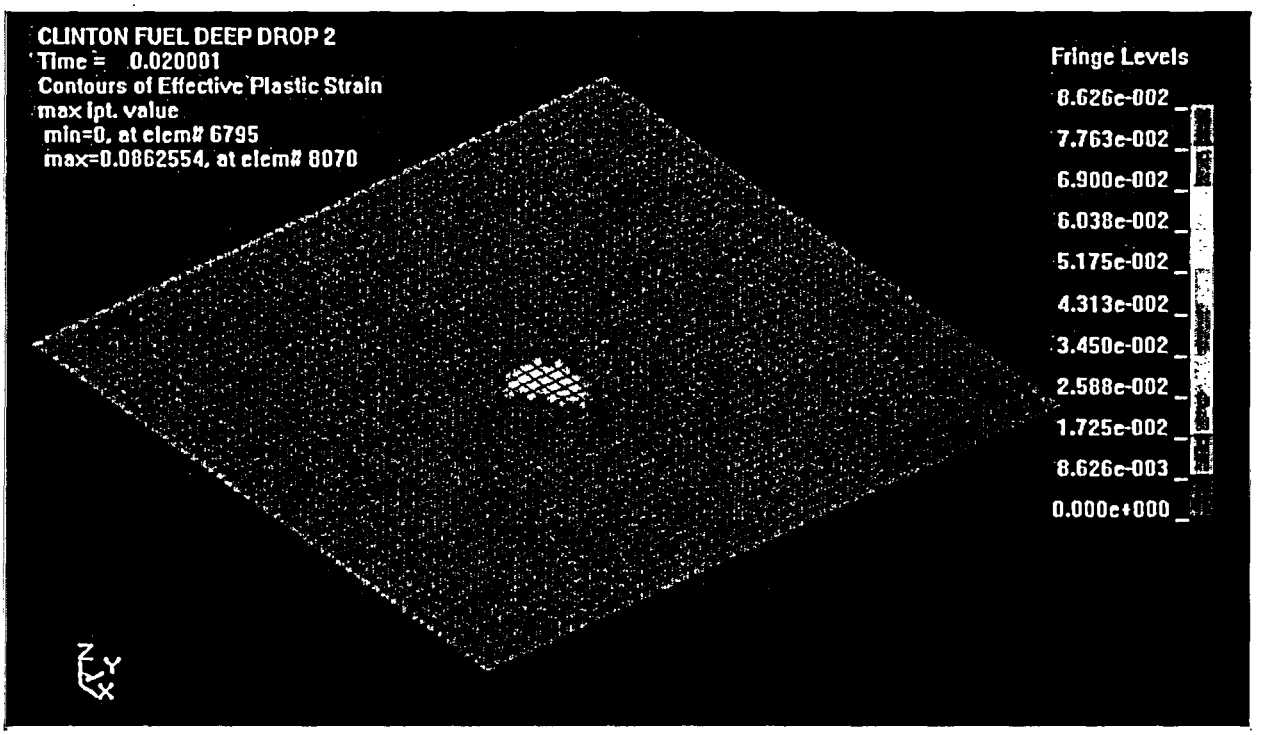

Fig. 7.5.3 "Deep" Drop Scenario 2: Maximum Von Mises Stress – Liner

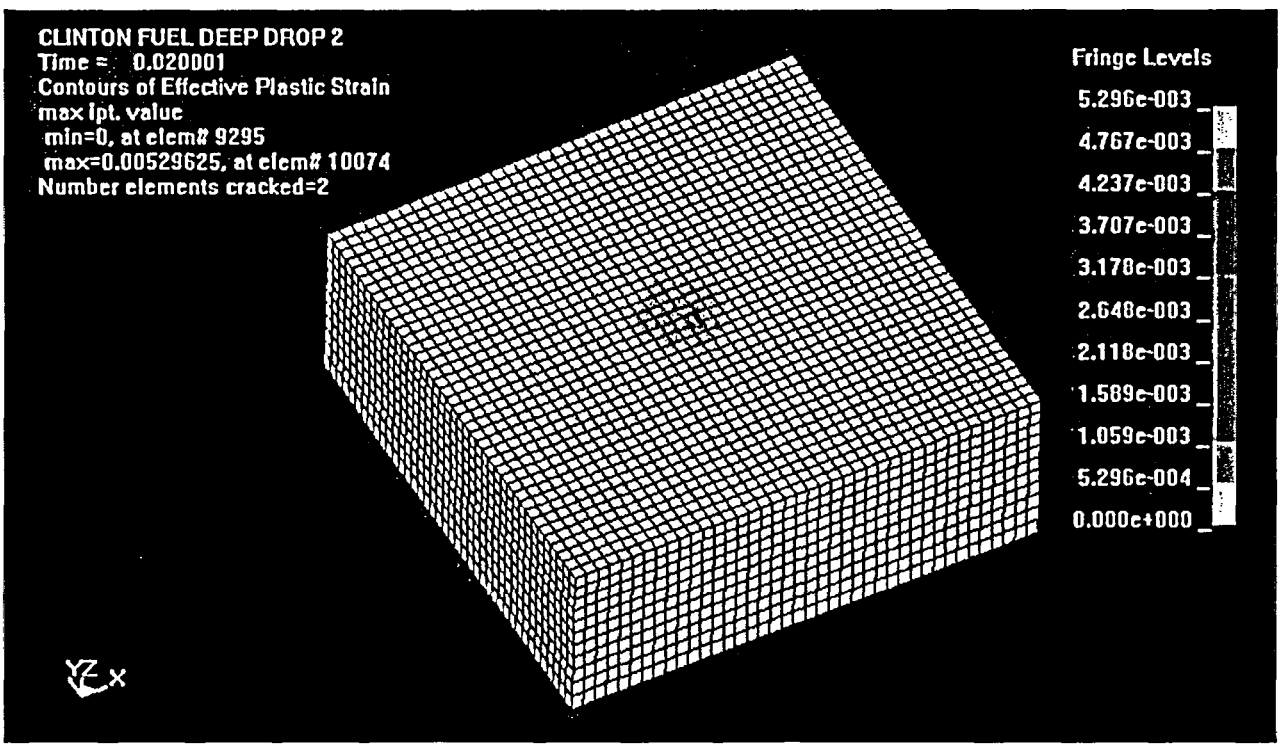

Fig. 7.5.4 "Deep" Drop Scenario 2: Maximum Effective Strain – Concrete

8.0 FUEL BUILDING STRUCTURAL INTEGRITY EVALUATIONS

Structural integrity evaluations of the regions of the reinforced concrete structure affected by the proposed fuel storage capacity expansion are summarized in this section. The introduction of racks into the Fuel Cask Storage Pool during Phases 1 and 2 and installation of new racks in the Spent Fuel Pool (SFP) during Phase 2, as shown in Figures 1.1.1 through 1.1.3 will affect the structure by imposing a hydrodynamic pressure on the walls adjacent to the new racks and additional loads on the pool floor through the pedestal bearing pads.

8.1 Introduction

Figure 8.1 shows a plan view of the SFP and adjacent Fuel Cask Storage Pool. The SFP and Fuel Cask Storage Pool each consist of four walls with floor slabs on grade. The floors of both pools are constructed above 21'-10" of controlled compacted fill material and consist of a 6 inch mud mat overlain with 9'-8" of reinforced concrete, topped with 6 inches of grout and covered with a ¼" thick liner. This brings the level of the floor up to the 712'-0" plant elevation. The concrete floor provides substantial strength, due to its thickness, placement on grade and the fact that it is heavily reinforced with #11 and #18 reinforcement bars.

A review of Figure 8.1 indicates that the western wall of the SFP will control the evaluation for the four walls surrounding this pool. The nominal rack-to-wall dimension of 2.5 inches (See Figure 1.1.2) is less for this wall than any of the other three walls. This wall is longer than the north and south walls and does not have any intermediate walls or floors providing support. Therefore, an evaluation of the western wall of the SFP for the increased rack-to-wall hydrodynamic coupling pressures is performed. The adjacent transfer pool is considered to be empty for conservatism.

Similarly, by observation of Figure 8.1, the 36 inch thick south and west walls of the Fuel Cask Storage Pool are much thinner than the other two 72 inch thick walls. The southern wall controls, because this wall is longer than the west wall and contains less reinforcement in the horizontal direction.

The structural evaluations of the affected portions of the SFP and Fuel Cask Storage Pool are conducted using finite element models of the controlling walls extending the full width of the pools. Figures 8.2 and 8.3 show the SFP west wall and Fuel Cask Storage Pool south wall finite element models, respectively.

Results for individual load components are combined using the factored load combinations mandated by the Clinton Power Station USAR [8.1], and are based on the "ultimate strength" design method. Bending moment capabilities are checked for appropriate sections on each wall in each direction (vertical and horizontal) for concrete structural integrity. Due to the compressive nature of the axial loads, the relationships between bending moment capacity and compression loads are conservatively neglected. Shear capability is evaluated along all sections of the affected walls. Load combinations and structural capacity assessments follow requirements of the plant USAR [8.1] and the American Concrete Institute Code (ACI 318) [8.2].

The SFP and Fuel Cask Storage Pool floor slabs are not included in the finite element model. The global adequacy of the slab and underlying subsoil remains satisfactory to withstand the additional loading imposed by the rack. This assertion is derived from the fact that the slab is a continuous structure with the same capacities in the Fuel Cask Storage Pool as in the SFP in areas beneath existing racks with similar fuel storage density and associated loading. Local stresses in the liner and underlying concrete imposed by the rack pedestals are addressed in Sections 6.9.6, 8.6, and 8.7.

The thermal loading in the reinforced concrete structure is considered in the manner specified in the applicable codes. The temperature gradients considered (see Section 8.4.3) are those defined in Section 5.0 and the plant USAR [8.1]. Consistent with standard design practices, the temperature gradient established for the pool walls is intended to subsume local thermal effects such as direct heat deposition into the concrete from the absorption of gamma radiation from the stored spent fuel.

8.2 Description of the SFP West Wall and Fuel Cask Storage Pool South Wall

The west wall of the SFP is 6' thick, 36' long and 43' high spanning in elevation from the top of the slab at 712' to the mezzanine floor at 755'. This wall is shared by the Transfer Pool and has no lateral support against out of plane displacements. The transfer gate from the SFP to the Transfer Pool creates a 4' wide by 27' deep discontinuity in the SFP west wall and is considered in the model, as shown in Figure 8.2. The horizontal reinforcement in this wall increases approaching the floor slab. The vertical reinforcement remains consistent through the height except for a local area near the floor slab in the middle of the base of the wall.

The south wall of the Fuel Cask Storage Pool is 3' thick, 17' long and 43' high spanning in elevation from the top of the floor slab at 712' to the mezzanine floor at 755'. This wall has lateral support against out of plane displacements from a 3' thick floor at Elevation 739'. The horizontal reinforcement is consistent throughout the height of the wall. The vertical reinforcement varies along the length and height of the wall.

In both analyses, the walls are fixed against out-of-plane and horizontal in-plane translations and three rotational degrees of freedom, but are free to displace in the vertical direction for all dead and seismic loadings. The boundary conditions are modified to allow for in-plane displacements due to thermal expansion.

8.3 Analysis Procedures

The reinforced concrete walls are subjected to individual "unit" load cases covering the service conditions (the structural weight of the concrete structure, the hydro-static water pressure and the temperature gradient) and seismic induced loads (structural inertial loads, hydro-dynamic water loads, and rack-structure interaction dynamic loads) for operating basis earthquake (OBE) and safe shutdown earthquake (SSE) conditions. The service condition loads are considered as static acting loads; the seismic induced loads for both OBE and SSE seismic events are obtained from the application of acceleration spectra provided in the plant USAR [8.1] with input seismic acceleration

amplifiers defined on the basis of a frequency analysis of the structure. Results from the seismic load cases are combined using the square root of the sum of the squares (SRSS) and then combined with the static load.

The reinforced concrete is considered elastic and isotropic. The elastic characteristics of the concrete are independent of the reinforcement contained in each structural element for the mechanical load cases when un-cracked cross-sections are assumed. This assumption is valid for all load cases with the exception of the thermal loads, where, for a more realistic description of the reinforced concrete cross-section behavior, the assumption of cracked concrete is used. To simulate the cracking patterns, the original elastic modulus of the concrete is reduced in accordance with the methodology suggested by ACI 349 [8.3]. Table 8.1 summarizes the concrete properties employed in the structural evaluation of the SFP west wall and Fuel Cask Storage Pool south wall.

8.4 Definition of Loads Included in Structural Evaluation

These definitions apply to both the SFP west wall and Fuel Cask Storage Pool south wall.

8.4.1 Static Loading (D = Dead Loads)

1) Dead weight includes the weight of the wall.
2) The hydrostatic water pressure acting on the wall.

8.4.2 Seismic (E = OBE; E' = SSE)

1) Horizontal hydrodynamic inertia loads due to the contained water mass and sloshing loads in the entire SFP (considered in accordance with [8.4]) that arise during a seismic event.
2) Horizontal hydrodynamic pressures between spent fuel rack and pool wall caused by rack motions during a seismic event.
3) Vertical hydrodynamic pressure due to acceleration of the contained water mass.
4) Seismic inertia force of the walls from the wall mass.

8.4.3 Thermal Loading (T_o)

A steady-state thermal gradient is defined by the bulk pool temperature of 134°F (Section 5) and the Fuel Building ambient of 70°F given in [8.1]. The bulk pool temperature is applied to both the SFP and Fuel Cask Storage Pool.

8.4.4 Load Combinations and Acceptance Criteria

No live loads are defined for the areas under consideration. Results from a suite of unit load analyses are used to form appropriate load cases and then combined in accordance with the load combinations specified in Table 3.8-1.2 of the plant USAR [8.1].

The final load combinations evaluated for structural integrity are:

Normal Loading Combination	$1.4\,D + 1.7\,T_o$
Severe Environmental Loading Combination	$1.4\,D + 1.7\,T_o + 1.9\,E$
Abnormal Loading Combination	$1.0\,D + 1.0\,T_o + 1.0\,E'$
Extreme Environmental Loading Combination	$1.0\,D + 1.25\,E$
Abnormal / Severe and Extreme Loading Combination	$1.0\,D + 1.0\,E'$

Note that seismic loads, after the SRSS combination, are directed so that they add to the hydrostatic pressure and wall self-weight.

Moments and shears computed for each load combination are compared with their respective capacities. Consistent with the intent of the guidance provided in the ACI literature, and recognizing that there is always load re-distribution occurring in a concrete structure designed in accordance with ultimate strength methods, characteristic section widths (horizontal and vertical) are established over which moments are averaged and then compared with the averaged section capacity. Similarly, the transverse shear is averaged over the same section width to define the "section shear".

The ratios of the moment and shear capacities to their respective "section" values are referred to as the safety factor (SF). In computing the SF for section moments and shears, the presence of in-plane compressive loads, which act to increase capacities, are conservatively neglected.

8.5 Results of Reinforced Concrete Analyses

The structural integrity of the SFP west wall and Fuel Cask Storage Pool south wall are evaluated and the axial forces, the bending moments and the shear forces were computed for all load combinations. The reinforced concrete cross-sectional capacities were determined and used to obtain the safety factors of the structural elements for each load combination considered. Safety factors are acceptable if the safety factor exceeds 1.0. The calculated minimum safety factors for the sections of the walls for each load combination are:

SFP West Wall

Item / Direction	Safety Factor	Load Combination
Moment / Horizontal	1.23	Severe Environmental
Moment / Vertical	1.24	Normal
Shear / Horizontal	1.42	Severe Environmental
Shear / Vertical	1.26	Normal

Fuel Cask Storage Pool South Wall

Item / Direction	Safety Factor	Load Combination
Moment / Horizontal	1.07 *	Severe Environmental
Moment / Vertical	2.23	Normal
Shear / Horizontal	1.62	Severe Environmental
Shear / Vertical	1.52	Normal

* The bending safety factors conservatively neglect the additional load carrying capacity induced by the presence of axial compression.

8.6 Pool Liner Evaluation

The freestanding racks are supported on a ¼" thick stainless steel liner plate, which separates the bearing pad from the concrete pool floor. During a seismic event the racks may undergo a series of motions developing friction forces between the bearing pad and the pool liner. The friction loads shall not buckle or tear the liner plate or cause the liner seam welds to rupture. A strength assessment is performed to show that the stresses in the liner plate and the seam welds comply with ASME Code Section III stress limits [8.5]. Since the pedestal loads occurring during the seismic event are repetitive, a fatigue assessment of the liner using Miner's Rule is also performed. The fatigue assessments conservatively consider 20 OBE and one SSE events.

The calculated minimum safety factors for the SFP liner are:

Principal Stress in Liner	5.9
Shear Stress in Liner Weld	3.8
Cumulative Usage Factor	1.05×10^{-3}

The stresses in the liner comply with ASME Subsection NF stress limits. In accordance with ASME Subsection NB [8.6], the cumulative usage factor is below the limit of 1. Therefore, fatigue failure does not occur after twenty OBE and one SSE events.

8.7 Bearing Evaluation

Bearing pads are placed between rack pedestals and the spent fuel pool (SFP) floor to reduce the otherwise high local stresses in the SFP concrete slab by spreading the concentrated load of each pedestal over a larger concrete contact area. The vertical pedestal loads generated by the peak load are obtained from the dynamic analyses of the spent fuel racks subject to seismic loads.

The calculated minimum safety factors for local bearing stress on the concrete is:

Bearing Stress in Concrete Slab	1.19

8.8 Conclusions

Regions affected by the installation of racks in the Fuel Cask Storage Pool and the SFP are examined for structural integrity under bending and shearing action and bearing stress. It is determined that adequate safety margins exist when the factored load combinations are checked against the appropriate structural design strengths. For the most limiting load combination, the minimum safety factor remained above 1.0. Finally, it is also shown that local loading on the liner does not compromise liner integrity.

8.9 References

[8.1] Clinton Power Station USAR, Revision 10, October 2001.

[8.2] ACI 318-77, Building Code Requirements for Reinforced Concrete, American Concrete Institute, 1977.

[8.3] ACI 349-01, Code Requirements for Nuclear Safety Related Concrete Structures, American Concrete Institute, 2001.

[8.4] Nuclear Reactors and Earthquakes, TID-7024, United States Atomic Energy Commission, Division of Reactor Development, August 1963.

[8.5] ASME Code Section III, 1977 Edition.

[8.6] ASME Code Section III, Subsection NB, 1977 Edition.

Table 8.1 Reinforced Concrete Properties	
Concrete Strength	4,000 psi
Reinforced Concrete Density (typical)	150 lbf / ft^3
Un-cracked Concrete Modulus of Elasticity	3.6 x 10^6 psi
Concrete Poisson's Ratio	0.17
Concrete Coefficient of Thermal Expansion	5.5 x 10^{-6} in/in/°F
Reinforcement Strength	60,000 psi
Reinforcement Modulus of Elasticity	29 x 10^6 psi
Reference Temperature	70°F

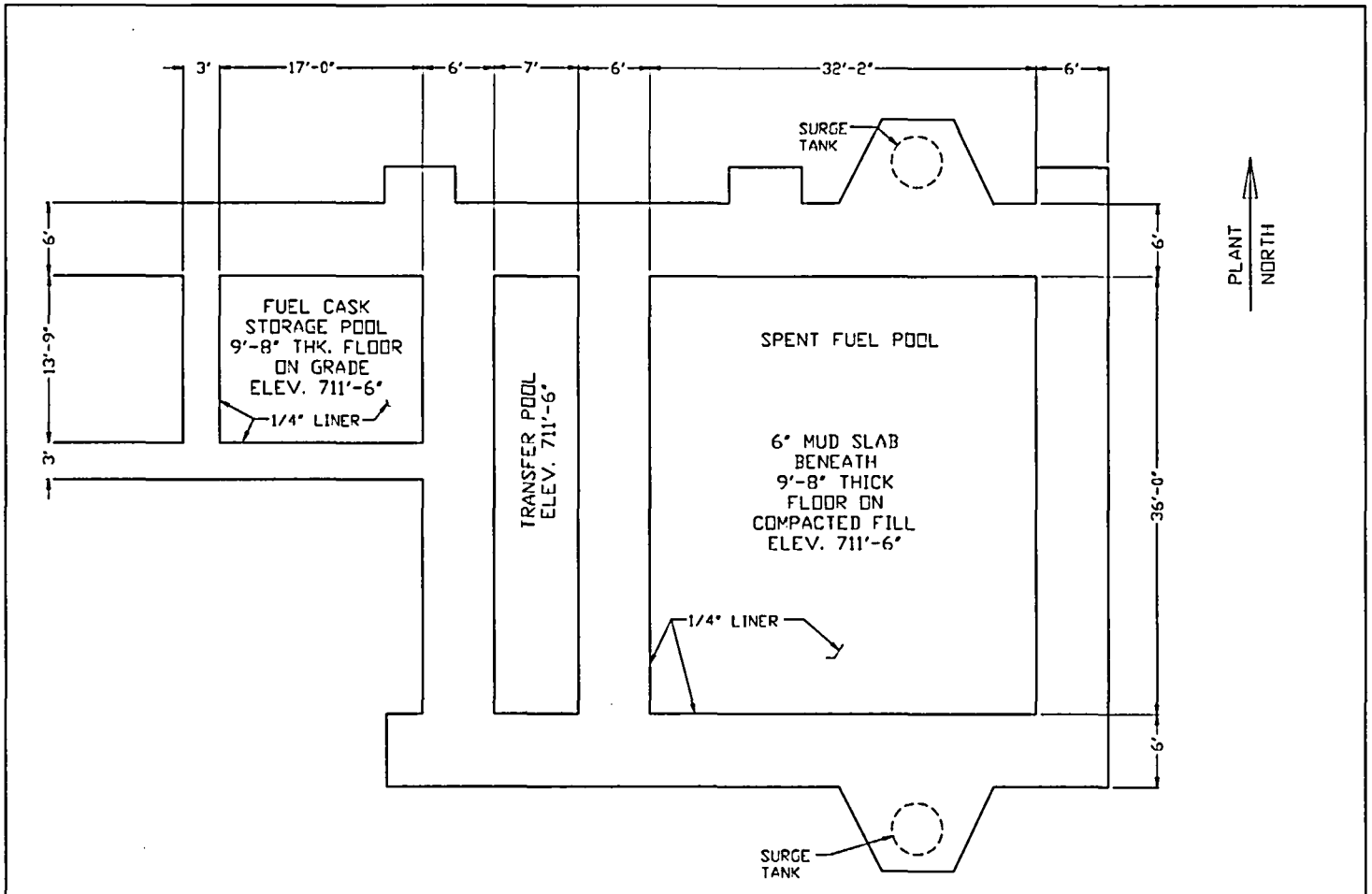

FIGURE 8.1

PLAN OF CLINTON SPENT FUEL POOL AREA

HI-2033124

PROJECT 1342

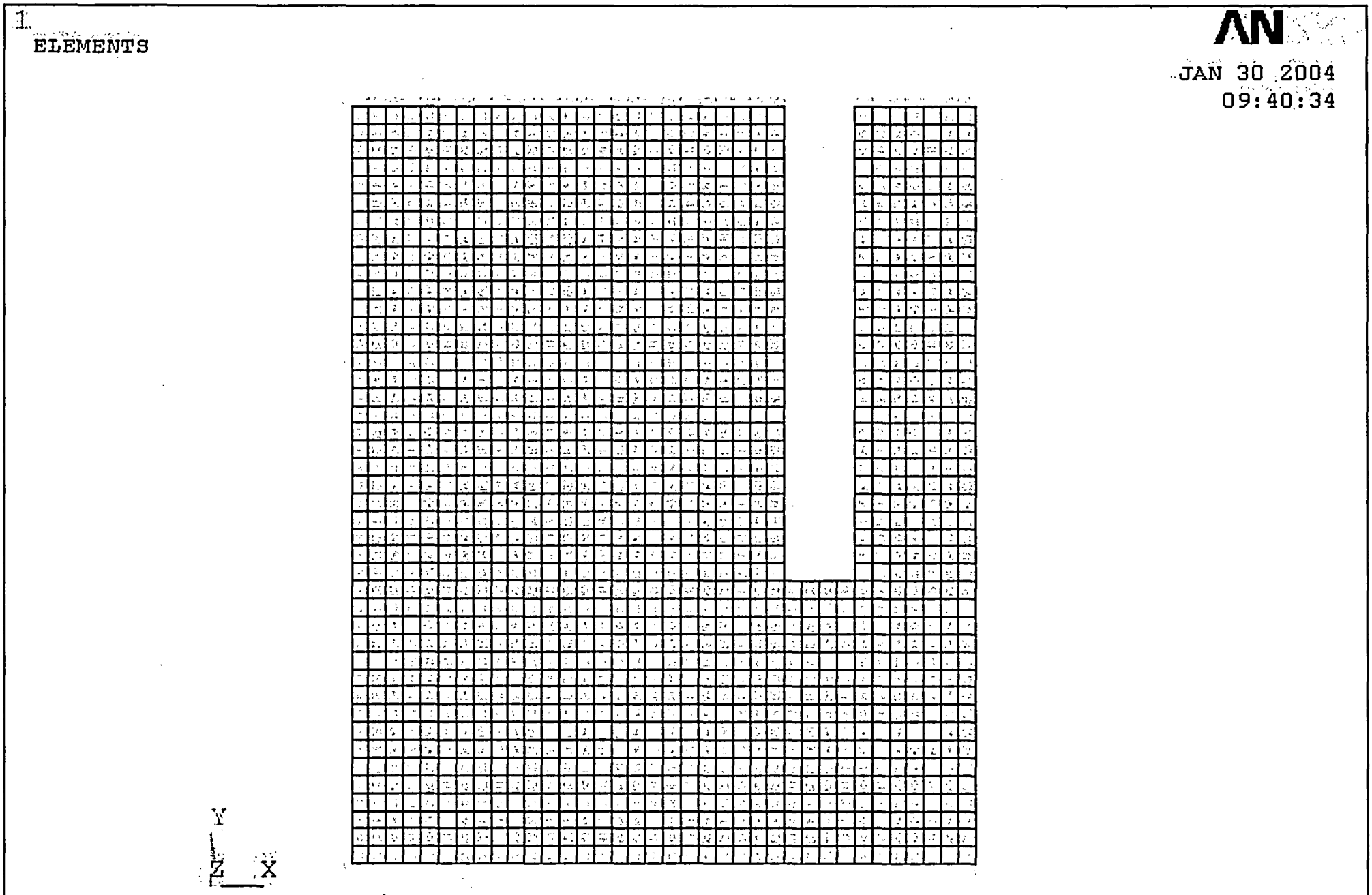

Figure 8.2 Spent Fuel Pool West Wall Finite Element Model, Proj 1342, HI-2033124

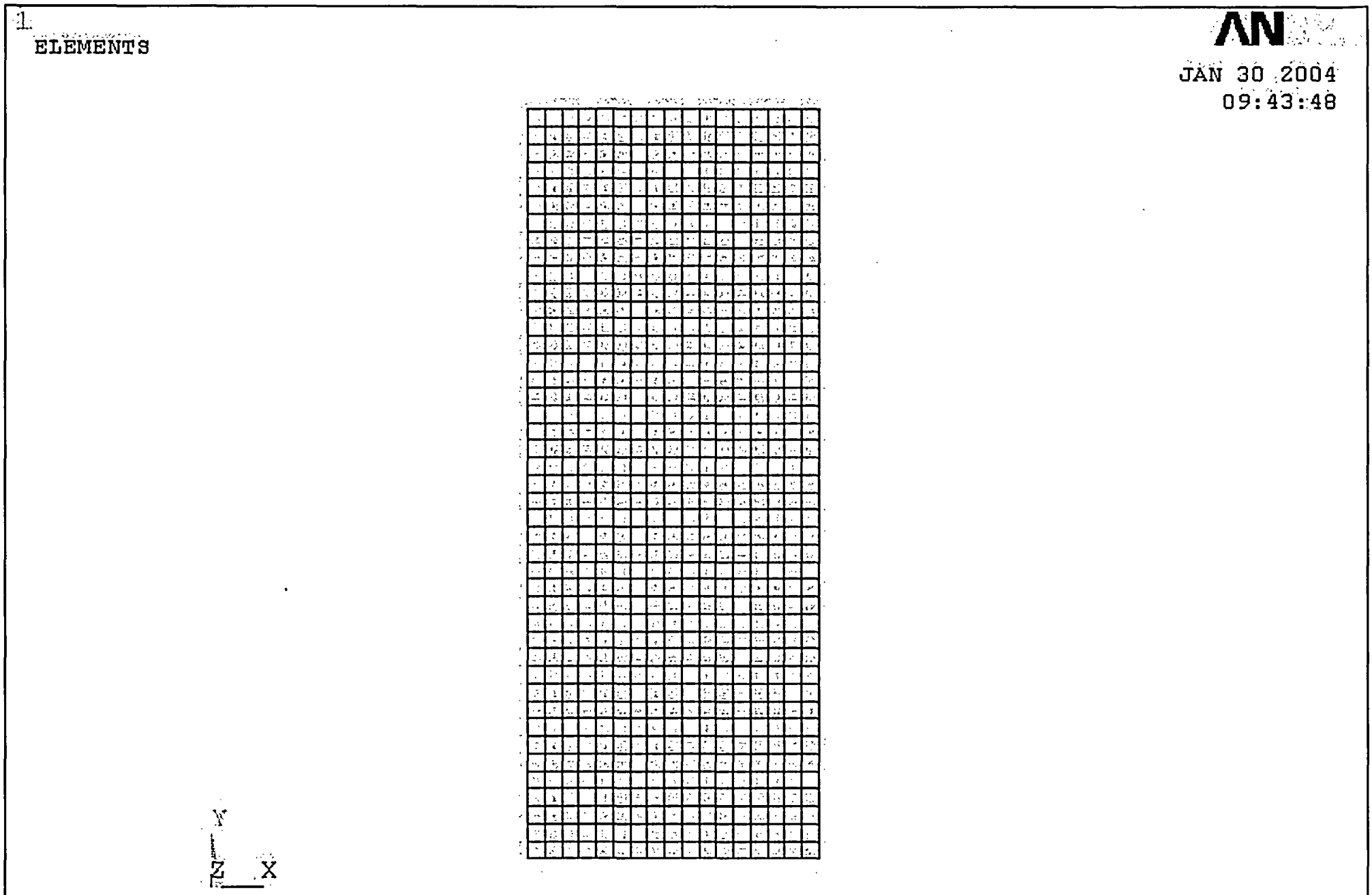

Figure 8.3 Fuel Cask Storage Pool South Wall FE Model, Proj 1342, HI-2033124

9.0 RADIOLOGICAL EVALUATION

9.1 Fuel Handling Accident

Increases in the fuel-storage capacity at Clinton do not require updating the analysis of the fuel-handling accident, for these doses were calculated in the recent past [9.1.1]. The factors affecting the doses, such as the depth of the pool, the exposure of the fuel elements considered when the accident occurs, etc. have not changed

9.2 Solid Radwaste

The necessity for resin replacement is determined primarily by the requirement for water clarity, and the resin is normally changed about once a year. No significant increase in the volume of solid radioactive wastes is expected with the expanded storage capacity. During fuel-storage expansion operations, small amounts of additional resins may be generated by the pool cleanup system on a one-time basis.

9.3 Gaseous Releases

Gaseous releases from the fuel storage building are combined with other plant exhausts. Normally, the contribution from the fuel storage building is negligible compared to the other releases, and no significant increases are expected as a result of the expanded storage capacity.

9.4 Personnel Exposures

During normal operations, personnel on the working level of the fuel storage area are exposed to radiation from the spent fuel pool. The dose rates experienced by personnel are not expected to increase with the increased storage capacity of the pools because the dose rate from the fuel in storage is negligible. The water above the stored fuel is sufficiently deep that the dose rate from that fuel is orders of magnitude lower than the low dose rate from the radionuclides in the pool water itself and the dose rate from a fuel assembly in transit. Consequently, though the dose rate from stored fuel will increase because more

spent fuel assemblies are stored, it will not increase to levels comparable to those attributable to other sources.

The radionuclide concentrations in the pool water are not expected to increase significantly, for the levels are determined principally from the mixing of primary system water with the pool water and the spalling of crud deposits from the spent fuel assemblies as they are moved in the storage pool during refueling operations. Although the overall capacities of the pools are being increased, the movement of fuel during given refuelings is independent of storage capacity.

There will be no change in the dose rate from a fuel assembly in transit, for the fuel parameters have not changed and the depth of water above the active portion of the assembly has not changed.

The concrete side walls of the fuel pool are six feet thick, providing sufficient shielding that the maximum dose rate at the outside surface of the concrete, from stored spent fuel, is two mr/hr if the pool is completely filled with fuel that has cooled only 24 hours.

The dose rate at the outer surface of the three-foot shield for the Fuel Cask Storage Pool would be high – 26 rem/hr -- in the hypothetical situation in which the racks in the Fuel Cask Storage Pool were filled with fuel cooled only 24 hours. If the three rows of storage cells closest to the wall were filled with old fuel that contributes negligibly to the dose rate at the outer surface, and the rest of the cells were filled with 24-hour fuel, the dose rate through the three-foot shield is reduced to 4.4 mr/hr. This fuel storage management scheme will be controlled by administrative controls implemented with procedural changes.

Operating experience has shown that there have been negligible concentrations of airborne radioactivity, and no increases are expected as a result of the expanded storage capacities. Area monitors for airborne activities are available in the immediate vicinities of the pools.

In summary, no increases in radiation exposure to operating personnel are expected. Consequently, neither the current health-physics program nor the area monitoring system needs to be modified.

9.5 Anticipated Exposures During Storage Expansion

All of the operations involved in increasing the storage capacity will utilize detailed procedures prepared with full consideration of ALARA principles. Similar operations have been performed in numerous facilities in the past, and there is every reason to believe that the expansion of storage capacity can be safely and efficiently accomplished at Clinton, with minimum radiation exposure to personnel.

Total occupational exposure for the operations required to increase storage capacity is estimated to be between 7 and 14 person-rem, as shown in Table 9.1. While individual task efforts and exposures may differ from those in Table 9.1, the total is believed to be a reasonable estimate for planning purposes.

The existing radiation protection programs at the plant are adequate for the storage-expansion operations. Where there is a potential for significant airborne activity, continuous air samplers will be in operation. Personnel will wear protective clothing and, if necessary, respiratory protective equipment. Activities will be governed by Radiation Work Permits, and personnel monitoring equipment will be issued to each individual. As a minimum, this will include pocket dosimeters. Additional personnel monitoring equipment (i.e., extremity badges or alarming dosimeters) may be utilized as required. Work, personnel traffic, and the movement of equipment will be monitored and controlled to minimize contamination and to assure that exposures are maintained ALARA.

At Clinton, some of the existing storage racks will be removed from service and washed down in preparation for packaging and offsite shipment. Estimates of the person-rem exposures associated with washdown and readying the old racks for shipment are included in Table 9.1. Shipping containers and procedures will conform to Federal DOT regulations and to the requirements of any state through which the shipment may pass, as set forth by the State DOT office.

9.6 References

[9.1.1] Site Boundary and Control Room Dose following a FHA in Containment using Alternative Source Terms, Stone & Webster Engineering Corporation calculation No. C-022, March 26, 2002.

Table 9.1 [†]

PRELIMINARY ESTIMATE OF PERSON-REM EXPOSURES DURING THE EXPANSION OF FUEL-STORAGE CAPACITY

Operation	Number of Personnel	Hours	Estimated Person-Rem Exposure [††]
Shuffle fuel	4	160	1.6 to 3.2
Remove/relocate existing racks	6	100	1.5 to 3.0
Clean and vacuum pool(s)	4	20	0.3 to 0.6
Remove underwater appurtenances and assist in rigging racks for moving (Divers)	4	24	1.9 to 3.8
Install/relocate new racks	6	60	1.0 to 2.0
Wash and decon old racks	3	20	0.2 to 0.3
Prepare old racks for shipment [†††]	4	60	0.6 to 1.2
TOTAL PERSON-REM EXPOSURE			7 to 14

[†] This tabulation presents the estimated exposures associated with the operations necessary to reposition the existing racks and install the new racks. The exposures are based on the experience obtained in increasing the capacities of many storage pools.

[††] Assumes a dose rate of 2.5 mr/hr (minimum) to 5 mr/hr (maximum), except for pool cleaning and vacuuming operations, which assume 4 to 8 mr/hr, and diving operations, which assume 20 to 40 mr/hr.

[†††] Maximum expected exposure, although details of preparation and packaging of old racks for shipment have not yet been determined.

10.0 INSTALLATION

10.1 Introduction

The installation phase of the Clinton fuel storage rack project will be executed by Holtec International's Field Services Division. Holtec, serving as the installer, is responsible for performance of specialized services, such as underwater diving and welding operations, as necessary. All installation work at Clinton is performed in compliance with NUREG-0612 (refer to Section 3.0), Holtec Quality Assurance Procedure 19.2, Clinton rack installation project specific procedures, and applicable Clinton procedures.

Crane and fuel bridge operators are trained in the operation of overhead cranes per the requirements of ANSI/ASME B30.2, and the plant's specific training program. Consistent with the installer's past practices, a videotape aided training session is presented to the installation team, all of whom are required to successfully complete a written examination prior to the commencement of work. Fuel handling bridge operations are performed by Clinton personnel, who are trained in accordance with Clinton procedures.

Rack lifting devices are required for the handling of new racks and existing racks. The lifting devices are designed to engage and disengage on lift points at the bottom of the racks. The lifting devices comply with the provisions of ANSI N14.6-1978 and NUREG-0612, including compliance with the design stress criteria, load testing at a multiplier of maximum working load, and nondestructive examination of critical welds.

A surveillance and inspection program shall be maintained as part of the installation of the racks. A set of inspection points, which have been proven to eliminate any incidence of rework or erroneous installation in previous rack projects, is implemented by the installer.

Underwater diving operations will be required to support some aspects of this project including, but not limited to, wall hanger/bracket interference removal and rack handling support.

Holtec International developed procedures will be used in conjunction with the Clinton procedures to cover the scope of activities for the rack installation and removal effort. Similar procedures have been utilized and successfully implemented by Holtec on previous rerack projects. These procedures are written to include ALARA practices and provide requirements to assure equipment, personnel, and plant safety. These procedures are reviewed and approved in accordance with Clinton administrative procedures prior to use on site. The following is a list of the Holtec procedures, used in addition to the Clinton procedures to implement the installation phase of the project.

A. Installation/Removal and Handling Procedure:

This procedure provides direction for the installation, removal, and handling of the new and existing storage rack modules in the Spent Fuel Pool and Fuel Cask Storage Pool, as applicable. This procedure delineates the steps necessary to receive the new racks on site, the proper method for unloading and uprighting the racks, staging the racks prior to installation, installation of the racks, and removal and packaging of existing racks. The procedure provides for the installation of the new racks, their height and level adjustments of the rack pedestals and verification of the as-built field configuration to ensure compliance with design documents.

B. Receipt Inspection Procedure:

This procedure delineates the steps necessary to perform a thorough receipt inspection of a new rack module after its arrival on site. The receipt inspection includes dimensional measurements, cleanliness inspection, visual weld examination, and verticality measurements.

C. Cleaning Procedure:

This procedure provides for the cleaning of a new rack module, if required. The modules are to meet the requirements of ANSI N45.2.1, Level B, prior to placement in the Fuel Cask Storage Pool or Spent Fuel Pool. Methods and limitations on cleaning materials to be utilized are provided.

D. Pre- and Post-Installation Drag Test Procedure:

These two procedures stipulate the requirements for performing a functional test on a new rack module prior to and following installation. The procedures provide direction for inserting and withdrawing an insertion gage into designated cell locations, and establishes an acceptance criterion in terms of maximum drag force.

E. ALARA Procedure:

Consistent with Holtec International's ALARA Program, this procedure provides guidance to minimize the total man-rem received during the rack installation project, by accounting for time, distance, and shielding. This procedure will be used in conjunction with the Clinton ALARA program.

F. Liner Inspection Procedure:

In the event that a visual inspection of any submerged portion of the pool liner is deemed necessary, this procedure describes the method to perform such an inspection using an underwater camera and describes the requirements for documenting any observations.

G. Leak Detection Procedure:

This procedure describes the method to test the pool liner for potential leakage using a vacuum box. This procedure may be applied to any suspect area of the liner.

H. Liner Repair and Underwater Welding Procedure:

In the event of a positive leak test result, underwater welding procedures may be implemented which provide for a weld repair, or placement of a stainless steel repair patch, over the area in question. The procedures contain appropriate qualification records documenting relevant variables, parameters, and

limiting conditions. The weld procedure is qualified in accordance with ASME Section XI , or may be qualified to an alternate code accepted by Amergen and Holtec International.

10.2 Rack Arrangement

The rerack project at Clinton will occur in two phases, as initially discussed in Section 1.0. In the initial phase, two new racks, to eventually be relocated to the Spent Fuel Pool in the second phase of the project, will be temporarily installed in the Fuel Cask Storage Pool. In the second phase of the project, the entire Spent Fuel Pool rack array will be changed, with the final array in the Spent Fuel Pool being comprised of both new and existing racks. This configuration requires new and existing racks to be placed closer to the pool walls. Therefore, the existing sparger pipes will need to be modified by removal of some portions. This modification is address by the pool thermal-hydraulic assessment, as discussed in Section 5.5 Additionally, three existing racks will be permanently installed in the Fuel Cask Storage Pool.

10.3 Rack Interferences

A survey was conducted to identify any objects which would interfere with rack installation or prevent usage of any storage locations. There are several permanently installed components interfering with the installation of the racks in the Fuel Cask Storage Pool and the Spent Fuel Pool. Those protrusions that require modification or removal to support the new rack array will be address during the rerack project. Removal or modification of wall protusions shall be done with the aid of diver, as necessary.

10.4 SFP Cooling

The pool cooling system shall be operated in order to maintain the pool water temperature at an acceptable level. It is anticipated that none of the installation activities will require the temporary shutdown of the Spent Fuel Pool cooling system.

If a temporary shutdown of the Spent Fuel Pool cooling system were required, the estimated time after shutdown to increase the pool bulk coolant temperature to a selected value of ≤120 °F will be determined. A temperature of ≤ 120 °F is chosen with enough margin such that cooling may be restored to ensure the pool bulk temperature will not exceed 150 °F.

10.5 Installation of New Racks and Removal of Existing Racks

Installation of the new racks, supplied by Holtec International, involves the following activities. The racks are delivered in the horizontal position. A new rack module is removed from the shipping trailer using a suitably rated crane, while maintaining the horizontal configuration. The rack is placed on the up-ender and secured. Using two independent overhead hooks, or a single overhead hook and a spreader beam, the module is up-righted into a vertical position.

The new rack lifting device is engaged in the lift points at the bottom of the rack. The rack is then transported to a pre-leveled surface where, after leveling the rack, the appropriate quality control receipt inspection is performed. (See 10.1B & D.)

The Fuel Cask Storage Pool or Spent Fuel Pool floor, as applicable, is inspected and any debris, which may inhibit the installation of the racks, is removed. The new rack module is lifted with the Fuel Building Crane and transported along the pre-established safe load path. The rack module is carefully lowered into the Fuel Cask Storage Pool or the Spent Fuel Pool. For the installation of racks along the eastern edge of the Spent Fuel Pool, Fuel Building Crane travel limits will preclude this crane from installing the racks past this travel limit. For these racks, a low profile crane is anticipated to be used to locate the rack to its final design location in the Spent Fuel Pool after its initial installation into the Spent Fuel Pool by the Fuel Building Crane. The use of a temporary crane in support of rerack operations is consistent with the process utilized at previous rerack projects including Beaver Valley, Callaway, Wolf Creek, V.C. Summer, McGuire, Davis Besse, and Three Mile Island.

Elevation readings are taken to confirm that the module is level and the pedestal heights are adjusted as necessary to achieve level. In addition, rack-to-wall and rack-to-rack off-set distances (gaps) are also measured. Adjustments are made as necessary to ensure compliance with design documents. The lifting device is then disengaged and removed from the Fuel Cask Storage Pool or Spent Fuel Pool under Health Physics direction. As directed by procedure, post-installation free path verification of individual cells is performed using an inspection gage.

For existing rack removal from the Spent Fuel Pool, the racks will be cleaned via pressure washing and surveyed by Health Physics prior to removal from the Spent Fuel Pool. As is the case for new rack placement, rack handling shall be completed by the Fuel Building Crane except for those where crane travel limits preclude this ability. In these instances, the low profile temporary crane will be used to lift and move the existing rack to a location in the Spent Fuel Pool that will allow access by the Fuel Building Crane for the ultimate removal of the existing rack from the Spent Fuel Pool. Safe movement of heavy loads is ensured by the processes discussed in Section 3.5.

10.6 Safety, Health Physics, and ALARA Methods

10.6.1 Safety

During the installation phase of the fuel storage rack project, personnel safety is of paramount importance. All work shall be carried out in compliance with applicable approved procedures.

10.6.2 Health Physics

Health Physics is carried out per the requirements of the Clinton Radiation Protection Program.

10.6.3 ALARA

The key factors in maintaining project dose As Low As Reasonably Achievable (ALARA) are time, distance, and shielding. These factors are addressed by utilizing many mechanisms with respect to project planning and execution.

Time

Each member of the project team is trained and provided appropriate education and understanding of critical evolutions. Additionally, daily pre-job briefings are employed to acquaint each team member with the scope of work to be performed and the proper means of executing such tasks. Such pre-planning devices reduce worker time within the radiological controlled area and, therefore, project dose.

Distance

Remote tooling such as lift fixtures, pneumatic grippers, a support leveling device and a lift rod disengagement device have been developed to execute numerous activities from the SFP surface, where dose rates are relatively low.

Shielding

During the course of the fuel storage rack project, primary shielding is provided by the water in the Spent Fuel Pool and Fuel Cask Storage Pool. The amount of water between an individual at the surface and an irradiated fuel assembly is an essential shield that reduces dose. Additionally, other shielding may be employed to mitigate dose when work is performed around high dose rate sources. If necessary, additional shielding may be utilized to meet ALARA principles.

10.7 Radwaste Material Control

Radioactive waste generated from the rack installation will be controlled in accordance with established Clinton procedures.

11.0 ENVIRONMENTAL COST / BENEFIT ASSESSMENT

11.1 Introduction

Article V of the USNRC OT Position Paper [11.1] requires the submittal of a cost/benefit analysis for a fuel storage capacity enhancement. This section provides justification for selecting installation of additional racks in the Fuel Cask Storage Pool and Spent Fuel Pool (SFP) as the most cost effective alternative.

11.2 Imperative for Additional Spent Fuel Storage Capacity

The specific need to increase the limited existing storage capacity of the Clinton Power Station (CPS) Spent Fuel Pool is based on the continually increasing inventory in the pool, the prudent requirement to maintain full-core offload capability, and a lack of viable economic alternatives.

Based on the current inventory of 1,312 fuel assemblies stored in the SFP and the anticipated future discharges of spent fuel, loss of full core reserve capacity will occur during the scheduled February 2006 refueling outage when an anticipated 312 fuel assemblies are permanently discharged and new fuel is loaded into the SFP during Operating Cycle 11. The projected loss of storage capacity in the pool would affect the owner's ability to operate the reactor.

11.3 Appraisal of Alternative Options

Adding fuel storage space to the Clinton Power Station SFP is the most viable option for increasing spent fuel storage capacity.

The key considerations in evaluating the alternative options included:

- Safety: Minimize the risk to the public.
- Economy: Minimize capital and O&M expenditures.
- Security: Protection from potential saboteurs, natural phenomena.

- Non-intrusiveness: Minimize required modifications to existing plant systems.
- Maturity: Extent of industry experience with the technology.
- ALARA: Minimize cumulative dose.
- Schedule: Minimize time to implement a plan which will maintain full-core offload capability for the distant future.
- Risk Management: Maximize probability of completing the expansion to support fuel storage needs.

Rod Consolidation Option

Rod consolidation has been shown to be a potentially feasible technology. Rod consolidation involves disassembly of a fuel assembly and the disposal of the fuel assembly skeleton outside of the pool (this is considered a 2:1 compaction ratio). The rods are stored in a stainless steel can that has the outer dimensions of a fuel assembly. The can is stored in the spent fuel racks. The top of the can has an end fixture that matches up with the spent fuel handling tool. This permits moving the cans in an easy fashion.

Rod consolidation pilot project campaigns in the past have consisted of underwater tooling that is manipulated by an overhead crane and operated by a maintenance worker. This is a very slow and repetitive process.

The industry experience with rod consolidation has been mixed thus far. The principal advantages of this technology are: the ability to modularize, moderate cost, no need of additional land and no additional required surveillance. The disadvantages are: potential gap activity release due to rod breakage, potential for increased fuel cladding corrosion due to some of the protective oxide layer being scraped off, potential interference of the (prolonged) consolidation activity which might interfere with ongoing plant operation, and lack of sufficient industry experience. The drawbacks associated with consolidation are expected to diminish in time. However, it is Amergen's view that rod consolidation technology has not matured sufficiently to make this a viable option for the present CPS SFP limitations.

On-Site Dry Cask Storage Option

Dry cask storage is a method of storing spent nuclear fuel in a high capacity container. The cask provides radiation shielding and passive heat dissipation. Typical capacities for BWR fuel are in the range of 68 assemblies that have been removed from the reactor for at least five years. The casks, once loaded, dried, and sealed are then stored outdoors on a seismically qualified concrete pad.

The U.S. DOE has embraced the concept of multi-purpose canisters (MPCs) obsolescing all existing licensed cask designs. Work is also continuing by several companies, including Holtec International, to improve licensed MPC systems that are capable of long storage, transport, and final disposal in a repository. However, it is noted that a cask system makes substantial demands on the resources of a plant. For example, the plant must provide for a decontamination facility where the outgoing cask can be decontaminated for release.

Several plant modifications may be required to support cask use, including: (1) tap-ins to the gaseous waste system, (2) chilled water to support vacuum drying of the spent fuel, and (3) piping to return cask water back to the Spent Fuel Pool/Fuel Cask Storage Pool. A seismic concrete pad would be needed to store the loaded casks. This pad may require a security fence, surveillance protection, a diesel generator for emergency power and video surveillance for the duration of fuel storage, which may extend beyond the life of the adjacent plant.

Other Storage Options

Other options such as Modular Vault Dry Storage and a new Fuel Storage Pool are overly expensive as compared to placing new racks in the Fuel Cask Storage Pool and Spent Fuel Pool. Due to the complexity of implementation, these options could not meet the required schedule for extending full-core offload capability.

11.3.1 Alternative Option Cost Summary

An estimate of relative costs in 2004 dollars for the aforementioned options is provided in the following:

Rack Installation:	$15 million
Rod consolidation:	$25 million
Dry Storage Horizontal Silo:	$35-45 million
Dry Storage Modular vault:	$56 million
Dry Storage Metal cask (MPC):	$68-100 million
New fuel pool:	$150 million

The above estimates are consistent with estimates by EPRI and others [11.2, 11.3].

To summarize, based on the required short time schedule, the status of the dry spent fuel storage industry, and the storage expansion costs, the most acceptable alternative for increasing the on-site spent fuel storage capacity at CPS is expansion of the wet storage capacity. First, there are no commercial independent spent fuel storage facilities operating in the United States. Second, the adoption of the Nuclear Waste Policy Act (NWPA) created a de facto nuclear fuel cycle requiring disposal. Since the cost of spent fuel reprocessing is not offset by the salvage value of the residual uranium, reprocessing represents an added cost for the nuclear fuel cycle which already includes the NWPA Nuclear Waste Fund fees. In any event, there are no domestic reprocessing facilities. Third, at over $½ million per day replacement power cost, shutting down Clinton Power Station is many times more expensive than addition of high density racks to the Fuel Cask Storage Pool and SFP.

11.4 Cost Estimate

The plant modification proposed for the CPS fuel storage expansion utilizes freestanding, poisoned spent fuel racks installed the Fuel Cask Storage Pool during Phase 1 of the project and the same style racks installed in the SFP during Phase 2.

The total capital cost is estimated to be approximately $15 million as detailed below.

	Phase 1	Phase 2
Engineering, design, project management:	$1 million	$1 million
Rack fabrication:	$2 million	$6 1/2 million
Rack installation:	$½ million	$4 million

As described in the preceding section, other fuel storage expansion technologies were evaluated prior to deciding on the use of additional racks. Storage rack capacity expansion provides a cost advantage over other technologies.

11.5 Resource Commitment

The expansion of the CPS spent fuel storage capacity via augmentation of racks in the SFP is expected to require the following primary resources per Unit:

Stainless steel:	112 tons
Neutron absorber:	12 tons, of which 5 ton is Boron Carbide powder and 7 tons are aluminum.

The requirements for stainless steel and aluminum represent a small fraction of total world output of these metals (less than 0.001%). Although the fraction of world production of Boron Carbide required for the fabrication is somewhat higher than that of stainless steel or aluminum, it is unlikely that the commitment of Boron Carbide to this project will affect other alternatives. Experience has shown that the production of Boron Carbide is highly variable, depends upon need, and can easily be expanded to accommodate worldwide needs.

11.6 Environmental Considerations

The proposed rack installation results in an additional heat load burden to the Spent Fuel Pool Cooling and Cleanup System due to increased spent fuel pool inventory, as discussed in Section 5.0. The

maximum bulk pool temperature will be limited to less than 150°F under normal refueling scenarios. The peak heat load from the spent fuel pool is less than 45 million Btu/hr, which is a minuscule fraction of the total operating plant heat loss to the environment and is well within the capability of the SFP cooling system. Consequently, the short duration of increased heat loading during an outage is not expected to have any significant impact on the environment.

The increased peak bulk pool temperature during a refueling results in a slightly higher increased pool water evaporation rate for a short period of time. This increase is within the Fuel Building HVAC system capacity and does not necessitate any hardware modifications for the HVAC system. Therefore, the environmental impact resulting from the increased heat loss and water vapor generation at the pool surface is negligible.

11.7 References

[11.1] OT Position Paper for Review and Acceptance of Spent Fuel Storage and Handling Applications, USNRC (April 1978).

[11.2] Electric Power Research Institute, Report No. NF-3580, May 1984.

[11.3] "Spent Fuel Storage Options: A Critical Appraisal", Power Generation Technology, Sterling Publishers, pp. 137-140, U.K. (November 1990).